SYNTHETIC AND NATURAL ORGANIC INHIBITORS FOR METAL CORROSION: PHYSICOCHEMICAL, ELECTROCHEMICAL, MORPHOLOGICAL AND QUANTUM MECHANICAL INVESTIGATIONS

Submitted to
University of Calicut
in partial fulfillment of the requirements
for the award of the Degree of

Doctor of Philosophy
in
Chemistry

By

VIDHYA THOMAS K

Under the guidance of

Dr. Joby Thomas K

RESEARCH AND POSTGRADUATE DEPARTMENT OF CHEMISTRY
ST. THOMAS' COLLEGE (AUTONOMOUS)
(UNIVERSITY OF CALICUT)
THRISSUR, KERALA – 680001
NOVEMBER - 2021

RESEARCH AND POSTGRADUATE DEPARTMENT OF CHEMISTRY
ST. THOMAS' COLLEGE
THRISSUR, KERALA-680001

(Nationally reaccredited at 'A' level by NAAC & affiliated to University of Calicut)

Dr. JOBY THOMAS K M.Sc.,M.Phil.,MBA,Ph.D

24-06-2022

CERTIFICATE

*I hereby certify that, this is the revised version of the thesis entitled "**Synthetic and natural organic inhibitors for metal corrosion: physicochemical, electrochemical, morphological and quantum mechanical investigations**" submitted by **Ms. Vidhya Thomas K** under my guidance after incorporating the necessary corrections/suggestions made by the adjudicators. Also certify that the contents in the thesis and the soft copy are one and the same.*

Dr. Joby Thomas K
(Supervising Teacher)

RESEARCH AND POSTGRADUATE DEPARTMENT OF CHEMISTRY
ST. THOMAS' COLLEGE (AUTONOMOUS)
THRISSUR, KERALA-68000
(Nationally reaccredited at 'A' level by NAAC & affiliated to University of Calicut)

Dr. JOBY THOMAS K. M.Sc.,M.Phil.,MBA,Ph.D
Former HOD & Associate Professor

2/11/2021

CERTIFICATE

This is to certify that the thesis entitled ***"Synthetic and natural organic inhibitors for metal corrosion: physicochemical, electrochemical, morphological and quantum mechanical investigations****" is an authentic record of research work carried out by* ***Ms. VIDHYA THOMAS K*** *under my supervision in partial fulfillment of the requirements for the degree of Doctor of Philosophy, in Chemistry of University of Calicut and further that no part thereof has been presented before for any other degree.*

Dr. Joby Thomas. K

(Supervising Teacher)

DECLARATION

I hereby declare that the thesis entitled, “Synthetic and natural organic inhibitors for metal corrosion: physicochemical, electrochemical, morphological and quantum mechanical investigations”, submitted to the University of Calicut in partial fulfillment of the requirements for the award of the Degree of Doctor of Philosophy in Chemistry is a bonafide research work done by me under the supervision and guidance of Dr. Joby Thomas. K, Former Associate Professor & Former Head, Department of Chemistry, St. Thomas’ College (Autonomous), Thrissur, Kerala.

I further declare that this thesis has not previously formed the basis of any degree, diploma or any other similar title.

2-11-2021 VIDHYA THOMAS K

To

My Family

ACKNOWLEDGEMENT

First of all, I thank God Almighty for His showers of blessing throughout my research to complete the work successfully. I would also like to express my deep and sincere gratitude to my Research Supervisor and my Mentor, Dr. Joby Thomas K for giving me the opportunity to do research and providing invaluable guidance throughout this research. I would always cherish this experience for the rest of my life, and it was a great privilege and honour to work and study under his guidance.

I should mention the love and great desire of two people Mr K V Thomas and Mrs Mary Thomas, my parents, which made me dream about these achievements. I am very much thankful to my Husband, Sabu A S, who helped me a lot to fulfil my ambition, especially spending his precious time introducing statistical analysis. Also, I express my thanks to my Son, Sister, Mother in law and Father in law for their tolerance and support.

The support rendered by the St. Thomas College Team – Dr. Fr Martin K A, Principal, Dr. K L Joy, Dr. Jenson P. O and Dr. Ignatius Antony, Former Principals, Dr. C L Joshy, HOD, Dept of Chemistry, all other faculty members of the Chemistry Department, Lab Assistants and Office Staffs has been really high. They served as a lighthouse in my journey towards the completion of this voyage.

I would like to express my sincere gratitude for the support and help rendered by my seniors Dr. Aby Paul, Dr. Vinod P. Raphael, Dr. Shaju K. S and Dr. Nimmy Kuriakose. Special thanks to Dr. Vinod P. Raphael for his constant guidance and support, which helped me greatly during the research period.

The support and help rendered by my research colleagues Sini, Bincy, Reeja, Ramesh, Dinoop, Anju, Martin, Savitha, Swathy, Rohini, Drishya, Siji, Aji, Akhila, Nithya, Neera, Sr. Jisha, Sr. Cinu, Raji and Memcy helped me a lot in completing this thesis, they sincerely worked as a unit. Really it was an honour to work with them.

I recollect the blessings and support from the faculty members, Dept. of Chemistry, St Josephs' College Irinjalakuda. I would like to express my sincere thanks to Dr. Naijil George, Dept. of Biotechnology, St. Joseph College, Irinjalakuda, for successfully completing the microbial induced corrosion studies. I also acknowledge Kavya from Biotechnology lab.

I hereby acknowledge the help rendered by the STIC-CUSAT and SAIF-MG University in analysing the compounds, which were really worthwhile to mention.

I also recall with gratitude the support and the motivation rendered by my dear friends and relatives. I sincerely thank the hard work of Mr. M I Pauly of Educare, Thrissur, who did the DTP work for this project.

I have no valuable words to express my thanks, but my heart is still full of the favours received from every person.

Vidhya Thomas K

ABBREVIATIONS

ICE	*Ixora coccinea* extract
CPE	*Croton persimilis* extract
TCE	*Tinospora cordifolia* extract
GCE	*Garcinia cambogia* extract
CILE	*Clerodendrum infortunatum* leaf extract
CIRE	*Clerodendrum infortunatum* root extract
DBE	*Dioscorea bulbifera* extract
HCA	Hydroxy citric acid
NHP2M	N-hydroxy-1-(pyridin-2-yl)methanimine
NHP3M	N-hydroxy-1-(pyridin-3-yl)methanimine
2PHEP	(E)-2-(1-(2-phenylhydrazono) ethyl)pyridine
2TAEP	(E)-2-(1-triazylidineethyl)pyridine
SCC	Stress corrosion cracking
HIC	Hydrogen-induced cracking
EIC	Environmentally induced cracking
CFC	Corrosion-fatigue cracking
GDP	Gross domestic product
VPIs	Vapour phase inhibitors
DMSO	Dimethyl sulphoxide
EIS	Electrochemical impedance spectroscopy
FTIR	Fourier-transform infrared
UV-Vis	Ultraviolet-visible
NMR	Nuclear magnetic resonance
LC-MS	Liquid chromatography-mass spectrometry
SCE	Saturated calomel electrode
OCP	Open circuit potential
ECN	Electrochemical noise

PSD	Power spectral density
FFT	Fast Fourier transform
MEM	Maximum entropy method
MM	Molecular mechanics
DFT	Density functional theory
SE	Semi-empirical
STO	Slater type orbitals
SEM	Scanning electron microscopy
AFM	Atomic force microscopy
MO	Molecular orbital
HOMO	Highest occupied molecular orbital
LUMO	Lowest unoccupied molecular orbital
RSM	Response surface methodology
CCD	Central Composite Design
ANOVA	Analysis of variance
BBD	Box-Behnken Design
MIC	Microbial induced corrosion
EPS	Extracellular polymeric substances
SRB	Sulphate reducing bacteria
SOB	Sulphur oxidizing bacteria
IB	Iron oxidizing/depositing bacteria
MnB	Manganese oxidizing/depositing bacteria
APB	Acid-producing bacteria
MHA	Mueller-Hinton agar
PCR	Polymerase Chain Reaction
XRD	X-ray diffraction spectroscopy
TEM	Transmission electron microscopy
IE	Inhibition efficiency

ABSTRACT

In recent years, green chemistry has been gaining traction in the research world, owing to a demand for chemical technologies and commercial products that are less toxic and generate less waste. One of the promising domains for applying green chemistry principles is the protection of metals from corrosion. Most industries work in an acidic environment that causes acid corrosion to metal, leading to the loss of metal. The best and favourable method to reduce metal degradation is the usage of corrosion inhibitors. Organic compounds with heteroatoms like N, O, S etc., in a conjugated system, have been commonly used as inhibitors, and they can interact with metal either by chemisorption or physisorption. The adsorptive layer formed on the metal surface protects from the acidic solution and thereby minimizing corrosion. Due to eco-friendliness, low cost, readily available and renewable sources of material, natural products like plant extracts can be used as green corrosion inhibitors

Microbial induced corrosion (MIC) is the destruction of a metal by the activity of living organisms either directly by enhancing the electrochemical reactions or indirectly because of their metabolic products. Various environments such as soil, natural waters, seawater, natural petroleum products and oil emulsion cutting fluids encounter the difficulties of corrosion by such biological activity. It is surprisingly high in the contribution of microbial corrosion loss towards total corrosion loss. In terms of MIC, corrosion inhibitors are known as “biocides”, which means spoiler of living organisms responsible for MIC. Schiff bases are synthetic organic compounds with potent activities in various disciplines such as medicine, agriculture and cosmetic products. Many Schiff bases exhibit anticancer, antitumor, antibacterial etc., properties. Schiff bases are popular compounds for synthesizing numerous antibacterial drugs due to their fast and

straightforward synthetic methods and their tendency to coordinate with their functional groups.

In the present course of investigation, synthetic and natural organic inhibitors were applied for MIC and acid corrosion, respectively. Their inhibition efficiency was evaluated using physicochemical, electrochemical, morphological and quantum mechanical investigations. For convenience and better understanding, the entire work has been presented in this thesis as nine chapters.

CHAPTER 1: Introduction and Review

This chapter deals with introduction to corrosion and MIC, mechanisms of corrosion, economic impact of corrosion, classification and factors affecting corrosion, necessity of corrosion control, methods of corrosion control, corrosion monitoring techniques and a thorough review of published work on natural plant products as corrosion inhibitors. This chapter also reviews synthetic organic compounds as metal corrosion inhibitors, Schiff bases as a metal corrosion inhibitor and Schiff bases as MIC corrosion inhibitors. This chapter is concluded by giving the scope and aim of the present investigations.

CHAPTER 2: Materials and Methods

The methods and reagents used for preparing natural plant extracts, their phytochemical screening, characterization and corrosion inhibition studies are included in this chapter. It also contains methods and reagents used for preparing medium for MIC inhibition studies, isolation and identification of bacterium from original seawater and MIC corrosion monitoring techniques.

CHAPTER 3: Corrosion inhibition efficiency analysis of *Ixora coccinea* extract on mild steel in 1.0 M HCl and 0.5 M H_2SO_4 using various corrosion monitoring methods like weight loss measurements, electrochemical studies, surface morphological, quantum

mechanical calculations and statistical analysis are explained in this chapter. All the results are briefly summarized at the end of this chapter.

CHAPTER 4: This chapter describes corrosion inhibition studies of *Croton persimilis* extract on mild steel in 1.0 M HCl and 0.5 M H_2SO_4 using various corrosion monitoring methods like weight loss measurements, electrochemical studies, surface morphological, quantum mechanical calculations and statistical analysis. All the results are briefly concluded at the end of this chapter.

CHAPTER 5: This chapter discusses the application of *Tinospora cordifolia* extract as a corrosion inhibitor on mild steel in 1.0 M HCl and 0.5 M H_2SO_4 using various corrosion inhibition studies like weight loss measurements, electrochemical studies, surface morphological, quantum mechanical calculations and statistical analysis. All the results are briefly pointed out at the end of this chapter.

CHAPTER 6: Corrosion monitoring analysis of *Garcinia cambogia* extract on mild steel in 1.0 M HCl and 0.5 M H_2SO_4 using weight loss measurements, electrochemical studies, surface morphological studies, quantum mechanical calculations and statistical analysis are illustrated in this chapter in detail. All the results are consolidated at the end of this chapter.

CHAPTER 7: This chapter narrates the application of *Clerodendrum infortunatum* extract as a green inhibitor for mild steel corrosion in 1.0 M HCl and 0.5 M H_2SO_4 using various corrosion monitoring methods like weight loss measurements, electrochemical studies, surface morphological, quantum mechanical calculations and statistical analysis. Here, plant leaf and root extracts were compared for their inhibition efficiency. All the results are briefly outlined at the end of this chapter.

CHAPTER 8: This chapter mainly focused on the anti-corrosion properties of *Dioscorea bulbifera* extract on mild steel in 1.0 M HCl and 0.5 M H_2SO_4 by employing various

corrosion inhibition studies such as weight loss measurements, electrochemical studies, surface morphological, quantum mechanical calculations and statistical analysis. All the results are briefly summarized at the end of this chapter.

CHAPTER 9: Isolation and identification of bacterium from original seawater and microbial induced corrosion (MIC) inhibition studies using synthetic organic inhibitors are described in detail in this chapter. Schiff bases derived from pyridine carbonyl compounds such as 1) *N*-hydroxy-1-(pyridin-2-yl) methanimine, NHP2M 2) *N*-hydroxy-1-(pyridin-3-yl) methanimine, NHP3M 3) (E)-2-(1-(2-phenylhydrazono) ethyl)pyridine, 2PHEP and 4) (E)-2-(1-triazylidineethyl) pyridine, 2TAEP are applied as MIC inhibitor on mild steel in marine environment. Corrosion inhibition properties of these inhibitors are established using weight loss measurements and electrochemical studies. Mechanism of MIC inhibition proves by surface analysis, microscopic surface analysis and *in vitro* antibacterial effects of inhibitors. All the results are briefly summarized at the end of this chapter.

Lastly, overall summary of thesis, followed by the bibliography are included and also the details of publications.

LIST OF CONTENTS

LIST OF TABLES

LIST OF FIGURES

CHAPTER 5

PREFACE

In recent years, the regulation of metal corrosion had a great interest in the field of scientific research. Ready availability, notable mechanical strength and affordable cost make mild steel a widely used alloy in industrial applications. However, the deterioration of mild steel remains a critical issue for the community by considering safety and economic matters. Acid media is used to clean boilers and massive equipment made from mild steel in large scale production units. But it causes metal corrosion. Mitigation of metal corrosion during acid treatment requires appropriate acid solutions. High-cost synthesis and hazardous influence on the atmosphere and human beings make synthetic inhibitors unfriendly inhibitors. The application of extracts from natural products like leaves, fruits, stems, seeds and roots as green corrosion inhibitors can overcome the limitations of the synthetic inhibitors. Plant products can adsorb the surface of the metal either by physical or chemical adsorption. This shielding behaviour of the natural products on the metal surface is due to numerous phytochemicals, which can interact with the metal surface by donating lone pair of electrons of heteroatoms, unsaturated and aromatic systems. Thus, the employment of eco-friendly corrosion inhibitors has a significant role in chemical research.

Microbial induced corrosion (MIC) is the destruction of a metal by the activity of living organisms either directly by enhancing the electrochemical reactions or indirectly because of their metabolic products. Various environments such as soil, natural waters, seawater, natural petroleum products and oil emulsion cutting fluids encounter corrosion by such biological activity. MIC is termed for corrosion by the occupancy and activities of microbes within biofilms at metal surfaces. Biocides are a standard chemical method applied as a MIC mitigation solution. Plant extracts are considered natural sources of antimicrobial agents. Schiff bases accounted for their high inhibition efficiency among

various synthetic organic inhibitors due to their electronic and structural properties. They can coordinate with the metal surface through π-electrons from double bonds and lone pairs of electrons from nitrogen.

The present work is an effort to find out potentially active natural corrosion inhibitors for mild steel in acid media and apply Schiff base inhibitors for MIC in marine environments. Some of the medicinal plants primarily available in our countryside are investigated as natural inhibitors for acid corrosion.

This thesis is divided into nine chapters.

CHAPTER 1: Introduction and Review

This chapter encompasses the introductory session and thorough review of this thesis. It provides an idea about the social and economic aspects of corrosion, types of corrosion, corrosion chemistry, and the need and methods for corrosion control. An introduction to MIC, causes of MIC and strategies to reduce MIC are also discussed in this chapter. The different experimental and quantum mechanical calculations adopted in the investigation for monitoring corrosion and the theories behind all these methods are included here. This chapter reviews natural and synthetic compounds as acid corrosion inhibitors and MIC corrosion inhibitors, respectively. This chapter is concluded by giving the scope and aim of the present investigations.

CHAPTER 2: Materials and Methods

This chapter deals with the experimental details regarding the whole work. The preparation of the extracts, materials and medium for acid corrosion are described here. The technical details of various corrosion monitoring studies, the operational aspects of quantum mechanical studies and statistical analysis methods are explained in this session. It also contains methods and reagents used for preparing medium for MIC inhibition studies, isolation and identification of bacterium from original seawater and

MIC corrosion monitoring techniques.

CHAPTER 3: *Ixora coccinea* Extract: Natural Corrosion Inhibitor for Mild Steel in Acid Media

This chapter discusses the corrosion inhibition behaviour of *Ixora coccinea* leaf extract (ICE). Phytochemical screening, FTIR spectroscopy, Weightloss measurements, Electrochemical impedance spectroscopy (EIS), Potentiodynamic polarization, Electrochemical noise measurements, adsorption, UV-Visible spectroscopy, temperature studies and surface morphological studies were carried out. Theoretical calculations of the major component ixorene have been performed. Statistical analysis of factors has also been studied using Response surface methodology and Central composite design. It was proved that ICE act as a good inhibitor for mild steel corrosion in 1 M HCl and 0.5 M H_2SO_4.

CHAPTER 4: *Croton persimilis* Extract: Natural Corrosion Inhibitor for Mild Steel in Acid Media

This chapter encompasses the study of the anti-corrosion behaviour of *Croton persimilis* leaf extract (CPE). The ethanolic extract of CPE was investigated as inhibitor for mild steel in 1 M HCl and 0.5 M H_2SO_4 media at room temperature. Electrochemical studies revealed the excellent inhibition capacity of CPE in 0.5 M H_2SO_4 than 1 M HCl, which was supported by adsorption studies, temperature and surface morphological studies. Theoretical calculations of the significant components neocrotocembraneic acid and stigmasterol have been performed. Statistical analysis of factors has also been studied using Response surface methodology and Central composite design.

CHAPTER 5: *Tinospora cordifolia* Extract: Natural Corrosion Inhibitor for Mild Steel in Acid Media

The inhibiting capacity of *Tinospora cordifolia* extract (TCE) has been evaluated on mild steel in 1M HCl and 0.5 M H_2SO_4 by physicochemical and electrochemical techniques and by utilizing statistical tools such as response surface methodology (RSM)

and Box-Behnken design (BBD) in this chapter. Surface properties have been ascertained by atomic force microscopy (AFM) to confirm the adsorption performance of the inhibitor molecules on the surface of the metal. Experimental results were found to agree with quantum chemical calculations of the active principle of TCE, Tinosponone.

CHAPTER 6: *Garcinia cambogia* Extract: Natural Corrosion Inhibitor for Mild Steel in Acid Media

This chapter illustrates the corrosion-resistant power of the ethanol extract of *Garcinia cambogia* (GCE) leaves for mild steel in 1 M HCl and 0.5 M H_2SO_4. Gravimetric, electrochemical and morphological studies have been established to authenticate inhibiting power of GCE. Quantum mechanical investigations of chief constituents, hydroxycitric acid and hydroxycitric acid lactone have been shown the anticorrosion behaviour of GCE. Statistical analysis using response surface methodology and Box-Behnken design was proved a good agreement with experimental results.

CHAPTER 7: *Clerodendrum infortunatum* Extract: Natural Corrosion Inhibitor for Mild Steel in Acid Media

This chapter deals with physicochemical, electrochemical and surface morphological studies of the inhibitive interaction of *Clerodendrum infortunatum* leaf and root extracts (CILE and CIRE) on the mild steel surface in 1 M HCl and 0.5 M H_2SO_4. The extracts showed appreciable efficiencies in varying inhibitor concentrations. The major components clerodin and scutellarin have also been analyzed for their inhibitory action. Predicted inhibition efficiency of CIRE at different CIRE concentrations and operating temperature in 1 M HCl evaluated by RSM was in perfect agreement with the data obtained from weight loss measurements.

CHAPTER 8: *Dioscorea bulbifera* Extract: Natural Corrosion Inhibitor for Mild Steel in Acid Media

This chapter explores the potent corrosion inhibition property of green *Dioscorea bulbifera* leaf extract (DBE) on the mild steel in 1 M HCl and 0.5 M H_2SO_4 using

physicochemical, electrochemical and surface morphological techniques. Three essential chemical components, bafoudiosbulbin A, diosgenin and kaempferol, have been subjected to quantum mechanical studies to supplement the corrosion inhibition mechanism of the leaf extract in more detail. By designing BBD, response surface methodology has been applied to validate the interdependence between DBE concentration, HCl concentration, and temperature on the inhibition efficiency. DBE was found to be an efficient corrosion inhibitor for mild steel corrosion exposed in 1 M HCl and 0.5 M H_2SO_4.

CHAPTER 9: Schiff Bases Derived from Pyridine Carbonyl Compounds: Synthetic Microbial Induced Corrosion Inhibitor for Mild Steel in Marine Environment

This chapter deals with microbial induced corrosion (MIC) behaviour of four synthetic inhibitors derived from pyridine carbaldehyde and acetyl pyridine on mild steel in the artificial seawater medium, 1) *N*-hydroxy-1-(pyridin-2-yl)methanimine, NHP2M 2) *N*-hydroxy-1-(pyridin-3-yl)methanimine, NHP3M 3) (E)-2-(1-(2-phenylhydrazono) ethyl)pyridine, 2PHEP and 4) (E)-2-(1-triazylidineethyl)pyridine, 2TAEP. It includes isolation and identification of bacterium from original seawater and corrosion monitoring methods like physicochemical and electrochemical techniques of these Schiff bases. Mechanism of corrosion was established by *in vitro* antibacterial effects of Schiff bases, surface analysis, microscopic surface analysis and UV-Vis spectroscopy.

An overall summary of these investigations is also reported at the end of this part, followed by the bibliography.

CHAPTER 1
INTRODUCTION AND REVIEW

From the beginning of humankind itself, metals have been an inevitable part of human life. There are various forms of metals all over the world. Some of the metals exist in their pure form, whereas some of them exist as their ores. Gold is an example of native metal, whereas iron is seen as its ores in this world. When two or more metals are combined, it will convert into a more effective form, i.e. alloy. Steel is an alloy of iron (Fe) that has improved properties than Fe. The unique characteristics of steel are high strength, thermal stability and corrosion resistance. It causes wide applications of steel, especially in the construction fields. Based on the requirement of steel, different elements are added to it. Manganese, molybdenum, chromium, nickel, vanadium, silicon and boron are alloying elements.

Manufacturing technology and the cost of a material is an essential criterion for the selection of an alloy. It is tough to manufacture an alloy with the property of corrosion resistance cheaply. Mild steel is one of the readily available and easily manufactured alloys. It is a less carbon alloy. Other alloying elements are also present in a very negligible amount. So it is affordable steel to all. But, it undergoes oxidation (corrosion) readily if it is not protected by inhibitors, coatings, cathodic protection etc.[1]

Corrosion

According to American Society for Testing and Materials' corrosion glossary, corrosion is defined as[2] "the chemical or electrochemical reaction between a material, usually a metal, and its environment that produces a deterioration of the material and its properties". Corrosion is a metal destruction activity influencing the action of metal in applications badly. It is a natural process due to the presence of surrounding

environments. When a pure metal is converted into its more stable metallic compounds (ores), it is known as corrosion[3]. The metallic compounds may be oxides, sulphides and carbonates. Rust is the corrosion product of ferrous metals. Adverse atmospheric conditions or aggressive media like acidic or basic solutions trigger corrosion in materials. All these natural deterioration processes cause acute damages to the surface of materials. Corrosion causes not only material loss but also economic loss. The financial loss due to corrosion is enormous all over the world every year. This loss can be divided into two cases 1) direct loss 2) indirect loss. Direct loss includes the cost of replacing and repairing corroded structures and machinery, galvanizing steel, modifying the metal by reforming it into alloy etc. Indirect loss can't be compensated by money, including the shutdown of industries, loss of products, and efficiency.

Each metal has different corrosion resistance power. The corrosion due to atmospheric exposure on steel, the most popular alloy, is uniform in nature. That is uniform corrosion. Localized corrosion is difficult to predict and reduce. Various type of corrosion exists in chemical industries due to the presence of offensive corrodents. According to DIN EN ISO 8044, corrosion[4] is the "physical interaction between a metal and its environment which results in changes of the properties of the metals and may lead to significant functional impairment of the metal, the environment or the technical system which they form a part".

Mechanism of corrosion

Local cell theory

According to De la Rive "corrosion occurs because of creating a large number of micro electrochemical cells or local cells at heterogeneities (impurities, defects, different phases, non-uniform stress distribution etc.,) on the metal surface[5]". This is the basics of Local cell theory of corrosion (Fig. 1.1). A change in electrical potential experienced

between two metals or between various portions of a single metal during the corrosion process. This voltage difference develops the current to go through the metal accounts for the reaction at anodic and cathodic areas. The difference in composition on the metal surface, surface inhomogeneity and stress due to metal operational works cause the development of anodic and cathodic areas on the metal surface.

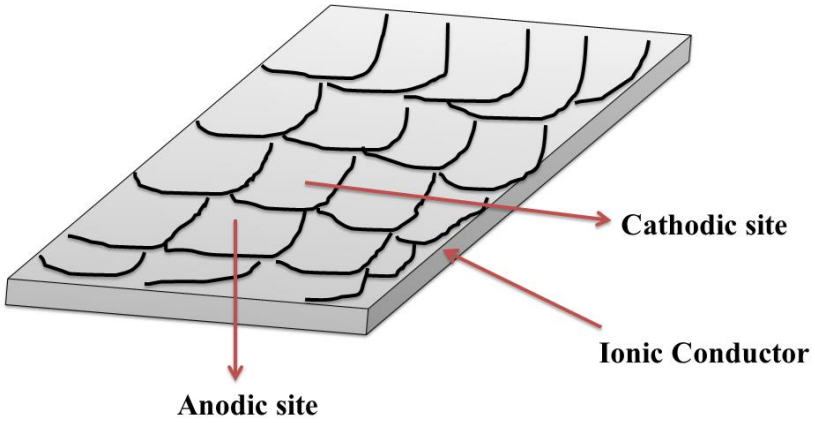

Fig. 1.1: Pictorial representation of local cell theory

Wagner and Trauds' theory

Primary mechanism of corrosion includes an occurrence of corrosion cells; however, it is not necessary to exist physically independent anodes and cathodes to take place corrosion. Instead of impurities and surface irregularities, some cathodic reactions must carry on concurrently on the metal surface. These cathodic reactions are the essential condition for corrosion as per Wagner and Trauds' theory[6].

Corrosion which is a metal dissolution process, can be explained using the following steps (Fig. 1.2):

- In the first step, Fe^0 getting oxidized into Fe^{2+} ion. Here iron is lost from the cathodic site, the smaller potential site to the aqueous solution.
- When Fe^{2+} formed, two electrons will be free to move through the metal surface to the cathodic site.
- Released electrons consume by oxygen in the water and converted into OH^-.

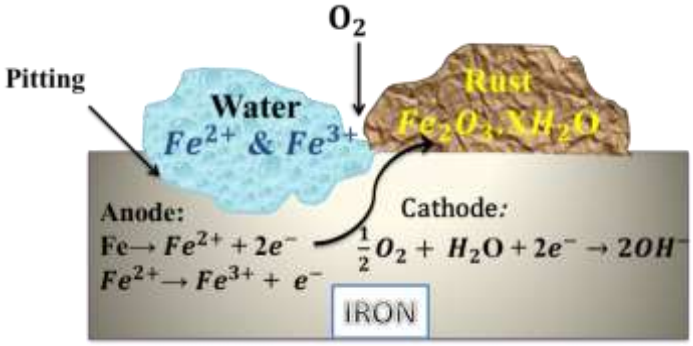

Fig. 1.2: Reactions involved in the corrosion of iron

Reaction at Anode: $Fe \rightarrow Fe^{2+} + 2e^-$ (1)

Reaction at Cathode: $\frac{1}{2}O_2 + H_2O + 2e^- \rightarrow 2OH^-$ If $P^H > 4$ (2)

If oxygen is not present, H^+ controls the reaction at the cathode to maintain the electrical circuit.

$2H^+ + 2e^- \rightarrow H_2\uparrow$ (3)

Hydroxyl ions react with Fe^{2+} to form the less soluble ferrous hydroxide, precipitating a white loosely clumped mass of fine suspended particles at the metal surface.

$Fe^{2+} + 2OH^- \longrightarrow Fe(OH)_2\downarrow$ (4)

This powder easily reformed into ferric hydroxide by oxidation.

$4Fe(OH)_2 + O_2 + 2H_2O \longrightarrow 4Fe(OH)_3$ (5)

Ferric hydroxide undergoes dehydration causes the occurrence of corrosion products on the metal surface.

$2Fe(OH)_3 \longrightarrow Fe_2O_3\downarrow + 3H_2O$ (6)

$Fe(OH)_3 \longrightarrow FeO(OH)\downarrow + H_2O$ (7)

It may lead to the precipitation of other aqueous ions since solid corrosion products are formed at the anodic site. It may attribute to the formation of traces of suspended mud, sand, clay etc., on the corrosion film. A porous film indicates that corrosion can occur continuously due to the penetration of metal ions up to the solution interface, whereas a tight adherent film shows the elimination of ionic diffusion.

Types of corrosion

The most adapted classification of corrosion provides the study of corrosion in depth[7, 8]. Corrosion failure analysis requires the knowledge of types of corrosion which is responsible for deterioration.

Uniform corrosion

It is also known as general corrosion[1]. It leads to the uniform thinning of corrosion over the metal surface. It is due to the existence of manifold anodes and cathodes working on metal surfaces like local corrosion cells. Uniform corrosion is made possible by the continuous movement of the anodic and cathodic sites over the surface. The impact of uniform corrosion can be easily judged because it is reproducible. Irrespective of the environment, the exposed metal surface is wholly corroded in this corrosion. The different environments are liquid electrolyte, gaseous electrolyte or hybrid electrolyte.

The anodic reaction of uniform corrosion is an oxidation process at all times. The cathodic reaction depends on the conditions: If $P^H < 7$ reduces hydrogen ions; If $P^H \geq 7$, it reduces dissolved oxygen. By applying paints, coatings or inhibitors, uniform corrosion can be prevented.

Galvanic corrosion

It is called dissimilar metal corrosion or bimetallic corrosion. It is formed by joining two different metals to build a wet corrosion cell (Fig. 1.3). The requirement of galvanic corrosion is an electrolyte and an electron-conducting path. Galvanic series determines which metal is acting as anode and cathode in the cell. The more negative metal will be the anode, and the more positive metal will be the cathode of the corrosion cell. The corrosion rate of the more active anode will increase, and of nobler cathode will decreases. The junction between two metals acutely undergoes corrosion. The voltage

difference between different metals leads to this corrosion. The conductivity of the electrolyte and the area ratio between cathode and anode are the two essential factors that determine the degree of attack. For example, galvanic corrosion results when aluminium alloy is coupled with steel and enhance the rate of corrosion of aluminium alloy which is the anode.

Fig. 1.3: Mild steel coupled with copper showing galvanic corrosion

Crevice corrosion

It is the same as pitting corrosion. In this corrosion, the total exposed area undergoes local changes in its chemistry. Reduction of oxygen in the crevice, increase in pH with increasing hydrogen ions and chloride ions are some of the initiations of crevice corrosion. Reduction of oxygen is a cathodic process that cannot exist under the crevice area causes metal dissolution.

Crevice corrosion may operate with any metal and adverse environment. However, certain metals and alloys specifically undergo crevice corrosion in particular environments because they depend on their oxide film at the surface of the material for the prevention of corrosion. Previous reports show that other than metallic material, wood, wax, plastic, rubber, concrete etc., are prone to crevice corrosion. It is generally exhibited in chloride environments.

Filiform corrosion

It is a form of crevice corrosion, also called “under film” corrosion. By the exposure of atmospheric moisture on painted surfaces, filiform corrosion takes place. Lacquers painted surfaces are mainly affected by this corrosion. Therefore, such quick-dry paints should avoid the prevention of this type of corrosion.

Pitting corrosion

Pitting corrosion is another form of crevice corrosion. It is self-nucleating localized corrosion. The attacking areas of pitting corrosion may include surface scratch or an emerging dislocation due to the applied tensile stresses or non-homogeneous composition (Fig. 1.4). Its initiation depends only on metallurgical factors.

Fig. 1.4: Pitting corrosion of mild steel

It is more harmful than uniform corrosion because it is not easy to detect and resist. Even a tiny pit can destruct the whole engineering system. After the initiation, the same cathodic reactions, such as oxygen depletion, hydrogen evolution etc., occurs in the pits as the crevice corrosion. The pits will act as an anode and the remaining metal surface act as a cathode. So, the metal loss will take place in small pits and reach higher rates than general corrosion. Large pits are challenging to corrode due to the mixing and restoring of oxygen, hydrogen or bicarbonate ions by water mobility.

Intergranular corrosion

Intergranular corrosion is a form of localized corrosion. It is a selective attack on the grain boundary area near them. The strength and ductility of a metal reduce because there is no damage to the centre of the grain. The attack is random, piercing into the metal and causing deterioration.

Stress corrosion cracking (SCC)

Structural components of a system may collapse before the due time when they are forced to the tensile stress and aggressive environment (Fig. 1.5). This phenomenon is called environmentally induced cracking (EIC). EIC includes three different forms of corrosion.

- Stress-corrosion cracking (SCC)
- Hydrogen-induced cracking (HIC)
- Corrosion-fatigue cracking (CFC)

Fig. 1.5: Stress-corrosion cracking of mild steel

Erosion corrosion

The word “erosion” implies destruction via mechanical force such as wear and tear. When erosion facilitates the rate of corrosion of a metal, it is known as erosion-corrosion. The critical reasons for erosion-corrosion are corrosive environment and

elevated fluid surface velocities. Unlike other corrosions, the surface of metal subjected to erosion-corrosion will be clear.

Necessity of corrosion control

For the years, the study of corrosion and its prevention methods have been gaining traction in the research world. This is due to:

- The utilization of a variety of metals and newly synthesized alloys has grown to a great extent.
- The need for metals in specific areas like aerospace, atomic energy etc. increasing in recent years.
- The increasing environmental pollution originates from aggressive corrosion conditions.
- Occasionally, the depletion of metal structures to thinner dimensions may be due to economic inducements; thus, the consequences of corrosion are extended to a necessary extent.
- The soaring trend toward prolonged time between support, swift restorative effort and the preference to track tasks involuntarily.
- The industry pays a heavy toll on corrosion. However, a considerable section of these costs could be conserved by an efficient implementation of well-known procedures for corrosion prevention paired with the growth of more effective approaches of protection[9].

Various nations reported in their studies that corrosion is a significant issue they face. The United States revealed that around 5% of the GDP was destroyed due to corrosion[3]. It has been considered that 20-25% of the current corrosion costs could be reserved by employing existing awareness of corrosion inhibition and control, i.e.,

applying recommended protective systems and upgrading design and materials selection[10, 11].

Beyond the economic loss of corrosion are safety matters. Human society focuses its attention on the security of a range of metallic structures susceptible to corrosion ruins. For example, aeroplanes constructed from extremely strong aluminium alloys and pressure vessels could threaten many lives if collapsed[12]. Besides all these, corrosion is severe destruction because it engenders the impoverishment of our natural resources. The enhancing industrial advancements of many countries cause an increased demand for metal resources to become more inadequate. It should also be suggested that the prevention of corrosion conserve energy[13]. In the concept that the extraction of all metals from their ores depleting vast amounts of energy. Preserving metals in their original state thus deliver a large quantity of energy. The applicability of corrosion to the community lies in the extensive use of metals exposed to various challenging environments[14].

Methods for corrosion control

The relevant stages of a component during its lifespan are design, construction and application. Corrosion inhibition has a vital role in each of these stages. Therefore, the breakdown of corrosion control in any of these stages will damage the component untimely.

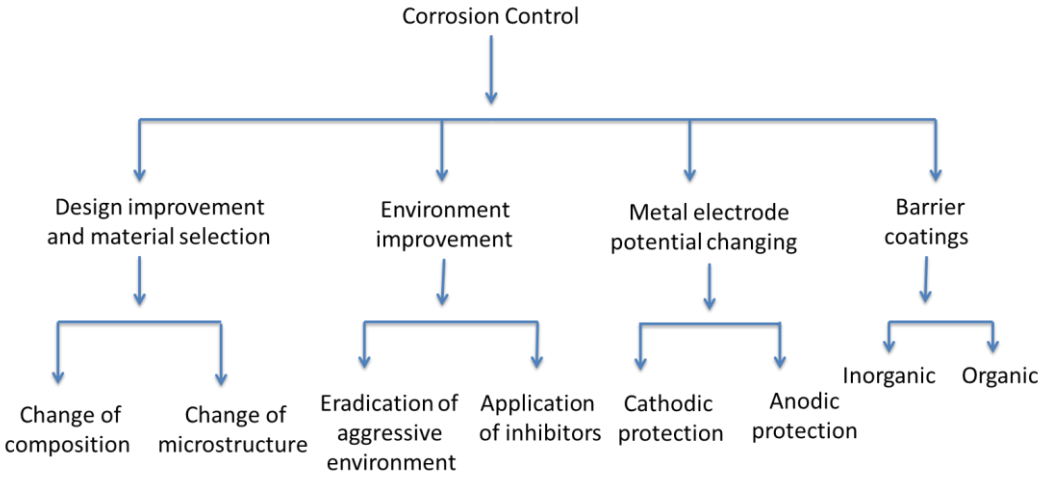

Fig. 1.6: Schematic representation of corrosion control methods

Corrosion control can be done by

- Improving the design and material selection
- Improving the environment
- Implementing barrier coats
- Implementing cathodic or anodic protection.

Materials selection and design

A proper design includes both mechanical and strength requirements, which means it allows free circulation of air instead of the build-up of dirt and stagnation of water. The selection of suitable material and its design is the initial step for corrosion control. For example, the relevance of metallurgical phase composition can be exemplified by the exfoliation of aluminium in marine life.

Improving the environment

There are two strategies for electrolyte management:

❖ ***Eradication of the aggressive components***

The following methods explain the removal of aggressive components:

1) Addition of oxygen scavengers, saturation of inert gases like N_2, evacuation etc., causes the removal of dissolved oxygen from the solution.
2) Neutralization reactions can remove corrosive acids or bases.
3) Prevention of humidity by any drying agents like silica gel.
4) Ion exchange or reverse osmosis can eradicate dissolved salts from the solution.
5) Relative humidity can also reduce by increasing the temperature above the surroundings.
6) Removal of solid particles causes the prevention of different aerations and crevice erosion.

❖ ***Application of inhibitors***

The use of corrosion inhibitors is an efficient and reliable method for shielding metals from deterioration in contact with aqueous solutions, especially in a closed system like cooling and heating systems[15]. Corrosion inhibitors are organic or inorganic compounds, which retard the rate of corrosion when added to the solution in a low concentration ranging from 1 to 15,000 ppm. Two probable working methods are for corrosion inhibitors to control metal corrosion in a corrosive environment[16]. 1) By the interaction with the corrosive species 2) By the interaction with the metal surface

Adsorption is the chief phenomenon through which corrosion mitigation happens on the metal surface by decreasing the rate of either or both the anodic and cathodic reactions. Inhibitors have a pronounced effect on the H_2 evolution reaction, such as aromatic and aliphatic amines; phosphorous, arsenic and antimony compounds; sulphur compounds and carbonyl molecules in the metal dissolution process. Some of the inhibitors create shielding to the metal surface by precipitating on it. Phosphate and bicarbonate salts of multivalent ions can form a passivation layer since they are insoluble. Another class of inhibitors works as redox agents by cathodic or anodic protection. Chromate is an example of a redox inhibitor that alters the potential of a metal surface and develops a passivation layer. Depending on the mechanism of inhibition, corrosion inhibitors are categorized into anodic, cathodic, mixed type and vapour phase inhibitors.

Anodic inhibitors

They are passivating inhibitors that inhibit metal corrosion by developing a barrier of oxide film on the metal surface. They affect the rate of anodic reactions in the corrosion process. There are two types of passivation by inhibitors 1) oxidizing 2) non-oxidizing. Nitrite, chromate, nitrate etc., passivate metal without oxygen. They belong to

oxidizing inhibitors. Some of the inhibitors like tungstate, molybdate, phosphate etc., passivate metal with oxygen. They are called non-oxidizing inhibitors. The important condition for an anodic inhibitor is that its concentration must be high in solution. Otherwise, it causes localized corrosion on the metal surface because the inhibitor doesn't adsorb the surface entirely.

Cathodic inhibitors

They affect the cathodic reaction and control the migration of ions to the cathodic site[17]. They can perform in different ways, such as cathodic poisons, cathodic precipitates and oxygen scavengers. Sulphites, bicarbonates etc., belong to cathodic inhibitors[18]. They are more advantageous than anodic inhibitors since cathodic inhibitors demand only a small amount of inhibitors.

Mixed-type inhibitors

They control both anodic and cathodic reactions of a corrosion process. The organic inhibitors usually act as mixed-type inhibitors by resisting metal dissolution at the anode and oxygen reduction at the cathode.

Vapour phase inhibitors (VPIs)

They have low vapour pressures ranging from 0.0002 to 0.4 mmHg. They can volatilize easily and adsorb on all surfaces situated in a confined space[19]. Their lifetime is so vast. So, they can retard the corrosion of metals used in storage, transport and electronic materials, such as circuit boards. VPIs are commonly used for the protection of steel. Hydrazine and morpholine are good examples of vapour phase inhibitors. They are carried with steam to prevent corrosion in condenser tubes.

Corrosion inhibitors are further classified into two based on compounds, i.e., organic and inorganic inhibitors.

Inorganic inhibitors

Molybdate anion, calcium nitrite, zinc phosphate, chromate, rare earth metal salts etc., belong to this category[20]. However, their application as an inhibitor is less due to its high toxicity, high cost and less solubility.

Organic inhibitors

Low toxicity, high solubility, coexistence with the protected metal and withstandable at various temperatures make them most popular in industrial fields. They form a protective film on the metal surface by performing either anodic, cathodic or mixed inhibitors. Plant extracts, amines, amino acids, heterocyclic compounds and Schiff bases are few examples of organic inhibitors in which Schiff bases are commonly used synthetic organic inhibitors. Condensation of an amino compound with aldehyde or ketone produces a Schiff base with a general formula $R_2C=NR$. It has been reported that Schiff bases have good corrosion inhibition capacity than their parent compounds. –CH=N- group involved in Schiff bases causes physical and chemical adsorption on the metal surface. Adsorption mainly depends on three factors. 1) structure of the inhibitor, 2) characteristics of the metal surface and 3) corrosive medium. Only the molecules having heteroatoms such as N, O and S and conjugated unsaturated π bonds can create adsorption film on the metal surface by donating lone pair of electrons and π electrons respectively[21,22].

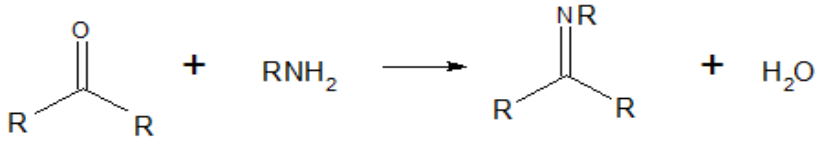

❖ ***Application of barrier coats***

A variety of barrier coatings may be employed to minimize localized corrosion on the metal surface. Barrier coatings protect the metal by high resistance to inhibit current flow between anode and cathode or dispossess oxygen diffusion. Metallic,

inorganic and organic coatings are different materials for protection. Thin coatings of materials can protect the metal from its environment with an acceptable barrier. Based on the service condition and economics for a certain process, the applicability of the barrier coating varies.

❖ ***Shifting the electrode potential***

According to the principle of anodic protection, a metal can protect either cathodically by decreasing its potential to the region of immunity or increasing the potential to the region of passivity. In the case of iron, elevation in the potential can be achieved by anodic polarisation or the addition of appropriate oxidizing agents. Metal protection by raising the potential is an excellent corrosion control method for iron-based metals and alloys in acid solutions since the region of passivity for iron is notably larger, as shown in Pourbaix diagram[23] (Fig. 1.7).

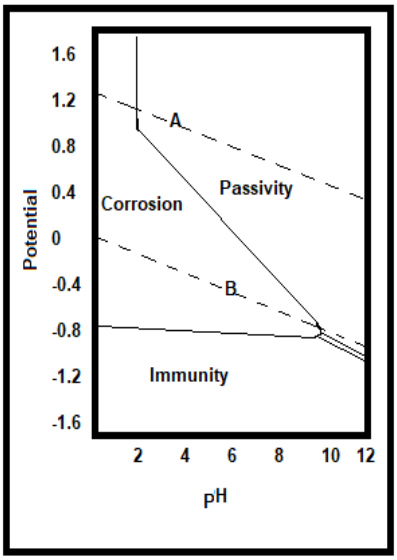

Fig. 1.7: Pourbaix diagram for iron in aqueous solution

Cathodic protection can be employed by sacrificial anodes or impressed current[24]. An electrolysis cell is built in the sacrificial method by connecting the metal to be protected with a more quickly destructed sacrificial metal intentionally. A sacrificial anode is set up from a metal having more negative potential than the metal to be

protected, which furnishes adequately high protective current. The potential difference between the sacrificial metal and the metal to be protected means the sacrificial metal deteriorates in preference to the metal to be protected. There are two necessary conditions for working the sacrificial anode method 1) for the flow of electrons from the sacrificial anode to the metal to be protected; a current path should be set up 2) There should be an electrolyte to carry the electrons. This method requires no external power source, whereas the impressed current method employs a power source to supply electrical power to the metal to be protected by the aid of an auxiliary electrode. Therefore, the impressed current method provides much longer protection than the sacrificial anode method since the former is connected by an outside power source[25].

Corrosion monitoring techniques

Corrosion analysis involves a quantitative measurement of the efficacy of corrosion regulation and evaluation of inhibition techniques. The significant advantages of corrosion monitoring may be summarized as[9].

- Better safety
- More eco-friendly
- A continuous and dynamic record of metal stability
- Lower performance costs

Weight loss measurements

One of the oldest direct measurement techniques of corrosion is the weight loss method, which employs metal weight loss over a coupon strip. The easiness of detection of small weight losses depends on the ratio between surface area and coupon weight. This prefers the shortest interval of time between weighing instead of a long time gap which will cause loss of rate of attack fluctuations. But, in the case of large samples, a long time interval of weighing is desired to monitor pitting attacks.

This method requires the weight loss of a metal exposed in the acid medium with and without inhibitor at a particular time interval in corrosion studies. Using the resulted weight loss values, corrosion rate (υ) and inhibition efficiencies (η%) are estimated by the following equations.

$$\upsilon = \frac{KW}{DSt} \quad (8)$$

where K =87600, W- an average weight loss of coupon (g), S- total area of the coupon (cm^2), D- density of metal (g cm^{-3}), t- period of immersion (h).

$$\eta\,\% = \frac{\upsilon_0 - \upsilon}{\upsilon_0} X100 \quad (9)$$

where υ_0 and υ indicate the corrosion rate of metal coupons immersed in acid solutions in the absence and presence of the inhibitor.

Electrochemical impedance spectroscopy (EIS)

Electrochemical impedance spectroscopy is the plot of electrode impedance against frequency. Dynamics of an electrochemical process is described graphically in EIS. It is an alternate current method that provides equivalent resistance and capacitance values in terms of interfacial phenomena.

A sinusoidal voltage perturbation of low amplitude is applied in the electrochemical system for EIS in a boundary of frequency. Frequency is the unique character of various processes involved in the electrochemical system since the processes evolved are distinct at each frequency. For an excitation signal ω, a linear system outputs a current frequency ω whereas; a non-linear system outputs a current with contorted frequency. The effect of non-linearity can be detected and applied for an electrode reaction in which the current-over potential function is non-linear beyond average ranges of overpotential. The flexibility of charging currents is the best part of all methods based on non-linearity. Charging currents are highly regulated to the excitation signals because double-layer capacitance has a more linear effect than faradaic impedance.

Corrosion behaviour can be analyzed using EIS at the metal/solution interface. In the corrosion process, the measured current is out of phase with the input voltage. Impedance is the fraction of input voltage to the output current. The fluctuation in magnitude and phase angle of impedance value gives elucidation of EIS. Electrical equivalent circuits are characteristic of the electrochemical reactions at the interface between metal and electrolyte. So, all the analysis of impedance data is focused on it.

Equivalent circuit of a cell is identical to the system in an electrochemical cell. The working of an electrochemical cell can render by an equivalent circuit of resistors and capacitors. As the real cell performs for a given signal, the equivalent circuit convey the current with the same amplitude and phase angle. Randle's circuit is the most commonly employed equivalent circuit. It consists of a solution resistance, a double layer capacitance (C_{dl}) and a charge transfer resistance (R_{ct}) or polarization resistance (R_p). Charge transfer reaction in the electrochemical cell makes the double layer capacitance parallel with the impedance[26]. Generally, double-layer capacitance on real cells acts as a capacitor. Fig. 1.8 represents Randle's circuit.

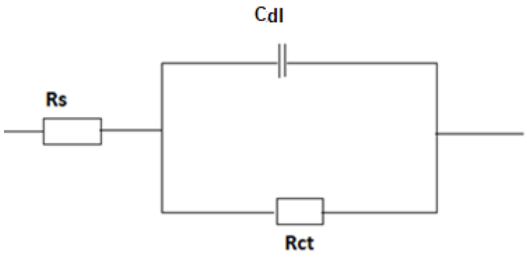

Fig. 1.8: Randle's circuit

This is the case of ideally behaving capacitors. Actually, capacitors perform as a constant phase element in the electrochemical system. This is because of the conjoining of the solution resistance and the surface capacitance due to microscopic roughness on the metal surface by corrosion attack, damage etc. Moreover, chemical in-homogeneities of the surface also lead to capacitance dispersion at the interface. These two factors cause the non-ideal behaviour of capacitors.

A sinusoidal voltage may be represented as

$$e = E\text{Sin}\omega t \quad (10)$$

where ω is the angular frequency.

Phase angle between I and E will be $\emptyset$ in real cases. So, it may be expressed as

$$i = I\text{Sin}(\omega t + \emptyset) \quad (11)$$

where $\emptyset$ is negative.

These equations may be utilized for the evaluation of simple circuits. When a pure resistance R is applied to this sinusoidal voltage, the current will be

$$i = (E/R)\text{Sin}(\omega t + \emptyset) \quad (12)$$

$$\text{where } E = IR \quad (13)$$

If $\emptyset$=0, then

$$i = (E/R)\text{Sin}\omega t \quad (14)$$

When a pure capacitor replaces the resistor, then current will be

$$i = \left(E/X_c\right)\text{Sin}(\omega t + \pi/2) \quad (15)$$

where the phase angle is $\pi/2$ and the current peaks come earlier than the voltage peaks. Real components are obtained along the abscissa, while imaginary components are availed along the ordinate. It is convenient to plot the current phase along the abscissa.

$$E = -jX_cI \quad (16)$$

$$\text{where } j = \sqrt{-1} \quad (17)$$

On comparing (13) and (16), it is clear that X_c has the exact characteristics of resistance except for the correlation between its magnitude and frequency. The magnitude of X_c is inversely proportional to frequency.

When resistance R and capacitance C are connected in series, a voltage E is applied. The sum of individual contributions of the resistor and capacitor is the total voltage drop.

$$E = E_R + E_C \tag{18}$$

$$E = I(R - jXc) \tag{19}$$

$$E = IZ \tag{20}$$

This Z vector is known as an impedance that links between voltage and current. Impedance can be expressed as

$$Z_\omega = Z_{Re} - jZ_{Im} \tag{21}$$

where Z_{Re} represents real components, and Z_{Im} indicates imaginary components of the impedance.

For the combination of resistors and capacitors, phase angles are between 0 and $\frac{\pi}{2}$. There are different forms of representations for recording fluctuations in impedance with frequency.

Bode and Nyquist plots are two other representations (Fig. 1.9). Bode plot[27] exhibits log $|Z|$ and $\emptyset$ against log ω, whereas Nyquist plot represents Z_{Re} against Z_{Im} for various ω.

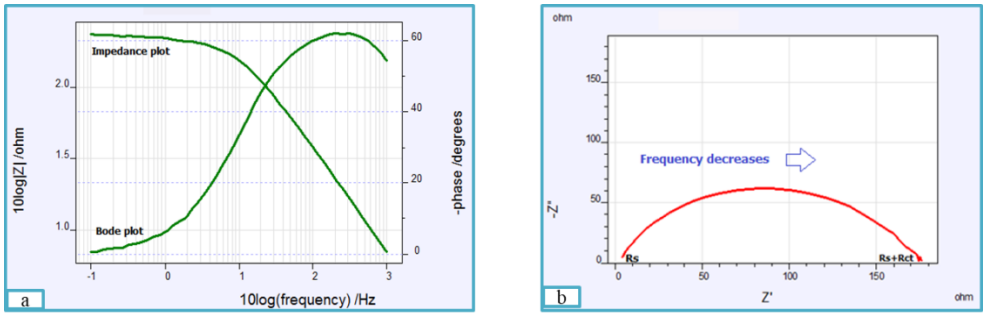

Fig. 1.9: a) Bode plot b) Nyquist plot

Bode plots precisely express frequency information. In the Bode plot, the same number of points is recorded for each decade. So, it is plotted over the observed

frequency region logarithmically. To find the initial resistor more easily, both Nyquist and Bode plots depict high frequency to low frequency. Nyquist plot is a popular representation of impedance since it is more interpretative than the other. In the Nyquist plot, the real part is plotted against the imaginary part and gives impedance values for various frequencies. Impedance decreases as frequency increases.

To counteract solution resistance between the counter and reference electrodes, three-electrode assembly is used in electrochemical systems. But, when the electrochemical cell is designed, there is a solution resistance between the reference electrode and the working electrode that should be accounted for. Impedance is a degree of the capacity of an electrical circuit to resist the conveyance of current, similar to resistance. But, impedance doesn't follow the simplifying properties of an ideal resistor. An ideal resistor

a) Obeys Ohm's law at all current and voltage values.
b) Its resistance value doesn't depend on the frequency
c) Alternate current and voltage signals through a resistor are in phase with each other.

EIS is a dominant technique for the quick and precise analysis of corrosion processes of various materials in different corrosive media[28]. It is also used to delineate coating integrity. Organic coatings have high resistivity. So, typical DC techniques can't employ for the analysis of corrosion[29]. EIS technique provides necessary parameters for estimating corrosion mechanisms such as coating capacitance, coating resistance, and interfacial corrosion process between metal and coating[30].

Nyquist plot is a semi-circular line for Randle's equivalent circuit. Real axis value at the high-frequency intercept, close to the origin, gives the solution resistance. In contrast, charge transfer resistance (polarization resistance) and solution resistance at the

low-frequency intercept gives total resistance. So, the measurement of the diameter of the semicircle provides charge transfer resistance. Other parameters obtained from the Nyquist plot are corrosion rate, corrosion current and capacitance of coating. Using R_{ct} values from Nyquist plots, the corrosion inhibition efficiency of an inhibitor can be determined by the following equation.

$$\eta\,\% = \frac{R'_{ct} - R_{ct}}{R'_{ct}} X100 \qquad (22)$$

where R'_{ct} and R_{ct} are the charge transfer resistance of the working electrode in the presence and absence of inhibitor, respectively.

Potentiodynamic polarization method

Polarization of an electrode results from dispelling the potential of an electrode from its original value at an open circuit. Polarisation leads to the conveyance of current at the electrode surface. This departure from the equilibrium condition leads to a potential difference between polarized and unpolarized electrode potential. That is referred to as overpotential (η)[31]. The degree of polarization can be obtained from the value of over potential η,

$$\eta = E - E_{eq} \qquad (23)$$

Polarization related to the charge transfer mechanism is known as activation polarization. The following equation connects reaction rate and overvoltage for activation polarization,

$$\eta_a = \pm\beta \log \frac{i}{i_0} \qquad (24)$$

where η_a represents overvoltage, β indicates a constant called Tafel constant or "β slope[30]", and i is the current density which explains the rate of oxidation or reduction. This equation is known as the Tafel equation.

Reaction rate in a corrosion process is equivalent to electric current due to the movement of electrons and ions from metal to solution and vice-versa. Potential of the metal also determine the reaction rate. If the potential of metal is more positive, then there is an increase in anodic reaction rate and a decrease in cathodic reaction rate. If the potential of metal is more negative, then the opposite phenomenon takes place on the reaction rate. So, the corrosion process can be monitored using current-potential curves. Polarization curves are current-potential curves under certain polarization conditions. Fig. 1.10a and b show the Tafel plot and linear polarization curve, respectively.

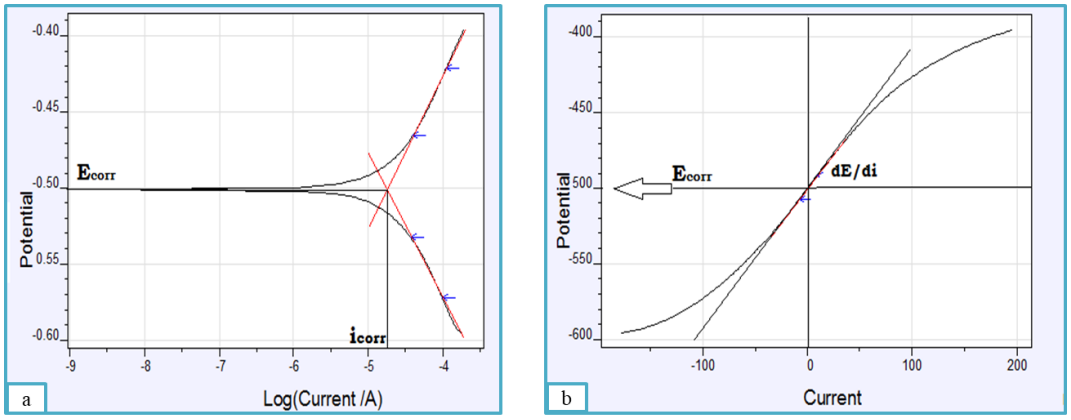

Fig. 1.10 a) Tafel plot b) Linear polarization curve

❖ ***Tafel extrapolation method***

It depends on the mixed potential theory discovered by Wagner and Traud[32]. Information availed from cathodic or anodic polarization measurements are applied in this method. The mixed potential at which anodic and cathodic reaction rates are equal is called open circuit potential (OCP)[33], or corrosion potential E_{corr} and corresponding current is called corrosion current density i_{corr}. Initially, the voltmeter records the corrosion potential of the metal concerning the reference electrode before the conveyance of cathodic current. After cathodic polarization, by applying external potential E (E_{corr}>>E), the applied or measured current density can be expressed similarly to the Butler-Volmer equation[34],

$$i_{app} = i_{corr}\{\exp[-\frac{\alpha_c}{RT} zF\eta]\} \quad (25)$$

where $\eta = E - E_{corr}$, (26)

α_c represents the charge transfer coefficients for cathodic reactions, η is the overpotential, z is the valency of metal, T is the absolute temperature, F and R represent Faraday constant and universal gas constant, respectively.

Tafel slope for cathodic polarization is given by,

$$b_c = \frac{2.303\ RT}{\alpha_c\ zF} \quad (27)$$

If anodic polarization takes place by applying $E>>E_{corr}$, the expression for the applied or measured current density is,

$$i_{app} = i_{corr}\{\exp\left[\frac{\alpha_a}{RT} zF\eta\right]\} \quad (28)$$

where α_a represents the charge transfer coefficients for anodic reactions.

Tafel slope for anodic polarization can be expressed as,

$$b_a = \frac{2.303\ RT}{\alpha_a\ zF} \quad (29)$$

Corrosion current density is different for inhibited and uninhibited corrosive media. Its value is lower in the inhibited medium since the inhibitor decreases the rate of the corrosion process. So, percentage inhibition efficiency can be calculated as,

$$\eta_{pol}\% = \frac{i_{corr} - i'_{corr}}{i_{corr}} X100 \quad (30)$$

where i_{corr} and i'_{corr} are the corrosion current densities in the absence and presence of the inhibitor.

Values of b_a and b_c help to determine the mechanism of inhibitor. If there is a large deviation only in b_a values of the inhibited media from the uninhibited one, it can be said that there is remarkable adsorption of inhibitor molecules on anodic site only. Similarly, the deviations in b_c value correspond to the influence of inhibitor molecules on the cathodic site only. On the other hand, if both b_a and b_c values considerably change, it

causes adsorption of inhibitor molecules on both anodic and cathodic sites, affecting both anodic and cathodic corrosion.

❖ ***Linear polarization method***

When anodic and cathodic reaction rates are equal, the potential acquired for the metal in corrosive solution is known as corrosion potential. After repositioning the corrosion potential E_{corr} of the metal, there will be a polarization resistance R_p which is the slope of the linear polarization curve dE/di. As the polarization resistance increases, corrosion current density i_{corr} lowers and thereby, corrosion rate also decreases. The relationship between i_{corr} and R_p is shown in the following equation[35].

$$i_{corr} = \frac{B}{R_p} \quad (31)$$

where B is a constant.

Polarization curves progressively diverge from the linear relationship on the logarithm of current density after the polarization of the metal is raised over 10 mV. In such cases, the measured potential E and current density 'i' relates to the following equation.

$$E - \eta = i_0 + b\log i \quad (32)$$

where η indicates the overpotential, i_0 represents the exchange current density, and b gives the Tafel slope dE/dlogi of the curve.

Polarization resistance R_p is different for inhibited and uninhibited corrosive media. Its value is higher in the inhibited medium since the inhibitor decreases the rate of the corrosion process. Polarisation resistance can be estimated from slope analysis of linear polarization curves. Using R_p values for inhibited and uninhibited media, percentage of corrosion inhibition efficiency can be calculated as,

$$\eta_{R_p}\% = \frac{R_p' - R_p}{R_p'} X100 \quad (33)$$

where R'_p and R_p are the polarization resistance values in the presence and absence of inhibitor, respectively.

Electrochemical noise measurements

Electrochemical noise (ECN) measurement is mainly used in corrosion inhibition analysis introduced by Iverson[36]. Electrochemical noise denotes current and potential fluctuations. This modern technique is widely accepted in corrosion inhibition analysis because a corroding metal at open circuit potential (E_{OCP}) can create random electrochemical noises since fluctuations are steady-state at the metal-solution interface. So, ECN measurements help to determine metal corrosion at E_{OCP} without any external potential. Random current and potential noise signals derived from corrosion processes can be applied to investigate the corrosion rate. Fig. 1.11a shows the current noise vs time plot. Corrosion mechanism can be evaluated using the pitting index value. Fig. 1.11b shows the pitting index curve. ECN signals can measure either separately or simultaneously. In separate measurements, either potential or current noise is analyzed at a particular time, whereas, in simultaneous measurement, both noise signals are analyzed at the same time. Potential noise can be interpreted from the potential between a working electrode and a zero-noise reference electrode or two similarly working electrodes, whereas current noise can be analyzed from the current between a working electrode and a counter electrode or between two similarly working electrodes in separate measurement. Simultaneous measurement is more advantageous since it employs a three-electrode assembly. Current noise is analyzed between a working electrode and a counter electrode, and potential noise is analyzed between a working electrode and a reference electrode.

There are two methods for ascertaining ECN data. 1) Frequency domain analysis, 2) Time-domain statistical method

❖ ***Frequency domain analysis***

Sum of various sinusoidal signals of relative phase, periodicity and amplitude give the waveform of any complexity. That is the fundamental concept of frequency domain analysis. An illustration of a time depending process is referred to as a spectrum in frequency domain analysis. An important parameter derived from this analysis is the power spectral density (PSD)[37]. Fig. 1.11c shows the PSD plot. It plots the logarithm of spectral power of potential or current Vs logarithm of the frequency. PSD doesn't affect time and signal statistics. Greater amplitude of potential and current noise increased the localized corrosion of metal.

❖ ***Time-domain statistical methods***

ECN data can be rendered as a spectrum in terms of frequency through auto-correlation of the time-domain data[38]. This can be made possible by two mathematical approaches 1) Fast Fourier transform (FFT) and 2) Maximum entropy method (MEM).

Fast Fourier transform

Fast Fourier transform (FFT) method works based on previously existing algorithms. Complex Fourier series can be analyzed using this faster machine calculation method. FFT method adopts discrete Fourier transform properties. FFT analysis is associated with two main problems as leakage and aliasing[39]. Leakage is due to the periodicity of finite time records in Fourier transform outputs. Too slow sampling rate causes aliasing.

Maximum entropy method

Even though Fourier transform is a prominent method among all spectral analysis methods, it is proper for only long record lengths. If the record length is small, then the spectral resolution is weak. In such situations, resolution can be intensified by applying the maximum entropy method proposed by Burg[40]. In this method, the auto-correlation

function gets extrapolated, and the entropy of the probability density function gets maximized. Thus, MEM is a data-dependent and nonlinear method widely operating in science and technology.

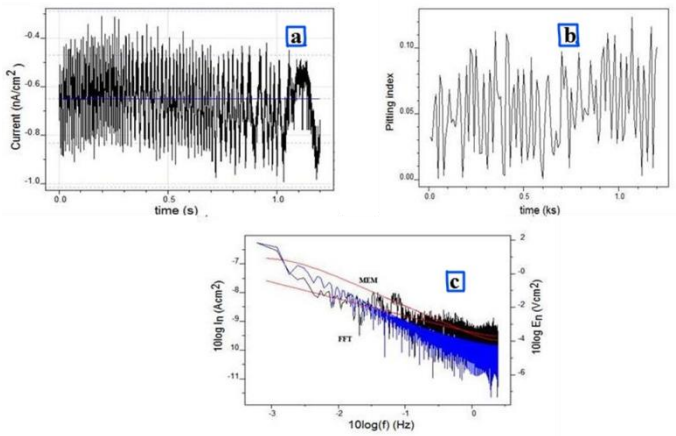

Fig. 1.11: a) Current noise vs time plot b) Pitting index curve c) PSD plot

Adsorption isotherms

Adsorption is the primary phenomenon observed in the inhibition action of inhibitors. Interaction between inhibitor molecules and the metal surface can be explained by adsorption isotherms perfectly[41]. Organic inhibitors affect anodic and/or cathodic corrosion processes after removing water molecules from the metal surface. Displacement of the water molecules and attachment of inhibitor molecules on the metal surface are determined by disturbing cathodic or anodic reactions or both. This can be achieved by developing a diffusion barrier or hindering reaction sites[42, 43, 44]. Different types of adsorption isotherms can demonstrate the properties of inhibitor molecules adsorbed on the metal surface, such as chemical composition, temperature and interfacial electrochemical potential between metal and solution[45].

❖ ***Langmuir adsorption isotherm***

Langmuir adsorption isotherm can be given by,

$$\frac{C}{\theta} = \frac{1}{K_{ads}} + C \qquad (34)$$

where θ is the extent of occupancy of adsorbed sites, C signifies the concentration, and K_{ads} implies the adsorption equilibrium constant.

This model explains the extent of occupancy of adsorbed sites by adsorbed molecules for a certain temperature and pressure of adsorbate[46]. According to Langmuir adsorption isotherm, there are many similar adsorption sites and little chance for lateral interaction.

❖ ***Freundlich adsorption isotherm***

It is commonly used in the determination of multisite adsorption for rough surfaces. The equation can represent it,

$$\theta = K_{ads}\, C \tag{35}$$

It is more suitable for rough surfaces than Langmuir adsorption isotherm[47].

❖ ***Temkin adsorption isotherm***

This model considers indirect adsorbate-adsorbate interactions on adsorption isotherms. It can be expressed as,

$$e^{f\theta} = K_{ads}\, C \tag{36}$$

where f denotes the molecular interaction constant.

❖ ***Frumkin adsorption isotherm***

This model supposes the multilayer adsorption of inhibitor molecules where there is an adsorbate-adsorbent interaction. It can be indicated as,

$$\frac{\theta}{1-\theta}\exp(f\theta) = K_{ads}\, C \tag{37}$$

El-Awady adsorption isotherm

This model can be explained by the equation,

$$\log\frac{\theta}{1-\theta} = \log K + y\log C \tag{38}$$

$$\text{where } K_{ads} = K_{1/y}\,, \tag{39}$$

y denotes the number of active sites. If 1/y<1, then it is multilayer adsorption, whereas if 1/y>1, then it is coverage of adsorbed molecules in more than one active site.

❖ ***Florry-huggin isotherm***

Florry-huggin isotherm is given by the following equation,

$$\log\frac{\theta}{C} = \log K_{ads} + \chi\log(1-\theta) \quad (40)$$

where χ is the polymer-solvent interaction parameter.

Temperature studies

Stability of the protective film of an inhibitor by adsorption on the metal surface can be described by performing temperature studies at elevated temperatures[48]. Various corrosion thermodynamic parameters such as entropy of corrosion (ΔS^*), enthalpy of corrosion (ΔH^*), activation energy for decay (with the electrical charge on the metal surface) and Arrhenius parameter (A) can be investigated by applying Arrhenius equation. Rate of corrosion and activation energy for corrosion is related in Arrhenius equation as,

$$K = A\exp(\frac{-E_a}{RT}) \quad (41)$$

where K represents the rate of corrosion, A is the pre-exponential factor known as Arrhenius parameter, E_a denotes the activation energy for corrosion, R is gas constant, and T is the temperature. When we plot a graph between log K and 1000/T, we get a straight line with a slope $\frac{-E_a}{2.303R}$ and intercept of log A.

Transition state theory helps to obtain ΔS^* and ΔH^* values[49], which is given by the following equations,

$$K = \left(\frac{RT}{Nh}\right)\exp(\frac{\Delta S^*}{R})\exp(\frac{-\Delta H^*}{RT}) \quad (42)$$

where N denotes Avagadro number and h gives Planck's constant.

This equation can be rearranged into logarithmic form as,

$$\log\frac{K}{T} = \log\frac{R}{Nh} + \frac{\Delta S^*}{2.303R} - \frac{\Delta H^*}{2.303RT} \quad (43)$$

When we plot a graph between log K/T and 1/T, we get a straight line with a slope $\frac{-\Delta H^*}{2.303R}$ and intercept of $\log\frac{R}{Nh} + \frac{\Delta S^*}{2.303R}$. From the slope and intercept, we can estimate the enthalpy and entropy of corrosion.

If the rate of corrosion increases as temperature increases, it may conclude that the nature of adsorption by the inhibitor is just physical adsorption. Stability of the adsorbed layer degrades at elevated temperatures. Or it can be said that the rate of desorption increases at elevated temperatures. If the adsorbed layer doesn't affect at higher temperatures, it may be chemisorption. When the activation energy of corrosion increases with inhibitor concentration, it can be said that the energy barrier for corrosion grows as possible[50]. It also emphasizes the existence of a complex compound formed by the interaction between the inhibitor and metal. Positive value of enthalpy of corrosion describes the endothermic character of the metal corrosion process. Negative values of the entropy of activation for corrosion mention a decrease in randomness for the activated complex, compared to the reactants that lead to a high corrosion rate. If the disorderliness of the activated complex increases with inhibitor concentration and ΔS* becomes positive values, it causes the prevention of metal corrosion at high rates.

Scanning electron microscopy (SEM)

Scanning electron microscopy (SEM) is a non-destructive method to examine the surfaces and cross-sections with a resolution at micron and nanometer levels. It is practical to gather facts about surface properties like crystalline nature, chemical composition, electrical behaviour, etc. When a high energy electron beam passes through a sample surface, emerging particles like electrons, X-rays and photons, etc., provide the surface's character. That is the basis of SEM.

SEM is supposed to be a valuable tool for corrosion inhibition studies. SEM image of a metal surface can distinguish between the surface morphology of corroded and non-corroded metals evidently. The mechanism of corrosion inhibition can prove by recording SEM images of metals exposed in the aggressive medium in the presence and absence of inhibitors because inhibitors may form a protective film on the metal surface[51].

Atomic force microscopy (AFM)

AFM is a well-known technique in which the surface topography of a sample can be explored at the microstructure level. So, it is widely employed in corrosion inhibition studies to establish barrier film formation on the metal surface.

AFM measures the force between a sharp probe and a sample surface at a minimum distance by touching the AFM tip on the surface and gives a 3D image of the surface on a nanoscale. The significant interactions between AFM tip and sample surface are van der Waals interactions[52]. Contact mode, tapping mode and non-contact mode are three imaging modes in AFM. Depending on the surface characteristics such as hardness, stickiness etc., the operating mode can be selected. Surface roughness parameters such as average roughness (R_a), root mean square roughness (R_q), and maximum peak-to-peak height (R_{pp}), which specify the topography of surfaces, are available from the AFM technique. Surface roughness parameters for the inhibited metal differ from the bare metal and the metal exposed in the aggressive medium. This reinforces the adsorption of inhibitor molecules on the metal surface in the corrosion reaction.

Quantum mechanical calculations

Quantum mechanical calculations can achieve interactions of compounds at the molecular level. It can simply investigate chemical problems on a computer because quantum mechanical calculations provide information about molecular geometry such as

bond lengths, angles, dihedrals, molecular energies, transition states, and chemical reactivity. Attainment of these problems is through the selection of different methods of computational chemistry. There are five broad classes of computational chemistry methods.

- Molecular mechanics (MM): It is a ball and spring model. Here ball indicates atoms, and spring represents the bond between them. So, a molecule can be considered as a collection of balls connected by springs. We can compute the energy of a given molecule by providing the normal spring lengths and the angles between them and stretching and bending energy. We can also obtain the geometry of a molecule with the least energy, i.e. geometry optimization.
- Molecular dynamics calculations: It is based on the laws of molecular motion. For example, it can predict the movement of an enzyme because it changes shape with respect to the binding substrate. Similarly, the activity of a swarm of water molecules around a solute molecule can be estimated.
- Ab initio calculations: Ab initio is a Latin word that means "from first principles". It is mainly focused on the Schrodinger equation. The energy of a molecule and wave function can be provided from this method by solving the Schrodinger equation for a molecule. The wave function for a molecule gives information about the electron distribution. We can ascertain the polar behaviour and which parts of it are probably affected by nucleophiles or electrophiles.
- Semi-empirical (SE) calculations: It also depends on the Schrodinger equation. However, SE calculations can’t employ in the analysis of highly complicated integrals. Instead, this method benefits from a kind of library of integrals assembled by obtaining the most suitable experimental values for calculated

terms like geometry or energy. It is called "semi-empirical" because it is comprised of theory and experiment.

- Density functional calculations: Density functional theory (DFT) calculations depend on the Schrodinger equation, same as ab initio and SE calculations. But, it estimates electron distribution as a function of electron density directly without using wave function. That is the significant difference in DFT calculations from the other two.

Molecular structure of the inhibitor has a vital role in the determination of corrosion inhibition potency. Corrosion inhibition potency of organic inhibitors has been effectively correlated to molecular orbital (MO) energy levels by employing quantum mechanical calculations[53,54,55]. DFT calculations have been contributed to the calculation of parameters such as energies of HOMO (highest occupied molecular orbital), LUMO (lowest unoccupied molecular orbital), dipole moment (μ) etc., with sufficient accuracy. Mechanism of corrosion resistance can be demonstrated concerning HOMO-LUMO interaction between filled orbitals of inhibitor molecules and vacant orbitals of metal. Lower change in energy value ($\Delta E = E_{LUMO} - E_{HOMO}$) is the benchmark for strong adsorption of inhibitor molecules on the metal surface. Ionization energy, electron affinity, chemical potential, electronegativity, hardness, and the number of transferred electrons are the typically obtained parameters using DFT.

- Ionization energy (I): Negative of the energy value of HOMO gives ionization energy. $I = -E_{HOMO}$ (44)
- Electron affinity (A): Negative of the energy value of LUMO gives electron affinity. $A = -E_{LUMO}$ (45)
- Electronegativity (χ): It can be obtained in terms of orbital energies as,

$$\chi = -\frac{(E_{HOMO}+E_{LUMO})}{2} \quad (46)$$

- Chemical potential (μ): It may express as the negative of the electronegativity. If the species is more electronegative, then energy drop is more, i.e. chemical potential decreases. So,

$$\mu = -\chi \quad (47)$$

- Hardness (η): It measures the reduction in electronegativity when a minute electronic charge is added to it. If the value of the hardness of an inhibitor is smaller, then its inhibition efficiency is high.

$$\eta = \frac{1}{2}(E_{LUMO} - E_{HOMO}) \quad (48)$$

- Number of transferred electrons (ΔN): The number of transferred electrons from the inhibitor molecule to the metal atoms can be calculated as[56],

$$\Delta N = \frac{(\chi_{metal} - \chi_{inhibitor})}{2(\eta_{metal} + \eta_{inhibitor})} \quad (49)$$

Natural organic inhibitors as a tool for metal corrosion inhibition

Plants are made up of phytochemicals. They are producing a large number of chemical constituents at a time. So, it is monotonous to isolate and separate the phytochemicals present in it. However, this difficulty can be overcome using advanced and sophisticated instrumental techniques like HPLC, GCMS etc.

Primary and secondary metabolites are major chemical compounds present in plants. Proteins, nucleic acids, lipids and carbohydrates belong to primary metabolites. Terpenoids, alkaloids and phenolics are the major secondary metabolites that are biosynthesized from primary metabolites. Secondary metabolites have broad applications in human lives, which can act as drugs, stimulants, functional foods, flavours, fragrances, natural insecticides and herbicides[57].

Terpenoids possess pharmacological characteristics like antibacterial, antiviral, anti-inflammatory, anticancer, anti-diabetic, etc. Alkaloids are the first isolated organic compounds from plants, known to be either medicinally beneficial or toxic. Flavonoids

are polyphenols mainly found in the plant kingdom with bright and striking colours. Anthocyanins, flavones, flavonols and their derivatives like isoflavonoids, neoflavonoids belong to the flavonoids family. They are important for human health, such as antioxidant, antibacterial, antiviral etc. They also have wide applications in the food industry.

In recent years, green chemistry has been gaining traction in the research world, owing to a demand for chemical technologies and commercial products that are less toxic and generate less waste. One of the promising domains for applying green chemistry principles is the protection of metals from corrosion. Most industries work in an acidic environment, which causes metal corrosion, leading to metal loss. The best and favourable method to reduce metal degradation is the usage of corrosion inhibitors. Organic compounds with heteroatoms like N, O, S etc., in a conjugated system, have been commonly used as inhibitors and can interact with metal either by chemisorption or physisorption. The adsorptive layer formed on the metal surface protects from the acidic solution and thereby minimizing corrosion. Due to eco-friendliness, low cost, readily available and renewable sources of material, natural products like plant extracts can be used as green corrosion inhibitors. Several plant-based extracts successfully inhibited the corrosion of metals in corrosive environments. These are listed in Table 1.1 and structures of active constituents listed in Table 1.1 are given in Fig. 1.12 and Fig. 1.13.

K. K. Anupama et al. have been studied the effect of corrosion behaviour of methanolic extracts of leaves of *Ruta graveolens* (RGE) in 1 M HCl for mild steel using gravimetric and electrochemical techniques in 2016[48]. RGE exhibited 98% inhibition efficiency at 4 v/v% from EIS studies. Theoretical calculations were also proved with experimental results. Rutin is the active component present in RGE that supported the adsorption mechanism of the extract on the mild steel surface.

Table 1.1: List of natural organic inhibitors with their active constituents, material/medium used and inhibition efficiency (IE%)

Inhibitors	Active constituents	Material/medium	IE%
Ruta graveolens	1) Rutin	Mild steel/1 M HCl	98.00
Tinospora cordifolia	2) Borapetoside F	Low-carbon steel/ 0.5 M H_2SO_4	87.18
Terminalia chebula	3a) Gallic acid 3b) Methyl gallate	Low-carbon steel/ 0.5 M H_2SO_4	94.07
Ficus religiosa	4a) Myricetin 4b) Serotonin 4c) Campesterol	Mild steel/ 0.5 M H_2SO_4	92.26
Asparagus racemosus	5) Sarsasapogenin	Mild steel/0.5 M H_2SO_4	93.25
Achyranthes aspera	6) Oleanolic acid	Mild steel/0.5 M H_2SO_4	90.79
Aloe vera	7a) Anthraquinone 7b) p-Coumaric acid 7c) Calleic acid 7d) Ferulic acid	Mild steel/0.5 M H_2SO_4 Stainless Steel/0.5 M H_2SO_4	88.90 99.10
Cinnamomum verum	8) Eugenol	Mild steel/1 M HCl Mild steel/0.5 M H_2SO_4	99.00 96.55
Chlorophytum borivlianum	9) Saponins	Mild steel/1 M HCl Mild steel/ 0.5 M H_2SO_4	90.00 83.00
Punica grantum	10a) Pelargonidin 10b) Pelletierine 10c) Gallic acid 10d) Ellargic acid	Mild steel/1 M HCl Mild steel/0.5 M H_2SO_4	80.60 91.00
Allium sativum	11) Allicin	Mild steel/well water	90.00
Geissospermum laeve	12) Geissospermine	C38 steel/1 M HCl	92.00
Lemongrass extract	13a) Neral 13b) Geranial 13c) β- myrcene 13d) Nerol	Carbon steel/produced oilfield water	58.19
Strychnos nuxvomica, *Piper longum* and *Mucuna pruriens*	14a) Brucine 14b) Piperine 14c) L-DOPA	Copper/3 M HNO_3	91.60 80.00 71.60
olive leaves	15a) Hydroxylyrosol 15b) Oleuropein	Carbon steel/2 M HCl	93.00
Rice hulls	16) β-Sitosterol	Mild steel/1 M H_2SO_4	95.00
Saraca ashoka	17) Epicatechin	Mild steel/0.5 M H_2SO_4	95.48
Musa paradisica	18) Gallocatechin	Mild steel/1 M HCl	89.00
Fennel essential oil	19a) Limonene 19b) β-Pinene	Carbon steel/1 M HCl	77.00
Cinnamon essential oil	20a) E-Cinnamaldehyde 20b) δ – Cadinene 20c) β- Cubebene	Copper/0.5 M H_2SO_4	87.24

In 2020, Akhil Saxena and coworkers investigated that ethanol extracts of fruits of *Tinospora cordifolia* showed 87.18% effectiveness at 500 mg/L inhibitor concentration using potentiodynamic polarization studies[58]. Weight loss, EIS studies, SEM and AFM analyses were also supported for their corrosion effectiveness. Borapetoside F is the chief component that leads to adsorption on the metal surface following the Langmuir adsorption isotherm. In 2019, inhibiting power of ethanol extracts of seeds of *Terminalia chebula* has been studied by Akhil Saxena et al. using electrochemical and surface morphological studies[59]. It exhibited 94.07% inhibition potency at 500 mg/L inhibitor concentration in 0.5 M H_2SO_4 for low-carbon steel from potentiodynamic polarization studies. DFT calculations based on the active constituents, gallic acid and methyl gallate, were observed with experimental results.

In 2018, Rajesh Haldhar and coworkers reported that ethanol extracts of the fruits of *Ficus religiosa* showed an extreme inhibition efficiency of 92.26% at 500 mg/L in 0.5 M H_2SO_4 for mild steel using electrochemical and gravimetric estimations[60]. The major components present in the extract are myricetin, serotonin, and campesterol, which cause adsorption film on the metal surface, thereby decreasing the corrosion rate. Akhil Saxena et al. suggested that ethanol extract of fruits of *Achyranthes aspera* exhibited 90.79% protecting power at 500 mg/L in 0.5 M H_2SO_4 for mild steel using potentiodynamic polarization studies in 2018[61]. They investigated that the adsorption behaviour of oleanolic acid, an active component present in the extract, cause a decrease in corrosion rate. Inhibition effect of colourless liquid extract from aloe vera in 0.5 M H_2SO_4 for mild steel and stainless steel was reported by A. A. Ayoola et al. in 2020[62]. It revealed that aloe vera extract showed a maximum protection capacity of 88.9% for mild steel and 99.1% for stainless steel at 10 v/v%. In 2018, K. K. Anupama et al. reported that ethanol extract of leaves of *Cinnamomum verum* exhibited a maximum inhibition power of

99.73% in 1 M HCl and 96.55% in 0.5 M H_2SO_4 using potentiodynamic polarization studies[63].

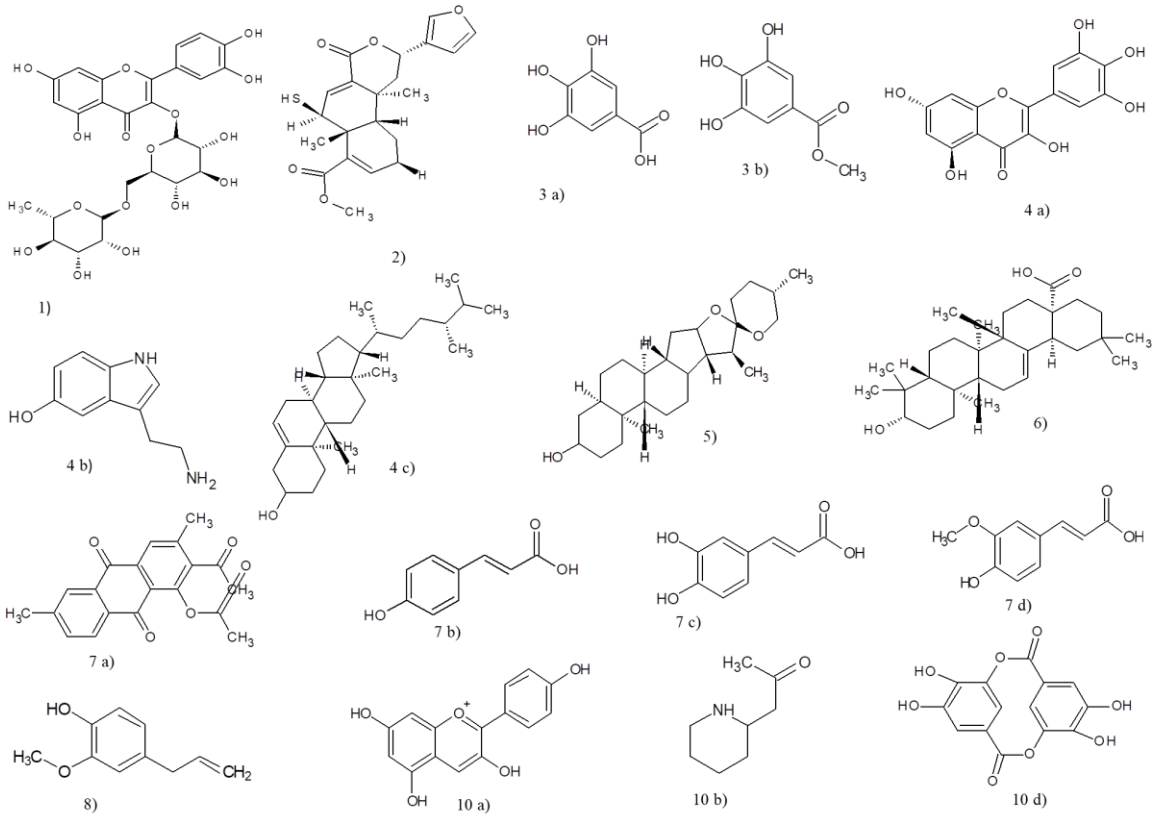

Fig. 1.12: Structures of active constituents of natural organic corrosion inhibitors (1-10)

In 2013, Gopalji et al. suggested that aqueous extracts of roots of *Chlorophytum borivlianum* showed an extreme inhibition effect of 90% and 83% in 1 M HCl and 0.5 M H_2SO_4 respectively in weight loss measurements[64]. In 2012, Maduabuchi A. Chidiebere et al. showed that ethanol extract of seeds of *Punica grantum* exhibited a maximum inhibition potency of 80.6% and 91% in 1 M HCl and 0.5 M H_2SO_4, respectively, using EIS studies[65]. In 2018, N. Karthiga and coworkers reported that aqueous extract of garlic exhibited 90% inhibition efficiency in well water for mild steel in weight loss measurements[66]. Inhibition ability of alkaloid extract of *Geissospermum laeve* in 1 M HCl with 100 mg/L for C38 steel was investigated by M. Faustin et al. in 2014[67]. It exhibited 92% inhibition power from weight loss measurements. In 2017, M. A. Deyab et al. suggested that water extract of lemongrass showed 58.19% protection power with

400 ppm concentration in produced oilfield water for carbon steel from weight loss measurements[68]. It was also supported by EIS studies, potentiodynamic studies and quantum chemical calculations. Savita and coworkers discovered that *Strychnos nuxvomica, Piper longum and Mucuna pruriens* seed extracts could act as a green inhibitor in 3 M HNO_3 for copper with the maximum corrosion resistance 91.60%, 80% and 71.6% respectively at 0.2 g/L from weight loss measurements in 2016[69].

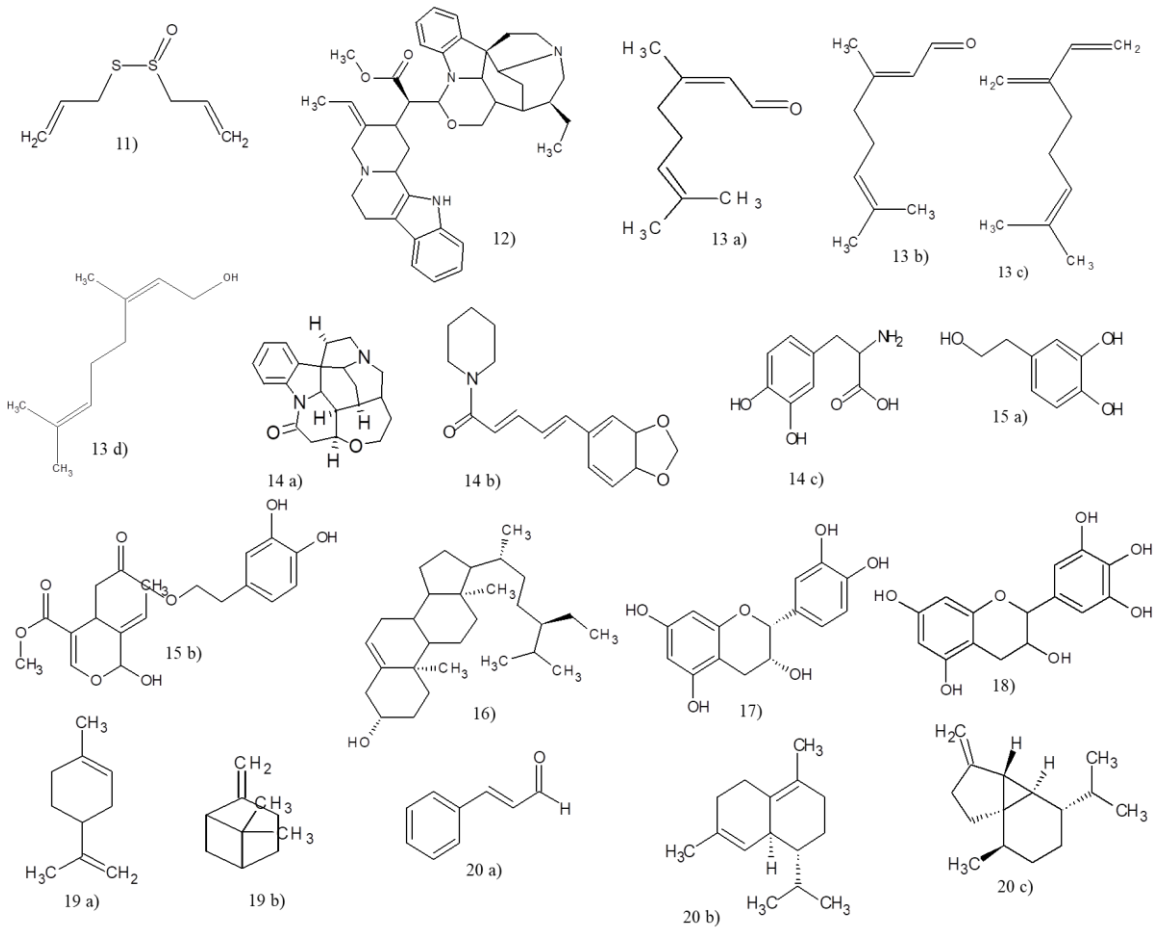

Fig. 1.13: Structures of active constituents of natural organic corrosion inhibitors (11-20)

A.Y. El-Etre has been conducted polarization techniques to evaluate the inhibiting capacity of aqueous extract of olive leaves. It exhibited an extreme corrosion inhibition efficacy of 93% in 2 M HCl for mild steel with 900 ppm inhibitor concentration in 2007[70]. In 2017, Mayakrishnan Prabakaran et al. reported that β-Sitosterol isolated from rice hulls revealed an extreme inhibition capacity of 95% in 1 M

H_2SO_4 for mild steel with 500 ppm inhibitor concentration from weight loss measurements[71]. In 2018, Akhil saxena and coworkers reported that ethanol extract of seeds of *Saraka ashoka* showed the best inhibition power of 95.48% at 100 mg/L inhibitor concentration in 0.5 M H_2SO_4 for mild steel from polarization measurements[72]. Gopal Ji et al. suggested that raw banana peel extract is a good green corrosion inhibitor with 89% protecting power in 1 M HCl for mild steel at 300 mg/L inhibitor concentration from EIS studies in 2014[73].

Performance of fennel essential oil as a corrosion inhibitor in 1 M HCl for carbon steel with 77% corrosion resistance power at 3 mL/L was studied by N. Lahhit et al. in 2011 using polarization studies[74]. In 2017, K. Dahmani et al. reported that cinnamon essential oil has 87.24% corrosion inhibition potency in 0.5 M H_2SO_4 for copper at 150 ppm inhibitor concentration from EIS calculations[75].

Synthetic organic inhibitors as a tool for metal corrosion inhibition

Acid cleaning, oil and gas industries tremendously utilize synthetic organic inhibitors for inhibiting corrosion of metals, especially for iron and its alloys, like mild steel and carbon steel. This metal passivation is mainly through the phenomenon of adsorption. Adsorption film formed by organic inhibitors is more uniform and covered than those created by inorganic inhibitors. So, inorganic inhibitors cause localized corrosion on the metal surface. The most commonly observed organic inhibitors are heterocyclic compounds that possess heteroatoms such as sulfur, phosphorus, nitrogen and oxygen. The lone pair of electrons present in these heteroatoms involve in the adsorption mechanism. Table 1.2 shows some of the synthetic organic inhibitors used for metal corrosion, and Fig. 1.14 exhibits the structures of these synthetic organic inhibitors.

Table 1.2: List of synthetic organic corrosion inhibitors

Authors	Synthetic organic inhibitor
A.M. Fekry et al.	1a) 4-(4-methoxyphenyl)-6-(yridine-3-yl)-1H-pyrazolo[3,4-b]42yridine-3-amine
	1b) 4-phenyl-6-(42yridine-3-yl)-1H-pyrazolo [3,4- b]42yridine-3-amine
	1c) 6-(42yridine-3-yl)-4-(thiophen-2-yl)-1H-pyrazolo[3,4-b]42yridine-3-amine
	1d) 4-(furan-2-yl)-6-(42yridine-3-yl)-1H-pyrazolo[3,4-b]42yridine-3-amine
Sutter et al.	2a) Benzotriazole
	2b) Mercaptobenzimidazole
	2c) Mercaptobenzoxazole
	2d) Mercaptobenzothiazole
Gurmeet Singh et al.	3) 4,6-dihydroxypyrimidine
Ezhilarasi et al.	4) 1-acetyl-4,5-dihydro-5-phenyl-3-(thiophen- 2yl) pyrazole
Dr. Mushtaq J. Meften	5) 6,12,14-trithia-1,4,8,10-tetraaza-tricyclo [9.4.0.03,9] pentadeca-3(9),10-dien-2-one
A. S. Fouda et al.	6a) 2-styrylbenzo[d] oxazole
	6b) 4-(€-2-(benzo[d] oxazol-2-yl)vinyl)-N,N-dimethyl benzenamine
	6c) 4-(€-2-(benzo[d]thiazol-2-yl)vinyl)-N,N-dimethyl benzenamine
J. Aljourani et al.	7a) Benzimidazole
	7b) 2-methylbenzimidazole
	7c) 2-mercaptobenzimidazole

A. M. Fekry et al. have been investigated the inhibiting capacity of some newly synthesized aromatic heterocyclic inhibitors for mild steel in 1 M H_2SO_4 using hydrogen evolution reaction and electrochemical techniques[76]. Sutter and coworkers have been studied the effect of four different aromatic heterocyclic inhibitors for copper corrosion, and they are characterized through their C^{13} and H^1 NMR spectroscopy methods[77]. Applicability of dihydroxypyrimidine as a corrosion inhibitor for mild steel in 1 N phosphoric acid has been recorded by Gurmeet Singh and coworkers[78]. They observed the adsorption behaviour of inhibitors at different temperatures using electrochemical studies. All the inhibitors mentioned above are aromatic amine derivatives that develop

an adsorption film on the metal surface by coordinating their non-bonding and π-electrons with vacant d-orbital of the metal surface.

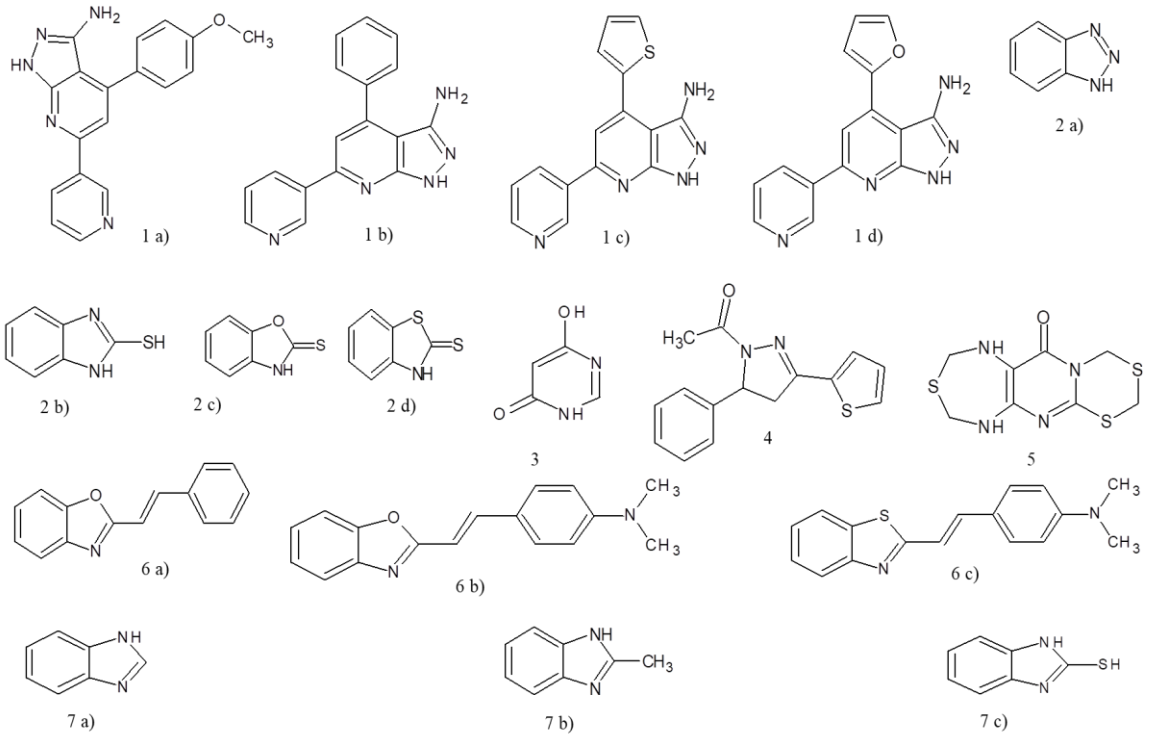

Fig. 1.14: Structures of synthetic organic corrosion inhibitors

Ezhilarasi et al. reported the effect of corrosion inhibition properties of a pyrazole based ionic liquid in 1 M HCl and 1 M H_2SO_4 on mild steel using weight loss and electrochemical techniques[79]. The structure of the inhibitor was characterized by FTIR, ^{1}H NMR and ^{13}C NMR. Dr Mushtaq J. Meften synthesized a new heterocyclic compound and characterized it by liquid chromatography, LC-MS, ^{1}H NMR and ^{13}C NMR[80]. He verified the applicability of the synthesized inhibitor as an anti-corrosive agent in 15% HCl on C38 carbon steel using the gravimetric method, gasometrical method, EIS, and X-ray diffraction (XRD) spectroscopy. Corrosion inhibition efficiency of three heterocyclic compounds for carbon steel in 1 M HCl has been analyzed by A.S. Fouda et al. using various physicochemical and electrochemical techniques[81]. J. Aljourani and coworkers have been studied the inhibition efficacy of some benzimidazole derivatives on carbon steel in 1 N HCl and 1 N H_2SO_4 using adsorption

and electrochemical studies[82]. They also verified the synergistic effect of halide ions on inhibition efficiency when it adds with inhibitors.

Schiff bases as a tool for metal corrosion inhibition

Schiff bases accounted for their high inhibition efficiency among various synthetic organic inhibitors due to their electronic and structural properties. They can coordinate with the metal surface through π-electrons from double bonds and lone pairs of electrons from nitrogen. Many researchers reported that different types of Schiff base compounds could apply in corrosion inhibition processes. Table 1.3 shows some of the Schiff bases used as inhibitors for metal corrosion in acidic media and Fig. 1.15 exhibits and their structures.

Shaju K. S et al. have been investigated the effect of corrosion resistance offered by a polynuclear Schiff base compound in 0.5 M H_2SO_4 on mild steel employing weight loss measurements, EIS and potentiodynamic polarization studies[83]. They also pointed out that the efficiency was enhanced by adding potassium iodide with inhibitor, and adsorption studies proved it. Nimmy Kuriakose and coworkers have been studied the corrosion inhibition behaviour of a Schiff base derived from the condensation reaction between thiophene-2-carbaldehyde and tryptophan in 1 M HCl for mild steel corrosion using gravimetric and electrochemical methods[84]. Synthesis of some novel Schiff base compounds and anti-corrosive behaviour of those inhibitors in 1 M HCl on mild steel has been conducted experimentally and theoretically by Hany M. Abd El-Lateef et al.[85]

Aby Paul and coworkers discovered that a Schiff base derived from 3-Formylindole and 4-aminobenzoic acid has potential for corrosion inhibition in 1 M HCl on mild steel and copper by employing weight loss measurements, EIS and potentiodynamic polarization studies[86]. Adsorption mechanism of the synthesised inhibitor was proved by calculating thermodynamic parameters.

Table 1.3: List of Schiff base corrosion inhibitors

Authors	Schiff base
Shaju K. S et al.	1) Anthracene-9(10H)-one-3-aminopropanoic acid
Nimmy Kuriakose et al.	2) Thiophene-2-carbaldehyde tryptophan
Hany M.Abd El-Lateef et al.	3a) Sodium 3-[{[1-carboxy-3-(methylthio)propyl] imino}methyl]-4-hydroxybenzenesulfonate 3b) Sodium 3-{[(1-carboxy-2-phenylethyl) imino]methyl}-4-hydroxybenzenesulfonate
Aby Paul et al.	4) 3-formylindole-4-aminobenzoic acid
Yue Meng et al.	5a) 3-pyridine carboxaldehyde-4-phenyl thiosemicarbazide 5b) 4-pyridine carboxaldehyde-4-phenyl thiosemicarbazide
Parul Doharea et al.	6a) N^2,N^6-bis(4-ethylbenzylidene)pyridine-2,6-diamine 6b) N^2,N^6-dibenzylidenepyridine-2,6-diamine 6c) N^2,N^6-bis(4-nitrobenzylidene)pyridine-2,6-diamin
Sam John et al.	7a) Anisoin-N(4)-methyl(phenyl)thiosemicarbazone 7b) Furoin-N(4)-methyl(phenyl)thiosemicarbazone
A. Yurt et al.	8a) 2-((1E)-2-aza-2-pyrimidine-2-ylvinyl) thiophene 8b) 2-((1Z)-1-aza-2-(2-pyridyl)vinyl) pyrimidine 8c) 2-((1E)-2-aza-2-(1,3-thiazol-2-yl)vinyl) thiophene 8d) 2-((1Z)-1-aza-2-(2-thienyl)vinyl) benzothiazole
M. G. Hosseini et al.	9a) N,N-ethylen-bis(salicylidenimine) 9b) N,N-isopropylien-bis(salicylidenimine) 9c) N-acetylacetone imine N-(2-hydroxybenzophenone imine)ortho-Phenylen
C. Sini Varghese et al.	10a) 2-pyridine carbaldehyde oxime 10b) 3-pyridine carbaldehyde oxime

Yue Meng et al. synthesized two novel pyridine Schiff base derivatives[87]. They accounted for the corrosion inhibition property of the synthesized compound in 1 M HCl on mild steel, including experimental and theoretical studies. SEM and X-ray photoelectron spectroscopy analyses were employed to justify the formation of adsorption film on the mild steel surface. Synthesis, characterization and corrosion inhibition studies of three pyridine-based Schiff bases in 1 M HCl for mild steel has been

carried out by Parul Dohare et al., incorporating electrochemical and theoretical studies[88]. DFT calculations and Monte Carlo simulations were conducted to correlate metal-inhibitor interaction. Sam John and coworkers have been investigated the corrosion inhibition ability of two N(4)-substituted thiosemicarbazone compounds in 1 M HCl for mild steel using weight loss, electrochemical and surface morphological studies[89]. The mechanism of interaction between the inhibitor and mild steel was further justified by molecular dynamic simulations. Potentiodynamic polarization and ac impedance techniques have been conducted to evaluate the inhibition efficiency of some Schiff bases in 1 M HCl on carbon steel by A. Yurt et al.[90] Polarisation studies were revealed that examined Schiff bases could act as an anodic inhibitor.

M. G. Hosseini et al. have been investigated the effect of protecting power of three new Schiff bases in 0.5 M H_2SO_4 for mild steel using EIS and Tafel polarization studies[91]. Thermodynamic calculations were proved that the nature of adsorption was physisorption. Electrochemical and gravimetric evaluations on anti-corrosive properties of pyridine-carbaldehyde derivatives in 1 M HCl on carbon steel were carried out by C. Sini Varghese et al[92]. Mechanism of adsorption was determined by calculating thermodynamic parameters.

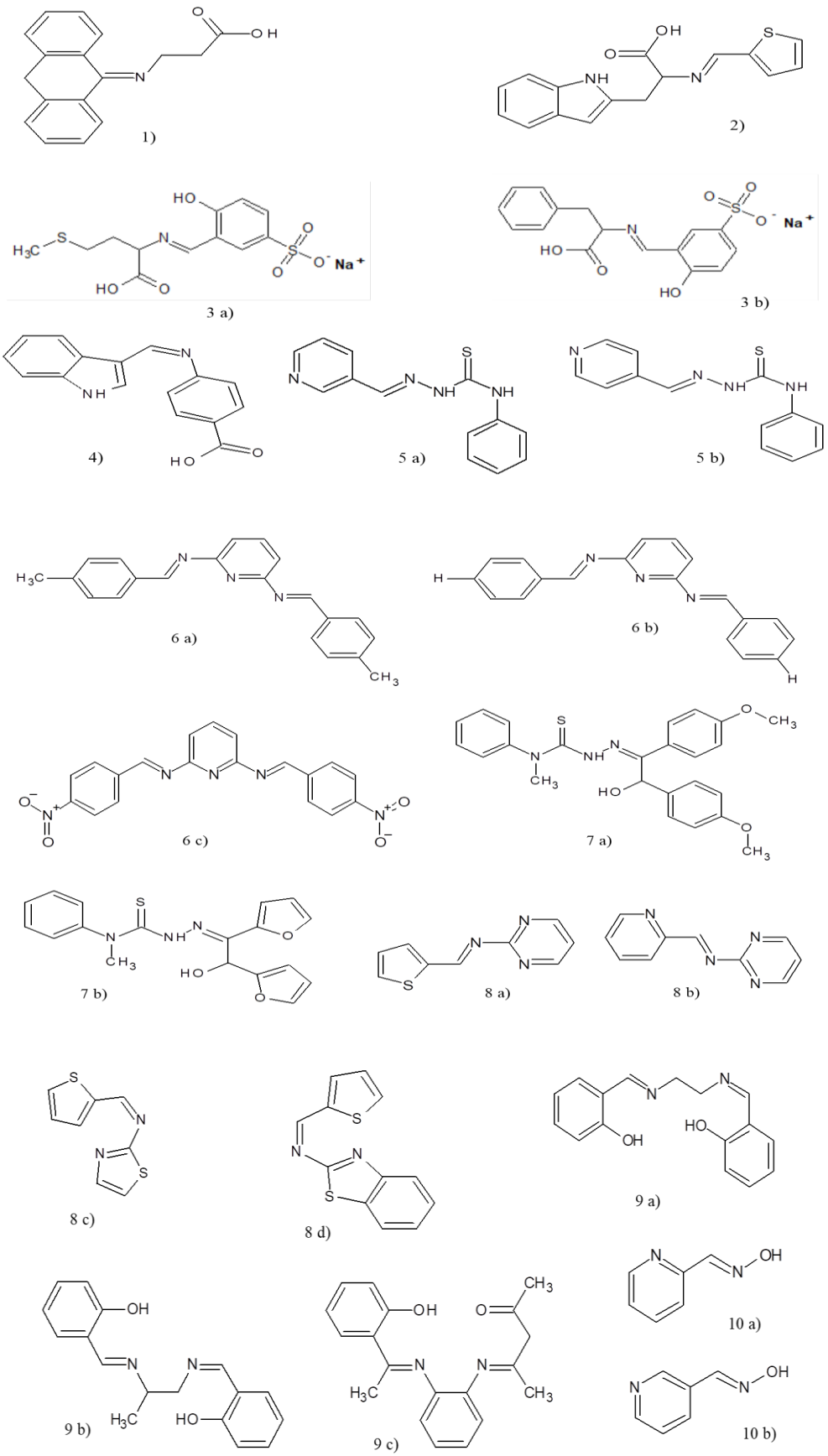

Fig. 1.15: Structures of Schiff base corrosion inhibitors

Schiff bases as a tool for microbial induced corrosion inhibition

Microbial induced corrosion (MIC) is the destruction of a metal by the activity of living organisms either directly by enhancing the electrochemical reactions or indirectly because of their metabolic products. Various environments such as soil, natural waters, seawater, natural petroleum products and oil emulsion cutting fluids encounter the difficulties of corrosion by such biological activity. It is surprisingly high in the contribution of microbial corrosion loss towards total corrosion loss. MIC is termed for corrosion by the occupancy and activities of microbes within biofilms at metal surfaces[93]. The term 'biofilm' was introduced in 1978[94]. By definition, it is a "matrix-enclosed bacterial populations" attached to one another or surfaces. Biofilms are a vital part of the destruction process in MIC. Biofilms are formed by creating extracellular polymeric substances (EPS) such as lipids, polysaccharides, nucleic acids, and proteins[95]. The proximity of biofilms to metal surfaces generates an electrochemical disturbance that allows electron transfer at the anode. Locales at which microbes set apart the metal is mentioned as an anode. The cathodic sites are places of oxygen availability at which corrosion could occur. So, it is difficult to deal with biofilm in mechanical systems.

MIC applies to metals and non-metallic surfaces such as concrete and causes drastic industry losses. MIC has attracted much research interest and attention from researchers and engineers in the last few years, especially with developing new and sophisticated surface morphological and electrochemical techniques that can determine the influence of microorganisms on electrochemical reactions and corrosion chemistry.

Most of the microorganisms causing microbial corrosion are chemotrophs that use chemicals as an energy source[96]. They are as follows:

- Sulphate reducing bacteria (SRB)
- Sulphur oxidizing bacteria (SOB)

- Iron oxidizing/depositing bacteria (IB)
- Manganese oxidizing/depositing bacteria (MnB)

Micro-organisms operate in different ways:

- By generating sludge and deposits which causes crevice corrosion;
- By developing corrosive environments through their metabolic products, or by demolishing corrosion inhibitors;
- By quickest interaction with the corrosion reactions.

Some of the aerobic bacteria like the sulphur oxidisers and the iron bacteria are capable of producing aggressive corrosion environments. For example, the sulphur oxidisers mainly observed in metalliferous mines, oil fields etc., can oxidise elemental sulphur or sulphur containing compounds to H_2SO_4[97]. They proliferate in acidic environments and can generate deposits of sulphuric acid concentrations up to 5 wt%. The sulphur-oxidising bacteria (SOB) cause a mass loss in metals, alloys and even in non-metals, even though the mechanism of corrosion is just acid attack. *Thiobacillus ferrooxidans* is SOB, can form sulfuric acid utilizing sulfur or sulphide.

Another class of aerobic bacteria is the iron bacteria which are mainly found in soil waters and supply waters oxidise ferrous iron to ferric hydroxide precipitates. They tend to develop tubercles on the steel surface of supply pipes. It may cause crevice corrosion in steel pipes. It also made a suitable habitat for the anaerobic bacteria. Iron bacteria can oxidize and/or deposit iron oxides extracellularly or intracellularly[98]. Iron bacteria derive energy from Fe(II) oxidation process with Fe(III). *Pseudomicrobium sp.* and *Gallionella sp*. are fundamental species that belong to iron-oxidizing bacteria. These species can oxidize Mn^{2+} to Mn^{3+} also. Iron reducing bacteria causes depolarization of mild steel surface by modifying the protective oxide film on it.

Another class of bacteria are acid-producing bacteria (APB) which creates the most harmful metabolites, i.e., acids. For example, acetic and butyric acids. APB can readily be confined under the biofilms and generate acids leads to under film corrosion[99]. One of the acetic acid-producing bacteria, *Acetobacter aceti*, facilitated the corrosion process by destroying a protective calcareous film formed due to cathodic polarization. Similarly, *Thiobacillus* can produce sulfuric acid that is hugely corrosive. There are three ways to enhance corrosion for the produced acids:

(1) Prone to more cathodic reactants.

(2) Coordination with metal ions.

(3) Eradicating the passive film and obstructing the passivation.

Sulphate-reducing bacteria (SRB) are a group of anaerobic bacteria that reduce dissolved sulphate to sulphide by ingesting hydrogen and bringing about corrosion to steel frameworks[100]. They can double the effect of metal corrosion. The corrosion rate is stimulated through the cathodic reaction of the corrosion couple, which is achieved via a better mechanism of elimination of hydrogen from the metal surface. Or the corrosion process can also be enhanced from the sulphide layers created from their metabolic products. SRB can be considered the predominant supporter of MIC due to their metabolic activity to provide H_2S. Mechanism of anaerobic bacterial corrosion is as follows:

Anodic reaction: $4Fe \rightarrow 4Fe^{2+} + 8e^{-}$

Dissociation of water: $8H_2O \rightarrow 8H^{+} + OH^{-}$

Cathodic reaction: $8H^{+} + 8e^{-} \rightarrow 8H$

Cathodic depolarization: $SO_4^{2-} + 8H \rightarrow S^{2-} + 4H_2O$

$Fe^{2+} + S^{2-} \rightarrow FeS$

Corrosion products: $3Fe^{2+} + 6OH^{-} \rightarrow 3Fe(OH)_2$

Overall reaction: $4Fe + SO_4^{2-} + 4H_2O \rightarrow 3Fe(OH)_2 + FeS + 2OH^-$

Based on the nature of the soil, sulphate-reducing and sulphur-oxidising bacteria can take effect periodically. Rainy season enhances the multiplication of sulphate-reducing bacteria where the soil is moistened and doesn't expose it to air circulation. In contrast, dry season prospers the growth of sulphur oxidisers by oxidising the sulphide compounds produced in metabolism to sulphuric acid. It leads to the immense destruction of buried metal structures.

Manganese oxidizing bacteria can catalyze Mn(II) oxidation to MnO. It resulted in the growth of visible and easily noticeable extracellular deposits of insoluble manganese oxides[101]. Various organisms tend to catalyse manganese oxidation, such as bacteria, fungi, algae and even eukaryotes. Two Mn(II) oxidation mechanisms by bacteria are 1) indirect and 2) direct. There are free radicals for hydrogen peroxide, superoxide, and OH radicals in the indirect method. In the direct method, Mn(II) oxidation is made possible by Mn-binding compounds like proteins, cell wall compounds and Mn oxidizing enzymes.

Slime-forming bacteria belong to either aerobic or anaerobic. They lead to creating differential aeration cells and capsules on the biofilm surface. The slime capsules can protect the biomass formed inner side from the application of antimicrobial compounds.

Microorganisms enhance metal corrosion by interfering at the interface between the metal and the electrolyte. They are exposed to the atmosphere by attaching themselves to metal surfaces, then colonizing, multiplying, and forming a biofilm. Biofilm contains metabolites of microbes and their extracellular polymeric substance (EPS). Biofilm formation leads to change in pH, dissolved oxygen, nutrient contents, temperature, and pressure, which cause the MIC of metals and alloys. 20%–25% of the

overall financial loss of corrosion was due to MIC. MIC is fundamentally an electrochemical phenomenon, the same as other types of corrosion. All structural materials associated with the water and soil are possible to suffer from MIC. Among these factors, water is essential for the life of microorganisms, and hence, water is predominant to occur MIC. Mainly, it has been explained that microbes in any condition, such as temperature, salinity, nutrients, etc., cause localized corrosion.

MIC inhibition strategies

According to the types of apparatus and proper maintenance required, MIC mitigation has different strategies (Fig.1.16).

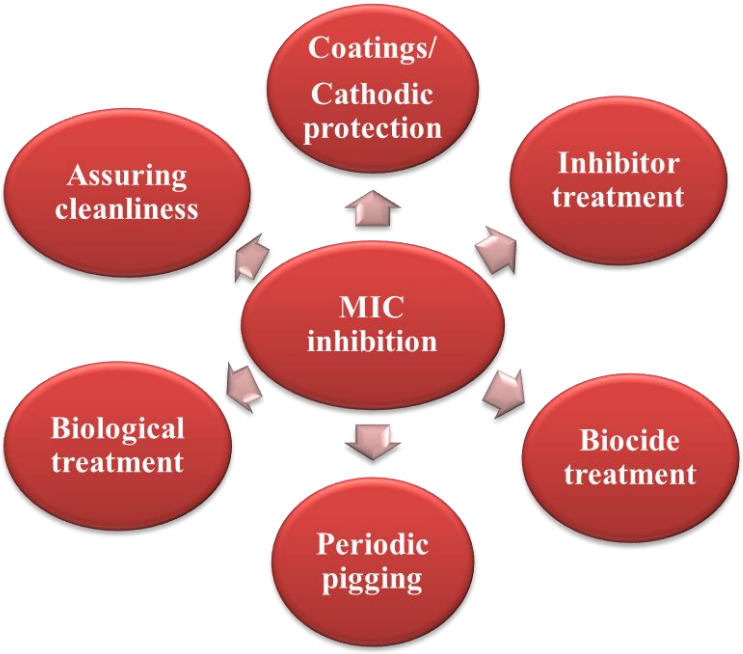

Fig. 1.16: Schematic representation of MIC inhibition strategies

❖ ***Periodic pigging***

It is a mechanical strategy used in oil and gas pipelines to mitigate MIC. Usually, in pipelines, a mechanical pig carrying compact plastic plates is applied to empty garbage from the inner parts of the pipe prior to injection of biocide. This mitigating strategy removes bits of biofilm and maintains solid particles, encouraging the immediate

activity of biocides[102,103]. Pigging is a non-harmful method for the review and washing of pipelines. But, it is not an excellent strategy to inhibit MIC.

❖ ***Cleanliness***

An immaculate operational state that does not enter solids, oxygen, waste, polluted waters etc., Compatible throw out of solid waste, washing, and drying are various processes involved in this method. It is a simple technique to preclude or at least control internal pollution.

❖ ***Cathodic protection and coatings***

It is mainly the least laborious, economically sound, and most effective MIC inhibition method for vessels and tanks. In underground pipelines, removal of covering is the root cause of corrosion in this area. Polymeric compounds are the chief constituents of industrial coatings[104]. Polystyrene and epoxy resin are highly stable industrial coatings towards microbial attack. Coatings are able to defend aggressive synthetic compounds, which are produced by some acid-producing bacteria that may cause corrosion.

❖ ***Biological treatment***

It is the most advanced method for inhibiting MIC, i.e. applying particular bacteria to inhibit the growth of the bacteria which cause MIC. Nitrate reducing bacteria are used to fight against SRB, which creates corrosion.

❖ ***Biocides/Inhibitors***

Corrosion inhibitors are chemicals used to considerably decrease the overall corrosion rate by affecting anodic, cathodic, or both types of reactions. In terms of MIC, these chemicals are known as “biocides”, which means spoiler of living organisms responsible for MIC. Biocides are a standard chemical method applied as a MIC mitigation solution, especially in oil and gas industries[105]. The biocides may be single or

a group of two or more compounds employed to kill microorganisms or destroy microbial growth. Feasibility of a biocide depends on the properties of microbes to be destroyed and the operating conditions of the material structures. So, it is instructed to do *in vitro* experiment to determine the exact dosages of the biocides suitable for the material systems prior to direct application. The authoritative criteria for a reliable industrial biocide are:

(i) Selective toward microbes to be killed.

(ii) Effective with and without all other compounds present in the working system.

(iii) Cheap.

(iv) Retard corrosion.

(v) Biodegradability.

Biocides interfere with the bacterial existence in order to prevent biofilm formation on the metal surface. So, this method is successful in controlling sulphate reducers. Biocides can be classified into two categories: oxidizing biocides and non-oxidizing biocides[106]. Freshwater systems are the favoured system for oxidizing biocides. Chlorine, bromine and chlorine-containing compounds such as bleach and chlorine dioxide are commonly oxidizing biocides, producing an affordable biocide hypochlorous acid. Hypochlorite is another oxidizing biocide used for drinking water and in oil field waters. Oxidizing biocide is more reactive than non-oxidizing biocides[107].

Non-oxidizing biocides are synthetic molecules that can be employed in various operating systems. They are appreciably financially beneficial in structural materials having reduced hydrocarbon contents[108]. Table 1.4 summarizes some of the non-oxidizing inhibitors.

Table 1.4: Some of the non-oxidizing inhibitors with their advantages and disadvantages

Non-oxidizing inhibitor	Advantages	Disadvantages
Formaldehyde	▪ Financially sound	▪ Carcinogenic ▪ Required large amounts
Glutaraldehye	▪ Relatively not sensitive to sulphide	▪ Demobilization by amines and oxygen
Quaternary amine compounds	▪ Broad activity ▪ Constancy ▪ Inertness towards other substances	▪ Delayed action ▪ Foaming
Carbamates	▪ Effective against SRB	▪ Required large amounts ▪ React with metal ions
Metronidazole	▪ Active against SRB ▪ Unresponsive to various substances	▪ Unique for anaerobic microorganisms
Isothiazolone	▪ Broad activity ▪ Degradable	▪ Highly expensive ▪ Not applicable to sour medium

Hsu et al.[109] investigated the antimicrobial activity, and corrosion mitigation power of a non-poisonous biocide, called benzyldimethyldodecylammonium chloride (BDMDAC), against 304 stainless steel corrosion dipped in a *Desulfovibrio desulfuricans* inoculated solution. Environmental rules and regulations about safety concerns on the application of biocides forced to synthesize environmentally-friendly biocides. This compound proved to be a green microbial corrosion inhibitor. Table 1.5 exhibits some of the recently reported synthetic MIC inhibitors.

Wang J. et al.[110] reported that sodium pyrithione functioned as a microbial corrosion inhibitor on carbon steel using weight loss, electrochemical and molecular modelling. Planktonic and sessile SRB were target microbes, and 80% inhibition efficiency was reported. Shaban S. M. et al.[111] studied the MIC inhibition behaviour of alginates polymeric cationic surfactants on mild steel in 1 M HCl by G (+ve) and G (-ve) bacteria and fungi using spectroscopic tools like FTIR and ^{1}H NMR, physicochemical,

electrochemical and surface morphological studies. They found that these inhibitors behaved as a mixed-type inhibitors.

Table 1.5: Recently reported biocides for inhibiting MIC

Sl. No.	Metal/Medium/Bacteria	Biocide/Inhibitor
1	Planktonic and sessile SRB on X80 carbon steel	Sodium pyrithione
2	Mild steel in 1 M HCl by G (+ve) and G (-ve) bacteria and fungi	Alginates polymeric cationic surfactants
3	SRB	*Polyalhia longifolia* plant
4	Mixed SRBs culture	ZnO-interlinked chitosan nanoparticles
5	Sulfate-reducing microorganisms	Zinc pyrithione
6	Mild steel in cold water by *Bacillus thuringiensis* EN2	Ginger extract
7	Sulfidogenic bacteria	Cationic Gemini surfactants
8	5.49% NaCl against Sulfidogenic bacteria from oil-field water tank	Cationic Gemini surfactants
9	Carbon steel in 0.5 M HCl against SRB	Tetra hydroxyl methylphosphonium sulphate with fatty acids
10	API 5L X80 line pipe steel in artificial seawater by SRB	Neem extract
11	Carbon steel and stainless steel in oilfield environments by *Bacillus subtilis* A1 and *Streptomyces parvus* B7	*Allium sativum*

Vaithiyanathan S. et al.[112] discovered that *Polyalhia longifolia* plant has green corrosion inhibition power against SRB. They confirmed this fact utilizing TEM, SEM, FTIR, potentiodynamic polarization and weight loss studies. Rasool K. et al.[113] reported that mixed SRBs culture isolated from oilfields increased MIC and ZnO-interlinked chitosan nanoparticles mitigated corrosion establishing SEM, TEM, XRD and FTIR monitoring techniques. Carlson H. K. et al.[114] analyzed the MIC of sulfate-reducing microorganisms (SRM) and inhibition using potent biocide zinc pyrithione by high-

throughput (HT) approach. Narenkumar J. et al.[115] disclosed a green MIC inhibitor ginger extract to apply for mild steel corrosion. Cooling water was the medium, and *Bacillus thuringiensis* EN2 was the target microbes. Ginger extract showed 80% inhibition efficiency at 20 ppm of ginger extract and, calculated by weight loss, electrochemical, XRD and FTIR techniques. Labena A. et al.[116] studied corrosion inhibition properties of cationic gemini surfactants by sulfidogenic bacteria by employing redox potential and sulphide productivity. It was found that this inhibitor destroyed the biofilm growth at 0.1 mM concentration of surfactants. Labena A. et al.[117] also experimented with the same inhibitor in 5.49% NaCl against sulfidogenic bacteria from an oil-field water tank. They said that 97% corrosion inhibition power at 5 mM inhibitor concentration conducting sulphide production, redox potential and corrosion inhibition studies. Aiad I. A. and coworkers[118] proved MIC inhibition power of Tetra hydroxylmethylphosphonium sulphate with fatty acids on carbon steel in 0.5 M HCl by SRB employing FTIR, ^{1}H NMR, surface tension, critical micelle, weight loss and electrochemical methods. The inhibition effect of Neem extracts on the MIC of API 5L X80 line pipe steel by a sulphate-reducing bacterial (SRB) consortium was recommended by Shaily M. Bhola and team[119]. They carried out FESEM coupled with EDS and electrochemical studies to establish a 50% reduction power of MIC rate. Punniyakotti Parthipan and coworkers[120] suggested that *Allium sativum* as a green MIC inhibitor on carbon steel and stainless steel in oilfield environments in the presence of *Bacillus subtilis* A1 and *Streptomyces parvus* B7 by conducting weight loss and electrochemical techniques.

Schiff bases are synthetic organic compounds with potent activities in various disciplines such as medicine, agriculture and cosmetic products. Many Schiff bases exhibit anticancer, antitumor, antibacterial etc., properties. Schiff bases are popular

compounds for synthesizing numerous antibacterial drugs due to their fast and straightforward synthetic methods and their tendency to coordinate with their functional groups. Some recently reported Schiff bases as MIC inhibitors for metal surfaces in various environments in the presence of microorganisms mentioned below.

Nabel A. Negm et al.[121] synthesized four active Schiff base surfactants (Fig. 1.17a) derived from ketoglutaric acid and fatty alcohol as corrosion inhibitors with the properties of SRB biocide. They confirmed the inhibition efficiency of synthesized Schiff bases using weight loss studies. The surface properties of the Schiff bases were estimated using surface tension-log concentration profiles.

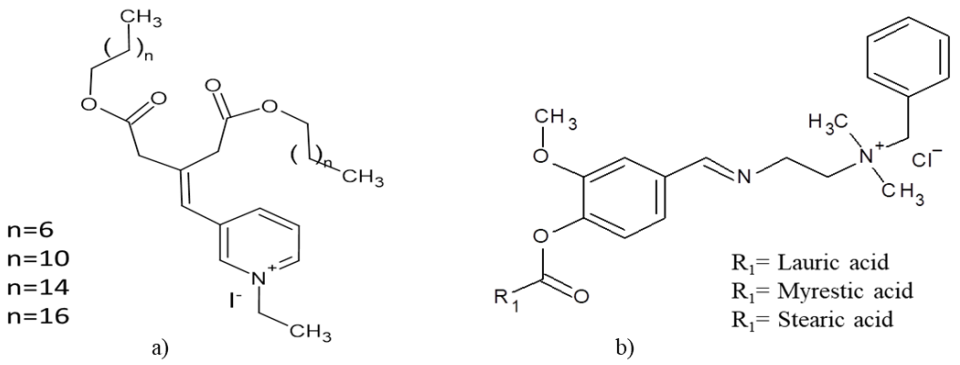

Fig. 1.17: Structure of a) quaternary ammonium Schiff base-alkyl ketoglutarate b) Schiff base derived from vanillin

Atef S. K. and coworkers[122] prepared three Schiff base surfactants (Fig. 1.17b) derived from vanillin and fatty acids and characterized them using FTIR and ^{1}H-NMR techniques. A mixed culture of SRB isolated from an oil field tank was targeted to prove the antimicrobial effect of the newly synthesized Schiff bases. They concluded that Schiff base cationic surfactants were suitable MIC inhibitors for industrial applications.

Samy M. Shaban and coworkers[123] reported three Schiff base cationic surfactants (Fig.1.18) derived from 4-dimethylaminobenzaldehyde and monoethanolamine acted as MIC inhibitors for carbon steel in acid medium against SRB. They applied physicochemical and electrochemical studies to confirm the inhibition behaviour of the synthesized Schiff bases.

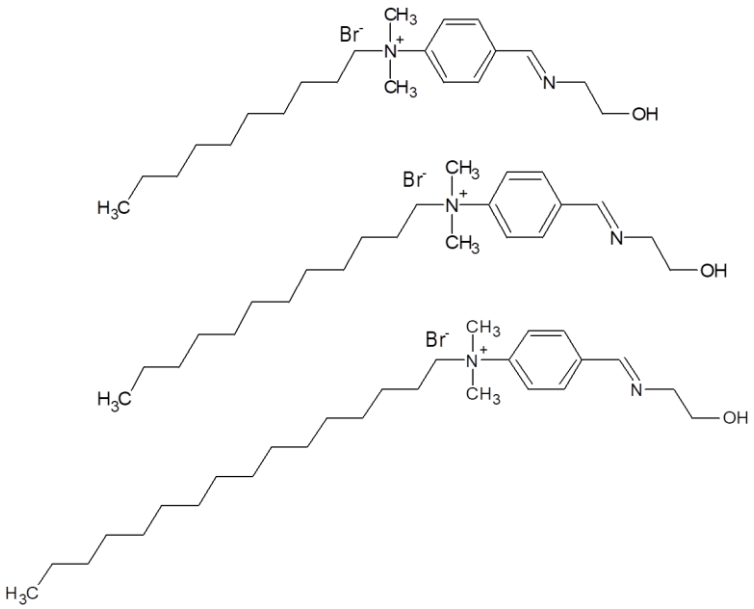

Fig. 1.18: Structures of three Schiff bases derived from 4-dimethylaminobenzaldehyde

Nabel A. Negm et al.[124] carried out a synthetic procedure for a series of Schiff base cationic surfactants (Fig.1.19) and their transition metal complexes by condensation reaction between fatty amines and 4-diethyl aminobenzaldehyde to study the biocidal activity of these compounds against SRB.

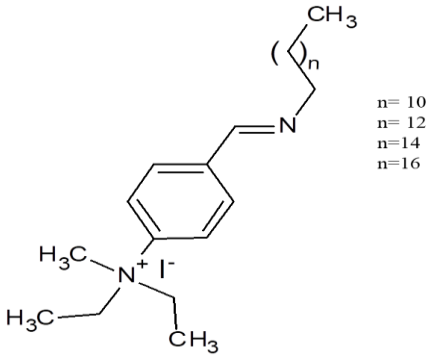

Fig. 1.19: Structure of Schiff base derived from 4-diethyl aminobenzaldehyde

It was reported that parent Schiff bases and their metal complexes showed remarkable biocidal activity.

Various recognition and effective approaches are being developed to fight MIC, yet more advancement is essential. Numerous problems want to be identified and addressed by using new technologies that will regulate MIC. Application of

environmental friendly biocides/inhibitors to substitute other harmful inhibitors will be cost effective and eco-friendly. Predominant issue that have to be studied in future is associated to the selection of methodologies. More deep knowledge of mechanisms related to every MIC inhibitory process could likewise be a significant area of future research.

Scope and objectives of the present investigation

Natural plant products are a source of myriads organic compounds having the potential to donate lone pair of electrons from the compounds to the metal surface. Hence, plant products can function as effective corrosion inhibitors. Many researchers were investigated natural plant products like leaf, seed, root, fruit, flower etc., as an efficient, eco-friendly corrosion inhibitor on the mild steel surface in aggressive acid environments.

The present research concentrates on extracting seven different natural plant products such as *Ixora coccinea* extract (ICE), *Croton persimilis* extract (CPE), *Tinospora cordifolia* extract (TCE), *Garcinia cambogia* extract (GCE), *Clerodendrum infortunatum* extract (CILE and CIRE) and *Dioscorea bulbifera* extract (DBE) and monitoring them as corrosion inhibitors for mild steel in 1 M HCl and 0.5 M H_2SO_4 media. FTIR and UV-Visible spectroscopy are used to characterise functional groups in extracts and determine the metal-binding ability of the extracts, respectively. Weight loss measurements, electrochemical studies such as EIS, potentiodynamic polarization and noise measurements are proposed to investigate the corrosion inhibition efficiency of extracts. Surface characterisations are carried out using SEM and AFM. It is also suggested to clear the mechanism of corrosion inhibition by evaluating various adsorption isotherm models. The impact of temperature on corrosion mitigation efficiency is examined, and deriving thermodynamic parameters of activation like

enthalpy, entropy and energy. Quantum mechanical calculations are also recommended to achieve energies of HOMO, LUMO and other quantum mechanical parameters. The impact of temperature, extract concentration and acid concentration on inhibition efficacy is also analysed by statistical tools like response surface methodology and Box-Behnken Design/Central Composite Design.

Schiff bases have a significant role in industrial, catalytic and pharmaceutical fields due to their adaptability and simple synthetic preparations. They have functional groups containing hetero atoms, unsaturated bonds can donate lone pair of electrons and function as potential corrosion inhibitors. Many synthetic compounds like Schiff bases, quaternary ammonium compounds, heterocyclic compounds etc. and natural plant extracts were reported as microbial induced corrosion inhibitors for microorganisms on the metal surfaces in various media. However, the literature survey exhibited that Schiff bases derived from heterocyclic compounds like acetyl pyridine and pyridine carbaldehydes were not investigated as MIC inhibitors.

Herein, previously reported four Schiff bases derived from 2-acetylpyridine, pyridine 2-carbaldehyde and pyridine 3-carbaldehyde such as N-hydroxy-1-(pyridin-2-yl) methanimine (NHP2M), N-hydroxy-1-(pyridin-3-yl) methanimine (NHP3M), (E)-2-(1-(2-phenylhydrazono) ethyl)pyridine (2PHEP) and (E)-2-(1-triazylidineethyl) pyridine (2TAEP) are employed as microbial induced corrosion inhibitors against microorganisms isolated from seawater on mild steel. Various corrosion monitoring techniques like weight loss measurements, electrochemical studies such as EIS, potentiodynamic polarization techniques are also presented to determine the MIC mitigation efficiency of these compounds. The changes observed in the metal surface are examined using optical micrographs of the metal surfaces. The mechanism of MIC inhibition is determined by surface analysis such as XRD and FTIR of corrosion products. The affinity of Schiff

base inhibitor towards metal surface confirmed by taking UV-Visible spectra of inhibitor and ferric salt solutions individually and combined. Antibacterial effects of Schiff base inhibitors were studied to verify the inhibition mechanism.

CHAPTER 2
MATERIALS AND METHODS

This chapter introduces the materials, preparative methods, characterization and corrosion monitoring techniques employed for the natural and synthetic corrosion inhibitors.

Natural corrosion inhibitors

Preparation of extracts

Ethanol extracts, prepared from plant leaves, were acted as inhibitor solutions against mild steel corrosion in acid media. Plant leaves were collected from different areas of Thrissur District. They were washed with distilled water to clean any dust particles attached to them and shade dried for two weeks. Dried leaves were then made fine grain using a grinder. 5 g of the powdered sample was refluxed with 100 ml ethanol for 4 hrs. It was then filtered after keeping overnight and concentrated into 50 ml. The selected plants and the major phytochemicals present in them, used for the application as corrosion inhibitors are listed in Fig. 2.1.

Experimental and quantum mechanical calculations were applied to evaluate the inhibition potential of plant leaves. Literature survey was the essential source for the identification of the principal constituents of the leaves. Among the various phytochemicals, one or two components were then selected to explain the mechanism of corrosion inhibition experimentally and theoretically.

Materials and medium

Weight percentage of the mild steel used: carbon 2.95 % and iron 97.05%. Mild steel metal sheet was cut into 1x1x0.059 cm dimension, and then they were

smoothened using an abrasive material with different grades such as 100, 220, 440, 800, 1000, 1500 and 2000 and cleaned with distilled water, followed by acetone.

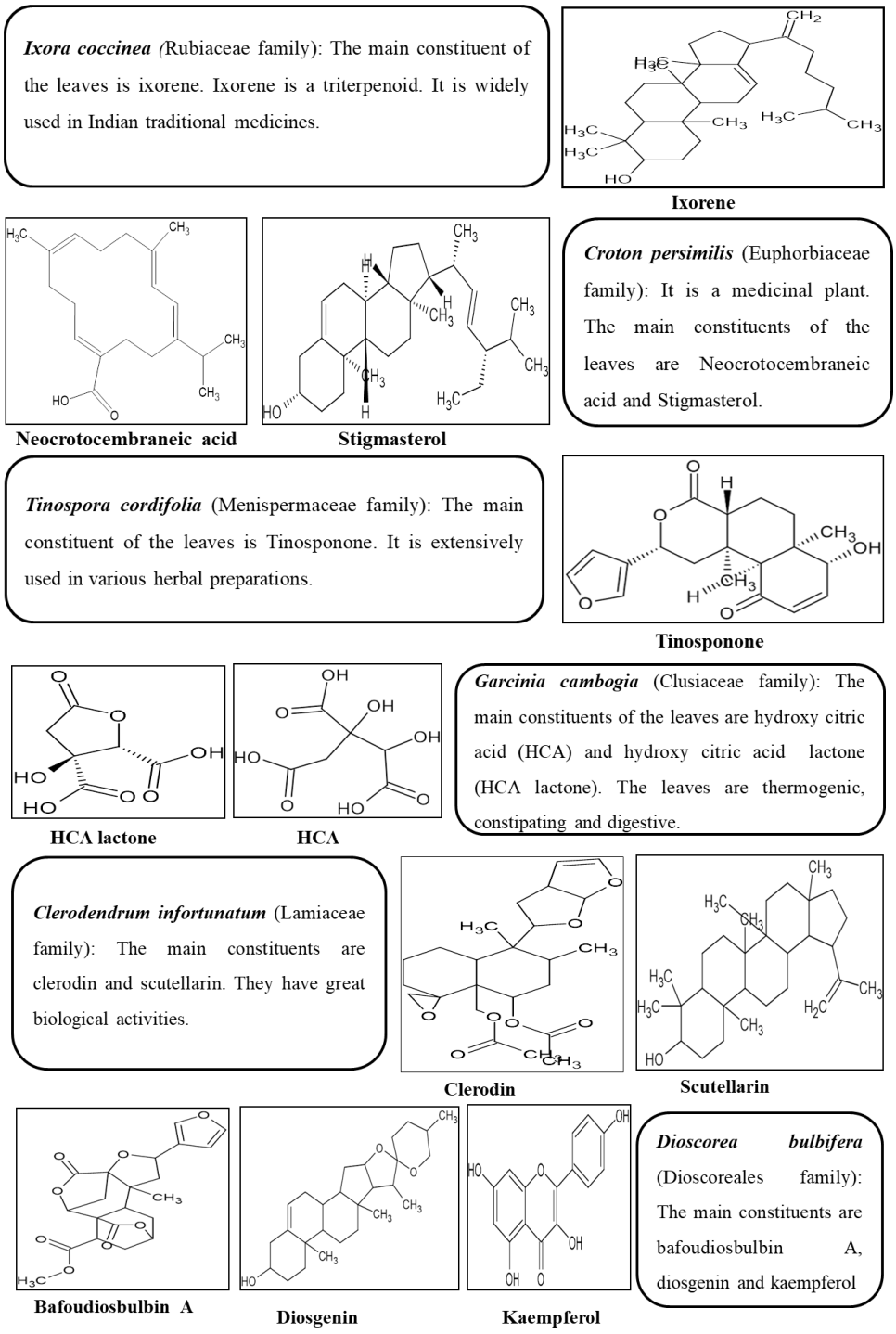

Fig. 2.1: Plant extracts and structure of significant constituents

Analytical pure (Merck) HCl and H_2SO_4 were used for preparing 1 M HCl and 0.5 M H_2SO_4. To analyze the effect of temperature on corrosion rate, a thermostat was used at temperatures 303 K, 313 K, 323 K and 333 K.

Ethanol, Mayer's reagent, chloroform, potassium ferrocyanide, NaOH, lead acetate, con. H_2SO_4 of Merck was used to conduct the phytochemical screening.

Merck samples of chromium acetate, cobalt acetate, copper acetate, manganous acetate, ferric chloride, sodium chloride and zinc acetate were used to determine the metal-binding capacity of alcoholic extract of plant leaves.

Spectral analysis

❖ ***FTIR spectroscopy***

IR spectra of extracts were examined to recognize the functional groups present in extracts for the studies and Spectrum Two FTIR spectrometer (Perkin Elmer, USA) was employed.

❖ ***UV-Visible spectroscopy***

The UV-Visible absorption spectra of 5 ppm plant extract, 5 ppm metal salts and an equal mixture of these two solutions were recorded using UV-Visible spectrophotometer, Shimadzu UV-1800, to study the metal-binding ability of plant extract. Chromium acetate, cobalt acetate, copper acetate, manganous acetate, ferric chloride, sodium chloride and zinc acetate were used to prepare 5 ppm metal salt solution.

Screening of phytochemicals

The phytochemicals of plant extract were tested by the standard methods[125,126,127,128]:

- Mayer's test: It is an identification test for alkaloids. 3 drops of freshly prepared Mayer's reagent were mixed with 1 ml of plant extract in a test tube. If it precipitates in white colour, the presence of alkaloids in the extract can be confirmed.

- Salkowaski's test: It is an identification test for steroidal compounds. 2 ml of chloroform was used to dissolve 5 ml of extract in a test tube and then was mixed with conc.H_2SO_4 to form a lower layer. Occurrence of reddish-brown colour at the interface is the confirmatory test for steroids in the extract.
- Test for phenolic compounds: 1% of ferric chloride solution was added to 1% potassium ferrocyanide in equal amounts. Then it was mixed with 2 ml of extract in a test tube. Visibility of bluish-green colour was accounted for the presence of phenolic compounds.
- Test for flavonoids: 3 ml of extract was mixed with 2 ml of dilute NaOH solution. Presence of yellow colour indicates the existence of flavonoids.
- Test for Terpenoids: 1 ml of extract was added with 0.5 ml of chloroform and a few drops of conc.H_2SO_4. A reddish brown precipitate points out the presence of terpenoids in the extract.
- Froth test: It is a positive test for saponins. About 0.5 g of extract was dissolved in 10 ml distilled water. The aqueous solution was closed tightly and shaken for 30 seconds gently. Then it was kept for 30 minutes. Presence of honeycomb froth above the surface was considered as the identification of saponins.
- Lead acetate test: It is an identification test for tannins. Freshly prepared 1% lead acetate was added to 5 ml of plant extract. Appearance of yellow precipitate was considered as a positive test for the presence of Tannins
- Tests for cardiac glycoside: Aqueous extract was mixed with 2 ml of conc. H_2SO_4. Development of reddish-brown colour was intended to the presence of steroidal aglycone part of the glycoside

- Tests for coumarin: 2 ml of extract was treated with few drops of alcoholic NaOH solution. Presence of coumarins can be verified by the formation of yellow colour.
- Test for quinones: 1 ml of extract was added to conc.H_2SO_4 solution. Appearance of the colour showed the presence of quinones.

Weight loss measurements

Weight loss studies were conducted with and without 1-5 v/v% concentrations of plant extract in both acid solutions for 24 hrs immersion period at different temperatures. Smoothened mild steel coupons were pre-measured, pre-weighed and immersed in 50 ml 1 M HCl and 0.5 M H_2SO_4 solutions separately by adding 0 - 5 v/v% concentrations of plant extract. After the completion of the period of immersion, metal coupons were weighed and calculated its weight loss. Using the resulted weight loss values, corrosion rate (υ) and inhibition efficiencies (η%) were estimated by equations (8) and (9), respectively.

Electrochemical studies

Electrochemical impedance spectroscopy (EIS), polarization studies and electrochemical noise studies were performed using Ivium CompactStat-e electrochemical work station and IviumSoft software with a three-electrode electrochemical cell. A pictorial representation of three-electrode assembly is shown in Fig. 2.2.

For all the electrochemical studies, a saturated calomel electrode behaved as the reference electrode. For EIS and linear polarization studies, a platinum electrode was acted as the counter electrode, and the mild steel having 1 cm^2 exposed surface area was employed as a working electrode.

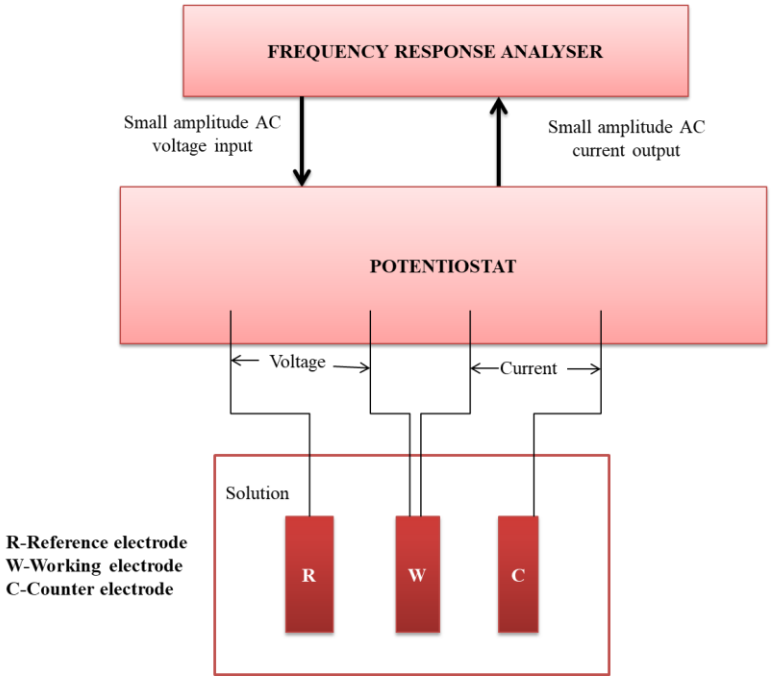

Fig. 2.2: Pictorial representation of a three-electrode assembly

The mild steel samples with 1 cm^2 exposed surface area were utilized as counter and working electrodes for electrochemical noise measurements. Reference electrode was same as EIS and potentiodynamic polarization studies. Measurements were carried at room temperature using 1 M HCl and 0.5 M H_2SO_4 with various plant extract concentrations (1- 5 v/v %).

The EIS parameters were measured over a frequency span of 1 KHz to 100 mHz and 10 mV signal breadth. Corrosion inhibition power of plant extracts was calculated from R_{ct} values obtained from Nyquist plots by the equation (22).

Current-potential relationship of mild steel samples in the test solution was evaluated using the open circuit potential method by potentiodynamic polarization studies. Applied potential range for the working electrode was from -250 to +250 mV compared to the corrosion potential (E_{corr}) with a scan rate of 1 mV/sec. Surveillance of anodic and cathodic curves was accomplished to derive corrosion current density (i_{corr}), and then the percentage of inhibition potency (η_{pol}%) as shown in equation (30).

Electrochemical noise studies were carried out for a period of 1200s.

Adsorption isotherms

Mechanism of corrosion inhibition between inhibitor molecules and mild steel metal was illustrated using adsorption isotherms. Several adsorption isotherms like Langmuir, El-Awady, Frumkin, Temkin, Freundlich, and Flory-Huggins were considered for the study. Best suitable isotherm was detected using the correlation coefficient (R^2) value[44]. As the concentration of the inhibitor increases, the surface coverage (θ) also increases. Adsorption of inhibitor molecules on the metal surface leads to decreased active surface area exposed to the acid media, thereby reducing metal corrosion.

Scanning electron microscopy

Surface characterization of mild steel coupons submerged in 1 M HCl and 0.5 M H_2SO_4 media comprising 5 v/v% of plant extract was examined by a scanning electron microscope JEOL Model JSM- 6390LV. The immersion period for the mild steel in contact with acid media and plant extract was 24 hrs.

Atomic force microscopy

Surface mechanism of plant extract on mild steel was further strengthened by an atomic force microscope WITEC ALPHA300 RA. Mild steel coupons employed for analysis and the immersion periods are the same as in SEM analysis.

Quantum mechanical calculations

Quantum mechanical parameters of active principles of plant extract were calculated using DFT method by GAMMES software. Correlation factor used was B3LYP and STO-3G as the basis set. This method provides a correlation between the corrosion inhibition efficiency of the inhibitor molecules and their electronic properties[129]. Calculated parameters such as E_{HOMO}, E_{LUMO} and ΔE were used to evaluate the corrosion inhibition behaviour of the compound.

Response surface methodology (RSM)

Response surface methodology (RSM) is the established optimization technique in current years. It describes the effect of a quantitative response on process factors, individually or with one another, and generates an empirical model illustrating the proper quantity of processes[130]. Response is a dependent variable, and process factors are known as independent/predictor variables or factors. RSM can apply for maximizing or minimizing the responses.

Generally, response surfaces are performed by a second-order regression model. A second-order regression model is also called a full quadratic equation for 'k' number of factors, shown in equation (50).

$$Y = a_0 + a_1X_1 + \dots a_kX_k + a_{12}X_1X_2 + \dots a_{k-1,k}X_{k-1}X_k + a_{11}X_1^2 + \dots a_{kk}X_k^2 \quad (50)$$

The favoured method of response surface design is Central Composite Design, CCD[131]. Fig. 2.3 is a schematic representation of CCD that is a two-level full factorial or fractional factorial design having centre points and axial points. Centre point is positioned at the centre, whereas the axial points are located at the middle of the levels of a factor. So, the axial points are coordinated with (-1, 0), (1,0), (0, -1), and (0, 1). Fig. 2.3 is a 3^2 factorial for which a full quadratic model can be suited for the response surface. When more centre points are inserted, the lack of fit has to be tested. The distance between the centre and the axial points is designated by α.

Accuracy of the prediction model can be evaluated by producing consistent and stable variance over the complete ranges of the independent/predictor variables. The statistical significance of an independent variable is verified by performing an analysis of variance (ANOVA). If the p-value is less than the significance level (0.05), then the full quadratic model of independent variables significantly influence the dependent variable[132]. When R-square and adjusted R-square values are close to unity, the model

parameters can perfectly explain the variation of dependent variables suggesting, a tremendous practical significance.

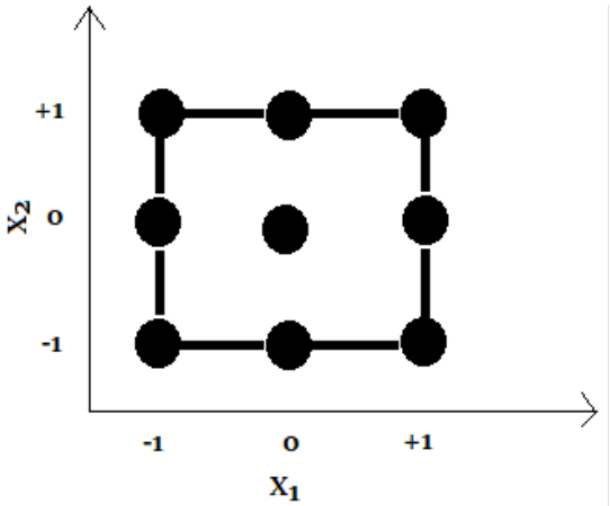

Fig. 2.3: Schematic representation of CCD with α=1

Normal probability plot gives information about the distribution of residuals[133]. If the residuals follow approximately a straight line, then it is a normal distribution for the residuals. The residuals vs fitted plots reveal the predictability of the residuals[134]. Lack of clear pattern in residuals vs fitted plot suggests no unpredictability of the residuals. Then, the residuals can be regarded as homogenous. Residuals vs the observation order plot imply the correlation between the observation number and the residuals.

Box-Behnken Design (BBD) is another attractive design for RSM to fit a second-order model[135]. BBD requires only three levels for each factor and a fewer number of experimental runs. BBD places a mid-level between the low-level and high-level factors, neglecting the extreme axial points as in CCD. Comparing to CCD, BBD uses face points beside the corner points. The assessment of the coefficients of a second-order model is more straightforward when a mid-level point is added. In BBD, 2^2 full factorial is employed as the base design. Then, applying mid-levels for the other factors, orthogonal blocks are produced.

Analysis and demonstration for the results of BBD are the same as CCD. CCD is the traditional fractional factorial design of experiments. So, it has all the merits of fractional factorial design. In addition, CCD is rotatable, whereas BBD is nearly rotatable or rotatable for some particular designs[136]. CCD can make possible a fourth-order model since it contains five levels for each factor. At the same time, BBD can set only a second-order model because there are only three levels for each factor. BBD could be more beneficial for more well-informed processes in practice, while CCD could be more interested in comparatively unknown processes. That's why CCD is used frequently compared to BBD since most RSM studies are performed to find something new. Even so, for more refinement and optimization, BBD is the more precise method.

In short, both designs have their merits and demerits. The designers can select any of these two based on the optimization goals. Composite desirability function used for the optimization technique. Overall predictability for responses by the independent factors can measure in it.

❖ ***RSM for maximum corrosion inhibition efficiency***

RSM helps to discover the optimum parameter condition to attain the maximum inhibition efficiency. Experimental design and analysis were performed using Minitab 19 programming tool, and CCD/BBD was applied to include possible experimental runs. The independent factors used in CCD were temperature (X_1) and inhibitor concentration (X_2), whereas those in BBD were temperature (X_1), inhibitor concentration (X_2) and acid concentration (X_3). Inhibition efficiency was the corresponding response. Table 2.1 shows the level of independent factors of BBD/CCD with coded and uncoded forms. The generalized full quadratic model for the three factors X_1, X_2 and X_3 in BBD is shown in equation (51) and that in CCD is given in equation (52).

$$Y = a_0 + a_1X_1 + a_2X_2 + a_3X_3 + a_{12}X_1X_2 + a_{13}X_1X_3 + a_{23}X_2X_3 + a_{11}X_1^2 + a_{22}X_2^2 + a_{33}X_3^2 \quad (51)$$

$$Y = a_0 + a_1X_1 + a_2X_2 + a_{11}X_1^2 + a_{22}X_2^2 + a_{12}X_1X_2 \quad (52)$$

where Y is the predicted value of corrosion inhibition efficiency. a_0 is a constant, a_1, a_2 and a_3 are constants indicating the effect of factors X_1, X_2 and X_3. a_{12}, a_{13} and a_{23} are interaction constants between the two factors X_1X_2, X_1X_3 and X_2X_3. Quadratic constants of X_1, X_2 and X_3 are represented by a_{11}, a_{22} and a_{33}.

Table 2.1: Level of factors of BBD/CCD with coded and uncoded form

Sl. No.	Factor	Code	Unit	Level of factors		
				Low (-1)	Center (0)	High (1)
1	Temperature	X_1	K	313	323	333
2	Inhibitor concentration	X_2	v/v%	1	3	5
3	Acid concentration	X_3	M	0.5	1	1.5

Synthetic corrosion inhibitors

Materials and methods

The Schiff base derivatives were synthesized from pyridine-2-carbaldehyde, pyridine-3-carbaldehyde and 2-acetylpyridine of analar grade chemicals procured from Fluka. The reagents hydroxylamine hydrochloride, semicarbazide hydrochloride, phenylhydrazine hydrochloride, sodium acetate, NaCl, KCl, $CaCl_2$. $2H_2O$, $MgSO_4$. $7H_2O$, $MgCl_2$. $6H_2O$, $NaHCO_3$ were acquired from E-Merck. The medium utilized for the synthetic purpose was pure ethanol.

❖ ***Preparation of metal samples***

For weight loss measurements, metal samples of 1x1x0.059 cm dimension were used and polished using emery papers. The exact surface area and thickness of the metal samples were accurately determined using vernier callipers and screw gauge, then weighed accurately using an electronic balance. For electrochemical studies, metal samples of 10x2x0.059 cm dimension were used and polished with emery papers.

❖ ***Synthesis of inhibitors***

1) Synthesis of N-hydroxy-1-(pyridin-2-yl)methanimine (NHP2M)

Ethanolic solution of pyridine-2-carbaldehyde (2 mmol) was carefully transferred to the mixture of an aqueous solution (5 ml) of hydroxylamine hydrochloride (2 mmol) and sodium acetate (4 mmol). It was refluxed on a water bath for 20 minutes, and then cooled in the ice bath. It yielded pale pink coloured crude- NHP2M, then filtered and dried.

2) Synthesis of N-hydroxy-1-(pyridin-3-yl)methanimine (NHP3M)

Ethanolic solution of pyridine-3-carbaldehyde was added to a 1:2 aqueous mixture of hydroxylamine hydrochloride and sodium acetate taken in a round bottom flask. After mixing thoroughly, it was refluxed on a water bath for 20 minutes. The clear solution was cooled in an ice bath. It was precipitated the white coloured compound - NHP3M. Then, it was filtered and dried.

3) Synthesis of (E)-2-(1-(2-phenylhydrazono)ethyl)pyridine (2PHEP)

Ethanolic solution of phenylhydrazine hydrochloride mixed carefully with a hot ethanolic solution of 2-acetylpyridine. Refluxed for 3 hours on a water bath, then concentrated. It yielded orange crystals - 2PHEP.

4) Synthesis of (E)-2-(1-triazylidineethyl)pyridine (2TAEP)

A hot ethanolic solution of 2-acetylpyridine was transferred to an ethanolic solution of semicarbazide contained in a round bottom flask. Then the mixture was refluxed for 3 hours on a water bath. It concentrated and collected light rose coloured crystals - 2TAEP.

Fig. 2.4 shows the structures of the four synthetic inhibitors used in the present course of studies.

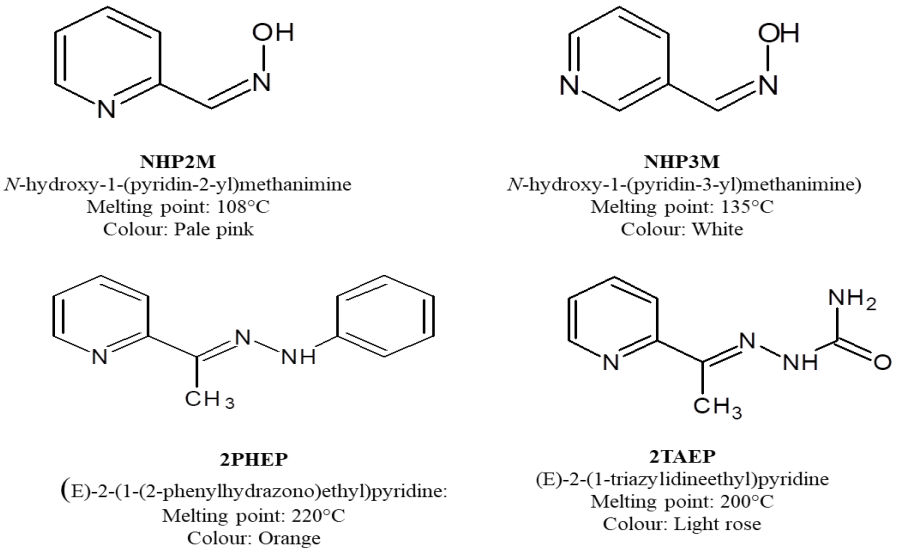

NHP2M
N-hydroxy-1-(pyridin-2-yl)methanimine
Melting point: 108°C
Colour: Pale pink

NHP3M
N-hydroxy-1-(pyridin-3-yl)methanimine)
Melting point: 135°C
Colour: White

2PHEP
(E)-2-(1-(2-phenylhydrazono)ethyl)pyridine:
Melting point: 220°C
Colour: Orange

2TAEP
(E)-2-(1-triazylidineethyl)pyridine
Melting point: 200°C
Colour: Light rose

Fig. 2.4: Structures of the four synthetic inhibitors understudy

❖ ***Preparation of artificial seawater broth***

An artificial salt mixture closely resembling the composition of ocean water for culturing marine bacteria was prepared.

Chemicals required:

NaCl - 24.600 g

KCl - 0.670 g

$CaCl_2$. $2H_2O$ - 1.360 g

$MgSO_4$. $7H_2O$ - 6.290 g

$MgCl_2$. $6H_2O$ - 4.660 g

$NaHCO_3$ - 0.180 g

Components of the artificial seawater media are separately weighed and suspended in 1 litre of double-distilled water. pH is read using a digital pH meter and adjusted to 7.5 using 1 N HCl or 1 N NaOH. The mixture is heated thoroughly to dissolve all components and allocated to 250 ml conical flasks. The resulting medium is sterilized by autoclaved at 15 lbs pressure at 121^{o}C for 15 min and allowed to cool to room temperature before inoculation.

❖ ***Culturing of marine bacteria***

Seawater was collected from Snehapuram beach, Vadanappilly, Thrissur. All samples were collected in the morning between 7.00 AM to 8.00 AM using a sterile glass bottle and transported immediately to the lab. 100 ml of this water were filtered through Whatman filter paper using Vacuum Filtration Apparatus. Microorganisms trapped in the filter paper is used as the inoculum for the culture. Sterilized and cooled artificial seawater media in the conical flask and is inoculated with a wire loop. Metal strip of dimension 1 cm x 1 cm was introduced into the flask and then incubated in a BOD incubator at 25^{o}C. Every day the flasks were shaken for one minute and examined for bacterial growth. The first subculture was done after 14 days of inoculation. Then the periodic subculturing was done on every seventh day. The metal strip was transferred to the new flask during the subculturing process.

Isolation of corrosion causing bacteria

To isolate the corrosion causing bacteria pour plate method[137] was used. Artificial seawater agar was made by incorporating 2% agar in the original seawater media. Microorganisms grown on artificial seawater media is serially diluted, and 0.1 ml from each dilution is transferred to a series of sterile Petri plates. After sterilization, the media is cooled to 45^{o}C and poured into the Petri plate. The media and inocula were mixed thoroughly by swirling and allowed to solidify. The plates were then incubated at room temperature for 2-3 days. Single-cell colony emerged was further isolated by streak plate technique using the same medium. Then it was subcultured on the artificial seawater agar slants and kept as stock cultures. Stock cultures for the experiments were preserved at 4^{0}C and subcultured frequently. Paraffin overlay technique was applied to keep permanent stock cultures[138]. Paraffin overlay technique employed an artificial seawater agar slant for inoculation of a single cell colony and incubated at room temperature (28 ±

2°C). Sterile liquid paraffin was used to envelop the top of the culture at the end of 18 hrs of incubation. At the same time, vials were overlaid by a sterile rubber cap.

Identification of the bacterium

Depends on the morphological and biochemical properties, the selected single cell colony MICBT7 was identified as summarized in Bergey's Manual of Systematic Bacteriology[139]. Further, to authenticate the identity, molecular ribotyping was also carried out. It was performed by employing the partial gene sequence of 16S rRNA.

❖ ***Isolation of genomic DNA***

It involved the following steps[140].

- Transferred mid-log phase culture of the bacteria (40 ml) into a sterile oakridge tube and centrifuged at 5000 rpm for 10 minutes at 4°C.
- Rejected the supernatant solution and dehydrated the pellet blot.
- Dissolved the cell pellet in 8.75 ml TE buffer.
- Then, 10 mg/ml Proteinase K and 10% SDS (l ml) were mixed thoroughly and incubated at 37°C for 1 hr.
- A 1:1 mixture of phenol and chloroform was transferred, mixed, and maintained for 10 minutes at 4°C.
- Centrifuged at 10,000 rpm for 10 minutes at 4^0C, the supernatant was added to a sterile tube using a sterile cut tip.
- Above mentioned two steps were repeated three times.
- Aqueous phase was transferred into a sterile 50 ml beaker, with 0.1 ml of 5 M sodium acetate (pH 5.2) and 20 ml of isopropanol.
- DNA gets precipitated, collected and then washed with 70% ethanol.
- Dissolved the precipitated DNA in 1 ml TE buffer.

❖ ***Agarose gel electrophoresis***

Agarose gel electrophoresis[140] was performed to examine the nature of the DNA precipitated. In this electrophoresis, 0.8% (w/v) agarose gel was employed. After loading 10 µl of the DNA onto the agarose gel, electrophoresis was conducted at 80 V for 1 hr. In other words, up to the migrating dye (Bromophenol blue) had passed over a two-thirds distance of the gel, electrophoresis continued. Lambda DNA cut with EcoR I and HindIII (Bangalore Genei) was applied as the marker. 0.5 mg/ml ethidium bromide solution was employed to stain the agarose gel for 20 minutes. A UV transilluminator was operated to give the exact vision of the gel.

❖ ***Ribotyping***

Universal primer pair for 16S rDNA was applied for executing Ribotyping. A fragment of the 16S rRNA gene (l.5 kb) was amplified from the genomic DNA[141]. 16S rDNA was amplified by employing the forward (l6SF) and reverse (l6SR) primers with the corresponding sequence as follows:

Sequence:

16SF 5' AGTTTGATCCTGGCTCA 3'

16SR 5' ACGGCTACCTTGT TACGACTT 3'

❖ ***Polymerase Chain Reaction (PCR)***

A thermal cycler (Eppendorf master cycler personal) rendered PCR function under a set of conditions.

PCR mix composition

Deionized water - 12.5 µl

Enyme buffer - 2.5 µl

dNTP - 10 mM

Forward primer - 10 picomol

Reverse primer - 10 picomol

Sample DNA - 50 mg

Taq polymerase (1/10) - 0.6 U

PCR conditions

- Initial denaturation at 94°C for 2 minutes.
- Denaturation at 94°C for 45 seconds.
- Annealing at 59°C for l minute.
- Primer extension at 72°C for 2 minutes.
- Steps 2, 3 and 4 were repeated 29 times.
- Final extension at 72°C for 10 minutes.
- Hold at 4°C.

Microbial corrosion monitoring methods

The generalized initial procedure for weight loss and electrochemical studies can be explained using Fig. 2.5. The concentration of inhibitor was 100 ppm for all corrosion studies.

❖ ***Weight loss measurements***

In weight loss measurements, the metal samples of 1 cm^2 were immersed in artificial seawater broth in a hanging position with the help of fishing lines for 21 days in three systems: control (without bacteria), biotic (with bacteria) and biocide (with bacteria and inhibitor). Corrosion rate and inhibition efficiencies were calculated from the weight loss measurements data using the equations (8) and (9). The rate of corrosion was expressed in terms of mm/year.

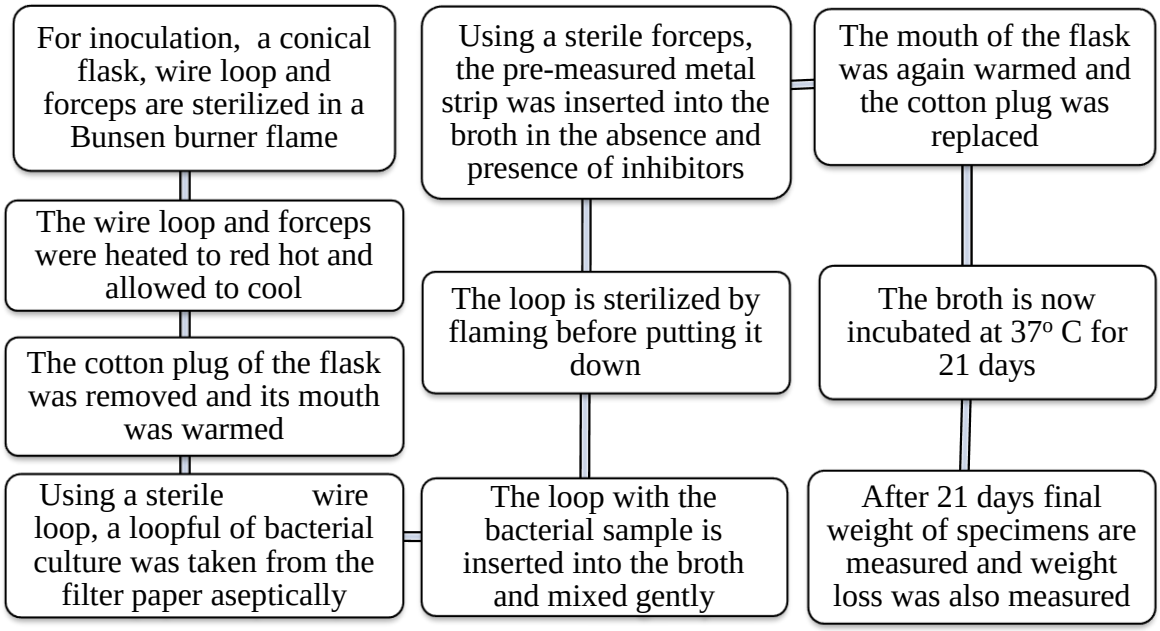

Fig. 2.5: Schematic representation of weight loss measurements

❖ ***Electrochemical impedance spectroscopy (EIS)***

Ivium compactstat-e electrochemical system was used for EIS studies. It was a three-electrode assembly. A saturated calomel electrode (SCE) was used as the reference electrode, and a platinum electrode with 1 cm^2 area was acted as the counter electrode. Working electrode was a metal sample with an exposed surface area of 1 cm^2 immersed in 100 ml artificial seawater broth containing control, biotic and biocide for 21 days (504 hrs) before the electrochemical measurements. EIS measurements were started after attaining a constant potential called OCP. It was carried out in the frequency range from 1 KHz to 100 mHz with an amplitude of 10 mV as an excitation signal. The percentage of inhibitions from impedance studies were estimated using charge transfer resistance values by the equation (22).

❖ ***Potentiodynamic polarization studies***

Electrochemical polarization studies of mild steel samples in control, biotic and biocide were conducted by recording anodic and cathodic potentiodynamic polarization curves. Polarization plots were derived in the electrode potential range from -250 to

+250 mV vs corrosion potential (E_{corr}) at 1 mV/sec scan rate. Corrosion current densities (i_{corr}) were rendered by extrapolating anodic and cathodic curves to the potential axis. The percentage of inhibition efficiency (η_{pol}%) was calculated from i_{corr} values using the equation (30). Polarization resistance (R_p) values were acquired from the slope analysis, and inhibition efficiency was estimated using the equation (33).

Surface analysis

❖ ***X-ray diffraction spectroscopy (XRD)***

Mild steel surfaces immersed in control, biotic and inhibitor systems after 21 days of incubation were used for X-ray diffraction spectroscopy (XRD). A computer controlled XRD system (PANalytical) was performed among 5º and 90º - 2θ with copper K-alpha radiation at a 40 kV, 25 mA rating.

❖ ***FTIR spectroscopy***

After 21 days of incubation, the mild steel coupons were taken outside the artificial sea water medium, and the surface film was scraped using a sterile spatula. FTIR spectra of the scratched corrosion products on the mild steel were conducted for control, biotic and inhibitor systems using KBr pellet method. The spectrum was recorded in the range 400-4000 cm^{-1} employing Shimadzu IR Affinity-1 model FT-IR spectrophotometer.

Microscopic surface analysis

After 21 days of incubation, the mild steel coupons were taken outside the artificial sea water medium and examined using a high-resolution optical microscope (Leica Stereo Microscope-No. S8ACO). This analysis focuses on studying the surface modifications that occurred for mild steel coupons when the metal coupons were exposed in control, biotic and inhibitor systems.

UV-Visible spectroscopy

UV-Visible spectra of Schiff base inhibitor and ferric salt solutions were recorded individually and combined (1:1 ratio) in an equal mixture of DMSO and water using UV-Visible spectrophotometer Shimadzu UV-1800. It helped to study the metal-binding ability of Schiff base inhibitors.

In vitro antibacterial effects of inhibitors

In vitro antibacterial effects of the Schiff base inhibitors 1) *N*-hydroxy-1-(pyridin-2-yl) methanimine, NHP2M 2) *N*-hydroxy-1-(pyridin-3-yl) methanimine, NHP3M 3) (E)-2-(1-(2-phenylhydrazono)ethyl) pyridine, 2PHEP and 4) (E)-2-(1-triazylidineethyl) pyridine, 2TAEP were carried out against *Escherichia coli*. Disc diffusion method was employed for antimicrobial susceptibility tests. To compare the antimicrobial activity of inhibitors, tetracycline was used as the standard antibiotic.

❖ ***Disc diffusion method***

Disc diffusion method is also called Kirby–Bauer test[142]. This method measures the degree of resistance of pathogenic microorganisms to various antimicrobial compounds. It involves different steps.

Mueller-Hinton agar (MHA) plates were prepared using the following components[143] at 7.4 pH.

Components:

Beef extract-2 g

Acid Hydrolysate of Casein-17.50 g

Starch-1.50 g

Agar-17 g (2%)

Distilled water-1000 ml

These components dissolved in distilled water and autoclaved after closing it with

a sterilized cotton ball at 121^0C for 15 minutes. Then cooled for half an hour and poured into a sterilized petri dish (diameter-90 mm and depth-4 mm) and placed in laminar flow hood chamber. Allowed the plate to solidify and examined each set of plates for sterility by incubating at 30-35^0C for 24 hrs.

For the preparation of inoculums growth method is used. From an agar plate culture, four to six isolated bacterial colonies having similar morphology was selected and then the growth is transferred to a tube consisting of nutrient broth (5 ml). Then incubation of the broth culture at 35^0C was done until it gains the turbidity of 0.5 McFarland standards. Normally 2-6 hrs will take to produce turbidity.

Selected bacterial strain, *Escherichia coli* of 24 hrs culture, was evenly spread into the surface of agar plates using sterile swab sticks. Sterile paper discs were dipped into different samples and placed gently on the plate. Using a micropipette samples were inoculated to the discs. Discs are then incubated at 37^0C for 24 hrs after placing it in a petri dish. The disc dipped in DMSO served as a negative control, and the tetracycline disc was acted as a positive control. Discs containing samples were allocated on the surface of the agar plate by means of forceps and then gently pressed down to attain uniform contact with agar plate. A minimum distance of 30 mm was preserved between the discs. Then the petri dishes were inverted and incubated at 37ºC for 24 hrs and observed for zone of inhibition. If the sample is resistant to the bacteria, there will be a zone around the bacteria called zone of inhibition where there is no bacterial growth. Zone of inhibition was then measured, and antibacterial activity was expressed in terms of the mean diameter of zone of inhibition in millimetres (mm) by comparing it with the standard antibiotic.

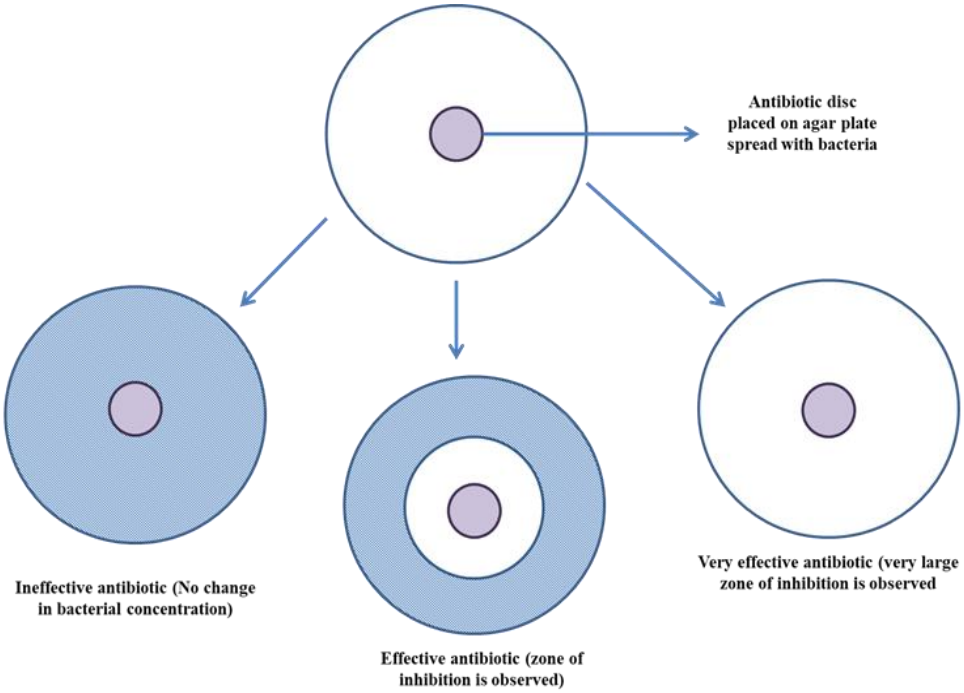

Fig. 2.6: Schematic representation of disc diffusion method

CHAPTER 3

IXORA COCCINEA EXTRACT: NATURAL CORROSION INHIBITOR FOR MILD STEEL IN ACID MEDIA

This chapter delineates the corrosion inhibition power of an eco-friendly green inhibitor *Ixora coccinea* extract (ICE), for mild steel in 1 M HCl and 0.5 M H_2SO_4 using various corrosion monitoring techniques. The major chemical constituent of *Ixora coccinea* leaves ixorene[144] (Fig. 3.1), subjected to theoretical calculations to evaluate the corrosion inhibition ability of the leaf extract in more detail.

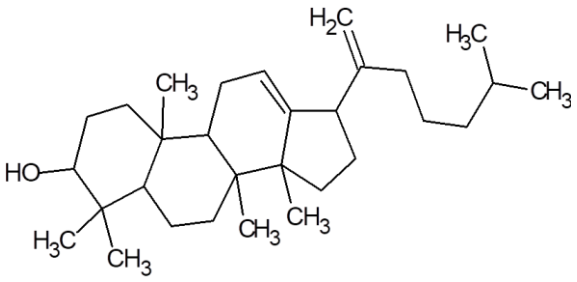

Fig. 3.1: Structure of ixorene

Ixora coccinea

Results and Discussion

Phytochemical screening of ICE

Standard identification tests were conducted to realize the phytochemicals present in ICE, and the results are given in Table 3.1.

FTIR spectroscopy

To identify the functional groups existing in ICE, FTIR spectroscopy of dried powdered *Ixora coccinea* leaves has been examined, shown in Fig. 3.2. A broad band observed at 3438 cm^{-1} indicates O-H stretching vibration. Two strong peaks at 2928 cm^{-1} and 2850 cm^{-1} are pointed alkyl C-H stretching bonds. The peaks at 1628 cm^{-1} and 1384 cm^{-1} represent aliphatic and aromatic C=C stretching bonds, respectively. The other significant peaks indicate the presence of minor components present in ICE.

Table 3.1 Phytochemical screening of ICE

Sl. No.	Compounds	Tests	Results
1	Alkaloids	Mayer's reagent	++
2	Steroids	Salkowaski's test	++
3	Phenolic compounds	Potassium ferrocyanide test	++
4	Flavanoids	Sodium hydroxide test	++
5	Saponins	Froth test	++
6	Tannins	Lead acetate test	––
7	Cardiac glycosides	Conc. sulphuric acid test	++
8	Coumarin	Alcoholic NaOH test	++
9	Quinones	Conc. sulphuric acid test	++

++ (present), – – (Absent)

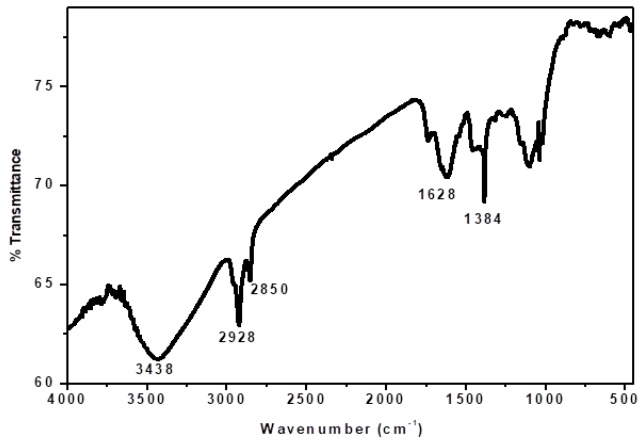

Fig. 3.2: FTIR spectrum of ICE

Weight loss measurements

❖ ***Effect of concentration***

The weight loss measurements of mild steel in 1 M HCl and 0.5 M H_2SO_4 solutions at room temperature with and without various concentrations (1-5 v/v %) of ICE for 24 hrs are recorded in Table 3.2. It is evident from the data that as the concentration of inhibitor is increased, the percentage inhibition efficiency also increases in both the acidic media. The results show that ICE is an efficient inhibitor in 1 M HCl, attaining maximum inhibition efficiency at 5% as 89.38%. This is because the

number of adsorbed organic molecules of inhibitor ICE on mild steel is more in HCl than H_2SO_4 medium.

Table 3.2: Weight loss measurements of mild steel with and without ICE in 1 M HCl and 0.5 M H_2SO_4 at room temperature for 24 hrs

Conc. (v/v %)	Corrosion rate (mm/yr)		Inhibition efficiency (η%)	
	1 M HCl	0.5 M H_2SO_4	1 M HCl	0.5 M H_2SO_4
Blank	3.95	35.57	-	-
1	0.60	12.23	84.77	65.61
2	0.56	11.52	85.75	67.58
3	0.52	9.05	86.73	74.53
4	0.47	8.77	87.98	75.32
5	0.41	7.83	89.38	77.96

❖ ***Effect of temperature***

Effect of temperature on the stability of the adsorption film formed by ICE on mild steel surface was explained by weight loss measurements in 1 M HCl and 0.5 M H_2SO_4 at elevated temperatures for 24 hrs. Inhibition efficacy was calculated and given in Table 3.3 and is graphically depicted in Fig. 3.3. Inhibition efficiency obtained for the highest concentration (5 v/v%) is 89.38 % in 1 M HCl. But when the temperature increases by 10 K, the efficiency lowered to 88.93 % and then went to 66.03 % for a further rise of 10 K, finally reaches 51.14% at the highest temperature (333 K). Similarly, in the case of 0.5 M H_2SO_4, the rate of corrosion enhances at elevated temperatures for the same concentration. This may be attributed to the instability of adsorbed film at higher temperatures. Higher temperature may cause desorption on the metal surface[58]. This indicates ICE molecules adsorb on the mild steel surface mainly by physisorption. So, temperature influences the action of inhibitor on the metal surface and thereby corrosion control.

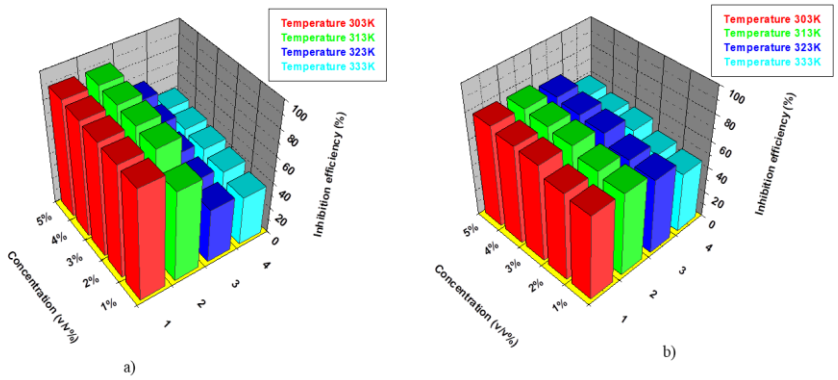

Fig. 3.3: Variation in inhibition efficiency of ICE in a) 1 M HCl b) 0.5 M H_2SO_4 at elevated temperatures

Table 3.3: Corrosion rate (υ) and inhibition efficiency (η%) of ICE in 1 M HCl and 0.5 M H_2SO_4 at different temperatures for 24 hrs

Medium	Conc. (v/v%)	υ (303 K)	η% (303 K)	υ (313 K)	η% (313 K)	υ (323 K)	η% (323 K)	υ (333K)	η% (333 K)
1 M HCl	Blank	3.95	-	13.11		22.05	-	31.77	-
	1	0.60	84.77	4.04	69.18	12.82	41.85	19.89	37.39
	2	0.56	85.75	2.06	84.28	11.68	47.02	18.19	42.74
	3	0.52	86.73	1.80	86.27	10.50	52.38	17.09	46.20
	4	0.47	87.98	1.59	87.87	8.62	60.90	16.43	48.28
	5	0.41	89.38	1.45	88.93	7.49	66.03	15.52	51.14
0.5 M H_2SO_4	Blank	35.57	-	58.27	-	86.25	-	106.2	-
	1	12.23	65.61	20.70	64.47	36.39	57.80	57.35	46.02
	2	11.52	67.58	19.05	67.30	34.44	60.06	54.47	48.73
	3	9.05	74.53	15.50	73.39	27.90	67.65	47.09	55.68
	4	8.77	75.32	14.49	75.13	25.99	69.86	45.99	56.71
	5	7.83	77.96	13.51	76.81	23.97	72.20	42.98	59.55

Using Arrhenius equation (41), plots of log K vs 1/T for metal corrosion in the presence and absence of ICE in acid media were obtained and are shown in Fig. 3.4 a) and Fig. 3.5 a). Activation energy of corrosion in acid media was calculated from the slopes of the plots. From transition state theory, thermodynamic parameters such as enthalpy of activation (ΔH^*) and entropy of activation (ΔS^*) were equated as in the equation (42). Fig. 3.4 b) and Fig. 3.5 b) show Arrhenius plots of log K/T vs 1/T. ΔH^* and ΔS^* values were derived from these plots and are given in Table 3.4 along with activation energy (E_a) and Arrhenius factor (A).

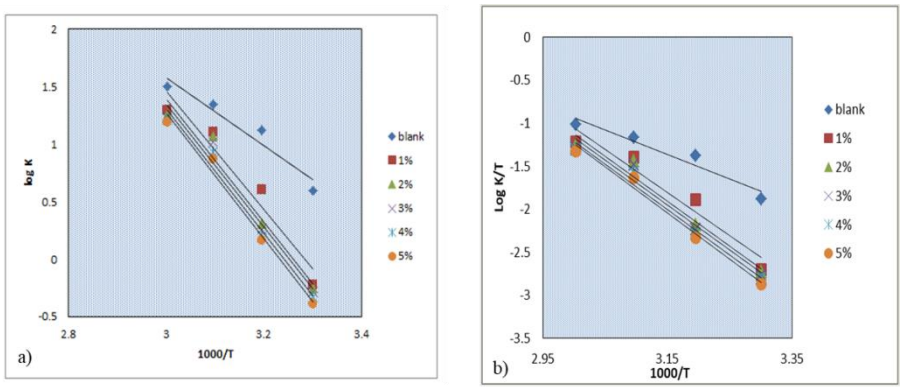

Fig. 3.4: Arrhenius plots of a) log K vs 1000/T b) log K/T vs 1000/T in the presence and absence of ICE in 1 M HCl

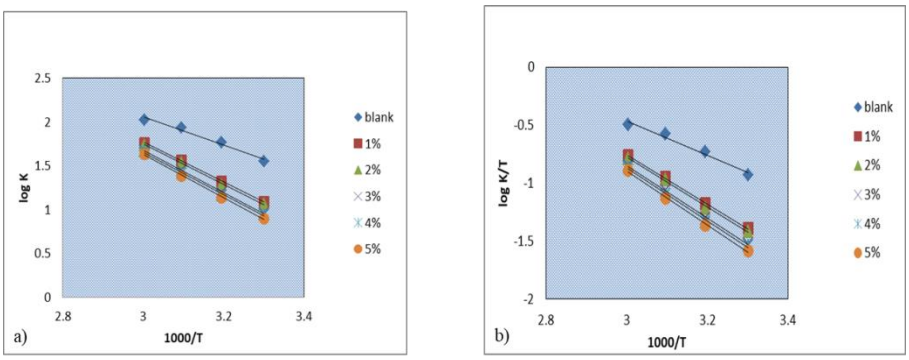

Fig. 3.5: Arrhenius plots of a) log K vs 1000/T b) log K/T vs 1000/T in the presence and absence of ICE in 0.5 M H_2SO_4

It exhibited that as the concentration of ICE increases, the activation energy of corrosion also enhances in both acids. This can be ascribed to the growing energy barrier with the increase in ICE concentration. It was evident that an activated complex compound was formed by the interaction of the inhibitor with mild steel. Positive enthalpy values were indicated that the corrosion process was endothermic. The values of ΔS* were also found to be raised as ICE concentration increases. Entropy of activation for corrosion was observed to be negative for blank solution mentioned that a decrease in randomness for the activated complex, compared to the reactants[145]. In the presence of ICE, the disorderliness of the activated complex getting increased, and ΔS* values became positive in the HCl medium. In the case of 0.5 M H_2SO_4, ΔS* values became less negative with increased ICE concentration.

Table 3.4: Thermodynamic parameters of mild steel corrosion with and without ICE in 1 M HCl and 0.5 M H_2SO_4

Medium	Conc. (v/v%)	E_a (kJ mol^{-1})	A	ΔH^* (kJ mol^{-1})	ΔS^* (J $mol^{-1}K^{-1}$)
1 M HCl	Blank	57.25	$3.58X10^{10}$	54.60	-44.77
	1	98.52	$7.94X10^{16}$	95.90	76.73
	2	102.55	$2.89X10^{17}$	99.90	87.47
	3	103.03	$3.16X10^{17}$	100.0	88.20
	4	103.87	$3.87X10^{17}$	101.0	89.88
	5	105.45	$6.32X10^{17}$	103.0	93.88
0.5 M H_2SO_4	Blank	30.96	8167704	28.30	-114.51
	1	43.64	$4.04X10^{8}$	41.00	-82.05
	2	44.06	$4.47X10^{8}$	41.40	-81.22
	3	46.42	$8.92X10^{8}$	43.80	-75.48
	4	46.54	$8.91X10^{8}$	43.90	-75.49
	5	47.62	$1.23X10^{9}$	45.00	-72.80

Adsorption isotherms

Mechanism of corrosion inhibition between inhibitor molecules and mild steel metal was illustrated using adsorption isotherms. Several adsorption isotherms like Langmuir, El-Awady, Frumkin, Temkin, Freundlich, and Flory-Huggins were considered for the study. The best suitable isotherm was detected using the value of the correlation coefficient (R^2).

From the values of R^2 in Fig. 3.6, it can be seen that Langmuir adsorption isotherm is the best suitable one for the adsorption of ICE on mild steel. The ΔG^0_{ads} calculated for ICE is -32.88 and -29.58 kJ/mol in 1 M HCl and 0.5 M H_2SO_4, respectively, showing that an electrostatic and chemical interaction exists between the inhibitor and the charged metal surface. ICE is composed of various organic compounds. The significant component of *Ixora coccinea* leaves is ixorene. Adsorption of all the ICE components on the mild steel surface may be attributed to the inhibitive action of the extract. Fig. 3.7 represents the predominant interaction of the significant component ixorene with the mild steel surface. By transferring electrons from the oxygen atom

present in -OH group and the interaction through the double bonds, ixorene molecules can be adsorbed onto the mild steel surface.

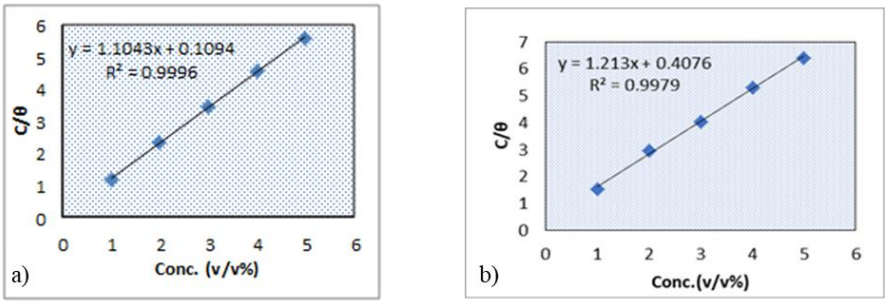

Fig. 3.6: Langmuir adsorption isotherm of ICE on mild steel in a) 1 M HCl b) 0.5 M H_2SO_4 at room temperature

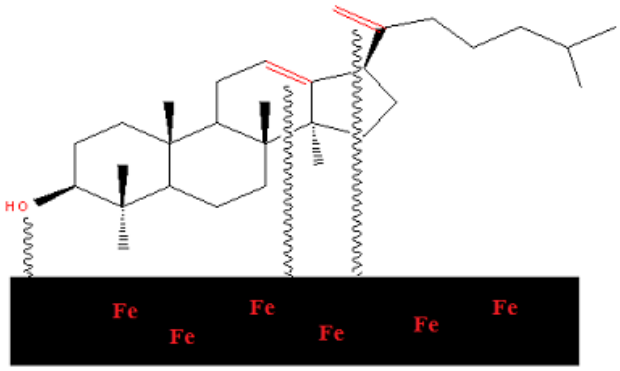

Fig. 3.7: Interaction diagram between ixorene and mild steel surface in acid media

UV-Visible spectroscopy

Metal-inhibitor interaction can be further established by studying UV-Visible spectroscopy. UV-Visible spectra were plotted for a) 5 ppm ICE, b) 5 ppm metal salt solution and c) equal proportions of the metal salt and ICE (Fig. 3.8). The UV spectrum of ICE exhibits a maximum absorbance of 2.045 at 666 nm. There is a sharp decrease in the intensity of ICE after binding with all the metal salts under study. In the case of $CoCl_2$, the maximum absorbance of 0.874 at 666 nm shows 57% decrease in the intensity after binding. In the case of chromium (III) acetate, the maximum absorbance of 1.208 at 666 nm exhibits 40% decrease in the intensity after binding. NaCl and Mn(II) acetate show almost the same reduction in intensity (51%) at 666 nm. Zn(II) acetate and Fe(III) chloride exhibit 1.053 and 1.018 at 666 nm, respectively indicates 50% decrease in

intensity. A significant reduction in intensity (58%) was observed in Cu(II) acetate as a maximum absorbance of 0.857 at 666 nm. This quenching may account for the strong affinity of ICE towards metal salts[146]. Thus, UV-Visible spectral studies prove the metal binding ability of ICE molecules.

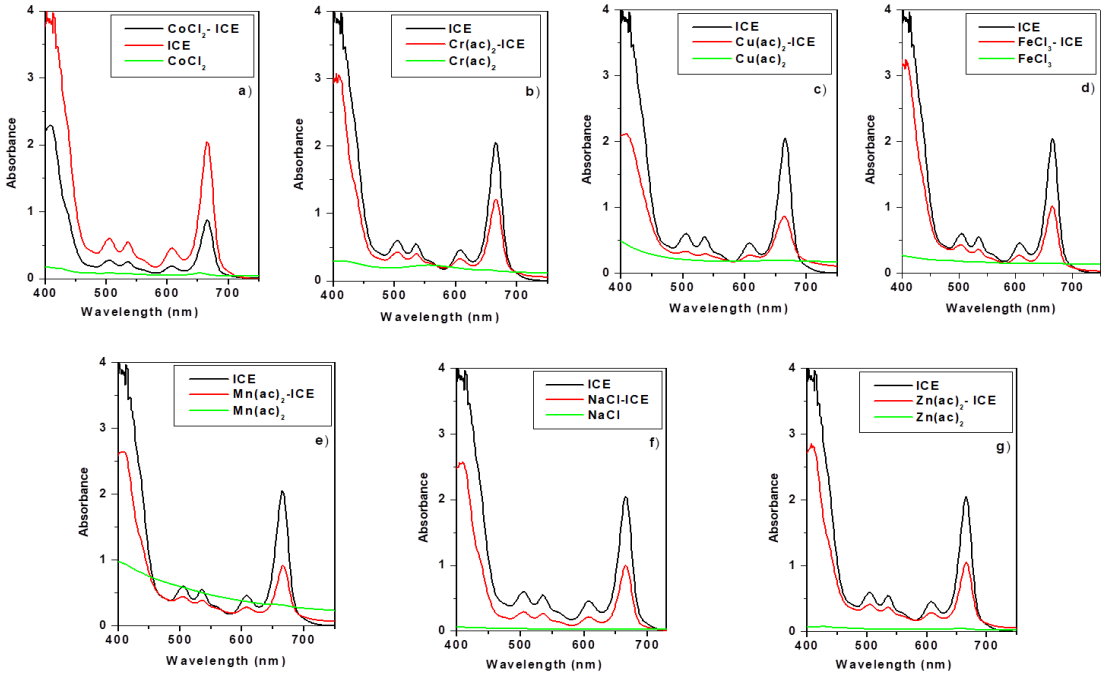

Fig. 3.8: UV spectra of a) ICE, $CoCl_2$ and ICE.$CoCl_2$ b) ICE, $Cr(ac)_2$ and ICE.$Cr(ac)_2$ c) ICE, $Cu(ac)_2$ and ICE.$Cu(ac)_2$ d) ICE, $FeCl_3$ and ICE.$FeCl_3$ e) ICE, $Mn(ac)_2$ and ICE.$Mn(ac)_2$ f) ICE, NaCl and ICE.NaCl g) ICE, $Zn(ac)_2$ and ICE.$Zn(ac)_2$

Electrochemical impedance spectroscopy

The equivalent circuit employed in this study is Randle's circuit (Fig. 1.8). It includes solution resistance R_s, charge transfer resistance R_{ct} and double layer capacitance C_{dl}. The deformities on the metal surface cause deviations from the ideal dielectric property of the metal. So, a constant phase element (Z) is preferred to C_{dl}[147].

$$Z = Q^{-1}(j\omega)^{-n} \qquad (51)$$

where Q is the measure of constant phase element, n is the power of the magnitude of constant phase element, ω is the angular frequency, and j is the imaginary unit. Based on the values of n, Z may be a resistance value.

Nyquist and Bode plots of mild steel without and with the inhibitor ICE using various concentrations (1-5 v/v %) in 1 M HCl and 0.5 M H_2SO_4 at room temperature are shown in Fig. 3.9 & Fig. 3.10. In Nyquist plots, it was seen that the low-frequency region is plotted to a straight line, and the high-frequency region is plotted to a semi-circle. The slight fall in the semi-circular plot may be ascribed to the heterogeneous and roughness of the mild steel. The straight-line portion represented the diffusion from the solution[148]. As the concentration of ICE is raised, the size of the loop also increases. This can be ascribed to the increase in the impedance of inhibited mild steel. The efficiency also increases in the process.

Table 3.5: Impedance parameters of mild steel in 1 M HCl and 0.5 M H_2SO_4 with and without ICE

Conc. (v/v%)	1 M HCl			0.5 M H_2SO_4		
	R_{ct} (Ωcm^2)	C_{dl} (μFcm^{-2})	η_{EIS}%	R_{ct} (Ωcm^2)	C_{dl} (μFcm^{-2})	η_{EIS}%
Blank	15.7	78.8	-	18.1	47.4	-
1	69.7	57.4	77.47	20.3	50.5	10.83
2	73.9	49.6	78.74	37.4	39.0	51.56
3	86.4	49.7	81.82	44.1	36.9	58.93
4	150	48.5	89.53	85.5	28.3	78.83
5	186	43.6	91.55	187	3.43	90.33

Impedance data obtained from the above equivalent circuit for both media are given in Table 3.5. On analyzing the data in Table 3.5, it has been noted that R_{ct} values were increased on the addition of ICE. It may be due to the increase in the rate of adsorption of ICE on the metal surface. As the concentration of inhibitor increases, double-layer capacitance (C_{dl}) decreases, which indicates that the thickness of the electrical double layer increases with respect to the concentration. This is due to the adsorption of inhibitor molecules on the mild steel surface[149]. The maximum inhibition

efficiency of 91.55% was seen at 5% concentration of ICE in 1 M HCl and 90.33% in 0.5 M H_2SO_4 at the same ICE concentration. From the impedance parameters, it was clear that ICE acted as a suitable corrosion inhibitor in both acid media. This result was matched with weight loss measurements.

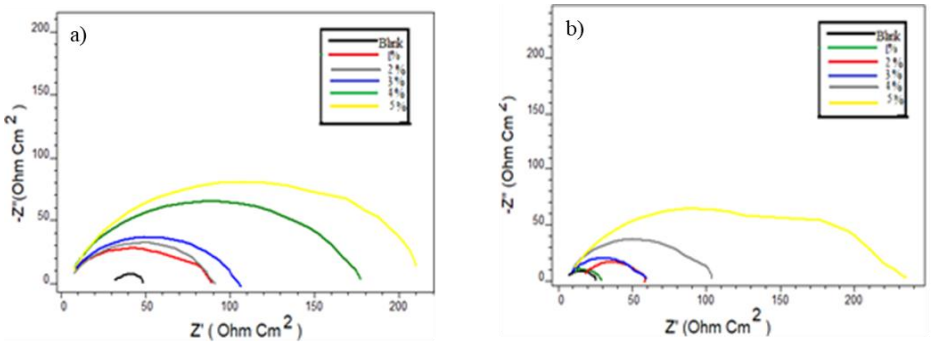

Fig. 3.9: Nyquist plots of mild steel with and without ICE in a) 1 M HCl and b) 0.5 M H_2SO_4

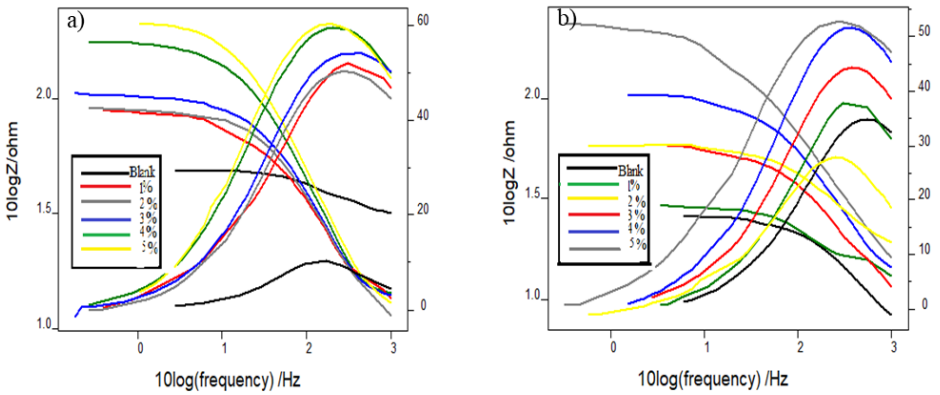

Fig. 3.10: Bode plots of mild steel with and without ICE in a) 1 M HCl and b) 0.5 M H_2SO_4

Potentiodynamic polarization studies

The potentiodynamic polarization data of mild steel in 1 M HCl and 0.5 M H_2SO_4 with and without ICE are given in Table 3.6, and corresponding Tafel plots are depicted in Fig. 3.11. Linear polarization curves are pictured in Fig. 3.12.

The potentiodynamic polarization data revealed that the greater the ICE concentration, the smaller is the corrosion current density (i_{corr}). The inhibition efficiency was also seen to increase. The inhibition efficiency of ICE for mild steel reached an upper limit of 93.67% in 1 M HCl solution and 87.02% in 0.5 M H_2SO_4 solution at higher

concentrations. From the slopes of Tafel plots, it is seen that both cathodic and anodic curves were influenced by the addition of various concentrations of ICE, which shows the mixed type inhibition character of ICE in both acids[150]. Linear polarization data were also reinforced with Tafel data.

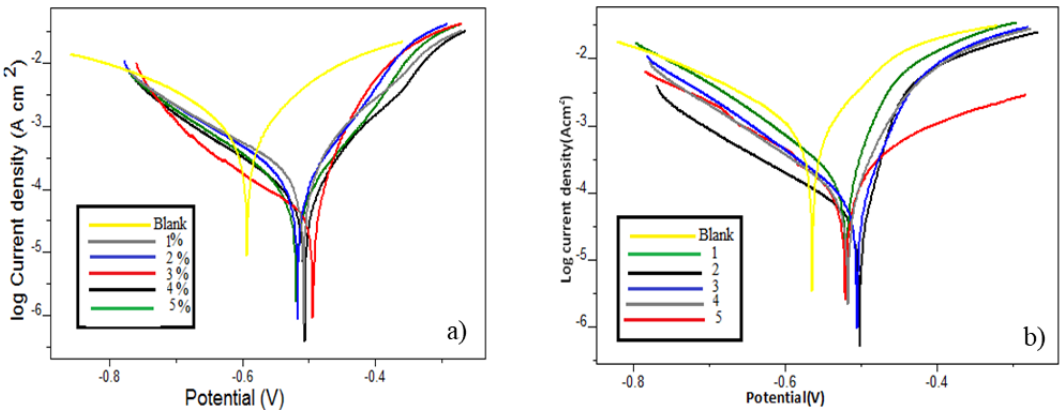

Fig. 3.11: a) Tafel plots of mild steel with and without ICE in a) 1 M HCl and b) 0.5 M H_2SO_4

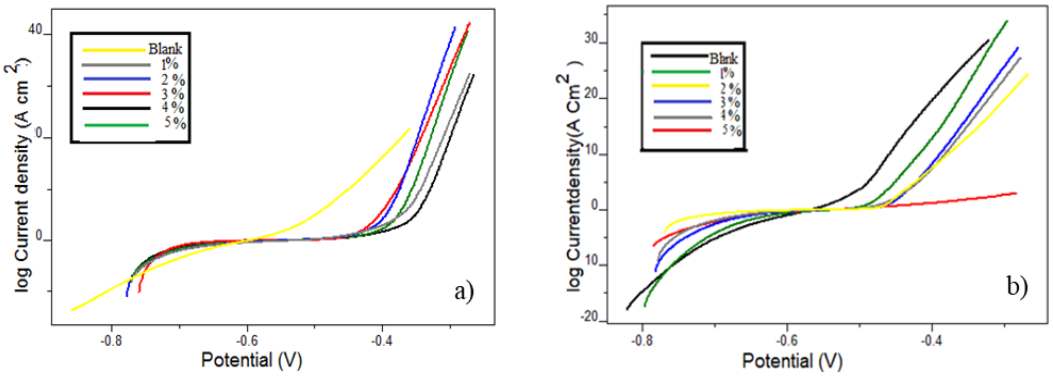

Fig. 3.12: Linear polarization plots of mild steel with and without ICE in a) 1 M HCl and b) 0.5 M H_2SO_4

Moreover, E_{corr} values of inhibited solution didn't vary noticeably (>85) regarding the blank solution. This trend was also assisted the mixed type inhibition character of ICE in acid media.

Electrochemical noise measurements

Fig. 3.13 represents the current noise for mild steel with and without various ICE concentrations (1, 3, 5 v/v %) in 1 M HCl and 0.5 M H_2SO_4. For inhibitor molecules, current and potential noise is lower than the uninhibited system. It was seen that

protecting power of ICE is increased as its concentration increases. Higher magnitude of potential noise signal of uninhibited acid media indicates appreciable localized metallic corrosion on the metal surface[151].

Table 3.6: Potentiodynamic polarization parameters of mild steel in 1 M HCl and 0.5 M H_2SO_4 with and without ICE

Medium	Conc. (v/v%)	Tafel data					Polarization data	
		E_{corr} (mV)	i_{corr} ($\mu A/cm^2$)	b_a (mV/dec)	$-b_c$ (mV/dec)	$\%\eta_{pol}$	R_p (ohm)	$\%\eta_{Rp}$
1 M HCl	Blank	-597.9	1240	166	221	-	33.14	
	1	-522.8	193.6	106	170	84.41	146.3	77.34
	2	-504.8	122.3	69	158	90.11	170.4	80.55
	3	-571.6	107.9	100	130	91.29	228.1	85.47
	4	-515.0	87.22	93	149	92.96	260.6	87.28
	5	-500.7	78.50	69	146	93.67	284.4	88.34
0.5 M H_2SO_4	Blank	-602.2	1616	184	193	-	25.3	
	1	-601.8	811.6	170	136	49.77	40.46	37.46
	2	-649.6	415.5	199	156	74.28	79.39	68.13
	3	-588.9	368.4	142	128	77.20	91.42	72.32
	4	-587.4	306.9	138	137	81.00	97.12	73.94
	5	-555.7	209.6	221	142	87.02	179.3	85.88

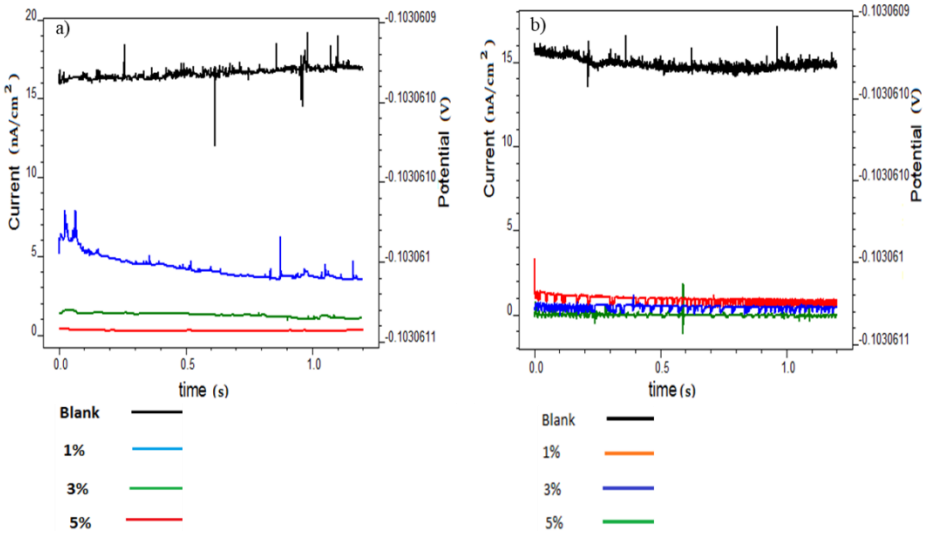

Fig. 3.13: Current noise plots of mild steel with and without ICE in a) 1 M HCl b) 0.5 M H_2SO_4

Power spectral density (PSD) was furnished by the frequency domain analysis of noise parameters. PSD plots in Fig. 3.14 revealed that the magnitude of the signals is higher for blank metal than metals with various concentrations of ICE (1, 3, 5 v/v %) in 1 M HCl and 0.5 M H_2SO_4. This indicated a considerable amount of localized corrosion on

the mild steel surface in the absence of ICE. As the concentration of ICE become greater, the magnitude of the noise signal decreases, showing its anti-corrosion property against mild steel in both acid solutions.

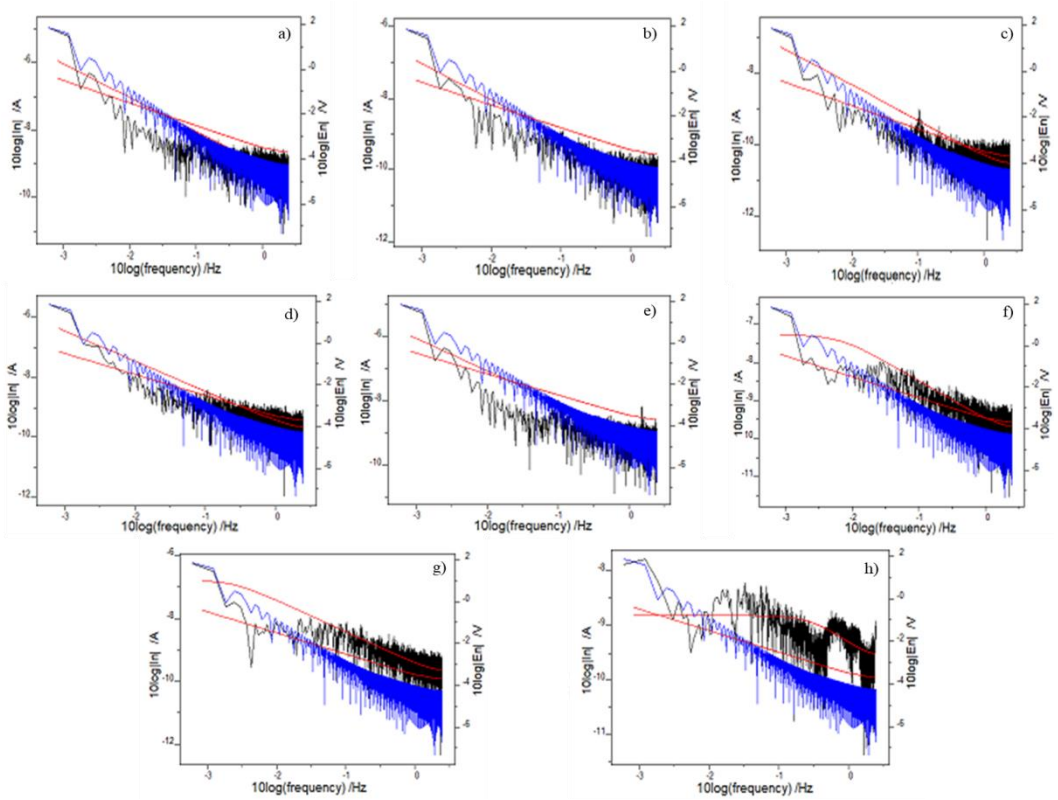

Fig. 3.14: Power spectral density plots of mild steel in 1 M HCl a) without ICE b) 1% ICE c) 3% ICE d) 5% ICE; Power spectral density plots of mild steel in 0.5 M H_2SO_4 e) without ICE f) 1% ICE g) 3% ICE h) 5% ICE

The extent of pitting corrosion can be understood by the pitting index value. Fig. 3.15 depicts pitting index curves for mild steel corrosion in 1 M HCl and 0.5 M H_2SO_4 in the presence and absence of various concentrations of ICE. Pitting index value of the mild steel in the blank solution of HCl was found to be minor, whereas its value was increased by adding 1, 3 and 5 v/v% ICE concentration and attained a higher value at the highest concentration under study. Similarly, in the blank experiment using 0.5 M H_2SO_4 solution, the pitting index value was lower and increased with various ICE concentrations. The high value of the pitting index indicated the strong resistance power of ICE molecules against pitting corrosion of mild steel in 1 M HCl and 0.5 M H_2SO_4[152].

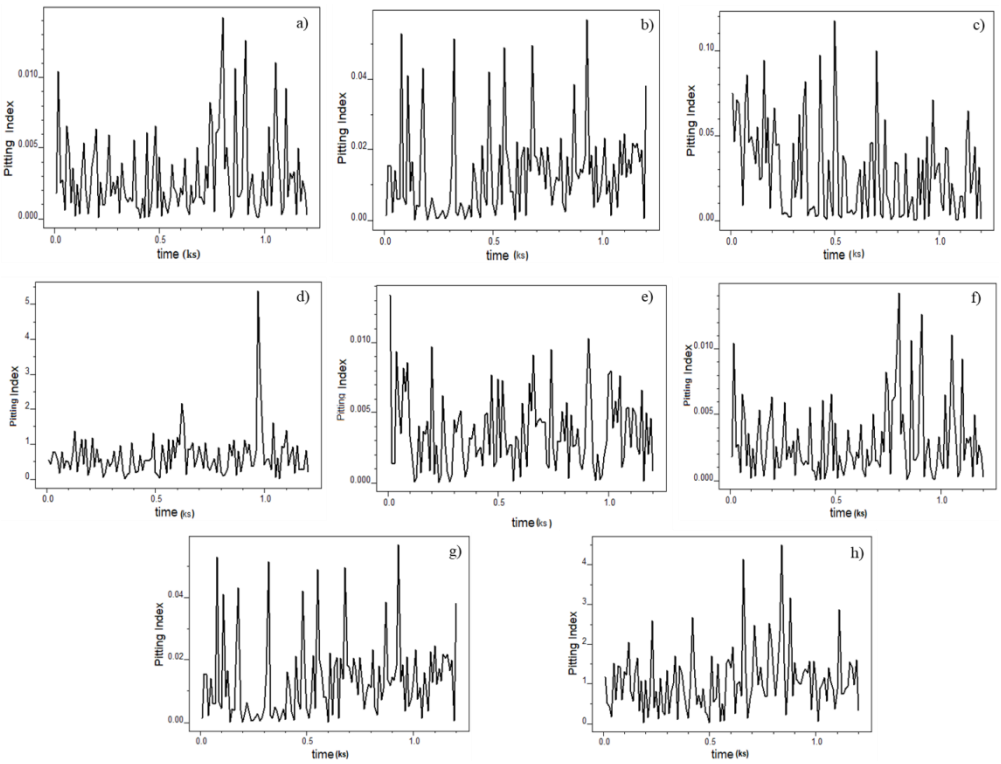

Fig. 3.15: Pitting index curves of mild steel in 1 M HCl a) without ICE b) 1% ICE c) 3% ICE d) 5% ICE; Pitting index curves of mild steel in 0.5 M H_2SO_4 e) without ICE f) 1% ICE g) 3% ICE h) 5% ICE

Scanning electron microscopy

To strengthen the understanding of the mechanism of ICE on the surface of mild steel, morphological studies were performed by taking the SEM images of metal coupons[153]. Fig. 3.16 a) shows the SEM picture of smoothening mild steel metal. Fig. 3.16 b, c, d, e shows the surface of mild steel metal after immersion in 1 M HCl and 0.5 M H_2SO_4, respectively, without and with ICE. The SEM images clearly exhibited that the surface is severely damaged in the absence of the inhibitor ICE. It could be seen that the surface corrosion is getting reduced in HCl solution with ICE and the surface is more smooth and perfect in it than H_2SO_4 solution. So it can be confirmed that ICE acts as an excellent green corrosion inhibitor in acidic media.

Quantum mechanical calculations

Quantum mechanical parameters like E_{HOMO}, E_{LUMO}, ΔE, Ionisation energy (I), Electron affinity (A), Chemical potential (μ), electronegativity (χ), hardness (η) and the

number of transferred electrons (ΔN) of ixorene are tabulated in Table 3.7. The HOMO and LUMO pictures of ixorene are depicted in Fig. 3.17. The ΔE value was found to be low for ixorene, which indicated that ICE has remarkable inhibition efficiency. The low ΔE value 4.884 eV of ixorene can be attributed to the low energy requirement for transferring electrons from HOMO of ixorene to the vacant orbitals of Fe. The high E_{HOMO} value (3.347) and low E_{LUMO} value (1.537) of ixorene were facilitated the strong interaction of inhibitor molecules on the mild steel surface[154]. The number of electrons transferred (ΔN) from inhibitor to metal can be calculated using equation (49) by assuming that chemical hardness and electronegativity of Fe metal is zero and 7 eV, respectively. The ΔN value of ixorene calculated as 1.2479 pointed out the interaction between donor-acceptor molecules. This, in turn, proved agreement between quantum mechanical calculations and experimental results.

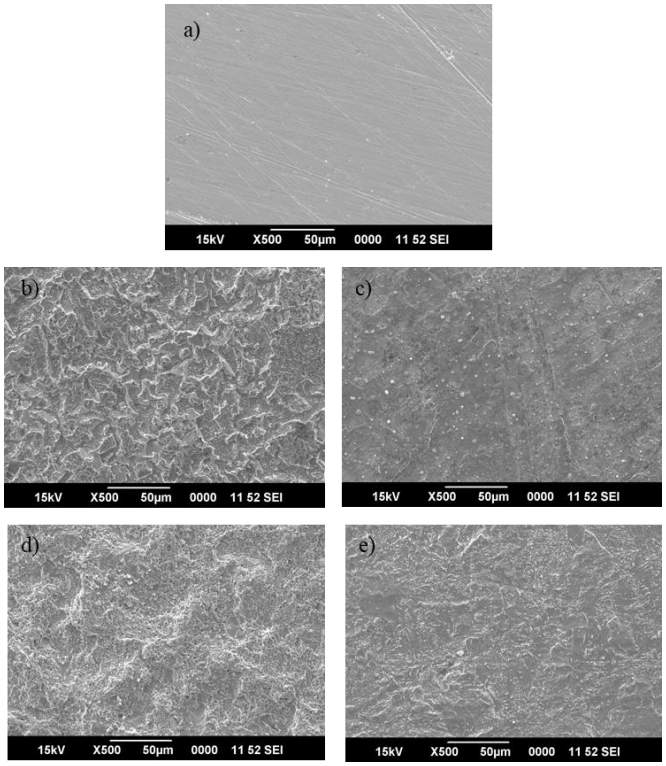

Fig. 3.16: SEM images of the surface of mild steel a) bare b) in 1 M HCl c) in 1 M HCl with ICE d) in 0.5 M H_2SO_4 e) in 0.5 M H_2SO_4 with ICE

Table 3.7: Quantum mechanical parameters (in eV) of ixorene

E_{HOMO}	E_{LUMO}	ΔE	I	A	μ	χ	η	ΔN
-3.347	1.537	4.884	3.347	-1.537	-0.905	0.905	2.442	1.2479

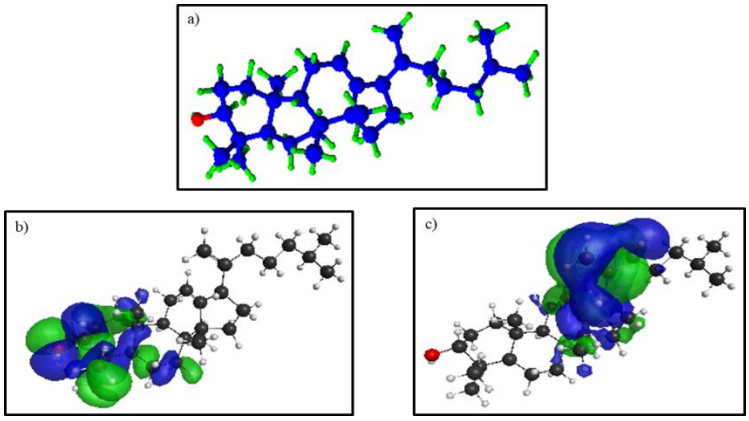

Fig. 3.17: a) Optimized geometry, b) HOMO and c) LUMO of ixorene

Statistical analysis

❖ ***Optimization of factors for inhibition efficiency (IE%)***

Screening experiments displayed that temperature and ICE concentration had a remarkable effect on the corrosion inhibition efficiency. So they were chosen as parameters in this investigation. Weight loss studies revealed that corrosion inhibition efficiency was upgraded in HCl medium than in H_2SO_4 medium. That motivated us to consider HCl solution as an acid medium. The design structure showing experimental results and predicted response for the test factors of central composite design (CCD) are summarised in Table 3.8.

A total of 9 experimental runs were performed in it. It was exhibited that corrosion inhibition efficiency improved tremendously with the increase in ICE concentration. The better inhibition efficiency that has been attained in this method was with 5 v/v% ICE concentration at 313 K working temperature. The proper combination of the two factors can be evaluated using RSM to get good inhibition efficiency. The

regression model satisfied the test factors and the inhibition efficiency shown in the quadratic equation (52).

$$IE = 10740 - 64.7X_1 + 32.8X_2 + 0.0976X_1^2 - 0.632X_2^2 - 0.075X_1X_2 \quad (52)$$

Using this quadratic equation, Analysis of variance (ANOVA) was then performed. ANOVA results having a significance level of 95% are displayed in Table 3.9.

Table 3.8: Experimental and predicted IE% from the weight loss measurements and CCD

Temp (X_1)	Conc (X_2)	IE%		Residual
		Experimental	Predicted	
313	5	88.93	81.4994	7.4306
333	1	37.39	24.8594	12.5306
313	1	69.18	59.3674	9.8126
333	5	51.14	40.9914	10.1486
313	3	86.27	72.9614	13.3086
323	5	66.03	51.4854	14.5446
333	3	46.2	35.4534	10.7466
323	1	41.85	32.3534	9.4966
323	3	52.38	44.4474	7.9326

Table 3.9: Analysis of variance for corrosion inhibition efficiency

Source	DF	Adj SS	Adj MS	F-Value	P-Value
Model	5	2770.86	554.17	37.43	0.007
Linear	2	2558.35	1279.18	86.39	0.002
Temp	1	2003.85	2003.85	135.33	0.001
ICE Conc	1	554.50	554.50	37.45	0.009
Square	2	203.51	101.76	6.87	0.076
Temp*Temp	1	190.71	190.71	12.88	0.037
ICE Conc*ICE Conc	1	12.80	12.80	0.86	0.421
2-Way Interaction	1	9.00	9.00	0.61	0.492
Temp*ICE Conc	1	9.00	9.00	0.61	0.492
Error	3	44.42	14.81		
Total	8	2815.29			

DF: degrees of freedom, Adj SS: adjusted sum of squares, Adj MS: adjusted mean of squares, F: Fischer's F-test value, P: probability

The noticeable parameter is the P-value in this Table which points out the significance of a factor on response. The degree of essentialness (α) was 0.05. It revealed

that the value of P was smaller than 0.05 for the two linear and one of the square terms. Among linear terms, the temperature was more significant than the ICE concentration. Square term of temperature is the only considerable term involved in squared terms. Pareto chart[155] (Fig. 3.18) also illustrates the significance of linear and non-linear terms on inhibition efficiency. The linear terms, such as temperature and ICE concentration, have a remarkable effect on the inhibition efficiency. In contrast, the square term of temperature has less influence on the response. Square term of ICE concentration and the two-way interaction term X_1X_2 have little effect on inhibition efficiency, same as ANOVA.

Accuracy of this quadratic model can be proved by Residual plots, as shown in Fig. 3.19. Normal probability plot conveyed that the residual distribution is normal since the residuals were merged into the straight line. Histogram of residuals represented that the residuals are distributed in a symmetric manner at all frequencies[156]. Versus order plot exhibited that observed runs were scattered within the fixed area of residuals which confirmed the accuracy of the regression model.

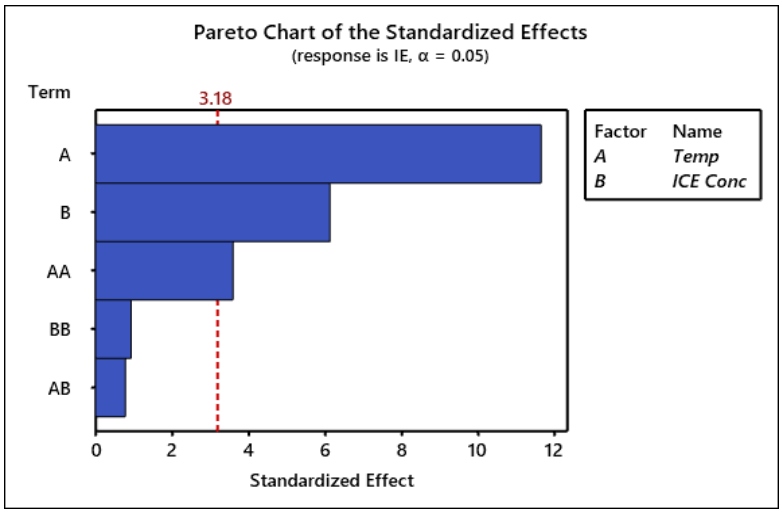

Fig. 3.18: Pareto chart of the standardized effects of mild steel

The perfect model for experimental results was inferred by agreeing to R^2 and R^2(adj) values to unity. In the present work, the R^2 and R^2(adj) values were 0.9842 and

0.9579, respectively, showing the most suitable predicted model for experimental values. Therefore, the results can be accurately analyzed by the model.

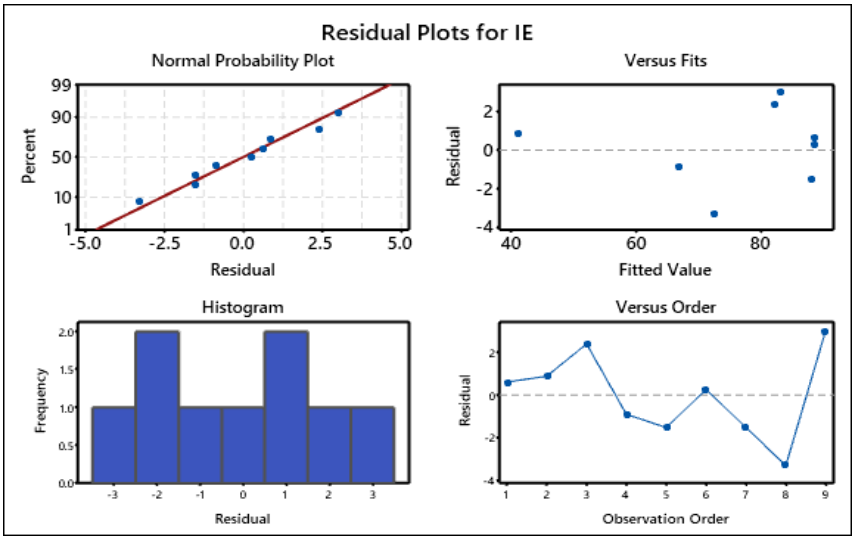

Fig. 3.19: Residual plots for inhibition efficiency

Main effects plots elucidate the effect of factors on the response. Fig. 3.20 shows the main effects plots for the fitted means of inhibition efficiency. Fig. 3.20 exhibited the highest inhibition efficiency reached at 5 v/v% concentration of ICE and at 313 K working temperature. At elevated temperatures, the kinetic energy of the inhibitor molecules increased, and the number of collisions between the molecules also enhanced. When the temperature goes up, the adsorbed film formed by the inhibitors on the metal surface is destroyed and thus, inhibition efficiency decreases. Whereas inhibition power of ICE and its concentration is directly proportional to each other. The corrosion rate was lowered in the presence of ICE molecules. As the concentration is added, the adsorption on the metal surface is enhanced and thus exhibits increased inhibition efficiency.

Contours and 3-D surface plots show the interconnection between the factors[157] and IE (%), represented in Fig. 3.21. It was worth mentioning that the inhibition efficiency goes up with ICE concentration for a particular temperature. But, inhibition efficiency and temperature are inversely proportional to each other. This relationship can

be attributed to the physical interaction between ICE molecules and the mild steel surface.

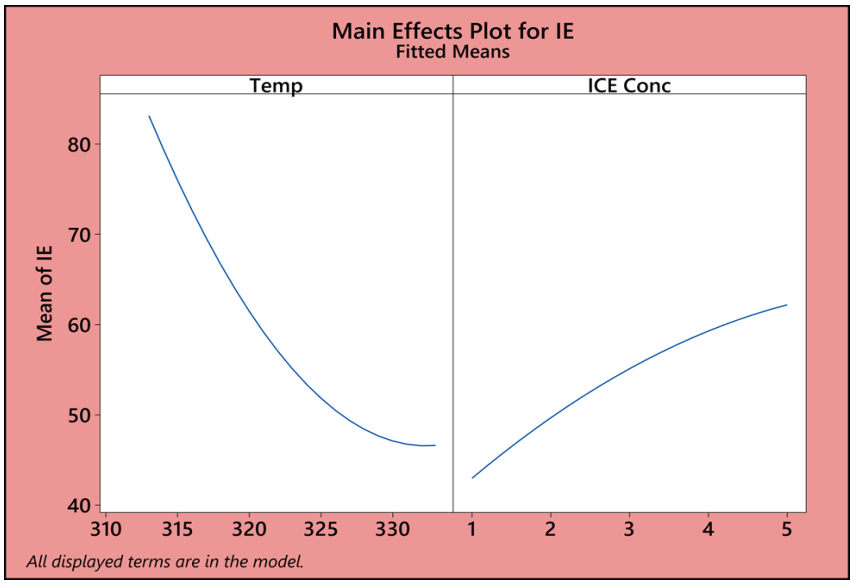

Fig. 3.20: Main effects plots for inhibition efficiency of mild steel in HCl medium

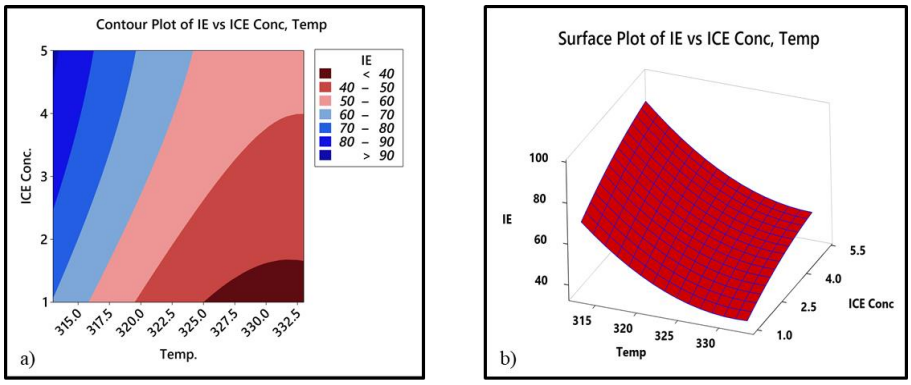

Fig. 3.21: a) Contour and b) 3-D surface plot for inhibition efficiency

❖ ***Response optimization***

Well organized quadratic equation (52) was used to optimize the independent factors such as temperature and ICE concentration to derive maximum IE (%). For the most feasible response, the desirability function method was applied. Response optimization plot for IE is exhibited in Fig. 3.22. The optimized conditions for best IE (%) identified were temperature (313 K) and ICE concentration (5 v/v %) for the HCl environment, and the corresponding predicted IE was 91.73 %, as given in Fig. 3.22.

Confirmation tests helped to verify the recurrence of the experimental outcomes and approve the accuracy of the model.

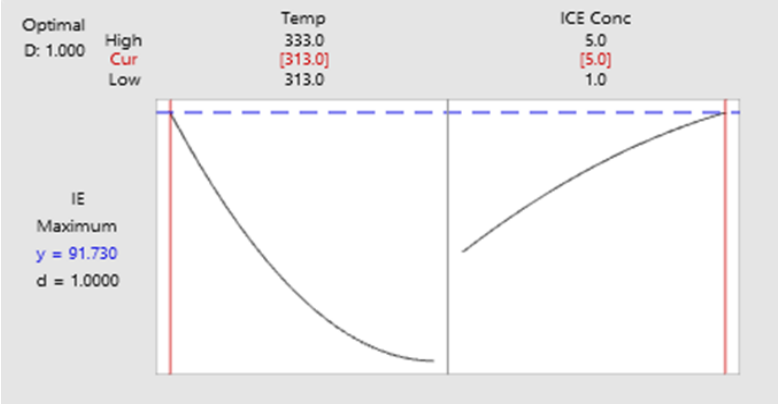

Fig. 3.22: Response optimization plot for inhibition efficiency

Conclusions

- *Ixora coccinea* leaf extract (ICE) acts as an efficient green inhibitor for corrosion of mild steel in 1 M HCl and 0.5 M H_2SO_4 medium. As the concentration of the inhibitor increases, the protecting power also increases. Temperature and inhibition efficiency are in inverse proportional relation
- On comparing, ICE in HCl medium shows higher efficiency than H_2SO_4 medium.
- Probability for the complexation of ICE with metal ions is confirmed by UV-Visible spectral studies.
- Electrochemical impedance analysis exhibits that charge transfer resistance increases and double layer capacitance decreases according to ICE concentration.
- Potentiodynamic polarization measurements exhibit mixed type character of ICE towards corrosion inhibition.
- Quantum mechanical calculations of ixorene, a major component present in ICE, supports the inhibition power of ICE.
- The adsorption studies of ICE shows that it obeys Langmuir adsorption isotherm.
- Surface morphological studies also confirmed the protecting power of ICE.

- Statistical analysis also verified the effect of temperature and concentration on inhibition efficiency of ICE towards mild steel corrosion.

CHAPTER 4

CROTON PERSIMILIS EXTRACT: NATURAL CORROSION INHIBITOR FOR MILD STEEL IN ACID MEDIA

This chapter presents preliminary phytochemical screening, metal-binding ability and corrosion inhibition properties of ethanolic leaf extract of *Croton persimilis* (CPE). *Croton persimilis* belongs to Euphorbiaceae family. The anti-corrosion effect of CPE in 1 M HCl and 0.5 M H_2SO_4 for mild steel has been explored by physicochemical, electrochemical and surface morphological studies. The major constituents present in the extract are neocrotocembraneic acid and stigmasterol[158]. There are various other minor constituents comprised, possessing either synergistic or antagonistic effects. Nevertheless, in this work, only significant components are regarded as the compounds accountable for corrosion inhibition. Major components of *Croton persimilis* leaves, neocrotocembraneic acid and stigmasterol have been subjected to quantum mechanical studies to evaluate the plant leaves' anti-corrosion effect. Structures of neocrotocembraneic acid and stigmasterol are shown in Fig. 4.1.

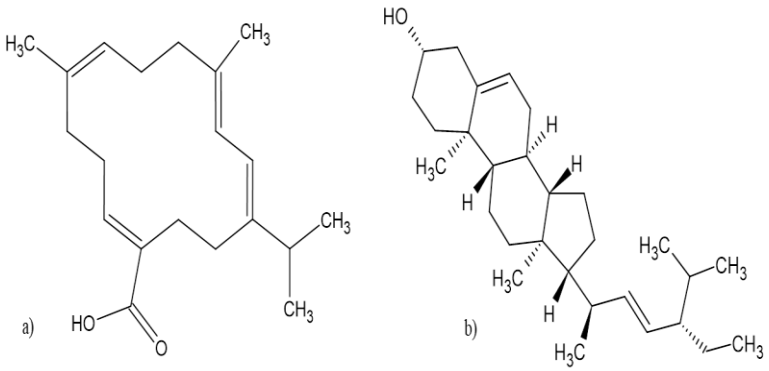

Fig. 4.1: Structures of a) neocrotocembraneic acid
b) stigmasterol

Croton persimilis

Results and Discussions

Phytochemical screening of CPE

The presence of various phytochemicals in CPE confirmed using different tests, and the results are summarised in Table 4.1

Table 4.1: Phytochemical screening of CPE

Sl. No.	Compounds	Tests	Results
1	Alkaloids	Mayers reagent	−−
2	Steroids	Salkowaski's test	++
3	Phenolic compounds	Potassium ferrocyanide test	++
4	Flavanoids	Sodium hydroxide test	++
5	Saponins	Froth test	++
6	Tannins	Lead acetate test	−−
7	Cardiac glycosides	Conc. sulphuric acid test	++
8	Coumarin	Alcoholic NaOH test	++
9	Quinones	Conc. sulphuric acid test	++

++ (present), − − (Absent)

FTIR spectroscopy

Predominant functional groups present in CPE were recognized by recording FTIR spectroscopy of CPE, shown in Fig. 4.2.

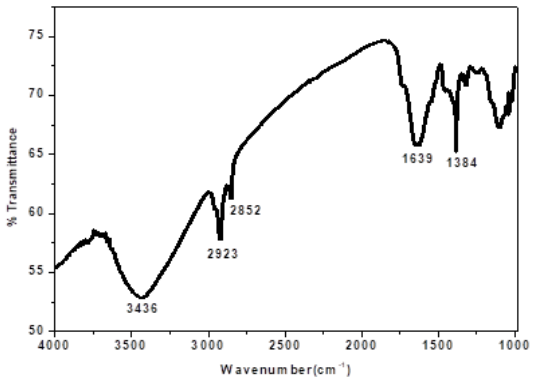

Fig. 4.2: FTIR spectrum of CPE

Broadband at 3436 cm^{-1} represents O-H stretching vibration. The two sharp peaks at 2923 cm^{-1} and 2852 cm^{-1} correspond to alkyl C-H stretching bonds. Alkyl and aromatic C=C stretching vibrations are indicated by the bands at 1639 cm^{-1} and

1384 cm^{-1}, respectively. The other prominent peaks reveal the existence of other constituents present in the CPE.

Weight loss measurements

❖ ***Effect of concentration***

Weight loss measurements reckon corrosion inhibition efficiency (η%) and corrosion rate (υ) on mild steel in acidic media such as 1 M HCl and 0.5 M H_2SO_4 with and without various concentrations (1-5 v/v %) of CPE have been recorded in Table 4.2. It was evident that an increment in inhibition capacity occurs in increasing the inhibitor concentration for both the acid solutions. It was observed that CPE is an excellent corrosion inhibitor in 0.5 M H_2SO_4, having maximum inhibition efficiency at 5 v/v% as 98.09%. In HCl medium, it was attained an extreme efficiency of 86.45% at 5 v/v%. The higher inhibition power in H_2SO_4 than HCl may attribute to the sufficient availability of metal sites on the surface of mild steel. It is because of the lesser adsorption of sulfate ions on the metal surface. Hence, the number of adsorbed organic molecules of inhibitor CPE on mild steel is more in the H_2SO_4 medium.

Table 4.2: Weight loss measurements of mild steel with and without CPE in 1 M HCl and 0.5 M H_2SO_4 at room temperature for 24 hrs

Conc. (v/v %)	Corrosion rate (mm/yr)		Inhibition efficiency (η%)	
	1 M HCl	0.5 M H_2SO_4	1 M HCl	0.5 M H_2SO_4
Blank	3.95	35.57	-	-
1	1.21	3.03	69.3	91.45
2	0.88	1.45	77.6	95.90
3	0.66	1.03	83.2	97.08
4	0.55	0.91	85.8	97.42
5	0.53	0.67	86.4	98.09

❖ ***Effect of temperature***

Temperature studies on the corrosion process have a crucial role in analyzing the stability of adsorbed film of inhibitor molecules on the mild steel surface. The extent of

decay is dependent on temperature and becomes severe in acidic media. In the present investigation, the influence of temperature on the corrosion inhibition was carried out by weight loss measurements for 24 hrs in 1 M HCl and 0.5 M H_2SO_4 by adding different concentrations of CPE at a temperature range of 303-333 K. The variation of corrosion inhibition efficiency with temperature is tabulated in Table 4.3. It is graphically represented in Fig. 4.3.

Table 4.3: Corrosion rate (υ) and inhibition efficiency (η%) of CPE in 1 M HCl and 0.5 M H_2SO_4 at different temperatures for 24 hrs

Medium	Conc. (v/v %)	υ (303 K)	η% (303 K)	υ (313 K)	η% (313 K)	υ (323 K)	η% (323 K)	υ (333 K)	η% (323 K)
1 M HCl	Blank	3.95	-	13.11	-	22.05	-	31.77	-
	1	1.21	69.36	8.07	38.44	14.06	36.23	23.41	26.31
	2	0.88	77.72	3.38	74.21	8.32	62.26	16.36	48.50
	3	0.66	83.29	2.19	83.29	5.94	73.06	12.56	60.46
	4	0.55	86.07	1.88	85.65	4.66	78.86	11.92	62.48
	5	0.53	86.58	1.76	86.57	4.49	79.63	11.69	63.20
0.5 M H_2SO_4	Blank	35.57	-	58.27	-	86.25	-	106.2	-
	1	3.03	91.48	15.7	73.05	33.39	61.28	48.95	53.93
	2	1.45	95.92	11.05	81.03	27.54	68.06	38.47	63.79
	3	1.03	97.10	6.27	89.23	18.94	78.04	28.65	73.03
	4	0.91	97.44	2.05	96.48	12.36	85.66	22.59	78.74
	5	0.67	98.11	0.74	98.73	7.92	90.81	16.52	84.45

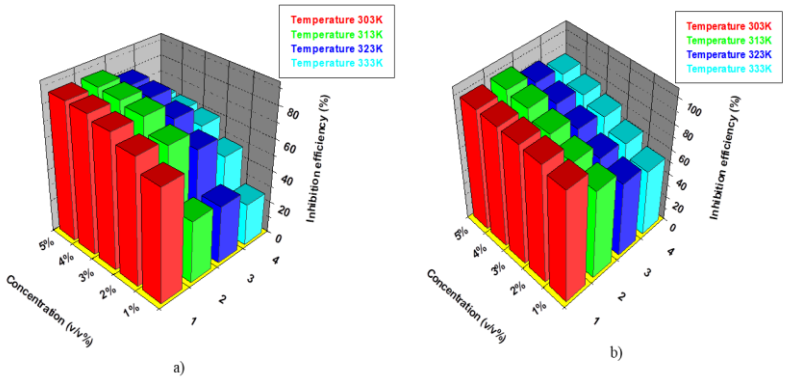

Fig. 4.3: Variation in inhibition efficiency of CPE in a) 1 M HCl b) 0.5 M H_2SO_4 at elevated temperatures

Fig. 4.3 expressed that the corrosion inhibition power of CPE decreased with an increase in temperature for the same concentration. This trend is because of the

destruction of the adsorbed film on the metal surface when the temperature rises. Protecting power of CPE in 0.5 M H_2SO_4 was 84.45% at extreme concentration and temperature understudy, whereas in 1 M HCl, it was decreased to 63.20% at the same concentration and temperature.

log K vs 1/T plots for mild steel coupons in acid solutions with and without CPE can be drawn with the help of Arrhenius equation (41), and they are shown in Fig. 4.4 a) and Fig. 4.5 a). From the curves' slope, the activation energy for the metal corrosion in 1 M HCl and 0.5 M H_2SO_4 was derived. Thermodynamic parameters such as enthalpy of activation (ΔH^*) and entropy of activation (ΔS^*) were calculated using transition state theory. Plots of log K/T vs 1/T for metal corrosion in 1 M HCl and 0.5 M H_2SO_4 are shown in Fig. 4.4 b) and Fig. 4.5 b). The calculated values of properties such as activation energy (E_a), enthalpy of activation (ΔH^*) and entropy of activation (ΔS^*) are given in Table 4.4. On comparing the activation energy of corrosion with and without CPE, it was clear from the table that its value is higher in the presence of CPE. In contrast, it is lower in the absence of CPE for both acid solutions. The positive value of enthalpy revealed the endothermic behaviour of metal corrosion reactions. On close examination of E_a and ΔH^* values at a maximum concentration of 5 v/v%, it was clear that metal corrosion has experienced higher activation energy and enthalpy of activation in 0.5 M H_2SO_4 medium. This data dramatically justifies CPE molecules being more strongly adsorbed on the mild steel surface in 0.5 M H_2SO_4 than 1 M HCl. As the concentration of CPE increases, the values of ΔS^* also increases. Entropy of activation for corrosion was seen to be positive in the presence of CPE, which indicated that the activated complex's randomness is more than the reactants in both acid solutions. But the increase in randomness was more facilitated in H_2SO_4 than HCl medium.

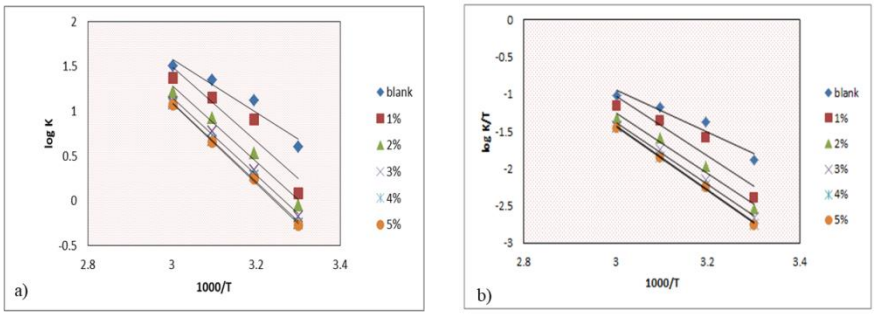

Fig. 4.4: Arrhenius plots of a) log K vs 1000/T b) log K/T vs 1000/T with and without CPE in 1 M HCl

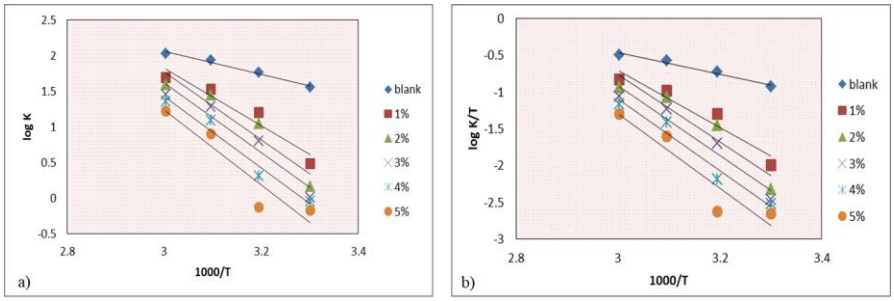

Fig. 4.5: Arrhenius plots of a) log K vs 1000/T b) log K/T vs 1000/T with and without CPE in 0.5 M H_2SO_4

Table 4.4: Thermodynamic parameters of mild steel corrosion with and without CPE in 1 M HCl and 0.5 M H_2SO_4

Medium	Conc. (v/v %)	E_a (kJ mol^{-1})	A	ΔH^* (kJ mol^{-1})	ΔS^* (J $mol^{-1}K^{-1}$)
1 M HCl	Blank	57.24	3.58×10^{10}	54.6	-44.7842
	1	79.91	1.04×10^{14}	77.3	17.68331
	2	81.42	1.10×10^{14}	78.8	22.01056
	3	82.71	1.29×10^{14}	80.1	23.29342
	4	85.14	2.76×10^{14}	82.5	27.56323
	5	85.80	3.40×10^{14}	83.2	27.67812
0.5 M H_2SO_4	Blank	30.96	8.17×10^{6}	28.3	-114.51
	1	76.98	7.62×10^{13}	74.3	18.94702
	2	91.02	1.06×10^{16}	88.4	59.97935
	3	93.66	1.94×10^{16}	91.0	65.01504
	4	95.95	2.88×10^{16}	93.3	68.28921
	5	100.14	8.34×10^{16}	97.5	77.13518

Adsorption isotherms

Adsorption isotherms provide authentic facts concerning the interaction between inhibitor molecules and mild steel. The mechanism of corrosion inhibition is blocking the rate of cathodic reaction or hindering the anodic metal dissolution or both by the adsorption of inhibitor molecules on the surface of the metal. Among various isotherms

such as Langmuir, El-Awady, Frumkin, Temkin, Freundlich and Flory-Huggins isotherms, the most suitable isotherm in both acid media was Langmuir isotherm, which was found by correlation coefficient (R^2). Langmuir adsorption isotherms of CPE on mild steel surface in 1 M HCl and 0.5 M H_2SO_4 at room temperature are shown in Fig. 4.6. R^2 values were seen to be very close to unity in both acids.

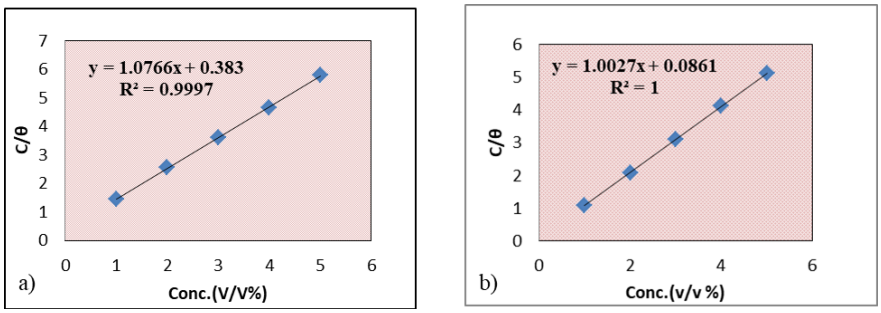

Fig. 4.6: Langmuir adsorption isotherm of CPE on mild steel in a) 1 M HCl b**)** 0.5 M H_2SO_4 at room temperature

ΔG^0_{ads} value determines the interaction between the charged molecule and the charged metal surface. In the present study, CPE on mild steel in 1 M HCl and 0.5 M H_2SO_4 exhibited ΔG^0_{ads} -29.73 and -33.47 $kJmol^{-1}$, respectively, indicating that CPE adsorbed on the metal surface by both electrostatic and chemical interaction[92].

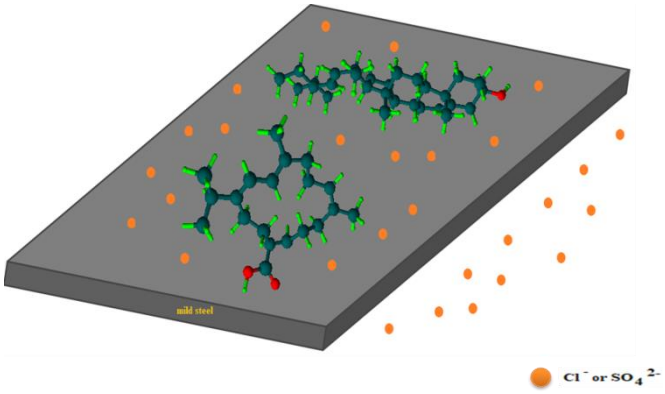

Fig. 4.7: Interaction diagram between CPE molecules and mild steel surface in acid media

Expected mechanism of corrosion inhibition of CPE on mild steel surface in acid is depicted in Fig. 4.7. Major components of CPE are neocrotocembraneic acid, stigmasterol. It may be suggested that the chief constituents of CPE adsorb on the metal

surface mainly by transferring electrons from oxygen atoms in –COOH and –OH functional groups and by the interaction with the unsaturated bonds.

UV-Visible spectroscopy

UV-Visible spectra were plotted to ascertain the metal-binding ability of CPE using various metal salt solutions shown in Fig. 4.8. UV spectrum of CPE exhibited a maximum absorbance of 0.279 at 404 nm and also an absorbance of 0.116 at 664 nm. There was a sharp decrease in CPE intensity after binding with all the metal salts used for the study. In $CoCl_2$, maximum absorbance of 0.165 at 402 nm showed 40% decrease in the intensity after binding. Chromium (III) acetate displayed maximum absorbance of 0.176 at 403 nm, which means 37% decrease in the intensity. For Mn(II) acetate maximum absorbance observed was 0.178 at 402 nm, which disclosed 36% decrease in the intensity after binding. NaCl and Zn(II) acetate showed a significant decrease in intensity as the maximum absorbance observed was 0.076 at 400 nm and 0.041 at 403 nm, respectively. Cu(II) acetate and Fe(III) chloride exhibit maximum absorbance of 0.039 at 662 nm and 0.026 at 661 nm, respectively. The decrease in intensity due to quenching may attribute to its strong affinity towards metal salts[146].

Electrochemical impedance spectroscopy

Analysis of impedance behaviour was conducted by an alternate current method such as electrochemical impedance spectroscopy, which helped evaluate current-potential responses at the metal/solution interface. Randle's circuit (Fig. 1.8) was acted as an equivalent circuit in the present work, including solution resistance R_s, charge transfer resistance R_{ct} and double layer capacitance C_{dl}. Regular and routine metal surface implies the ideal dielectric property of the metal. If there is any misshape in the metal surface, it will deviate from its ideal dielectric behaviour. So, a constant phase element is compensated for C_{dl}.

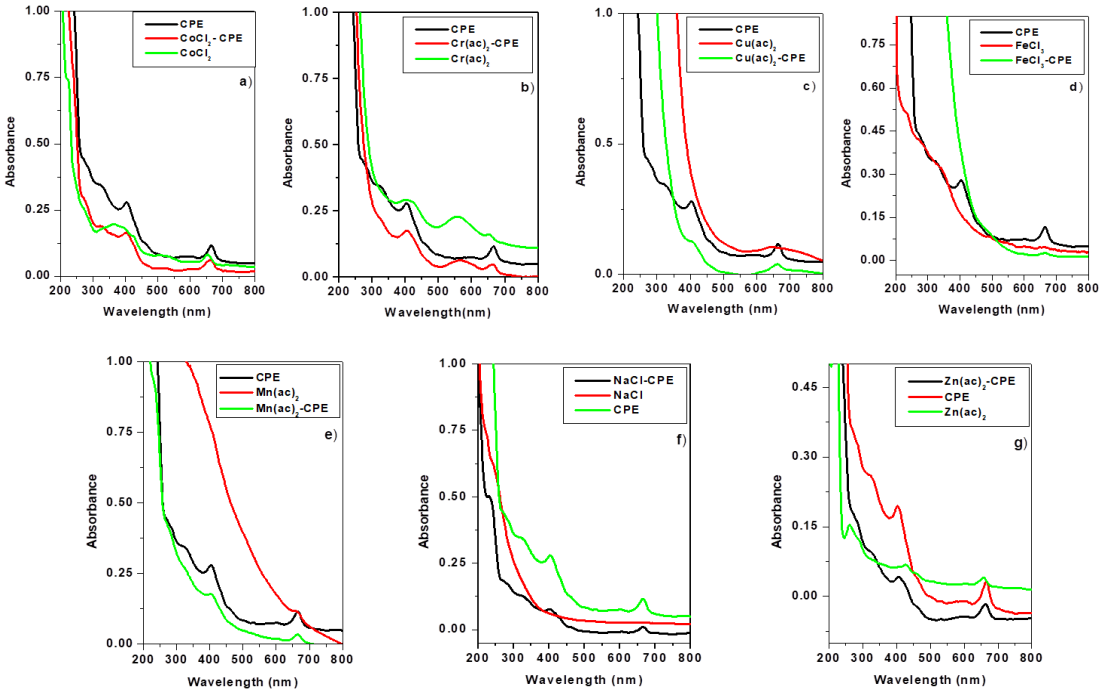

Fig. 4.8: UV spectra of a) CPE, $CoCl_2$ and CPE.$CoCl_2$ b**)** CPE, $Cr(ac)_2$ and CPE.$Cr(ac)_2$ c**)** CPE, $Cu(ac)_2$ and CPE.$Cu(ac)_2$ d**)** CPE, $FeCl_3$ and CPE.$FeCl_3$ e**)** CPE, $Mn(ac)_2$ and CPE.$Mn(ac)_2$ f**)** CPE, NaCl and CPE.NaCl g**)** CPE, $Zn(ac)_2$ and CPE.$Zn(ac)_2$

Impedance spectra include Nyquist and Bode plots for mild steel in 1 M HCl and 0.5 M H_2SO_4 by adding varying concentrations (0-5 v/v %) of the inhibitor CPE at room temperature are shown in Fig. 4.9 & 4.10. Impedance parameters gained from the impedance spectra for both media are given in Table 4.5. The highest semicircle was attained with a concentration of 5 v/v %; it successively decreased as the concentration decreases. This decreasing trend implied that as CPE concentration increases, the impedance of inhibited mild steel raised and lowered its corrosion rate.

From Table 5, it has been evident that charge transfer resistance (R_{ct}) was increased with CPE concentration. In contrast, double-layer capacitance (C_{dl}) was lowered, which indicated that the thickness of the electrical double layer increases with the concentration[74]. The increase in R_{ct} values predominant in the H_2SO_4 medium

pointed out that CPE molecules strongly resisted the charge transfer reaction of corrosion in that medium, which can be considered the rate-determining reaction.

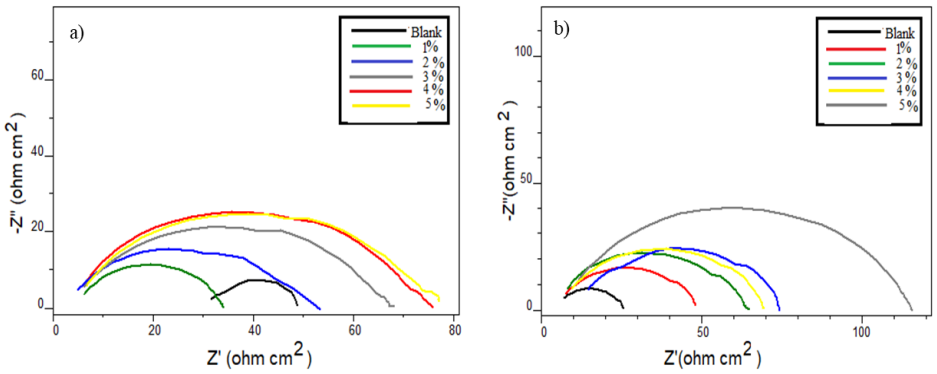

Fig. 4.9: Nyquist plots of mild steel with ad without CPE in a) 1 M HCl and b) 0.5 M H_2SO_4

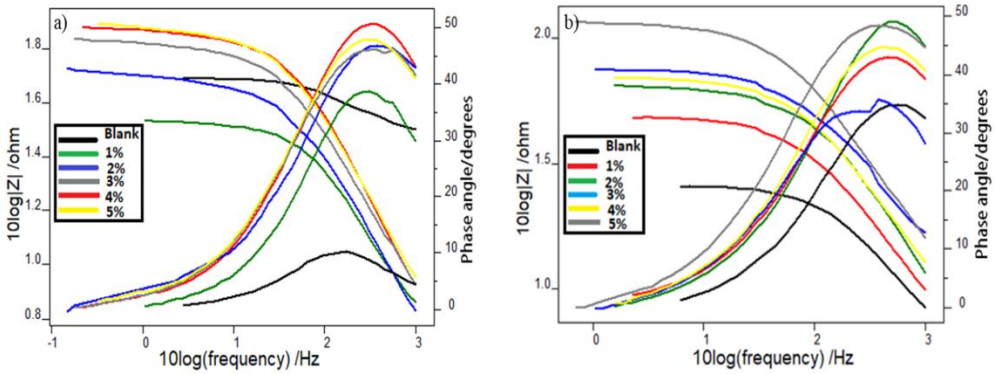

Fig. 4.10: Bode plots of mild steel with and without CPE in a) 1 M HCl and b) 0.5 M H_2SO_4

Table 4.5: Impedance parameters of mild steel in 1 M HCl and 0.5 M H_2SO_4 with and without CPE

Conc. (v/v %)	1 M HCl			0.5 M H_2SO_4		
	R_{ct} (Ωcm^2)	C_{dl} (μ Fcm^{-2})	η_{EIS}%	R_{ct} (Ωcm^2)	C_{dl} (μ Fcm^{-2})	η_{EIS}%
Blank	15.7	78.75	-	18.1	47.39	-
1	25.6	67.70	38.67	37.4	40.87	51.60
2	38.5	69.31	59.22	51.3	27.21	64.71
3	53.1	64.13	70.43	54.2	32.29	66.60
4	60.2	49.23	73.92	54.7	31.00	66.91
5	60.7	55.30	74.13	92.9	26.18	80.51

Decreasing trend of C_{dl} values is on account of the adsorption of inhibitor molecules on the mild steel surface. The decrease in C_{dl} value was more in the case of 0.5 M H_2SO_4, which showed an increase in surface coverage by CPE. It caused higher

inhibition potency in H_2SO_4 than in the HCl medium. Maximum inhibition efficiency of 74.13% and 80.51% was found at 5% concentration of CPE in 1 M HCl and 0.5 M H_2SO_4, respectively. This result was also in line with the data from weight loss measurements.

Potentiodynamic polarization studies

The potentiodynamic polarization curves such as Tafel plots (Fig. 4.11) and linear polarization plots (Fig. 4.12) of mild steel in 1 M HCl and 0.5 M H_2SO_4 with and without CPE are used to determine the polarization data, such as the corrosion current density (i_{corr}), the potential of corrosion (E_{corr}) current, cathodic slope (b_c), anodic slope (b_a), and inhibition power (η_{pol}%) which are given in Table 4.6. The polarization data showed that with the addition of inhibitor CPE, corrosion current density gets reduced. It can be ascribed to the interference in the anodic or cathodic process of corrosion or both. Thus, corrosion inhibition potency increased significantly in both acids. The inhibition efficiency of CPE for mild steel attained 80.88% in 1 M HCl and 84.09% in 0.5 M H_2SO_4 at the highest concentration under study. From Tafel plots in Fig.4.11, it is clear that both cathodic and anodic slopes were disturbed in a uniform manner which indicated the mixed type inhibition character of CPE in 1 M HCl and 0.5 M H_2SO_4, i.e., CPE behaves as an anodic and cathodic inhibitor[71].

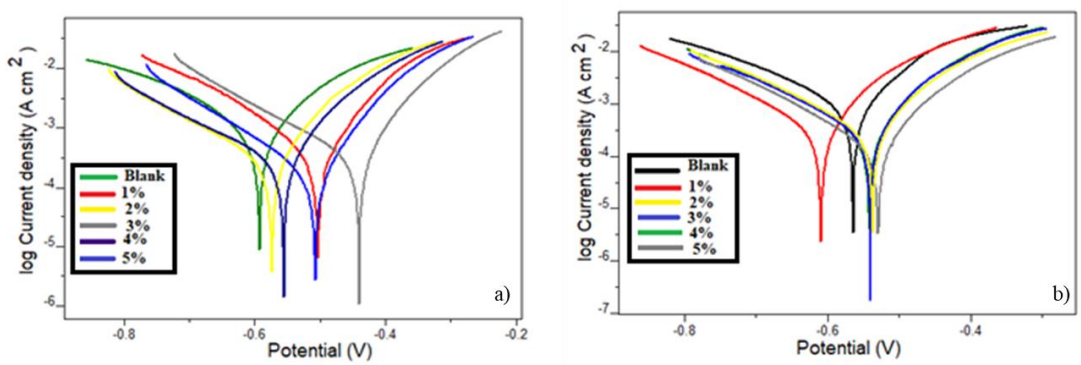

Fig. 4.11: Tafel plots of mild steel with and without CPE in a) 1 M HCl and b) 0.5 M H_2SO_4

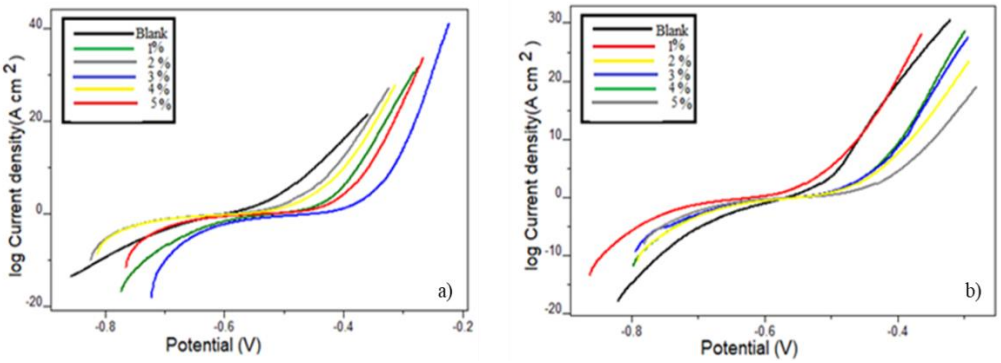

Fig. 4.12: Linear polarization plots of mild steel with and without CPE in a) 1 M HCl and b) 0.5 M H_2SO_4

Table 4.6: Potentiodynamic polarization parameters of mild steel in 1 M HCl and 0.5 M H_2SO_4 with and without CPE

Medium	Conc. (v/v%)	Tafel data					Polarization data	
		$-E_{corr}$ (mV)	i_{corr} ($\mu A/cm^2$)	b_a (mV/dec)	$-b_c$ (mV/dec)	$\%\eta_{pol}$	R_p (ohm)	$\%\eta_{Rp}$
1 M HCl	Blank	597.9	1240	166	221	-	33.14	-
	1	513.6	549.9	111	164	55.64	51.68	35.87
	2	607.7	398.8	138	173	67.82	72.97	54.58
	3	466.8	390.4	107	169	68.54	83.61	60.36
	4	589.2	364.9	132	185	70.56	91.77	63.88
	5	529.3	236.7	106	151	80.88	113.9	70.90
0.5 M H_2SO_4	Blank	602.2	1616	184	193	-	25.30	-
	1	645.1	576.6	153	150	64.29	56.95	55.57
	2	571.7	491.2	147	156	69.61	76.80	67.05
	3	575.4	486.3	141	160	69.92	86.96	70.90
	4	574.5	459.1	135	151	71.59	97.47	74.04
	5	560.9	256.9	131	143	84.09	115.7	78.13

Electrochemical noise measurements

Fig. 4.13 delineates the current noise for mild steel in the absence and presence of three different CPE concentrations (1, 3, 5 v/v %) in 1 M HCl and 0.5 M H_2SO_4. It is evident that when the concentration of CPE increased, its protecting power was also raised. The current and potential noise for the inhibited system was lower than the uninhibited system. The potential noise signal for the higher concentration of CPE (5 v/v%) was positioned at a lower magnitude, showing corrosion inhibition by the inhibitor. The signal was at a higher magnitude for uninhibited acid media, indicating appreciable localized metallic corrosion on the metal surface[154].

Power spectral density (PSD) plots originated from the frequency domain analysis of noise, shown in Fig. 4.14. Comparing the magnitude of the current noise signals for blank metal with inhibited metal was lower for the metal dipped in acid solution with various concentrations of CPE (1, 3, 5 v/v %) than the uninhibited acid solution. It connoted an appreciable amount of localized corrosion on the mild steel surface immersed in the uninhibited acid solution. For the highest concentration (5 v/v%), the magnitude of the current noise signals was attained the most negligible value suggesting its good corrosion inhibition nature and its value increasing as concentration decreased.

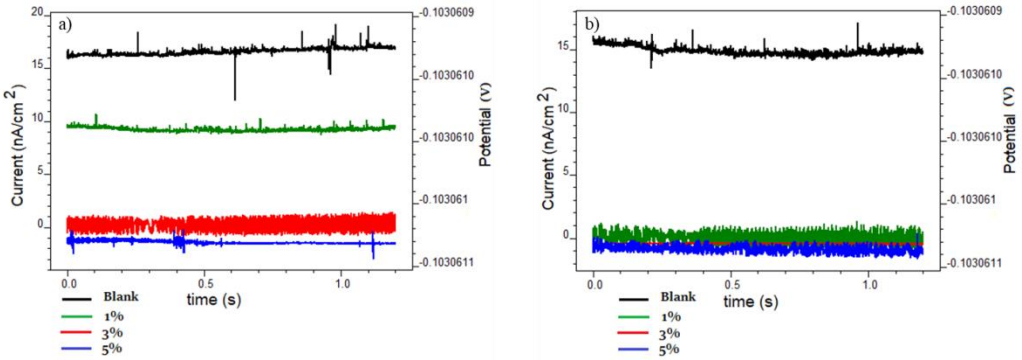

Fig. 4.13: Current noise plots of mild steel with and without CPE in a) 1 M HCl b) 0.5 M H_2SO_4

Pitting corrosion resistance power can be expressed by examining pitting index curves (Fig. 4.15). Contrary to PSD plots, the amplitude of the pitting index curve for blank metal was lower than the metal in the inhibited acid solution. It may be attributed to the worst mitigation to pitting corrosion offered by blank metal treated in an uninhibited acid medium. Pitting index value of the mild steel immersed in 1 M HCl containing 5 v/v% CPE solution was recorded smaller than that in 0.5 M H_2SO_4 solution having the same concentration of CPE. At the same time, pitting index value of the mild steel in the blank solutions of 1 M HCl and 0.5 M H_2SO_4 were observed to be smaller than inhibited metal.

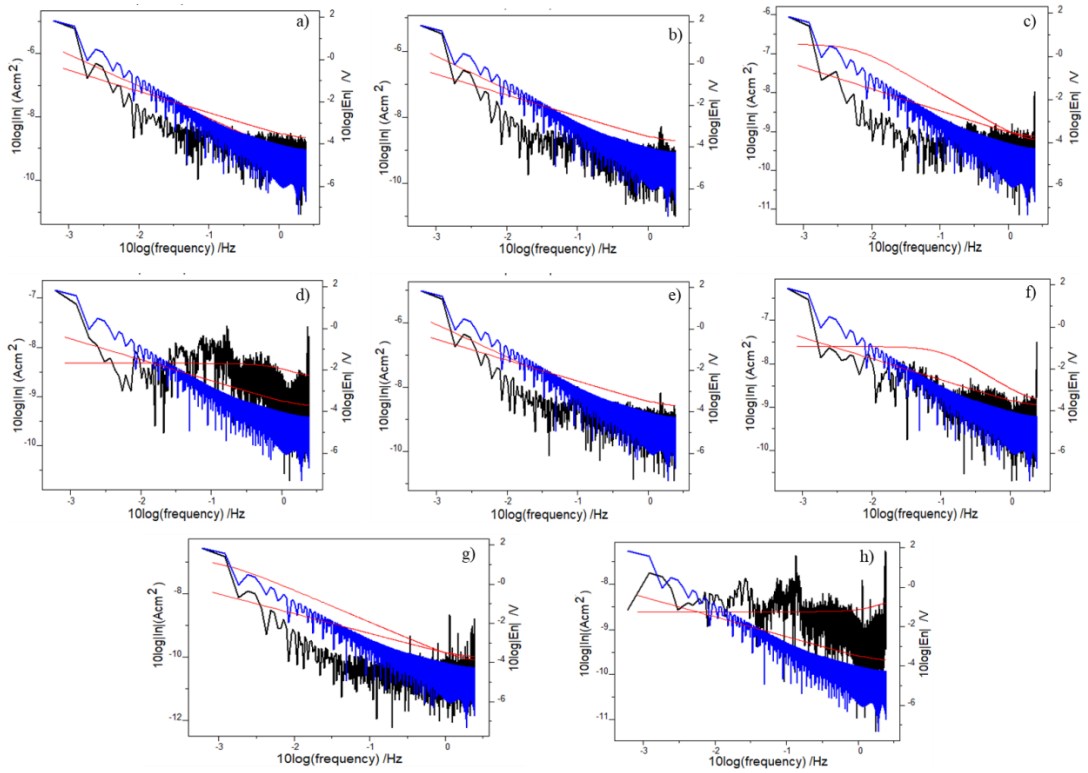

Fig. 4.14: Power spectral density plots of mild steel in 1 M HCl a) without CPE b) 1% CPE c) 3% CPE d) 5% CPE; Power spectral density plots of mild steel in 0.5 M H_2SO_4 e) without CPE f) 1% CPE g) 3% CPE h) 5% CPE

Scanning electron microscopy

Surface morphological studies can reinforce the adsorption mechanism by the inhibitor molecules of CPE on mild steel surfaces. Fig. 4.16 a) exhibits the SEM image of the surface of shining mild steel. Fig. 4.16 b), c), d) and e) reveals the SEM images of the surface of mild steel metal after the period of immersion in 1 M HCl and 0.5 M H_2SO_4, respectively, in the absence and presence of CPE. From Fig. 4.16, it was evident that the surface of the mild steel metal is seriously affected by the rust in the absence of the inhibitor CPE. It could be examined that the surface corrosion is lower in H_2SO_4 solution in the presence of CPE, and the surface is more transparent and refined in it than in the HCl solution. So it can be realized that CPE acts as an efficient green corrosion inhibitor in acidic media[159].

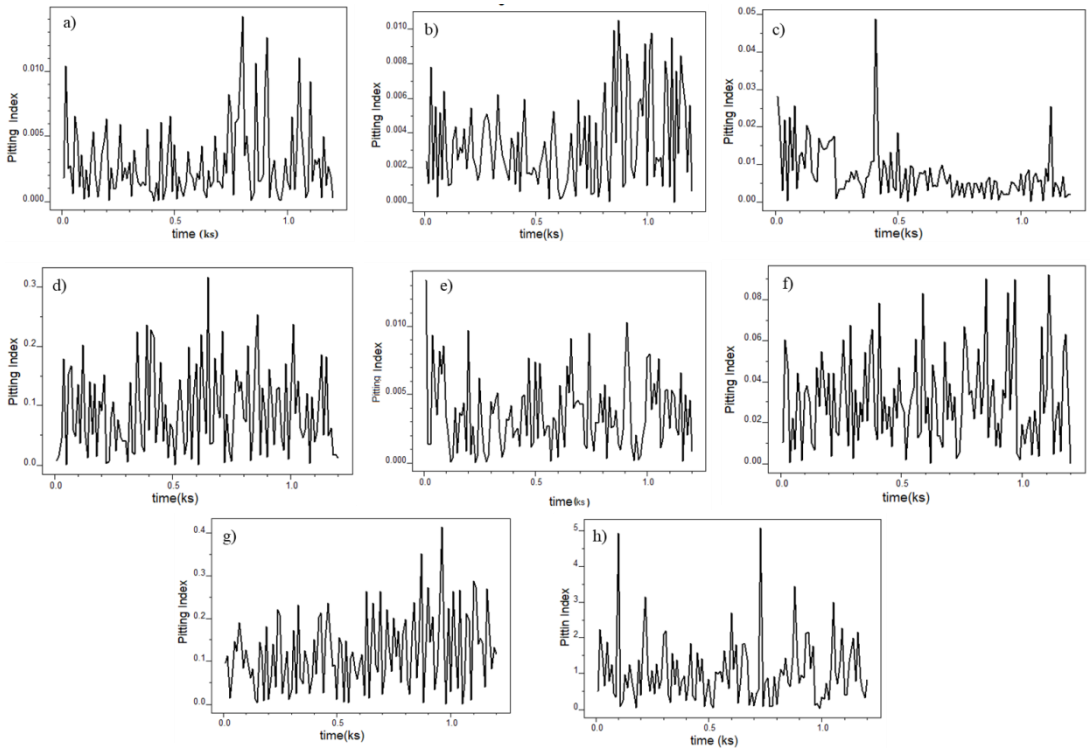

Fig. 4.15: Pitting index curves of mild steel in 1 M HCl a) without CPE b) 1% CPE c) 3% CPE d) 5% CPE; Pitting index curves of mild steel in 0.5 M H_2SO_4 e) without CPE f) 1% CPE g) 3% CPE h) 5% CPE

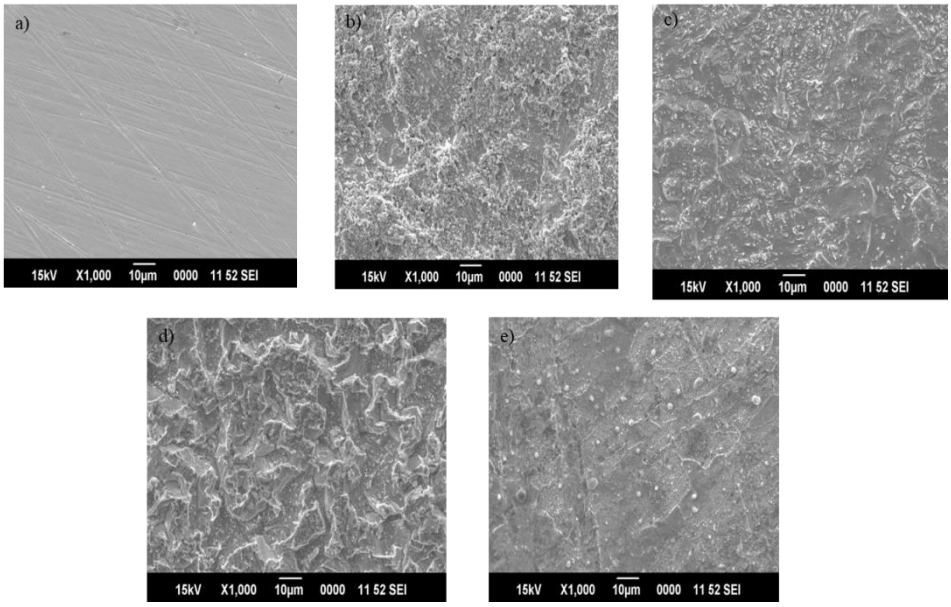

Fig. 4.16: SEM images of the surface of mild steel a) bare b) in 1 M HCl c) in 1 M HCl with CPE d) in 0.5 M H_2SO_4 e) in 0.5 M H_2SO_4 with CPE

Quantum mechanical calculations

Quantum mechanical parameters like E_{HOMO}, E_{LUMO}, ΔE, Ionisation energy (I), Electron affinity (A), chemical potential (μ), electronegativity (χ), hardness (η) and the

number of transferred electrons (ΔN) of neocrotocembraneic acid and stigmasterol are computed in Table 4.7. The optimized geometry, HOMO and LUMO pictures of neocrotocembraneic acid and stigmasterol are portraited in Fig. 4.17.

Table 4.7: Quantum mechanical parameters (in eV) of neocrotocembraneic acid (I) and stigmasterol (II)

Molecule	E_{HOMO}	E_{LUMO}	ΔE	I	A	μ	χ	η	ΔN
I	-2.135	1.081	3.21	2.13	-1.081	-0.527	0.52	1.608	2.01
II	-3.129	1.125	4.25	3.12	-1.125	-1.002	1.00	2.127	1.40

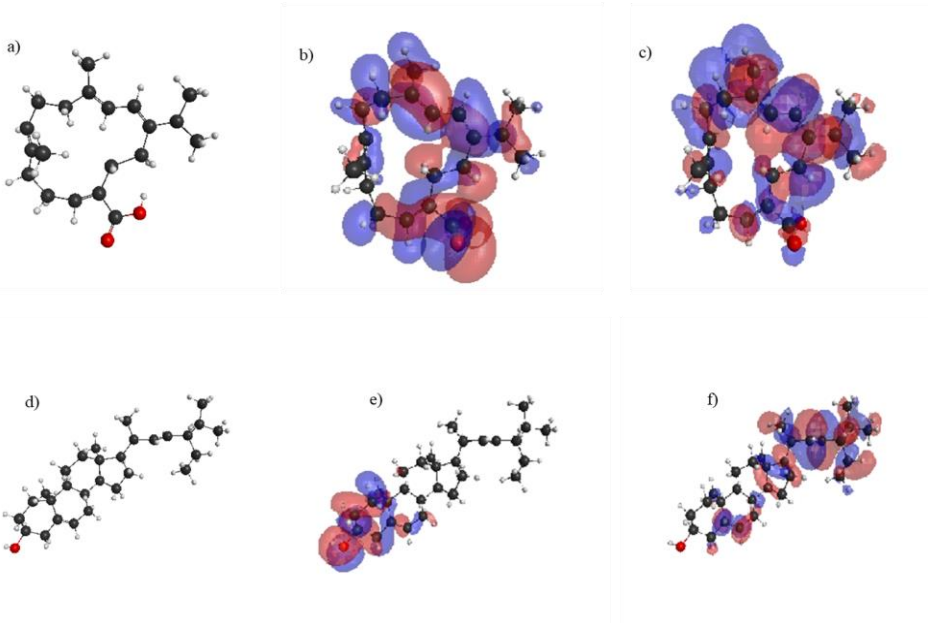

Fig. 4.17: a) Optimized geometry, b) HOMO and c) LUMO of neocrotocembraneic acid; d) Optimized geometry, e) HOMO and f) LUMO of stigmasterol

Adsorption of an inhibitor molecule on the metal surface is quantified by the value of change in energy (E_{LUMO} - E_{HOMO}). The ΔE value was low for neocrotocembraneic acid, facilitating the low energy condition for the transfer of electrons from HOMO of neocrotocembraneic acid to the vacant orbitals of Fe. This low ΔE value of 3.216 eV of neocrotocembraneic acid implies that CPE has significant protection efficiency. The ΔN values impart the concept concerning the relation between donor-acceptor molecules. If the value of ΔN is less than 3.6, the inhibitor molecules

tend to donate electrons to the metal surface[160]. Here the fraction of electrons transferred in neocrotocembraneic acid was 2.012, and for stigmasterol, it is 1.409. Presence of a conjugated double bond in neocrotocembraneic acid may enhance the donation of electrons to the metal surface. It may attribute to the high inhibition capacity of the major components. Thus, in turn, substantiates agreement between theoretical and experimental results.

Statistical analysis

❖ ***Optimization of factors for inhibition efficiency (IE%)***

Response surface methodology (RSM) yields optimized conditions concerning input values to acquire a proper response. From weight loss measurements, it was clear that the corrosion inhibition efficiency of CPE depends on its concentration and working temperature, and effective inhibition was obtained in 0.5 M H_2SO_4 than 1 M HCl medium. So, corrosion inhibition efficiency of the inhibitor and variables such as temperature and concentration of CPE in 0.5 M H_2SO_4 medium were connected through regression analysis. Parameters of the RSM technique are temperature in K (X_1) and concentration of CPE in v/v% (X_2).

The influence of temperature (X_1) and concentration of CPE (X_2) on inhibition efficiency (IE%) was described by a central composite design (CCD). There were nine experimental runs in CCD to optimize the parameters, which are given in Table 4.8. A full quadratic model was assigned to represent the inhibitor efficiency in response to the independent parameters in selected ranges:

$$IE = 2490 - 14.10X_1 - 7.81X_2 + 0.02027X_1^2 - 0.765X_2^2 + 0.0605X_1X_2 \quad (52)$$

Validity of this quadratic model can be verified using Residual plots shown in Fig. 4.18. On close observation of the normal probability plot, it has been seen that the response model for inhibition efficiency was fixed to the normal distribution. It suggests

that the established model required no response transformation, and there are no detectable problems with normality. Versus fits plot conveyed that there is a constancy in the variance of observations for all responses. Histogram of residuals indicated that the residuals are distributed uniformly for all frequencies[161]. Points of observed runs were distributed randomly within the fixed residuals, which authenticated the model's precision, and was established by Versus order plot. In short, all the plots in this figure verified the validity of the model to explain the inhibition efficiency of the inhibitor CPE.

Table 4.8: Experimental and predicted IE% from the weight loss measurements and CCD

Temp (X_1)	Conc. (X_2)	IE%		Residual
		Experimental	Predicted	
313	5	98.73	99.03913	0.30913
333	1	53.93	53.99153	0.06153
313	1	73.05	72.89313	-0.15687
333	5	84.45	84.97753	0.52753
313	3	89.23	89.02613	-0.20387
323	5	90.81	89.98133	-0.82867
333	3	73.03	72.54453	-0.48547
323	1	61.28	61.41533	0.13533
323	3	78.04	78.75833	0.71833

Table 4.9 explains the analysis of variance for corrosion inhibition efficiency. P-value determines whether the effect for that variable is significant or not. The selected value of α, degree of essentialness, was 0.05. Table 4.9 shows that for the linear and square terms, the P-value is less than α, which means they have a more significant effect on the response. Two-way interaction term has little effect on IE.

Pareto chart (Fig. 4.19) demonstrates that only linear terms significantly impact the inhibition efficiency. Squared terms for temperature (X_1^2) and concentration (X_2^2) are having no noticeable impact on the inhibition efficiency, and the response does not influence the two-way interaction term (X_1X_2). Value of coefficient (R^2) acquired for the predicted model was 0.9894, which indicated the best fit expected model for experimental values[162]. Therefore, the output can be easily interpreted by the model.

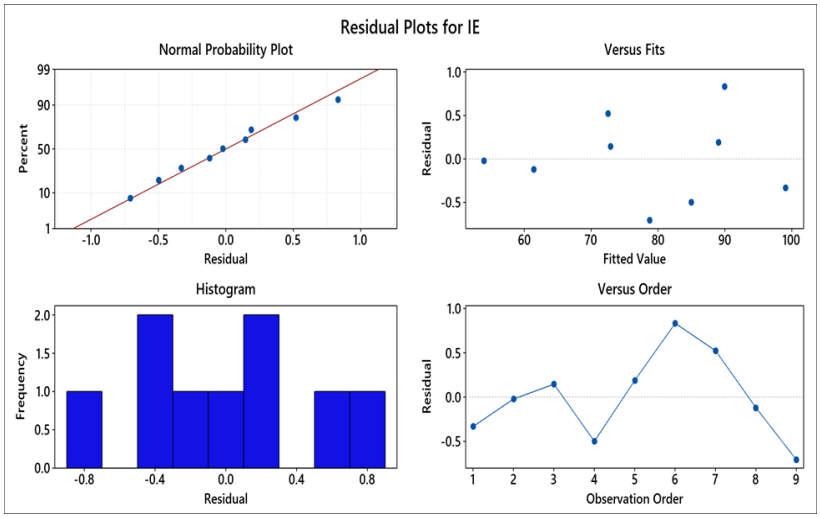

Fig. 4.18: Residual plots for inhibition efficiency

The impact of two parameters measured individually on IE% is plotted in the Main effects plots (Fig. 4.20). The figure shows that as CPE concentration increased from 1 to 5 v/v %, IE% also increased. It may be due to the coverage of active sites on the surface of mild steel metal with surplus CPE molecules. The type of adsorption exhibited by CPE molecules was physisorption because IE% decreased in higher temperatures. The results are precisely agreed with weight loss measurements.

Table 4.9: Analysis of variance for corrosion inhibition efficiency

Source	DF	Adj SS	Adj MS	F-Value	P-Value
Model	5	1667.74	333.549	527.87	0.000
Linear	2	445.32	222.660	352.38	0.000
Temp	1	256.15	256.150	405.38	0.000
Conc	1	189.17	189.169	299.37	0.000
Square	2	26.92	13.461	21.30	0.017
Temp*Temp	1	8.21	8.215	13.00	0.037
Conc*Conc	1	18.71	18.707	29.60	0.012
2-Way Interaction	1	5.86	5.856	9.27	0.056
Temp*Conc	1	5.86	5.856	9.27	0.056
Error	3	1.90	0.632		
Total	8	1669.64			

DF: degrees of freedom, Adj SS: adjusted sum of squares, Adj MS: adjusted mean of squares, F: Fischer's F-test value, P: probability

Interdependence of the parameters on the IE% was evaluated by plotting a contour and 3-D surface plot against two independent parameters in Fig. 4.21 a) and b),

respectively. It showed that the maximum corrosion inhibition efficiency was found for 5 v/v% concentration of CPE at 313 K. It can be attributed that elevated temperature causes an increase in the corrosion rate and obviously decreases the corrosion inhibition efficiency.

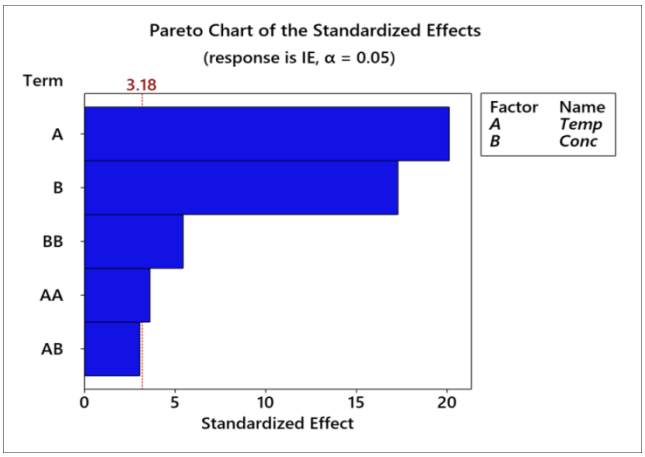

Fig. 4.19: Pareto chart of the standardized effects of mild steel

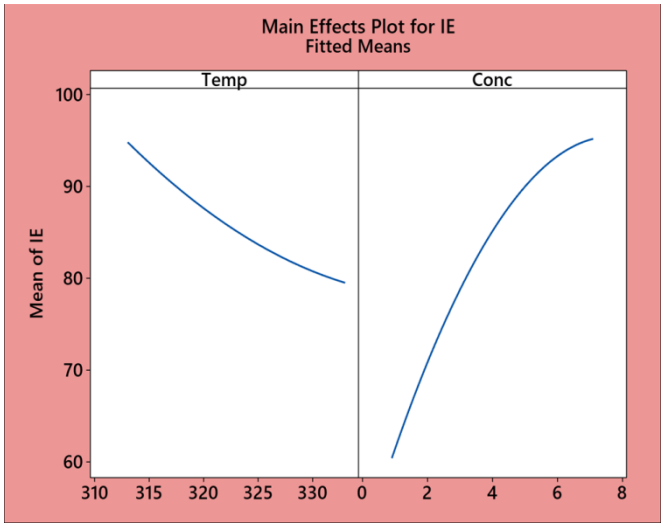

Fig. 4.20: Main effects plots for inhibition efficiency of mild steel in 0.5 M H_2SO_4

❖ ***Response Optimization***

Response optimization was performed to obtain the concentration of CPE and temperature at which a lower corrosion rate of mild steel in 0.5 M H_2SO_4. The maximum inhibition efficiency was investigated using the desirability function method by optimizing independent parameters presented in Fig. 4.22. The optimum temperature and

concentration parameters were 313 K and 5 v/v %, which yields the best result for the response of 99.06% inhibition efficiency.

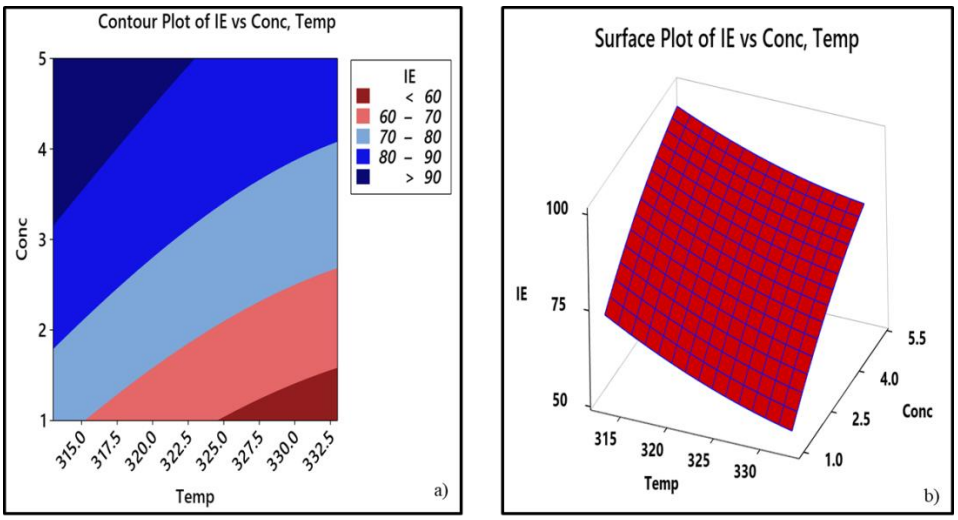

Fig. 4.21: a) Contour and b) 3-D surface plot for corrosion inhibition efficiency

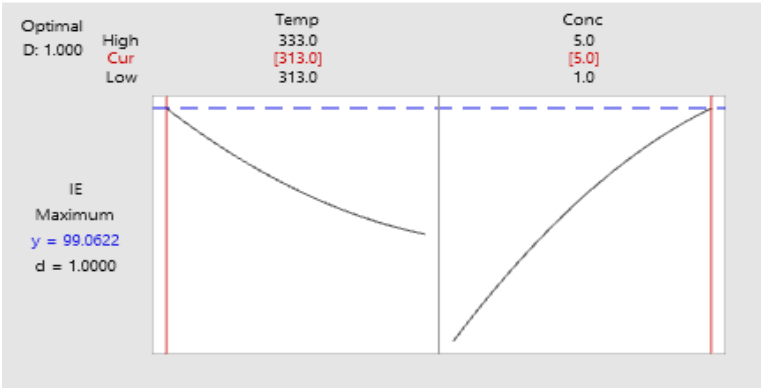

Fig. 4.22: Response optimization plot for inhibition efficiency

Conclusions

- Most of the tested metal salts exhibit good binding efficiency with CPE, which shows that they may be used to detect metal salts in different water sources.
- CPE behaves like an outstanding green corrosion inhibitor for mild steel in acidic environments.
- Weight loss studies reinforce the development of a protective barrier by CPE on the mild steel surface.

- Maximum inhibition potency of CPE in 1 M HCl and 0.5 M H_2SO_4 was calculated as 86.45% and 98.09%, respectively.
- The higher inhibition power in 0.5 M H_2SO_4 than 1 M HCl medium may attribute to the more adsorbed organic molecules of CPE on mild steel in 0.5 M H_2SO_4 medium than in 1 M HCl.
- Corrosion resistance power of CPE increases on adding the inhibitor concentration and decreases in elevated temperatures.
- The adsorption studies of CPE showed that it obeys Langmuir adsorption isotherm.
- CPE acts as a mixed-type inhibitor.
- Theoretical calculations of chief components of CPE such as neocrotocembraneic acid and stigmasterol are also establishing the corrosion inhibition potential of CPE.
- Predicted inhibition efficiency of CPE at various inhibitor concentrations and temperatures in 0.5 M H_2SO_4, investigated by RSM, was in agreement with the results obtained in weight loss measurements.

CHAPTER 5

TINOSPORA CORDIFOLIA EXTRACT: NATURAL CORROSION INHIBITOR FOR MILD STEEL IN ACID MEDIA

This chapter introduces *Tinospora cordifolia* extract's (TCE) inhibiting capacity on mild steel in 1 M HCl and 0.5 M H_2SO_4 by weight loss techniques, electrochemical and surface morphological studies. Effects of temperature, concentration of TCE and acid medium on inhibition efficiency are evaluated employing statistical tools such as response surface methodology (RSM) and Box-Behnken design (BBD). The research world has revealed medicinal characteristics of *Tinospora cordifolia* leaves, but their corrosion resistance properties with various competencies are not yet investigated. *Tinospora cordifolia* belongs to the Menispermaceae family, comprised of so many phytochemicals. Tinosponone is the major metabolite in *Tinospora cordifolia* leaf extract, which is a sesquiterpene[163]. Its structure is shown in Fig. 5.1. Berberine, tembetarine, tinocordioside, syringin, magnoflorine and 20-hydroxyecdysone are some of the minor chemical compounds in it.

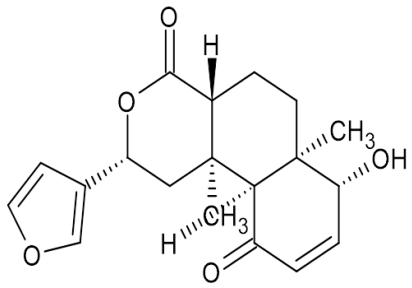

Fig. 5.1: Structure of tinosponone

Tinospora cordifolia

Results and discussions

Phytochemical screening of TCE

The presence of major phytochemicals in TCE was confirmed using different tests, and the results are given in Table 5.1.

Table 5.1: Phytochemical screening of TCE

Sl. No.	Compounds	Tests	Results
1	Alkaloids	Mayers reagent	−−
2	Steroids	Salkowaski's test	++
3	Phenolic compounds	Potassium ferrocyanide test	++
4	Flavanoids	Sodium hydroxide test	++
5	Saponins	Froth test	++
6	Tannins	Lead acetate test	++
7	Cardiac glycosides	Conc. sulphuric acid test	++
8	Coumarin	Alcoholic NaOH test	++
9	Quinones	Conc. sulphuric acid test	++

++ (present), − − (Absent)

FTIR spectroscopy

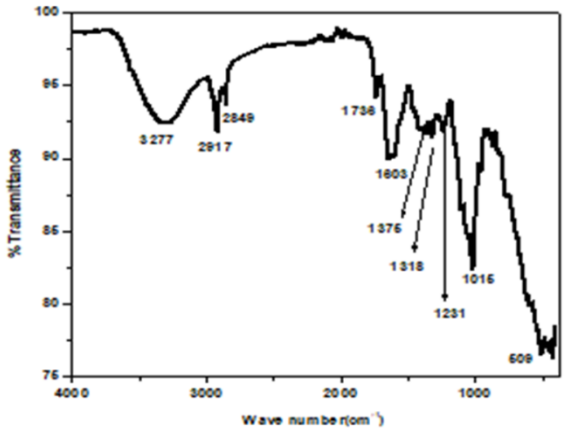

Fig. 5.2: FTIR spectrum of TCE

The FTIR spectrum of TCE revealed characteristic stretching and bending frequencies for various bonds, drawn in Fig. 5.2. Broadband at 3277 cm^{-1} denotes O-H stretching. Two sharp bands at 2917 cm^{-1} and 2849 cm^{-1} represents alkyl C-H stretching vibrations. >C=O stretching vibration appears at 1736 cm^{-1}. This peak can be assigned to six-membered cyclic lactones. The bands at 1603 cm^{-1} and 1318 cm^{-1} can be accredited to >C=C stretching vibrations. C-O bending pulse appears as a weak band at 1231 cm^{-1} and 1016 cm^{-1}. This peak can be ascribed to characteristic peaks for the furan ring. In summary, distinct peaks of TCE can be attributed to heteroatoms, aromatic rings, and unsaturated compounds.

Weight loss measurements

❖ ***Effect of concentration***

Corrosion inhibition efficiency (ηℵ) and corrosion rate (υ) found by weight loss technique on mild steel in 1 M HCl and 0.5 M H_2SO_4 with varying concentrations (0-5 v/v %) of TCE have been calculated. (Table 5.2)

Table 5.2: Weight loss measurements of mild steel with and without TCE in 1 M HCl and 0.5 M H_2SO_4 at room temperature for 24 hrs

Conc. (v/v %)	Corrosion rate (mm/yr)		Inhibition efficiency (ηℵ)	
	1 M HCl	0.5 M H_2SO_4	1 M HCl	0.5 M H_2SO_4
Blank	3.9500	35.570	-	-
1	0.7852	17.763	80.12	50.06
2	0.5731	13.370	85.49	62.41
3	0.4530	9.038	88.53	74.59
4	0.3365	7.533	91.48	78.82
5	0.2081	6.214	94.73	82.53

An augment in inhibition power was noticed from the data by raising TCE concentration in both acid media. Also seen that TCE behaves as an efficient green corrosion inhibitor in 1 M HCl, attaining maximum inhibition efficacy of 94.73% and 82.53% in 0.5 M H_2SO_4 at 5% TCE concentration. In HCl solution, TCE exhibit more inhibition capacity compared to H_2SO_4 solution. It may be due to the effective adsorption of Cl^- ions on the metal surface than SO_4^{2-} ions since halide ions are more electronegative. It may lead to more adsorption of cationic organic molecules on the metal surface to inhibit metal dissolution. At the same time, SO_4^{2-} ions were adsorbed on the metal surface poorly. It causes lesser surface coverage on metal. So, the fraction of TCE molecules adsorbed on mild steel surface is low, and hence, metal suffers a high corrosion rate in the H_2SO_4 medium.

❖ ***Effect of temperature***

Stability of the protective film of TCE by adsorption on mild steel surface was described by performing temperature studies[63]. Here, the impact of temperature on the corrosion control was accomplished by weight loss measurements in 1 M HCl and 0.5 M H_2SO_4 with varying TCE concentrations at different temperatures (303-333 K) for 24 hrs. Inhibition potential was calculated and given in Table 5.3 and graphically depicted in Fig. 5.3. It showed that the rate of corrosion rises with an enhancement in temperature for a fixed concentration. When the temperature raised from 303 K to 333 K, efficiency lowered from 94.73% to 62.64% for 5% TCE concentration in HCl medium. A similar observation can see in the H_2SO_4 medium, where the inhibition efficiency decreased from 82.53% to 66.61% for the same strength and temperature range. This trend may be ascribed to the metal surface changes such as instant engraving, crack, detachment of adsorbed film, decay, or reordering of the inhibitor when the temperature rises in both acids and thereby decreases inhibition potency. So, discrepancies in temperature influenced the metal disintegration, action of inhibitor either adsorption or desorption and corrosion control.

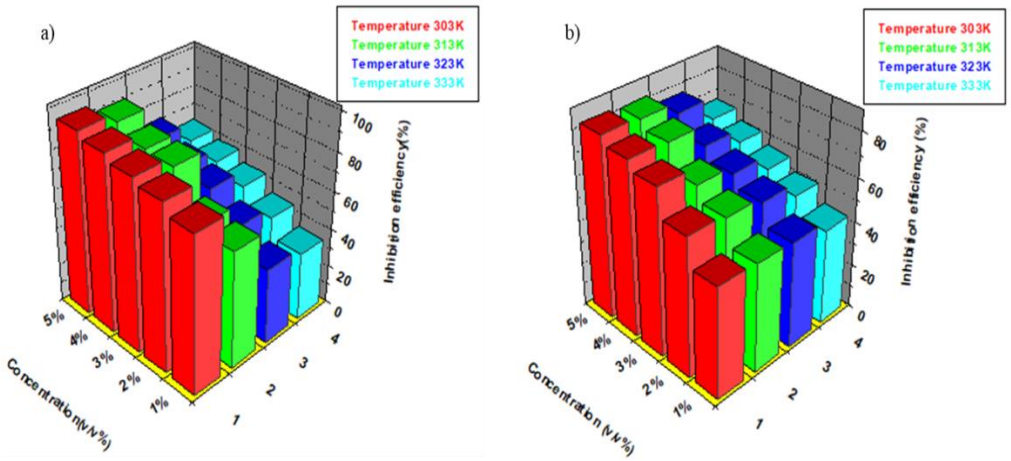

Fig. 5.3: Variation in inhibition efficiency of TCE in a) 1 M HCl b) 0.5 M H_2SO_4 at elevated temperatures

Table 5.3: Corrosion rate (υ) and inhibition efficiency (η%) of TCE in 1 M HCl and 0.5 M H_2SO_4 at different temperatures for 24 hrs

Medium	Conc. (v/v%)	υ (303K)	η% (303K)	υ (313K)	η% (313K)	υ (323K)	η % (323K)	υ (333K)	η% (333K)
1 M HCl	Blank	3.95	-	13.11		22.05	-	31.77	-
	1	0.78	80.12	5.23	60.11	13.54	38.61	20.48	35.54
	2	0.57	85.49	4.72	64.00	10.69	51.53	17.36	45.36
	3	0.45	88.53	2.15	83.60	8.23	62.68	14.69	53.76
	4	0.33	91.48	2.07	84.21	7.45	66.22	12.98	59.14
	5	0.20	94.73	1.26	90.39	6.15	72.11	11.87	62.64
0.5 M H_2SO_4	Blank	35.57	-	58.27	-	86.25	-	106.2	-
	1	17.76	50.06	29.69	49.04	44.95	47.88	60.04	43.49
	2	13.37	62.41	23.08	60.39	36.58	57.58	51.64	51.40
	3	9.03	74.59	19.36	66.77	31.95	62.95	45.91	56.79
	4	7.53	78.82	12.88	77.89	27.23	68.42	40.12	62.24
	5	6.21	82.53	10.77	81.51	20.14	76.64	35.48	66.61

Arrhenius equation was used to plot log K vs 1/T curves for metal corrosion in the presence and absence of TCE in acid media. Fig. 5.4 a) and Fig. 5.5 a) show Arrhenius plots. Slopes of the straight lines were fit to evaluate the activation energy of corrosion in acid media. Transition state theory renders the calculation of thermodynamic parameters such as enthalpy of activation (ΔH^*) and entropy of activation (ΔS^*). Linear plots of log K/T vs 1/T for the mild steel corrosion with and without TCE are shown in Fig. 5.4 b) and Fig. 5.5 b). All the thermodynamic parameters and activation energy derived from these plots were tabulated in Table 5.4, which established that the activation energy of corrosion increases with an increase in TCE concentration due to the growing energy barrier. It also emphasized an activated complex compound formed by the interaction between the inhibitor and mild steel[164]. Positive value of enthalpy described the endothermic character of the metal corrosion process[165]. ΔS^* values were also increased by adding TCE concentration. Negative values of the entropy of activation for corrosion in the absence of TCE mentioned a decrease in randomness for the activated complex compared to the reactants. Disorderliness of the activated complex increases as the concentration of TCE raises and ΔS^* possessed

positive values. In the case of H_2SO_4 medium, ΔS^* value in the absence of TCE was seen to be largely negative compared to other ΔS^* values in the presence of TCE, and it became less negative as concentration increases.

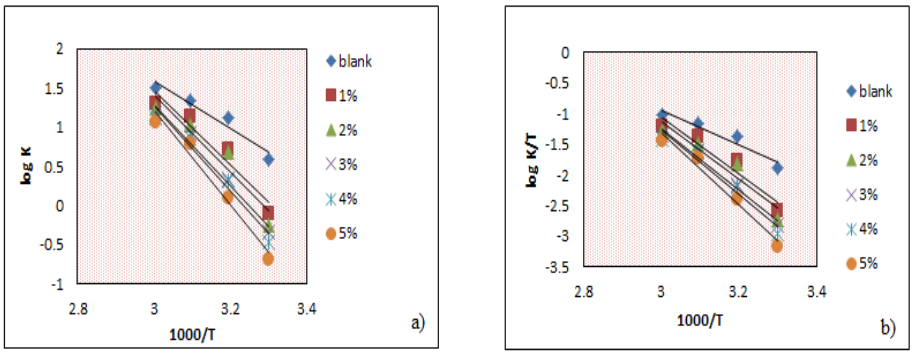

Fig. 5.4: Arrhenius plots of a) log K vs 1000/T b) log K/T vs 1000/T with and without TCE in 1 M HCl

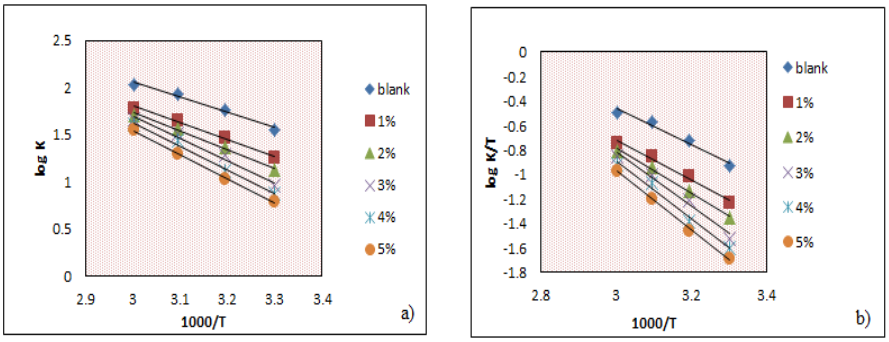

Fig. 5.5: Arrhenius plots of a) log K vs 1000/T b) log K/T vs 1000/T with and without TCE in 0.5 M H_2SO_4

Table 5.4: Thermodynamic parameters of mild steel corrosion with and without TCE in 1 M HCl and 0.5 M H_2SO_4

Medium	Conc. (v/v %)	E_a (kJ mol^{-1})	A	ΔH^* (kJ mol^{-1})	ΔS^* (J $mol^{-1}K^{-1}$)
1 M HCl	Blank	57.24	3.58×10^{10}	54.60	-44.78
	1	90.79	4.95×10^{15}	88.15	53.66
	2	93.51	1.13×10^{16}	90.87	60.51
	3	99.28	6.98×10^{16}	96.64	75.66
	4	103.28	2.76×10^{17}	100.64	87.09
	5	115.60	2.14×10^{19}	112.97	123.27
0.5 M H_2SO_4	Blank	30.96	8.16×10^{6}	28.30	-114.51
	1	34.23	1.47×10^{7}	31.59	-109.62
	2	37.95	4.82×10^{7}	35.31	-99.74
	3	45.29	6.31×10^{8}	42.65	-78.34
	4	48.42	1.66×10^{9}	45.78	-70.33
	5	49.06	1.73×10^{9}	46.42	-69.97

Adsorption isotherms

Adsorption isotherm studies provide interaction mechanism between inhibitor molecules and mild steel. Among different adsorption isotherm models such as Langmuir, El-Awady, Frumkin, Temkin, Freundlich, Flory-Huggins isotherms, the best adsorption isotherm model of TCE in 1 M HCl and 0.5 M H_2SO_4 was explored by fitting the extent of surface coverage (θ) and corrosion rate into it. Langmuir adsorption isotherm was found to be the best model with R^2 values of 0.9987 and 0.9974 in 1 M HCl and 0.5 M H_2SO_4, respectively. Fig. 5.6 represents Langmuir adsorption isotherms of TCE on mild steel in 1 M HCl and 0.5 M H_2SO_4 at room temperature.

Mechanism of adsorption can be estimated from the values of ΔG^0_{ads} which is related to adsorption equilibrium constant K_{ads}. In the present work, ΔG^0_{ads} for TCE-mild steel adsorptions were -30.37 and -27.15 kJ mol^{-1} in 1 M HCl and 0.5 M H_2SO_4, respectively, which showed the nature of adsorption of TCE molecules on mild steel surface as both physisorption and chemisorption[166]. K_{ads} values for TCE adsorption were calculated as 3362.475 and 931.185 in 1 M HCl and 0.5 M H_2SO_4, respectively. The higher inhibition potency of TCE in HCl than H_2SO_4 medium can be justified by evaluating the values of $K_{ads,}$ which was more significant for HCl than H_2SO_4.

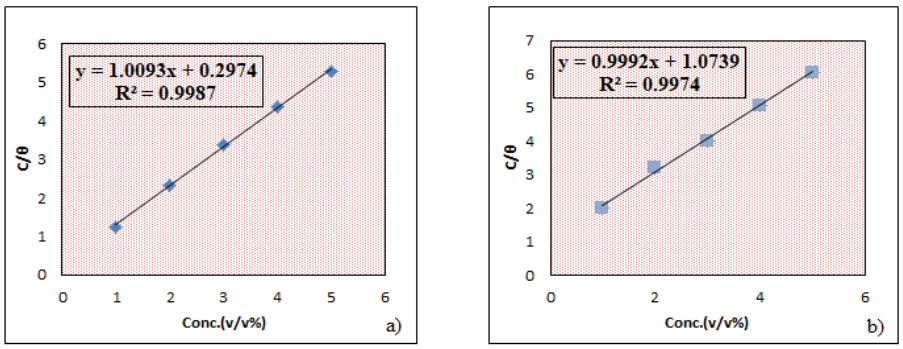

Fig. 5.6: Langmuir adsorption isotherm of TCE on mild steel in a) 1 M HCl and b) 0.5 M H_2SO_4

Fig. 5.7 portrays the possible surface behaviour of TCE molecules on mild steel. Even though TCE contains various components, the principal component is regarded as an authoritative compound for corrosion inhibition. The effective adsorption of tinosponone molecules by donating electrons from oxygen atoms in the furan ring, –OH, lactone functional groups, and π-electrons in the aromatic system causes the formation of a protective film on the metal surface and thereby mitigates metal corrosion. Moreover, tinosponone molecules may interact via back donation of 'd' electrons from the metal to π^* orbitals of tinosponone molecules. Besides this interaction, physisorption of TCE molecules was involved. Initially, chloride/sulfate ions present in the acid solution approach on the surface of mild steel and continue as a cathode. The cationic molecules of TCE, which are considerably larger than acid ions, were adsorbed on the metal surface by the substitutional adsorption process in the anodic and cathodic process of metal corrosion and decreased metal dissolution rate.

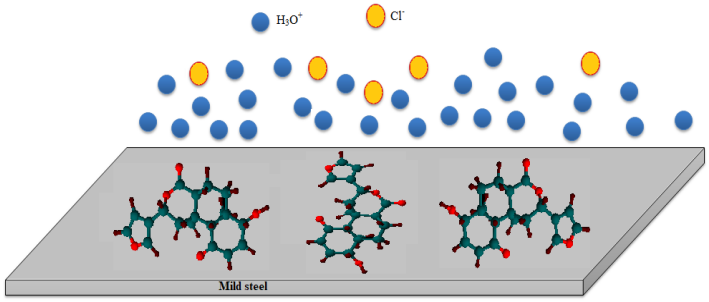

Fig. 5.7: Interaction diagram between tinosponone molecules and mild steel surface in acid media

Electrochemical impedance spectroscopy

The corrosion response of mild steel in 1 M HCl and 0.5 M H_2SO_4 solutions with various concentrations of TCE (0-5 v/v %) were demonstrated using EIS at 30^0C. In the present investigation, Randle's circuit (Fig. 1.8) was adjudged as an equivalent circuit. Fig. 5.8 and Fig. 5.9 shows Nyquist plots and Bode plots. Nyquist plots are not in an absolute semicircular shape. It can be interpreted as the result of surface inhomogeneity.

The adsorption phenomenon on the surface or development of porous or non-porous passivation layer on coating is the root cause for surface in-homogeneity[167]. Nyquist plots evinced a single capacitive loop for each concentration. It may be due to the occurrence of a charge transfer reaction at the electrode/solution interface. On examining the plots, it can be seen that the diameter of the semicircle increases by the addition of TCE concentration.

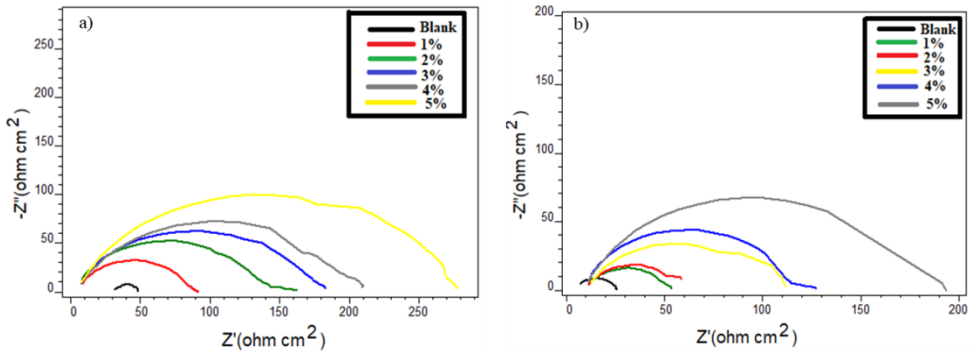

Fig. 5.8: Nyquist plots of mild steel with and without TCE in a) 1 M HCl and b) 0.5 M H_2SO_4

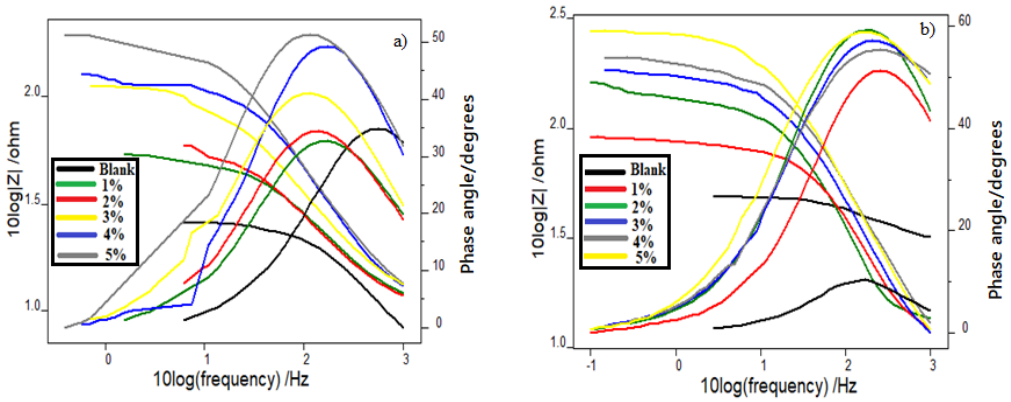

Fig. 5.9: Bode plots of mild steel with and without TCE in a) 1 M HCl and b) 0.5 M H_2SO_4

Table 5.5 clearly showed that R_{ct} values are directly proportional to TCE concentration, indicating that the mild steel corrosion is mitigated by the inhibitor TCE. Conversely, C_{dl} values decreased by the addition of TCE. This is due to a drop in the dielectric constant or a rise in the thickness of the electrical double layer. It recommends the formation of an interfacial protective layer between metal and acid[168]. Inhibition

efficiency of TCE attained 93.51% in 1 M HCl and 88.68% in 0.5 M H_2SO_4 for the highest concentration under supervision.

Table 5.5: Impedance parameters of mild steel in 1 M HCl and 0.5 M H_2SO_4 with and without TCE

Conc. (v/v %)	1 M HCl			0.5 M H_2SO_4		
	R_{ct} (Ωcm^2)	C_{dl} (μFcm^{-2})	η_{EIS}%	R_{ct} (Ωcm^2)	C_{dl} (μFcm^{-2})	η_{EIS}%
Blank	15.7	78.75	-	18.1	47.39	-
1	74.5	62.8	78.92	37.3	46.5	51.47
2	125	48.9	87.44	41.3	44.1	56.17
3	153	47.5	89.73	86.3	39.0	79.02
4	174	45.6	90.97	100	40.3	81.9
5	242	42.1	93.51	160	32.6	88.68

Potentiodynamic polarization studies

Potentiodynamic polarization studies on mild steel were carried out to evaluate the protective ability of TCE on the surface of mild steel in 1 M HCl and 0.5 M H_2SO_4. Fig. 5.10 and Fig. 5.11 exhibit Tafel and linear polarisation plots, and Table 5.6 reveal polarization parameters such as corrosion current densities (i_{corr}), corrosion potential (E_{corr}), cathodic Tafel slope (b_c), anodic Tafel slope (b_a) and polarization resistance (R_p). On close observation to the Table as mentioned above, it is clear that there was a remarkable decrease in i_{corr} values when TCE concentration increased. It can be pointed out that there is strong resistance in the corrosion process[55]. So, inhibition efficacy was found to be supplemented with an increase in concentration. The higher inhibition power on mild steel surface was displayed by 5% TCE concentration in HCl and H_2SO_4 media as 94.22% and 75%, respectively. A lower efficiency in H_2SO_4 than HCl medium was observed, similar to the weight loss and EIS studies. Linear polarization studies supplemented this observation. From Tafel plots, both cathodic and anodic Tafel slopes change appreciably in the presence of TCE, suggesting that TCE act as a mixed type inhibitor.

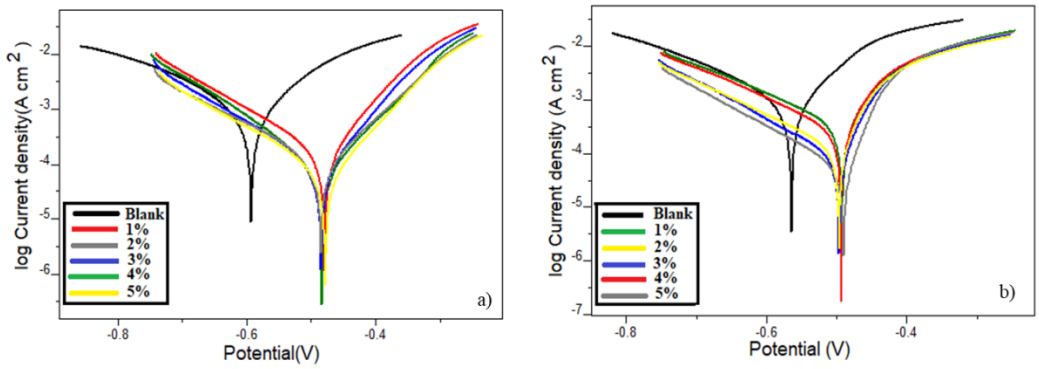

Fig. 5.10: Tafel plots of mild steel with and without TCE in a) 1 M HCl and b) 0.5 M H_2SO_4

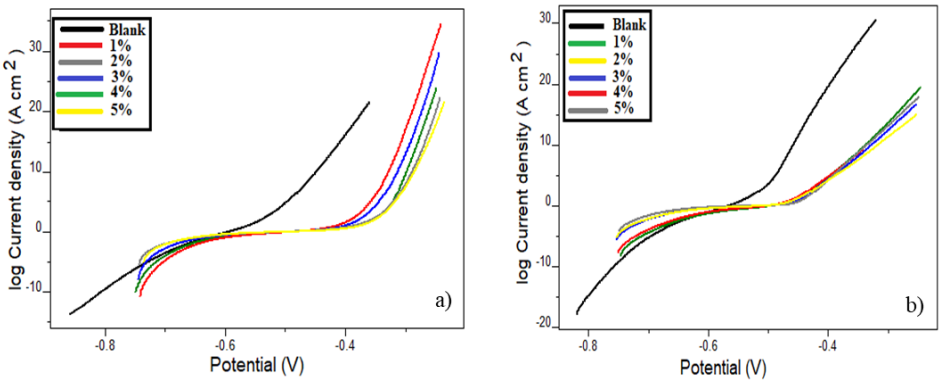

Fig. 5.11: Linear polarization plots of mild steel with and without TCE in a) 1 M HCl and b) 0.5 M H_2SO_4

Table 5.6: Potentiodynamic polarization parameters of mild steel in 1 M HCl and 0.5 M H_2SO_4 with and without TCE

Medium	Conc. (v/v %)	Tafel data					Polarization data	
		$-E_{corr}$ (mV)	i_{corr} ($\mu A/cm^2$)	$-b_c$ (mV/dec)	b_a (mV/dec)	η_{pol}%	R_p (ohm)	η_{Rp}%
1 M HCl	Blank	597.9	1240	221	166	-	33.14	-
	1	489.5	190.9	151	94	84.60	131.9	75.28
	2	486.9	105.1	176	91	91.52	228.9	85.5
	3	473.4	103.5	149	86	91.65	248.5	86.66
	4	472.6	82.12	132	85	93.35	273.9	87.90
	5	468.5	71.62	159	82	94.22	328.4	89.90
0.5 M H_2SO_4	Blank	602.2	1616	193	184	-	25.30	-
	1	562.8	845.2	184	210	46.70	50.35	49.75
	2	595.9	507.1	161	210	67.62	72.14	64.92
	3	599.6	445.1	137	199	71.46	78.24	67.66
	4	529.6	435.6	173	124	72.05	79.14	68.03
	5	609.5	388.0	143	194	75.00	92.12	72.53

Electrochemical noise measurements

Fig. 5.12 reveals the current noise for mild steel dipped in 1 M HCl and 0.5 M H_2SO_4 solutions containing various TCE concentrations (0, 1, 3, 5 v/v %). On inspection of the Figure, it was evident that the current noise for inhibited metal has a low value compared with uninhibited metal, which implies that TCE possesses considerable inhibition efficiency. As concentration increases, the value of current noise becomes lowered. The signal was at a higher magnitude for the blank experiment, indicating mild steel surface undergoes localized corrosion[154].

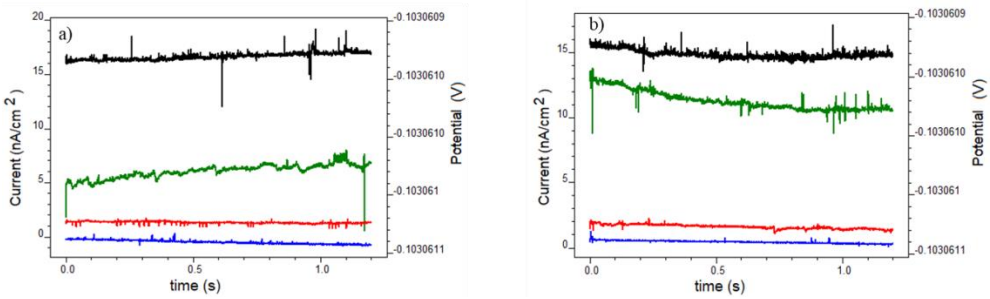

Fig. 5.12: Current noise plots of mild steel with and without TCE in a) 1 M HCl b) 0.5 M H_2SO_4

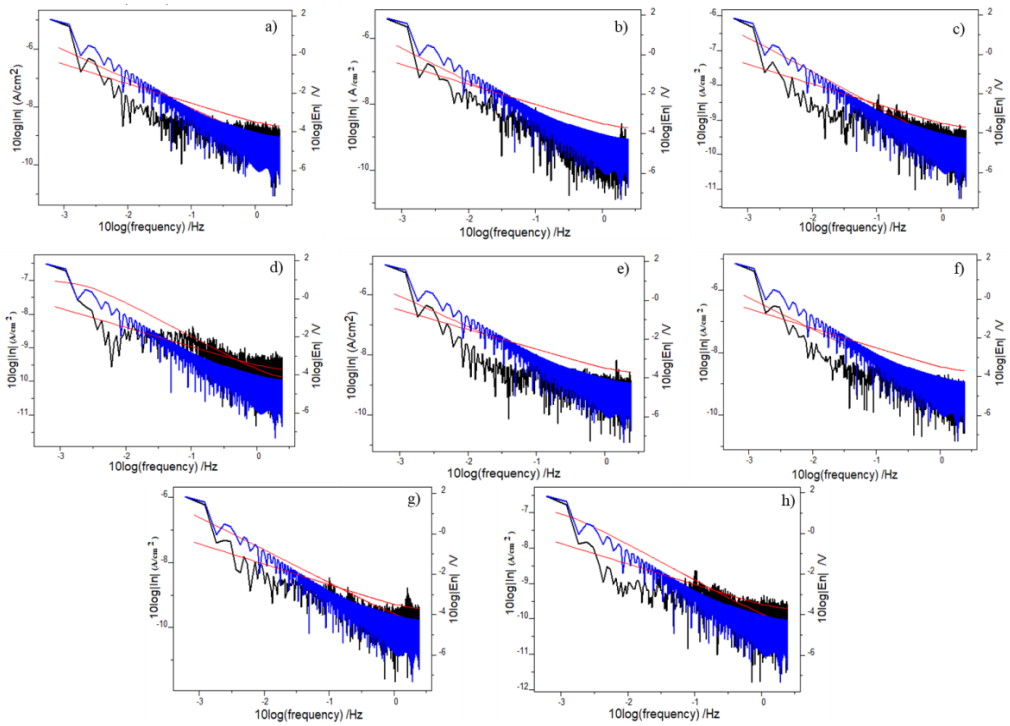

Fig. 5.13: Power spectral density plots of mild steel in 1 M HCl a) without TCE b) 1% TCE c) 3% TCE d) 5% TCE; Power spectral density plots of mild steel in 0.5 M H_2SO_4 e) without TCE f) 1% TCE g) 3% TCE h) 5% TCE

PSD plots for inhibited and uninhibited metal in acid media are shown in Fig. 5.13. It exhibited that magnitudes of current noise are relatively large for metal dipped in acid solution without TCE than the metal immersed in acid solution with TCE, which unequivocally establishing the inhibition action of TCE towards mild steel corrosion.

Pitting index is an assessment of the degree of resistance power to pitting corrosion. Fig. 5.14 shows pitting index curves for mild steel immersed in the absence and presence of various TCE concentrations. It was clear that as the concentration of TCE increases, the pitting index value rises. HCl pitting index value was higher for 5 v/v% concentration, while it was remarkably lower in the H_2SO_4 medium for the same concentration. From the pitting index values for blank and inhibited metal, it can be said that TCE can be acted as an inhibitor for mild steel in acid media[169].

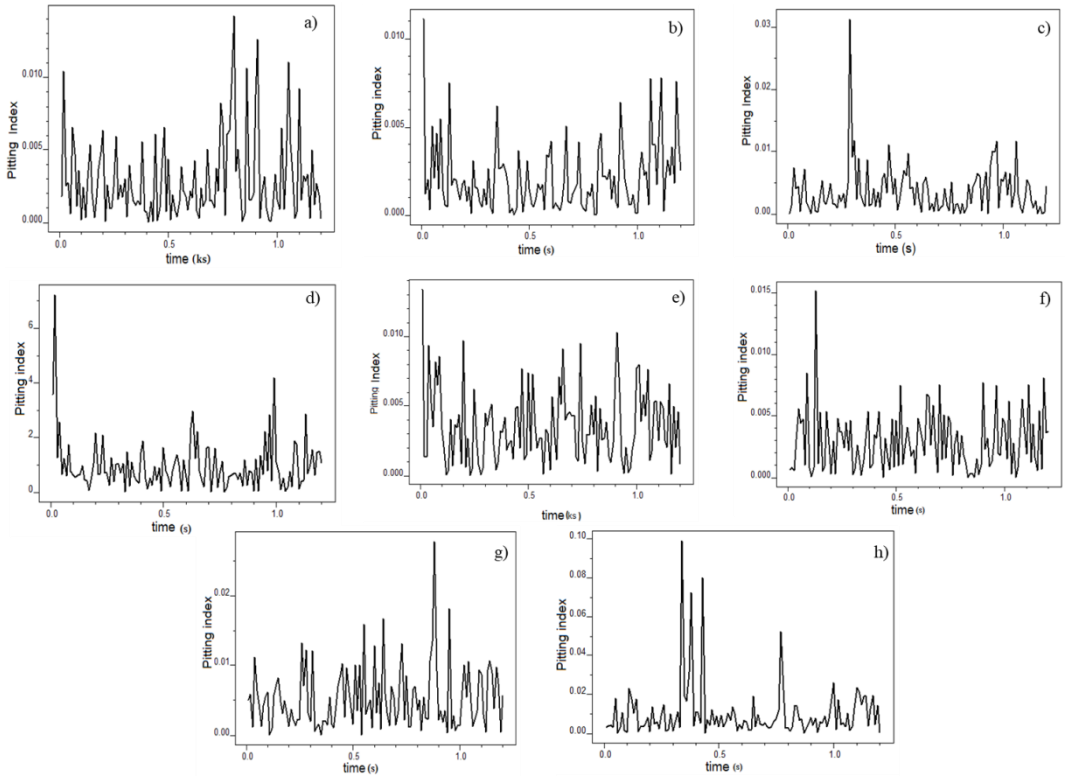

Fig. 5.14: Pitting index curves of mild steel in 1 M HCl a) without TCE b) 1% TCE c) 3% TCE d) 5% TCE; Pitting index curves of mild steel in 0.5 M H_2SO_4 e) without TCE f) 1% TCE g) 3% TCE h) 5% TCE

Atomic force microscopy

Surface mechanism of TCE on mild steel was further strengthened by AFM analysis. 3-D topography of smoothened metal, blank, metal coupons treated with 5 v/v% TCE in 1 M HCl and 0.5 M H_2SO_4 for 24 hrs are exhibit in Fig. 5.15 a–e, respectively. Surface roughness parameters such as average roughness (R_a), root mean square roughness (R_q), and maximum peak-to-peak height (R_{pp}), which specify the topography of surfaces, are provided in Table 5.7.

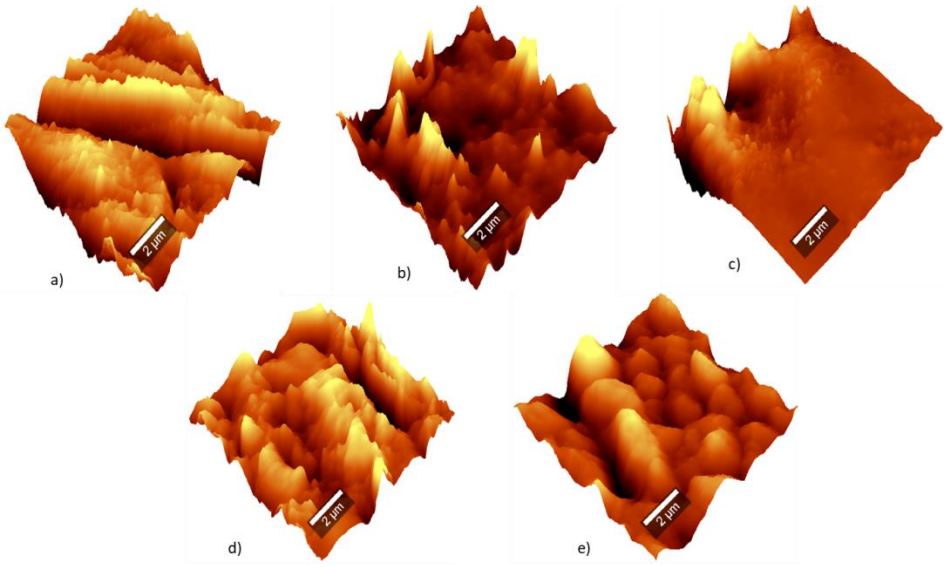

Fig. 5.15: Topography of mild steel surface a) smoothened b) in 1 M HCl c) in 1 M HCl with 5 v/v% TCE d) in 0.5 M H_2SO_4 e) in 0.5 M H_2SO_4 with 5 v/v% TCE

Table 5.7: Surface roughness parameters of mild steel by AFM analysis

Sample	R_{pp} (nm)	R_q (nm)	R_a (nm)
Smoothened mild steel	205.27	32.92	26.11
Mild steel in 1 M HCl	965.86	79.50	55.07
Mild steel in 1 M HCl with 5 v/v% TCE	646.53	51.65	29.57
Mild steel in 0.5 M H_2SO_4	2176.62	231.72	180.48
Mild steel in 0.5 M H_2SO_4 with 5 v/v%	1687.53	177.35	142.65

On analyzing the Table, it can be seen that surface roughness parameters for the smoothened metal were low, whereas the metal treated with 1 M HCl and 0.5 M H_2SO_4

were boosted due to the contact with aggressive media. Roughness parameters of the metal surface with TCE were in between that of smoothened and blank metals. It reinforces the adsorption of inhibitor molecules on the metal surface in the corrosion reaction[60]. It has also been noticed that the roughness parameters for the metal with TCE in 1 M HCl were lower than in 0.5 M H_2SO_4, implying that the former medium supports the mitigation of corrosion than the latter.

Quantum mechanical calculations

Quantum mechanical parameters of tinosponone such as energy values of HOMO and LUMO, ΔE, ionization energy (I), electron affinity (A), chemical potential (μ), electronegativity (χ), chemical hardness (η) and number of electrons transferred (ΔN) are computed in Table 5.8. The optimized geometry, corresponding HOMO and LUMO of tinosponone are pictured in Fig. 5.16. Formation of the adsorption layer on the mild steel surface by the donation of electrons can be demonstrated by the value of change in energy (E_{LUMO} - E_{HOMO}). The low ΔE value (4.178 eV) for tinosponone enables the shifting of electrons from HOMO of tinosponone to the vacant orbitals of Fe and makes TCE an excellent metal protection inhibitor. Value of ΔN less than 3.6 indicates a strong propensity for inhibitor molecules to supply electrons to the metal surface. For tinosponone ΔN value was found to be 1.4265, which may be ascribed to the excellent corrosion control of TCE[160]. So, theoretical calculations were in line with experimental results.

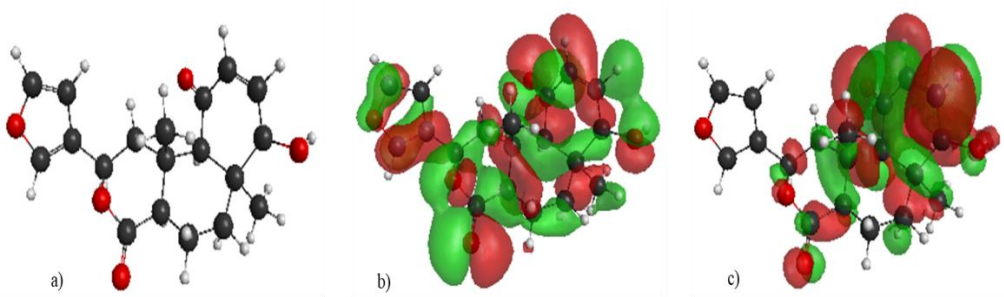

Fig. 5.16: a) Optimized geometry, b) HOMO and c) LUMO of tinosponone

Table 5.8: Quantum mechanical parameters (in eV) of tinosponone

E_{HOMO}	E_{LUMO}	ΔE	I	A	μ	χ	η	ΔN
-3.129	1.049	4.178	3.129	-1.049	-1.04	1.04	2.089	1.4265

Statistical analysis

❖ ***Optimization of factors for inhibition efficiency (IE%)***

Screening experiments revealed that temperature, TCE concentration, and acid concentration significantly influenced the corrosion inhibition efficiency. So they were selected as independent factors in this study. Weight loss studies showed that the corrosion rate was upgraded in H_2SO_4 medium than in HCl medium. That prompted us to select the HCl solution as an acid medium. The structure of the design and the three levels depending on the BBD of test factors are shown in Table 5.9, comprising experimental results and predicted response. A total of 15 experimental runs were obtained in it. It was demonstrated that corrosion inhibition efficiency increased with an increase in TCE concentration. This analysis reached maximum efficiency with 5 v/v% TCE concentration in 0.5 M HCl concentration at 313 K. To explore the exact combination of the three factors understudy for attaining the immense efficiency, RSM was applied for the optimization technique. The regression model between the test factors and the inhibition efficiency was created at that point, shown in equation (53). Inhibitor efficiency was designated as a function of the test factors in the selected levels using the quadratic equation (53).

$$IE = 5891 - 34.44\ X_1 + 30.3X_2 - 264.1\ X_3 + 0.0503\ X_1^2 - 1.387\ X_2^2 - 20.79\ X_3^2 + 0.922\ X_1X_3 - 1.62\ X_2X_3 - 0.0397\ X_1X_2 \quad (53)$$

where IE represents inhibition efficiency, X_1 denotes temperature, X_2 denotes TCE concentration and X_3 denotes acid concentration.

Using this regression model, analysis of variance (ANOVA) was then applied. ANOVA results with a significance level of 95% are illustrated in Table 5.10. The most

demanding parameter is P-value in this Table. P-value determined shows the significance of the impact of a factor on response[170]. The degree of essentialness (α) was chosen to be 0.05. It showed that the value of P was lower than 0.05 for the linear and square terms. The ANOVA results explained that TCE concentration was the factor having a significant influence on the response. Pareto chart (Fig. 5.17) describes that three linear terms such as temperature, TCE concentration and acid concentration have an appreciable impact on the inhibition efficiency in which TCE concentration has the most. Squared terms of temperature, TCE concentration and acid concentration were found to have a low influence on IE%. The two-way interaction term X_1X_3 also exhibited a small impact on IE%, whereas the remaining interaction terms X_1X_2 and X_2X_3 did not reveal any impact on the inhibition efficiency.

Table 5.9: Experimental and predicted IE% from weight loss measurements and BBD

Run order	Actual level of factors			IE%		Residual
	X_1	X_2	X_3	Experimental	Predicted	
1	313	1	1	60.11293	57.7645	2.34843
2	333	1	1	35.54071	36.4269	0.88619
3	313	5	1	90.39050	89.5043	0.88619
4	333	5	1	62.64005	64.9884	2.34835
5	313	3	0.5	84.60215	84.8844	0.28225
6	333	3	0.5	55.68507	52.7327	2.95237
7	313	3	1.5	60.13363	63.0860	2.95237
8	333	3	1.5	49.66637	49.3841	0.28226
9	323	1	0.5	39.46750	41.5337	2.06620
10	323	5	0.5	74.32543	74.9294	0.60397
11	323	1	1.5	32.80916	32.2052	0.60396
12	323	5	1.5	61.17699	59.1108	2.06619
13	323	3	1	62.68992	62.6899	0.00001
14	323	3	1	62.68992	62.6899	0.00001
15	323	3	1	62.68992	62.6899	0.00001

The better fit model for experimental results is indicated by the closeness of R^2 and R^2(adj) value to unity. Here, the R^2 and R^2(adj) values were 0.9892 and 0.9697,

respectively indicate the best fit predicted model for experimental values. Therefore, the outcomes can be quickly evaluated by the model.

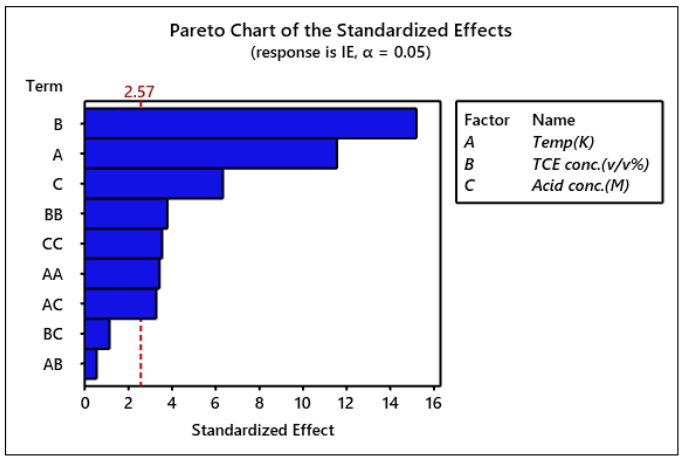

Fig. 5.17: Pareto chart of the standardized effects of mild steel

Table 5.10: Analysis of variance for corrosion inhibition efficiency

Source	DF	Adj SS	Adj MS	F-Value	P-Value
Model	9	3607.35	400.82	50.79	0.000
Linear	3	3185.58	1061.86	134.55	0.000
Temp	1	1051.27	1051.27	133.21	0.000
TCE Conc.	1	1818.13	1818.13	230.37	0.000
Acid Conc.	1	316.19	316.19	40.06	0.001
Square	3	323.62	107.87	13.67	0.008
Temp*Temp	1	93.38	93.38	11.83	0.018
TCE Conc.*TCE Conc.	1	113.65	113.65	14.40	0.013
Acid Conc.*Acid Conc.	1	99.73	99.73	12.64	0.016
2-Way Interaction	3	98.15	32.72	4.15	0.080
Temp*TCE Conc.	1	2.53	2.53	0.32	0.596
Temp*Acid Conc.	1	85.10	85.10	10.78	0.022
TCE Conc.*Acid Conc.	1	10.53	10.53	1.33	0.300
Error	5	39.46	7.89		
Lack-of-Fit	3	39.46	13.15	*	*
Pure Error	2	0.00	0.00		
Total	14	3646.81			

DF: degrees of freedom, Adj SS: adjusted sum of squares, Adj MS: adjusted mean of squares,

F: Fischer's F-test value, P: probability

Main effects plots supplement the outcomes obtained from the regression analysis[171]. It represents how to control tested factors that influence the response. Fig. 5.18 explains the main effects plots for the fitted means of inhibition efficiency. It

showed that the maximum inhibition efficiency was observed for 5 v/v% concentration of TCE at an operating temperature of 313 K at 0.5 M concentration of HCl. Rise in temperature causes a hike in the kinetic energy of the inhibitor molecules and the speed of collision between the molecules. This inclination hinders and destroys the development of adsorbed film inhibitors on the metal surface. So, when the temperature goes up, inhibition efficiency decreases. A close tendency was examined with the concentration of HCl as it was raised from 0.5 M to 1.5 M. Whereas inhibition power of TCE augmented when its concentration was increased from 1 to 5 v/v%. The corrosion rate was much boosted in the absence of an inhibitor and reduced when the inhibitor was present. Thereby adsorption of inhibitor molecules enhances, and efficiency also increases.

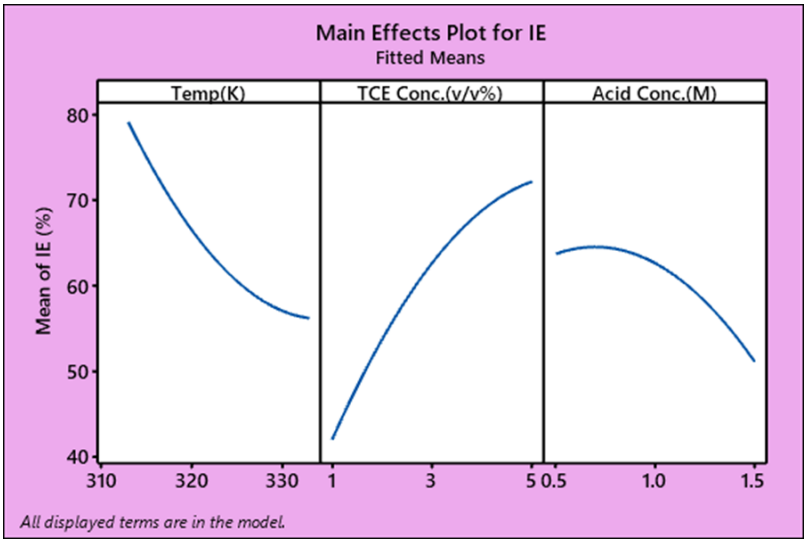

Fig. 5.18: Main effects plots for inhibition efficiency of mild steel in HCl medium

If the change in response is disparate for two factors, there will be an interaction between them. Fig. 5.19 exhibits the interaction plot for inhibition efficiency. Crossed lines in the interaction plot indicate a significant interaction between the factors, whereas parallel or straight lines point out little interaction[134]. From Fig. 5.19, it has been examined that the two-way interaction terms were trivial as there are no crossed lines except in Temp-Acid concentration interaction term, X_1X_3. Outcomes of ANOVA

analysis also revealed that the P-value was higher than 0.05 for two-way interactions, and only one interaction term has a lower P-value, i.e., X_1X_3.

Contours and 3-D surface plots demonstrate the inter-dependence of the tested factors on IE (%) and are presented in Fig. 5.20. It was exhibited that the inhibition efficiency goes up when TCE concentration rises for a given temperature. But, inhibition efficiency and temperature have a reverse relationship. This trend can be ascribed to the physical adsorption of TCE molecules on the mild steel surface. Similarly, inhibition efficiency and acid concentration are inversely proportional.

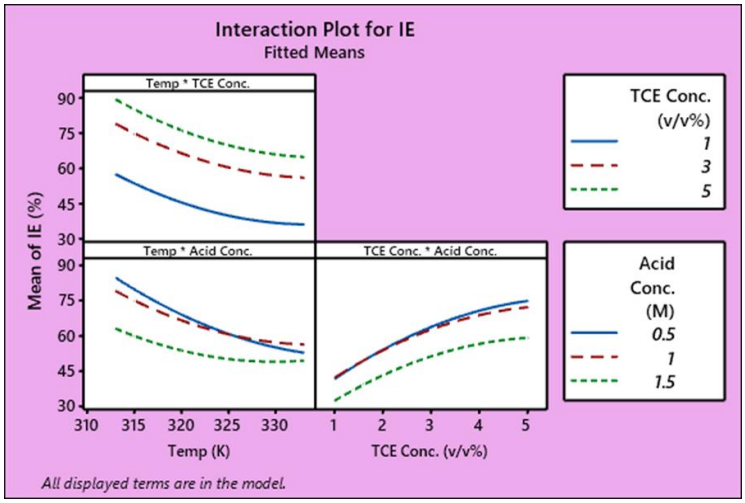

Fig. 5.19: Interaction plot for inhibition efficiency

❖ ***Response optimization***

Well organized numerical model in equation (53) was used with the goal of optimizing the independent variables such as temperature, TCE concentration and acid concentration to bring about the maximum IE. For the most remarkable and feasible response, the desirability function method was employed by improving tested factors[172]. Response optimization plot for IE is shown in Fig. 5.21. The anticipated optimum factors identified were temperature (313 K), TCE concentration (5 v/v%), and acid concentration (0.5 M) for the HCl environment and the corresponding predicted IE was 96.82%, as depicted in Fig. 5.21. Confirmation tests achieved validation of the optimal factor settings and the amelioration of the IE. Confirmation tests were also helped to

verify the recurrence of the experimental outcomes and approve the prescient model's accuracy.

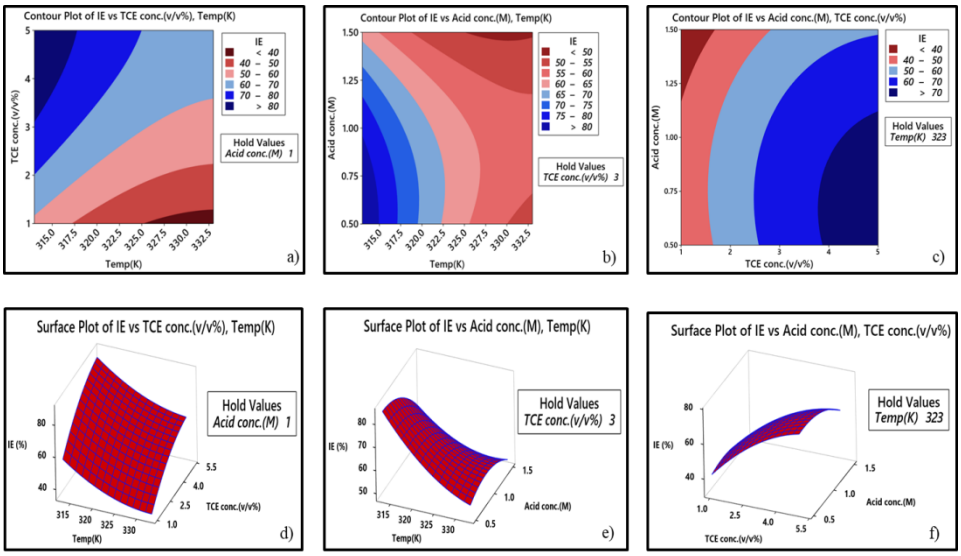

Fig. 5.20: a, b & c) Contours and d, e & f) 3-D surface plots for inhibition efficiency

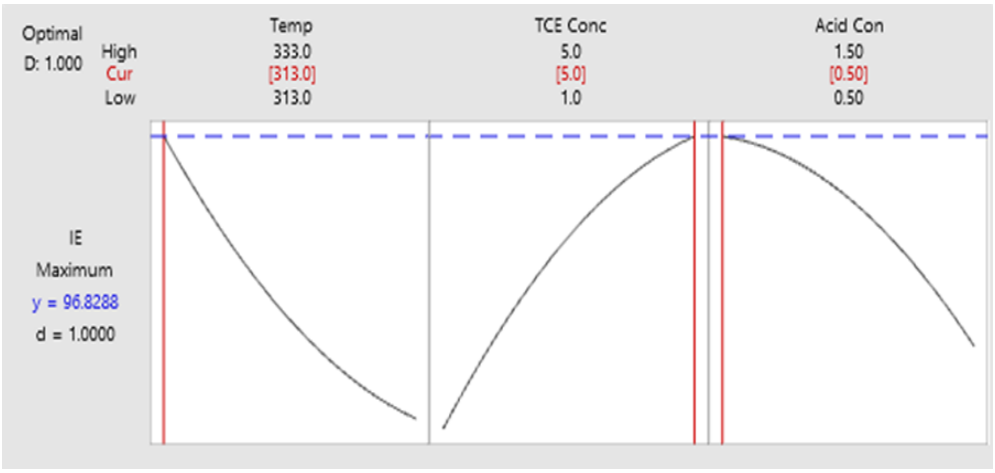

Fig. 5.21: Response optimization plot for inhibition efficiency

Conclusions

- TCE inhibitor was found to diminish and retard the corrosion of mild steel exposed in 1 M HCl and 0.5 M H_2SO_4.
- Weight loss studies showed that boosting the TCE concentration causes an increase in inhibition efficiency due to the adsorption of TCE molecules on the metal surface.

- In comparison, an increment in temperature reduces its inhibition potential due to the desorption of the adsorbed layer.
- Maximum inhibition potency of TCE in 1 M HCl and 0.5 M H_2SO_4 was calculated as 94.73% and 82.53%, respectively.
- Langmuir adsorption isotherm was reckoned to be good adsorption of TCE molecules on mild steel surface in both acid media.
- The variation in surface morphology of mild steel was studied by AFM, which furnished strong proof for developing a protective film on mild steel with TCE in an acidic media.
- Quantum chemical investigations were also supported to confirm the inhibition efficiency of TCE.
- Response surface methodology provides comprehensive information about the interrelation between the factors and the acceptance of the optimum parameter setting. Regression model could describe the results obtained from experiments in good agreement.

CHAPTER 6

GARCINIA CAMBOGIA EXTRACT: NATURAL CORROSION INHIBITOR FOR MILD STEEL IN ACID MEDIA

This chapter illustrates the corrosion-resistant power of the ethanol extract of *Garcinia cambogia* (GCE) leaves for mild steel in 1 M HCl and 0.5 M H_2SO_4. Gravimetric, electrochemical and morphological studies have been established to authenticate inhibiting power of GCE. Although GCE contains numerous bioactive components, organic acids such as hydroxycitric acid (HCA) and hydroxycitric acid lactone HCA lactone) (Fig. 6.1) are the leaf extract's primary class of compounds[173]. Quantum mechanical investigations of HCA and HCA lactone have been established the anticorrosion behaviour of GCE.

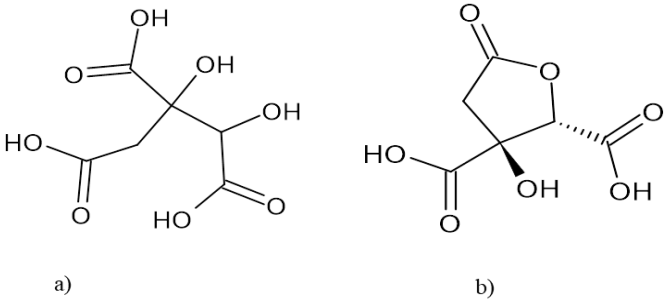

Fig. 6.1: Structure of a) hydroxycitric acid b) hydroxycitric acid lactone

Garcinia cambogia

Results and discussions

Phytochemical screening of GCE

Based on the standard screening tests, major phytochemicals in GCE were confirmed, and the results are given in Table 6.1.

FTIR spectroscopy

Fig. 6.2 shows the FTIR spectrum of GCE, which revealed characteristic stretching and bending frequencies for various bonds. Broad band at 3281 cm^{-1} indicates O-H stretching vibration, which is a hydrogen bonding band. Two sharp peaks at 2917

cm^{-1} and 2850 cm^{-1} exhibit alkyl C-H stretching bonds. >C=O stretching band occurs at 1731 cm^{-1}. This peak may be assigned to carboxylic acids. The peaks at 1622 cm^{-1} and 1463 cm^{-1} can be accredited to aliphatic and aromatic C=C stretching vibrations. C-O stretching vibration appears as a weak band at 1242 cm^{-1} and 1031 cm^{-1}. In short, well-defined peaks of GCE can be ascribed to heteroatoms, aromatic rings, and unsaturated compounds.

Table 6.1: Phytochemical screening of GCE

Sl. No.	Compounds	Tests	Results
1	Alkaloids	Mayers reagent	−−
2	Steroids	Salkowaski's test	++
3	Phenolic compounds	Potassium ferrocyanide test	++
4	Flavanoids	Sodium hydroxide test	++
5	Saponins	Froth test	++
6	Tannins	Lead acetate test	++
7	Cardiac glycosides	Conc. sulphuric acid test	++
8	Coumarin	Alcoholic NaOH test	−−
9	Quinones	Conc. sulphuric acid test	++

++ (present), − − (Absent)

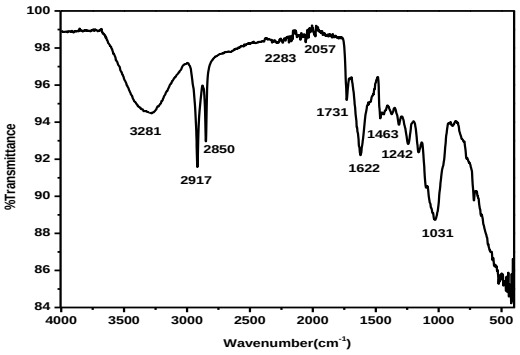

Fig. 6.2: FTIR spectrum of GCE

Weight loss measurements

❖ ***Effect of concentration***

The period of the adsorption layer's existence on the metal surface can be estimated in weight loss measurements. The inhibition efficiency (ɳ%) and corrosion rate (υ) were tabulated in Table 6.2. It can be seen that as GCE concentration raised, metal

corrosion potency also got increased in 1 M HCl and 0.5 M H_2SO_4 solutions. Weight loss measurement is a long-term measurement that may differ considerably from short-term methods like electrochemical techniques. Because the previous one corresponds to the steady-state of the corrosion process, whereas the latter results in instantaneous corrosion rates.

Table 6.2: Weight loss measurements of mild steel with and without GCE in 1 M HCl and 0.5 M H_2SO_4 at room temperature for 24 hrs

Conc. (v/v %)	Corrosion rate (mm/yr)		Inhibition efficiency (η%)	
	1 M HCl	0.5 M H_2SO_4	1 M HCl	0.5 M H_2SO_4
Blank	3.95	35.57	-	-
1	1.77	18.83	55.12	47.06
2	1.44	16.92	63.49	52.41
3	1.20	15.08	69.53	57.59
4	1.08	13.22	72.48	62.82
5	0.32	8.70	91.73	75.53

GCE exhibited a lower η% value of 55.12% at a minimum concentration (1 v/v%) and an extreme η% value of 91.73% at the highest concentration (5 v/v%) in 1 M HCl at room temperature. In hydrochloric acid medium, GCE exhibited reasonably better metal corrosion inhibition efficacy than in sulphuric acid medium. In 0.5 M H_2SO_4, maximum η% reached 75.53% at 5 v/v%. Surface coverage is the determining factor for corrosion inhibition potential. At higher GCE concentrations, the number of obtainable inhibitor molecules built on the metal surface led to higher surface coverage and reduced acidic corrosion for mild steel. The electron-donating ability of hydroxyl groups, heteroatoms and unsaturated compounds present in GCE can be accredited to the inhibition capacity of GCE, which is comprised of multi-complex compounds. HCA has also sustained high electron density towards the metal surface. The extent of hydration of chloride ions is smaller than sulphate ions. It may cause specific adsorption of

chloride ions compared to sulphate ions[174]. Since the number of adsorbed Cl^- ions on the metal surface is sufficient to generate negative charges towards the acid media, the cationic form of hydroxycitric acid adsorbs to a large extent.

❖ ***Effect of temperature***

The influence of temperature on the metal dissolution process was analyzed by employing weight loss measurements at four different temperatures 303, 313, 323 and 333 K. Variation in corrosion rate and inhibition efficiency is depicted in Fig. 6.3 and is computed in Table 6.3.

It is evident from the data that temperature is directly proportional to the rate of corrosion. When the temperature increased from 303 K to 333 K, inhibition potency showed a noticeable decrease from 91.73% to 72.08% for 5% GCE concentration in HCl solution. Likewise, in the H_2SO_4 medium, inhibition potency decreased from 75.53% to 62.46% for the highest concentration under study. This trend may be attributed to the desorption of GCE molecules from the metal surface at elevated temperatures and thereby destroys protection film and causes metal destruction.

Arrhenius equation (41) was applied to calculate the activation energy of metal corrosion. Fig. 6.4 a) and Fig. 6.5 a) represent the plot of log K vs 1/T for mild steel in acid media with and without GCE. The equation (43) derived from transition state theory was employed to acquire thermodynamic parameters such as enthalpy of activation (ΔH^*) and entropy of activation (ΔS^*) values. Slope and intercept of the plot of log K/T vs 1/T (Fig. 6.4 b) and Fig. 6.5 b)) corresponds to ΔH^* and ΔS^* values. All the thermodynamic parameters were calculated in Table 6.4, involving activation energy (E_a) and pre-exponential factor (A). Examining Table 6.4, it was clear that the acid solution without GCE has more activation energy of metal corrosion than the acid solution with GCE. The increase in E_a values with GCE concentration causes a reduction in the metal

dissolution rate[175]. Endothermic behaviour of metal corrosion was revealed from the positive values of the enthalpy of activation. As the concentration of GCE increased, ΔH* and ΔS* values were also raised.

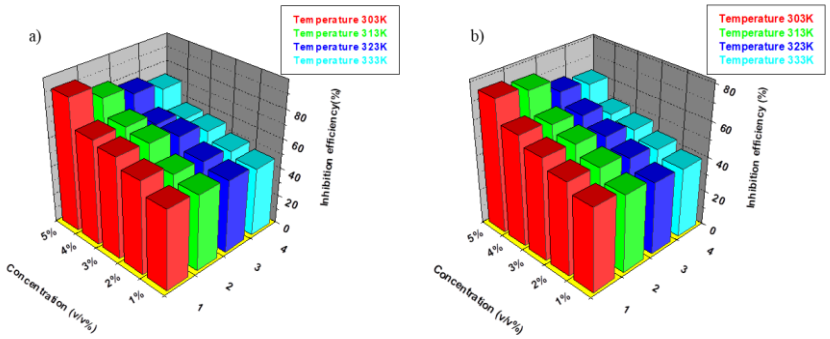

Fig. 6.3: Variation in inhibition efficiency of GCE in a) 1 M HCl b) 0.5 M H_2SO_4 at elevated temperatures

Table 6.3: Corrosion rate (υ) and inhibition efficiency (η%) of GCE in 1 M HCl and 0.5 M H_2SO_4 at different temperatures for 24 hrs

Medium	Conc. (v/v%)	υ (303 K)	η% (303 K)	υ (313 K)	η% (313 K)	υ (323 K)	η% (323 K)	υ (333 K)	η% (333 K)
1 M HCl	Blank	3.95	-	13.11		22.05	-	31.77	-
	1	1.77	55.12	6.23	52.48	10.94	50.40	16.78	47.18
	2	1.44	63.49	5.72	56.37	10.09	54.25	15.56	51.02
	3	1.20	69.53	4.15	68.34	8.13	63.14	13.69	56.91
	4	1.08	72.48	3.79	71.09	8.05	63.50	13.28	58.20
	5	0.32	91.73	2.26	82.76	5.01	77.28	8.87	72.08
0.5 M H_2SO_4	Blank	35.57	-	58.27	-	86.25	-	106.2	-
	1	18.83	47.06	32.69	43.89	50.95	40.92	64.14	39.63
	2	16.92	52.41	28.58	50.95	45.58	47.15	59.64	43.87
	3	15.08	57.59	25.36	56.47	40.95	52.52	54.91	48.32
	4	13.22	62.82	22.98	60.56	36.23	57.99	51.92	51.13
	5	8.70	75.53	15.77	72.93	30.14	65.05	39.88	62.46

Adsorption isotherms

Weight loss measurements revealed that temperature and surface coverage are inversely proportional to each other. It denotes the reduced stability of the corrosion products at higher temperatures. Higher temperature may cause 1) advancement in kinetic oxidation reaction 2) increased rate of desorption. Moreover, the electrical

charge on the metal surface rises with temperature, indicating a reverse relation between surface coverage and temperature.

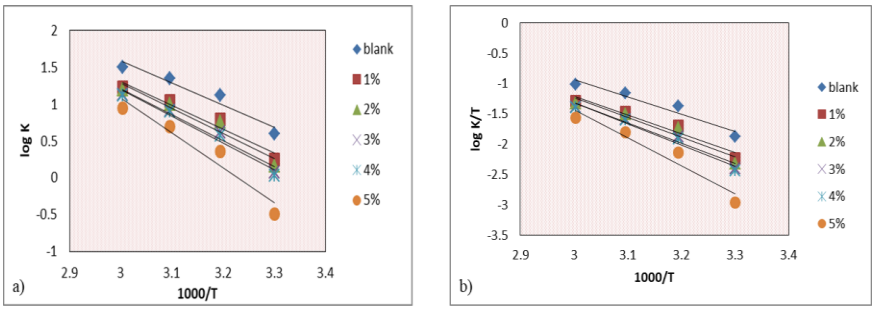

Fig. 6.4: Arrhenius plots of a) log K vs 1000/T b) log K/T vs 1000/T with and without GCE in 1 M HCl

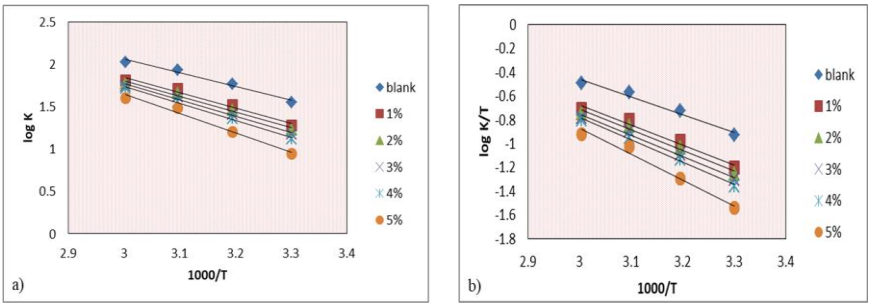

Fig. 6.5: Arrhenius plots of a) log K vs 1000/T b) log K/T vs 1000/T with and without GCE in 0.5 M H_2SO_4

Table 6.4: Thermodynamic parameters of mild steel corrosion with and without GCE in 1 M HCl and 0.5 M H_2SO_4

Medium	Conc. (v/v %)	E_a (kJ mol^{-1})	A	ΔH^* (kJ mol^{-1})	ΔS^* (J $mol^{-1}K^{-1}$)
1 M HCl	Blank	57.24	3.58×10^{10}	54.60	-44.78
	1	61.70	9.40×10^{10}	59.06	-36.76
	2	65.09	3.03×10^{11}	62.45	-27.00
	3	67.18	5.42×10^{11}	64.54	-22.19
	4	69.67	1.31×10^{12}	67.03	-14.83
	5	90.45	1.79×10^{15}	87.81	45.17
0.5 M H_2SO_4	Blank	30.96	8.16×10^{6}	28.30	-114.51
	1	34.72	1.92×10^{7}	32.08	-107.36
	2	35.72	2.54×10^{7}	33.08	-105.07
	3	36.63	3.22×10^{7}	34.01	-103.09
	4	38.32	5.50×10^{7}	35.68	-98.630
	5	43.88	3.31×10^{8}	41.24	-83.710

Adsorbed inhibitor molecules obstruct the availability of active adsorption sites on the metal surface. It may be due to the strong interaction between the inhibitor and metal surface than between the metal surface and water molecules.

Langmuir, El-Awady, Frumkin, Temkin, Freundlich and Flory-Huggins isotherms are usually employed to find the adsorption model for metal-inhibitor interaction. The best fit of all was found to be Frumkin isotherm which is a plot of log[1/c(θ/(1-θ))] vs θ for 1 M HCl. In contrast, Freundlich isotherm was found to obey in 0.5 M H_2SO_4, a plot of concentration vs θ. Fig. 6.6 a) and Fig. 6.6 b) shows Frumkin and Freundlich isotherm suited for the adsorption of GCE molecules on the metal surface in 1 M HCl and 0.5 M H_2SO_4 respectively.

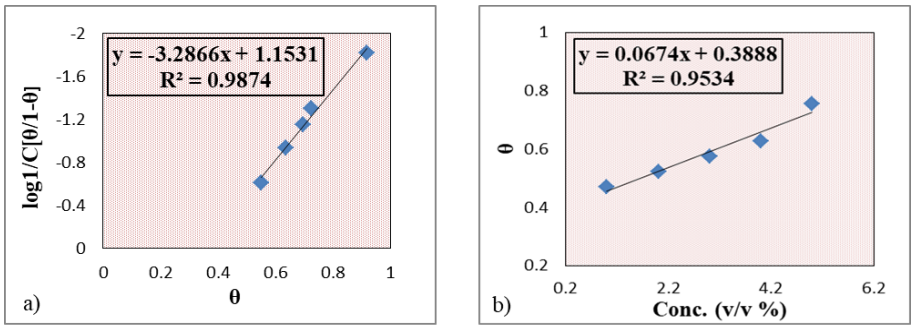

Fig. 6.6: a) Frumkin adsorption isotherm of GCE on mild steel in 1 M HCl and b) Freundlich isotherm of GCE on mild steel in 0.5 M H_2SO_4

Though the linearity of isotherm exhibited that the adsorption of GCE obeys Freundlich isotherm in H_2SO_4, appreciable deviation of the slope from unity suggested that the isotherm could not be tightly employed. The variation of the slope from unity may be described due to apparent heterogeneity on the metal surface in sulphuric acid medium[176].

From the relation between ΔG^0_{ads} and adsorption equilibrium constant K_{ads} as shown in equation (54), mechanism of adsorption of GCE molecules on the metal surface can be suggested.

$$\Delta G^0_{ads} = - RT \ln (55.5\ K_{ads}) \quad (54)$$

In the present research work, ΔG^0_{ads} for GCE-mild steel adsorptions were -26.98 and -29.70 kJ mol^{-1} in 1 M HCl and 0.5 M H_2SO_4, respectively, indicated the adsorption behaviour of GCE molecules on mild steel surface was both physisorption and chemisorption. K_{ads} values for GCE adsorption were calculated as 2572.016 and 867.227 in 1 M HCl and 0.5 M H_2SO_4, respectively. Higher value of K_{ads} pointed out that GCE molecules preferentially adsorb on the metal surface in HCl medium than H_2SO_4 medium.

UV-Visible spectroscopy

UV-Visible spectra were drawn to understand the metal-binding ability of GCE using various metal salt solutions shown in Fig. 6.7. UV spectrum of GCE displayed a maximum absorbance of 2.261 at 411 nm. Also noticed a sharp absorption band at 665 nm with an absorbance of 0.793. In addition, it showed another absorption band in the range of 505-535 nm. It can be assigned to the presence of various phytochemicals such as flavonoids, tannins, carotenoids, phenolic compounds and alkaloids. There was a sudden decrease in the intensity of these bands after binding with all the metal salts used for the present investigation. In $CoCl_2$, the maximum absorbance of 1.361 at 411 nm showed 39.9% decrease in the intensity after binding. Chromium (III) acetate revealed a maximum absorbance of 1.179 at 411 nm, implying a 47% decrease in the intensity. For Mn(II) acetate, maximum absorbance was 1.376 at 411 nm, which revealed 39% decrease in the intensity after binding. Cu(II) acetate and Zn(II) acetate exhibited a remarkable reduction in intensity as the maximum absorbance observed was 1.076 and 1.067 at 411 nm, respectively. Fe(III) chloride disclosed a maximum absorbance of 1.261 at 411 nm, with a 46% decrease in intensity. The lowering tendency was tremendous in the case of NaCl which showed 54% decrease in intensity. It may be due to quenching indicating a significant affinity of GCE towards metal salts[177].

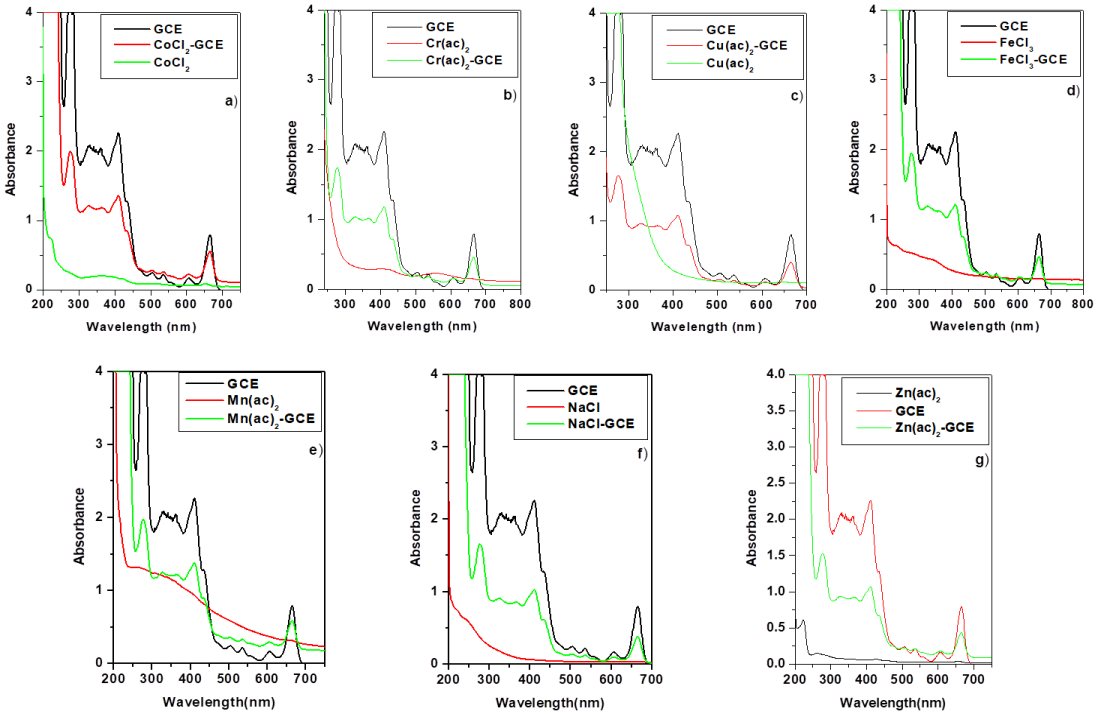

Fig. 6.7: UV spectra of a) GCE, $CoCl_2$ and GCE.$CoCl_2$ b**)** GCE, $Cr(ac)_2$ and GCE.$Cr(ac)_2$ c**)** GCE, $Cu(ac)_2$ and GCE.$Cu(ac)_2$ d**)** GCE, $FeCl_3$ and GCE.$FeCl_3$ e**)** GCE, $Mn(ac)_2$ and GCE.$Mn(ac)_2$ f**)** GCE, NaCl and GCE.NaCl g**)** GCE, $Zn(ac)_2$ and GCE.$Zn(ac)_2$

Electrochemical impedance spectroscopy

Impedance responses for mild steel corrosion in 1 M HCl and 0.5 M H_2SO_4 with and without GCE are presented in Fig. 6.8 and Fig. 6.9 as Nyquist and Bode plots, respectively. The depressed semi-circular shape of the Nyquist plot reveals that the metal dissolution process undergoes the charge transfer reaction[178]. The retarding capacity of metal corrosion by GCE molecules was realized from an increase in the diameter of the Nyquist plot with respect to concentration. Bode plots illustrate that as the concentration of GCE increased, phase angle peaks became higher and broader compared to the blank experiment. Table 6.5 outlines the result of impedance analysis assisted with Randle's equivalent circuit (Fig. 1.8). The percentage of inhibition efficiency was calculated using equation (22).

On inspection of the Table above mentioned, it was clear that R_{ct} values increased with GCE concentration, whereas C_{dl} values showed the opposite trend. The increase in R_{ct} values denotes higher inhibition efficiency by adding GCE. The drop in C_{dl} values can be ascribed to the adsorption of GCE molecules left behind water molecules at the metal solution interface. It causes the development of an adsorption layer on the mild steel surface and reduces the metal corrosion rate.

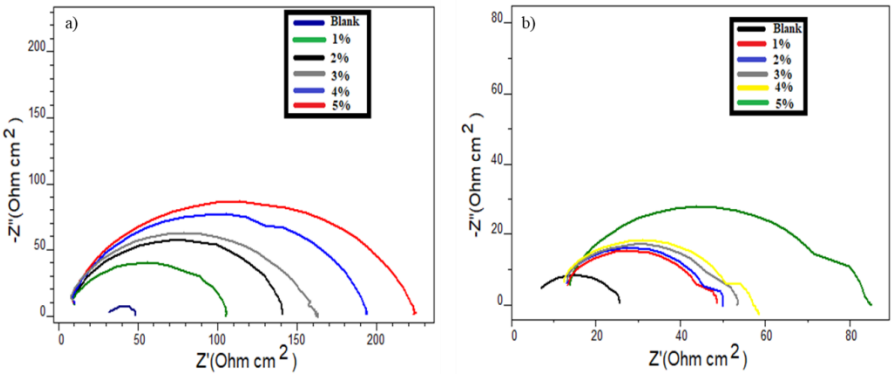

Fig. 6.8: Nyquist plots of mild steel with and without GCE in a) 1 M HCl and b) 0.5 M H_2SO_4

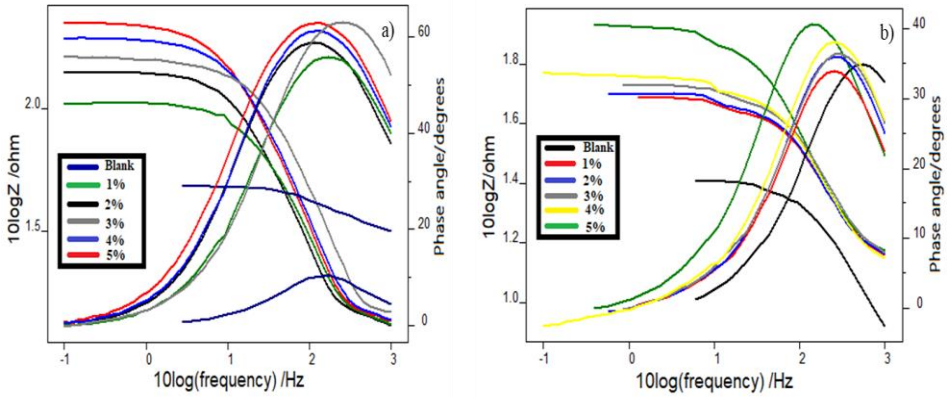

Fig. 6.9: Bode plots of mild steel with and without GCE in a) 1 M HCl and b) 0.5 M H_2SO_4

GCE showed considerably good metal protection in hydrochloric acid than sulphuric acid. In HCl, efficiency reached a maximum of 89.73%, whereas, in sulphuric acid, the extreme efficiency attained only up to 72.06%. This result was in exact agreement with weight loss measurements.

Table 6.5: Impedance parameters of mild steel in 1 M HCl and 0.5 M H_2SO_4 with and without GCE

Conc. (v/v %)	1 M HCl			0.5 M H_2SO_4		
	R_{ct} (Ωcm^2)	C_{dl} (μFcm^{-2})	η_{EIS}%	R_{ct} (Ωcm^2)	C_{dl} (μFcm^{-2})	η_{EIS}%
Blank	15.7	78.8	-	18.1	47.4	-
1	32.1	72.0	51.09	33.5	48.0	45.97
2	40.6	62.4	61.33	35.1	48.8	48.43
3	44.2	60.9	64.47	38.4	45.4	52.86
4	48.8	56.9	67.82	42.2	46.9	57.10
5	153	53.6	89.73	64.8	43.6	72.06

Potentiodynamic polarization studies

Potentiodynamic polarization studies explained changes in the anodic dissolution of mild steel and cathodic hydrogen reduction in the presence and absence of GCE as the metal corrosion controlled by redox reactions. Fig. 6.10 and Fig. 6.11 reveal Tafel and linear polarization plots in 1 M HCl and 0.5 M H_2SO_4 with varying GCE concentrations for mild steel. i_{corr} values can be obtained by extrapolating the linear fragment of the anodic and cathodic Tafel plot through the E_{corr} values. Tafel plots exhibited that GCE has appreciably changed the slope of curves at all concentrations, indicating that oxidation-reduction reactions were controlled by adding GCE into acid solutions. It may diminish the anodic dissolution of mild steel and restrict the cathodic hydrogen evolution reactions[179]. Potentiodynamic polarization parameters acquired from Tafel and linear polarization plots and corresponding calculated inhibition efficiencies are summarized in Table 6.6. From the Table, it was clear that the corrosion potential values change from negative to more positive potential moving from uninhibited metal to inhibited metal dipped in an acidic environment. But, this change was not examined in a particular direction. This fact can be considered that the reason behind GCE was acted in a mixed mode of inhibition. This trend showed that GCE molecules encourage passivation of mild steel metal as a result of interaction between GCE and the metal surface, which cause successful sealing for the surface from further reaction. The higher concentration

brings about a lower current density and attained extreme inhibition capacity of 92.51% and 74.93% in 1 M HCl and 0.5 M H_2SO_4, respectively.

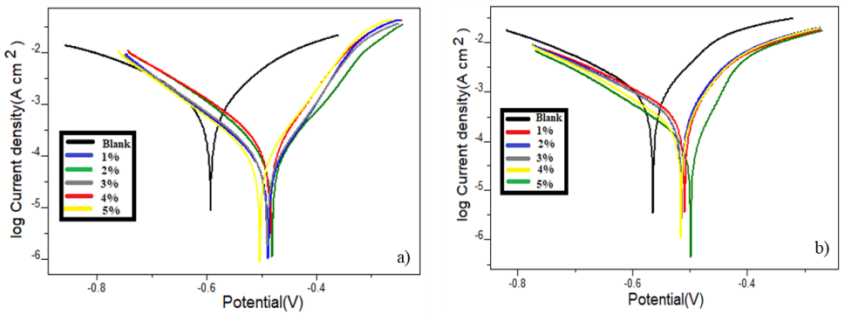

Fig. 6.10: Tafel plots of mild steel with and without GCE in a) 1 M HCl and b) 0.5 M H_2SO_4

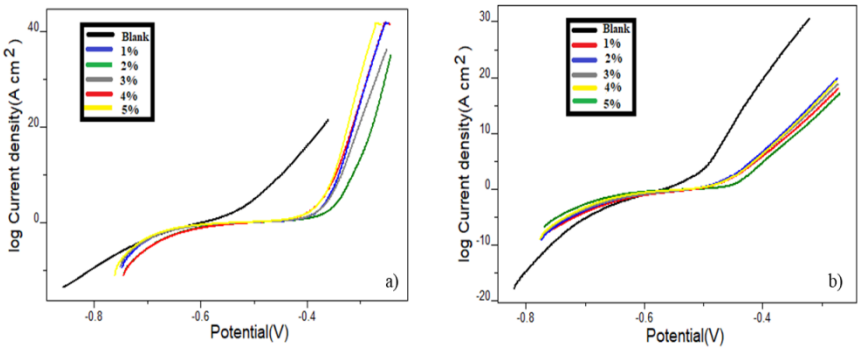

Fig. 6.11: Linear polarization plots of mild steel with and without GCE in a) 1 M HCl and b) 0.5 M H_2SO_4

Table 6.6: Potentiodynamic polarization parameters of mild steel in 1 M HCl and 0.5 M H_2SO_4 with and without GCE

Medium	Conc. (v/v %)	Tafel data					Polarization data	
		$-E_{corr}$ (mV)	i_{corr} (μAcm^2)	b_a (mV/dec)	$-b_c$ (mV/dec)	η_{pol}%	R_p (Ω)	η_{Rp}%
1 M HCl	Blank	597.9	1240	166	221	-	33.14	-
	1	492.2	441	97	172	64.43	68.92	51.91
	2	506.2	424	94	139	65.80	82.73	59.94
	3	507.3	378	104	157	69.51	84.99	61.00
	4	487.3	358	89	166	71.12	89.21	62.85
	5	495.3	92.8	72	132	92.51	217.5	84.76
0.5 M H_2SO_4	Blank	602.2	1616	184	193	-	25.30	-
	1	567.9	792	194	179	50.99	57.16	55.73
	2	574.7	743	186	174	54.02	60.06	57.87
	3	572.5	726	187	180	55.07	62.44	59.48
	4	581.6	567	176	152	64.91	82.82	69.45
	5	577.9	405	167	144	74.93	167.1	84.85

Polarization data revealed that potent corrosion inhibition could be ascribed to improved mild steel resistance against polarization when immersed in acid solutions with

GCE. In 1 M HCl polarization resistance value was 217.5 Ωcm^2 while in 0.5 M H_2SO_4, it was 167.1 Ωcm^2 at 5 v/v% GCE concentration. Due to multi-complex compounds present in the extract collected at the metal-acid interface may prevent further polarization of the mild steel, obvious from increased polarization resistance values with GCE concentration[180].

Electrochemical noise measurements

Pitting corrosion on mild steel can be easily detected from fluctuations of electrode potential. The current noise data for mild steel exposed in 1 M HCl and 0.5 M H_2SO_4 solutions with varying GCE concentrations are shown in Fig. 6.12. It exhibits that the amplitude of current noise decreased with an increase in GCE concentration, indicating the corrosion process has been dramatically prevented. PSD plots for metal dipped in 1 M HCl and 0.5 M H_2SO_4 containing various GCE concentrations are shown in Fig. 6.13. It shows that as frequency increases, magnitudes of current noise decreased. On inspecting the figure above mentioned, it is evident that the current noise for uninhibited metal was higher than inhibited metal in both acid solutions[181]. It agreed metal corrosion inhibition property of GCE in acid media was used to investigate.

Pitting index is also called pitting resistance equivalent number (PREN). It is an indicator of metal corrosion resistance[182]. Fig. 6.14 shows pitting index curves for mild steel exposed acid solutions in the absence and presence of various GCE concentrations. On examining the figure, it was clear that as GCE concentration increases, the pitting index value augments. Pitting index value was higher for the highest concentration under-study in the HCl medium, while lower in the H_2SO_4 medium for the same concentration. On comparing the pitting index values for blank and inhibited metal, it can be suggested that metal with GCE has excellent resistance power against corrosion in

the aggressive media. It also established the good anti-corrosion behaviour of GCE in 1 M HCl than 0.5 M H_2SO_4.

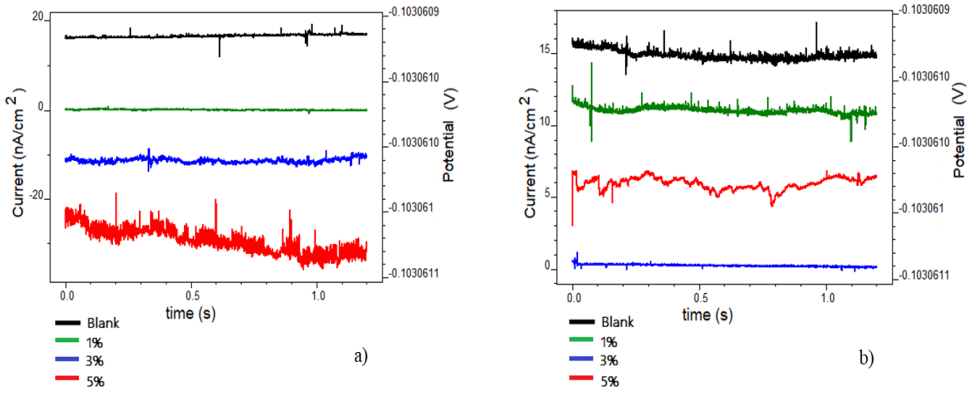

Fig. 6.12: Current noise plots of mild steel with and without GCE in a) 1 M HCl b) 0.5 M H_2SO_4

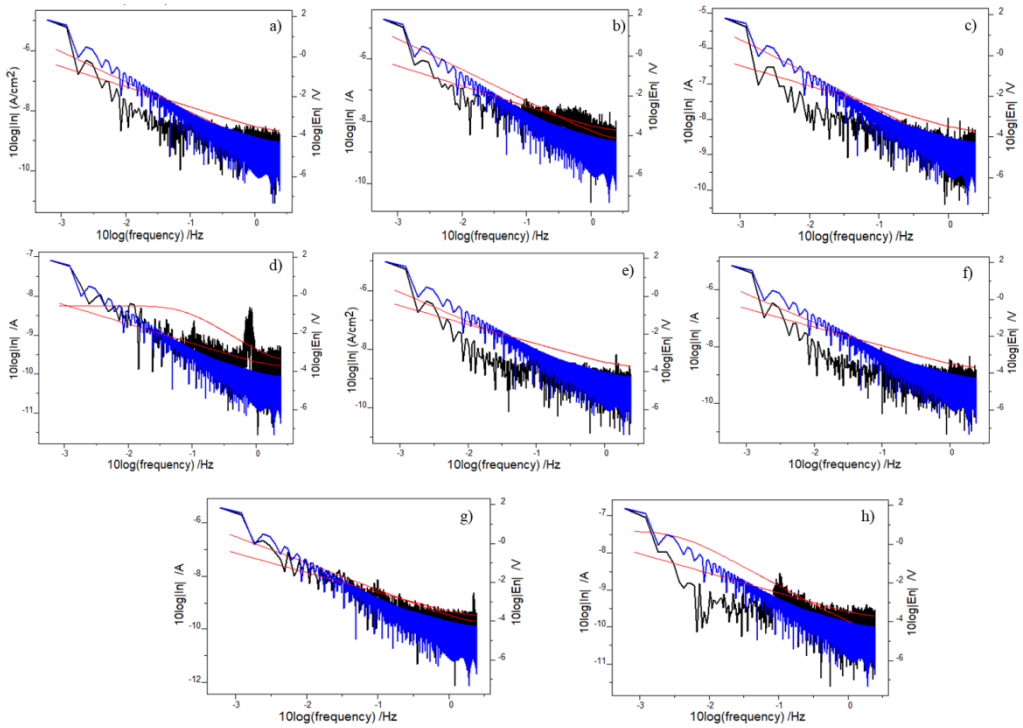

Fig. 6.13: Power spectral density plots of mild steel in 1 M HCl a) without GCE b) 1% GCE c) 3% GCE d) 5% GCE; Power spectral density plots of mild steel in 0.5 M H_2SO_4 e) without GCE f) 1% GCE g) 3% GCE h) 5% GCE

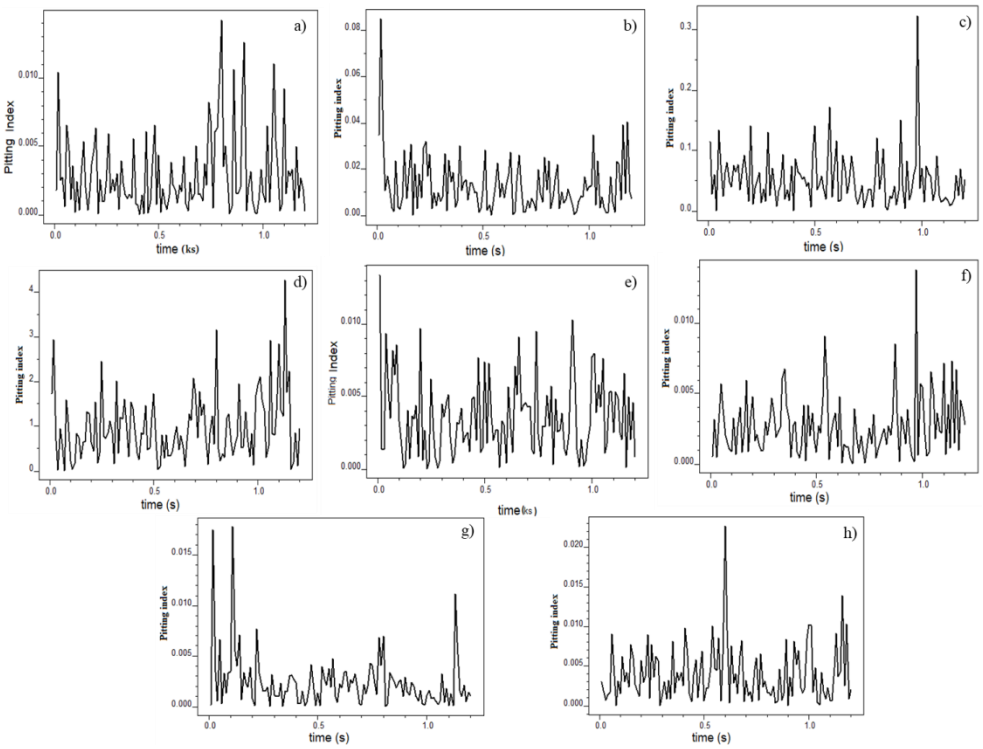

Fig. 6.14: Pitting index curves of mild steel in 1 M HCl a) without GCE b) 1% GCE c) 3% GCE d) 5% GCE; Pitting index curves of mild steel in 0.5 M H_2SO_4 e) without GCE f) 1% GCE g) 3% GCE h) 5% GCE

Atomic force microscopy

AFM analysis reinforces the surface interaction of GCE on mild steel since it is an effective method for surface morphological studies. 3-D images of AFM analysis for 24 hrs are shown in Fig. 6.15a-e. Surface roughness parameters are given in Table 6.7. Fig. 6.15 a) exhibits the surface topography of smoothened metal surface with an average roughness value (R_a) of 26.11 nm lower than the metal dipped in acid media. Fig. 6.15 b) and d) represent the corroded metal surface exposed in 1 M HCl and 0.5 M H_2SO_4, respectively. R_a values for the blank experiment were found to be higher than the metal dipped in acid solutions containing 5 v/v% GCE. Fig. 6.15 c) and e) displays the inhibited metal surfaces in 1 M HCl and 0.5 M H_2SO_4, respectively. The R_a values obtained for inhibited metal were in between smoothened metal and blank experiment. This indicates that a protective adsorption film of GCE molecules was developed on mild steel that maintained the metal surface fine and smooth. It has also been observed that

the roughness parameters for the metal with GCE in 1 M HCl were lower than in 0.5 M H_2SO_4. This fact further supported the higher inhibition power of GCE in HCl than in the H_2SO_4 medium.

Table 6.7: Surface roughness parameters of mild steel by AFM analysis

Sample	R_{pp}	R_q (nm)	R_a (nm)
Smoothened mild steel	205.27	32.92	26.11
Mild steel in 1 M HCl	965.86	79.50	55.07
Mild steel in 1 M HCl with 5 v/v% GCE	727.45	58.27	36.46
Mild steel in 0.5 M H_2SO_4	2176.62	231.72	180.48
Mild steel in 0.5 M H_2SO_4 with 5 v/v%	1026.18	120.38	86.46

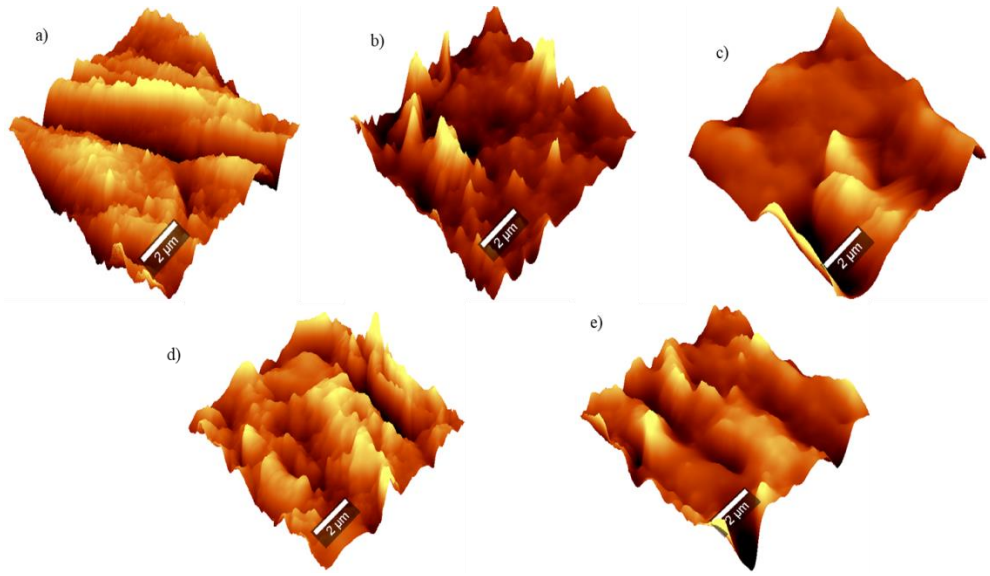

Fig. 6.15: Topography of mild steel surface a) smoothened b) in 1 M HCl c) in 1 M HCl with 5 v/v% GCE d) in 0.5 M H_2SO_4 e) in 0.5 M H_2SO_4 with 5 v/v% GCE

Quantum mechanical calculations

Spatial and electronic molecular structures of an inhibitor have a significant role in determining the inhibition potential. The optimized geometry, HOMO and LUMO of HCA and HCA lactone, two important GCE components, are shown in Fig. 6.16. Quantum mechanical parameters such as energies of HOMO (E_{HOMO}), LUMO (E_{LUMO}),

change in energy between HOMO and LUMO (ΔE), Ionisation energy (I), electron affinity (A), chemical potential (μ), electronegativity (χ), hardness (η) and the number of electrons transferred (ΔN) of HCA and HCA lactone are calculated and given in Table 6.8.

Table 6.8: Quantum mechanical parameters (in eV) of HCA (I) and HCA lactone (II)

Molecule	E_{HOMO}	E_{LUMO}	ΔE	I	A	μ	χ	η	ΔN
I	-2.131	0.090	2.22	2.13	-0.09	-1.02	1.02	1.11	2.692
II	-2.148	0.066	2.21	2.14	-0.06	-1.04	1.04	1.10	2.691

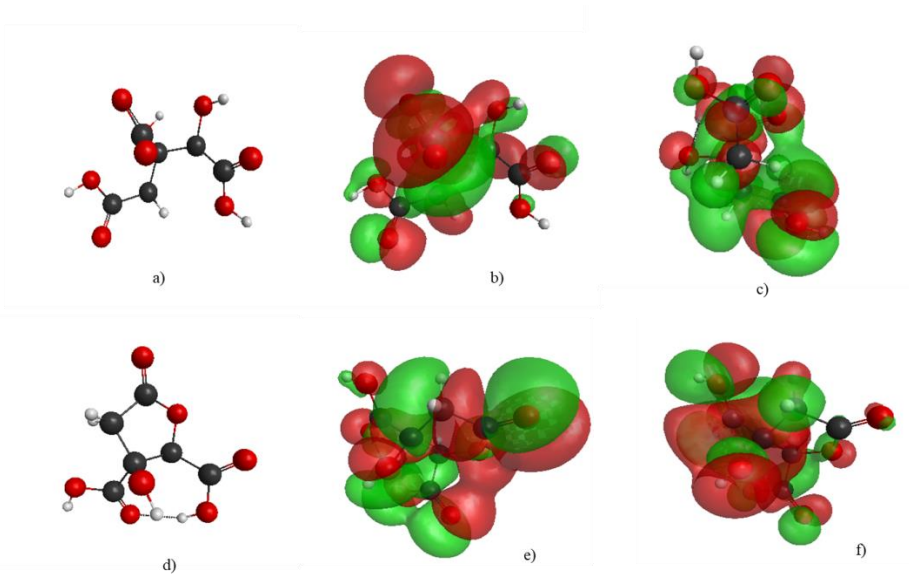

Fig. 6.16: a) Optimized geometry, b) HOMO and c) LUMO of HCA; d) Optimized geometry, e) HOMO and f) LUMO of HCA lactone

The lower change in energy (ΔE) values facilitate improved inhibition potentials as the lower ionization energy values. Table 6.8 revealed that the ΔE value for HCA lactone is smaller than HCA, indicating HCA lactone predominantly operates to decrease the energy gap and increase the possibility of electron donation. HCA also supplemented the high inhibition efficiency of GCE. The electronic chemical potential (μ) is a measure of electron's distribution in a molecule. Even though the electronic chemical potential (μ) can't predict the direction of a corrosion inhibition process, it is usually said that the adsorption of an inhibitor is encouraged by large values of μ[183]. The higher value of μ for

HCA and HCA lactone forms implies that the inhibition efficacy of GCE can be attributed to the effective interaction of these two major components.

Statistical analysis

❖ ***Optimization of factors for inhibition efficiency (IE%)***

Weight loss measurements showed that temperature, GCE concentration, and acid concentration considerably affected corrosion inhibition potential. So they opted as independent factors in this investigation. The Box-Behnken Design (BBD) structure and the three levels depending on the design of test factors (X_1, X_2 & X_3) for HCl and H_2SO_4 are shown in Table 6.9 and Table 6.10, respectively, incorporating experimental results and predicted response. A total of 15 experimental runs were found in it. It was described that corrosion inhibition efficiency is directly proportional to GCE concentration. This method attained an extreme inhibition efficiency with 5 v/v% GCE concentration in 0.5 M HCl and H_2SO_4 at 313 K. By applying RSM for the optimization, excellent efficiency was derived for the proper combination of the three factors used in the present analysis. The regression model was generated for the relation between test factors (X_1, X_2 & X_3) and inhibition efficiency, and they are shown in the quadratic equation (55) and (56) for HCl and H_2SO_4, respectively.

$$IE = 670 – 3.32\ X_1 + 27.55X_2 – 99.7\ X_3 + 0.00436\ X_1^2 + 0.013\ X_2^2 - 2.09\ X_3^2 - 0.0673\ X_1X_2 + 0.2833\ X_1X_3 + 0.841\ X_2X_3 \quad (55)$$

$$IE = 461 – 2.12\ X_1 + 4.44X_2 – 90.4\ X_3 + 0.00255\ X_1^2 + 0.349\ X_2^2 + 3.29\ X_3^2 - 0.0028\ X_1X_2 + 0.2337\ X_1X_3 + 0.287\ X_2X_3 \quad (56)$$

where IE represents inhibition efficiency, X_1 denotes temperature, X_2 denotes GCE concentration and X_3 denotes acid concentration.

Analysis of variance (ANOVA) was developed by applying this regression model[184]. ANOVA results with a significance level of 95% for HCl and H_2SO_4 are given

in Table 6.11 and Table 6.12, respectively. P-value is the most requiring value in this Table, which determine whether the factor is significant or not. The degree of essentialness (α) was selected to be 0.05. On close observation of the Table, it displayed that P-value was lower than 0.05 for linear and two-way interaction terms in HCl, whereas the linear and square term of GCE concentration has a P-value lower than 0.05. It explained that temperature, GCE concentration and acid concentration are the more significant terms. Pareto charts (Fig. 6.17) interpret that linear term GCE concentration has the most remarkable impact on inhibition efficiency in both acid media.

The better fit model for experimental data can be predicted by the closeness of R^2 and R^2(adj) value to unity. R^2 and R^2(adj) values obtained 0.9983 and 0.9954 for HCl and 0.9962 and 0.9895 for H_2SO_4, respectively. These values clearly proposed the best fit predicted model for experimental data. Therefore, the results can be quickly evaluated by the model.

Table 6.9: Experimental and predicted IE% from weight loss measurements and BBD in HCl medium

Run order	Actual level of factors			IE%		Residual
	X_1	X_2	X_3	Experimental	Predicted	
1	313	1	1	52.48	53.00	2.348
2	333	1	1	47.18	47.30	0.886
3	313	5	1	82.76	82.64	0.886
4	333	5	1	72.08	71.56	2.348
5	313	3	0.5	74.27	73.59	0.282
6	333	3	0.5	62.66	62.37	2.952
7	313	3	1.5	60.61	60.90	2.952
8	333	3	1.5	54.66	55.35	0.282
9	323	1	0.5	54.79	54.96	2.066
10	323	5	0.5	79.43	80.23	0.603
11	323	1	1.5	44.22	43.42	0.603
12	323	5	1.5	72.22	72.05	2.066
13	323	3	1	63.14	63.14	0.001
14	323	3	1	63.14	63.14	0.001
15	323	3	1	63.14	63.14	0.001

Table 6.10: Experimental and predicted IE% from weight loss measurements and BBD in H_2SO_4 medium

Run order	Actual level of factors			IE%		Residual
	X_1	X_2	X_3	Experimental	Predicted	
1	313	1	1	39.60	39.53	0.062
2	333	1	1	35.82	34.80	1.028
3	313	5	1	62.23	63.26	-1.028
4	333	5	1	58.23	58.29	-0.062
5	313	3	0.5	56.47	55.71	0.758
6	333	3	0.5	48.32	48.53	-0.207
7	313	3	1.5	46.13	45.92	0.207
8	333	3	1.5	42.65	43.41	-0.758
9	323	1	0.5	40.92	41.74	-0.821
10	323	5	0.5	65.05	64.78	0.269
11	323	1	1.5	33.45	33.72	-0.269
12	323	5	1.5	58.72	57.90	0.821
13	323	3	1	47.32	47.32	0
14	323	3	1	47.32	47.32	0
15	323	3	1	47.32	47.32	0

Table 6.11: Analysis of variance for IE% in HCl medium

Source	DF	Adj SS	Adj MS	F-Value	P-Value
Model	9	1807.96	200.88	335.49	0.000
Linear	3	1788.01	596.00	995.35	0.000
Temperature	1	140.67	140.67	234.92	0.000
GCE Conc.	1	1452.89	1452.89	2426.37	0.000
Acid Conc.	1	194.46	194.46	324.76	0.000
Square	3	1.86	0.62	1.04	0.452
Temperature*Temperature	1	0.70	0.70	1.17	0.328
GCE Conc.*GCE Conc.	1	0.01	0.01	0.02	0.906
Acid Conc.*Acid Conc.	1	1.01	1.01	1.68	0.251
2-Way Interaction	3	18.09	6.03	10.07	0.015
Temperature*GCE Conc.	1	7.24	7.24	12.09	0.018
Temperature*Acid Conc.	1	8.02	8.02	13.40	0.015
GCE Conc.*Acid Conc.	1	2.83	2.83	4.72	0.082
Error	5	2.99	0.60		
Lack-of-Fit	3	2.99	1.00	*	*
Pure Error	2	0.00	0.00		
Total	14	1810.96			

DF: degrees of freedom, Adj SS: adjusted sum of squares, Adj MS: adjusted mean of squares, F: Fischer's F-test value, P: probability

Table 6.12: Analysis of variance for IE% in H_2SO_4 medium

Source	DF	Adj SS	Adj MS	F-Value	P-Value
Model	9	1287.93	143.10	147.40	0.000
Linear	3	1273.00	424.33	437.08	0.000
Temperature	1	47.06	47.06	48.47	0.001
GCE Conc.	1	1114.86	1114.86	1148.34	0.000
Acid Conc.	1	111.08	111.08	114.42	0.000
Square	3	9.13	3.04	3.13	0.125
Temperature*Temperature	1	0.24	0.24	0.25	0.640
GCE Conc.*GCE Conc.	1	7.20	7.20	7.41	0.042
Acid Conc.*Acid Conc.	1	2.49	2.49	2.57	0.170
2-Way Interaction	3	5.80	1.93	1.99	0.234
Temperature*GCE Conc.	1	0.01	0.01	0.01	0.913
Temperature*Acid Conc.	1	5.46	5.46	5.63	0.064
GCE Conc.*Acid Conc.	1	0.33	0.33	0.34	0.586
Error	5	4.85	0.97		
Lack-of-Fit	3	4.85	1.62	*	*
Pure Error	2	0.00	0.00		
Total	14	1292.78			

DF: degrees of freedom, Adj SS: adjusted sum of squares, Adj MS: adjusted mean of squares, F: Fischer's F-test value, P: probability

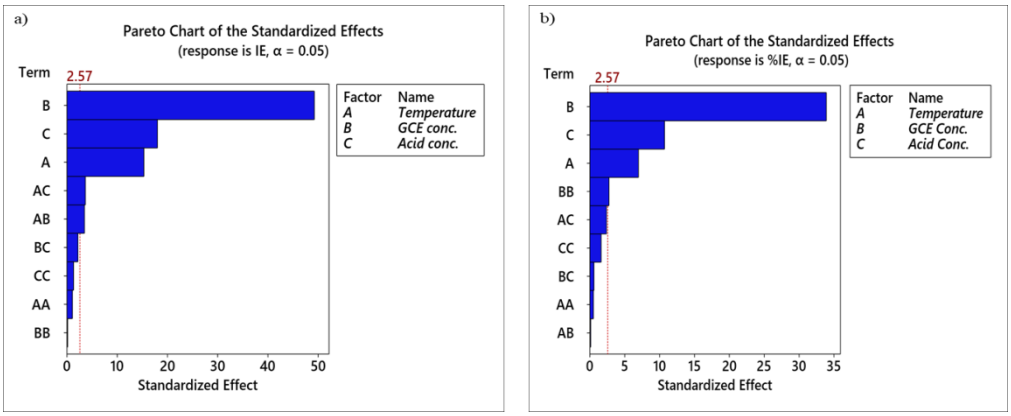

Fig. 6.17: Pareto chart of the standardized effects of mild steel in a) HCl b) H_2SO_4 medium

Main effects plots complement the results from the regression analysis. It illustrates the influence of tested factors on response. Fig. 6.18 shows the main effects plots for the fitted means of inhibition efficiency in HCl and H_2SO_4 media. On analyzing the figure above mentioned, it has been noticed that the maximum inhibition efficiency was with 5 v/v% concentration of GCE at an operating temperature of 313 K at 0.5 M concentration of HCl and H_2SO_4. As temperature rises, the kinetic energy of the inhibitor

molecules enhances and thereby, the velocity of bombardment between the molecules increases. This inclination tends to break down the formation of adsorbed film by inhibitors on the metal surface and decreases inhibition efficiency. A similar observation was found with an increase in acid concentration. At the same time, the inhibition capacity of GCE gets boosted by the addition of 1 to 5 v/v% GCE concentration. In the presence of inhibitor, the corrosion rate was decreased due to the adsorption of inhibitor molecules, and efficiency also increases.

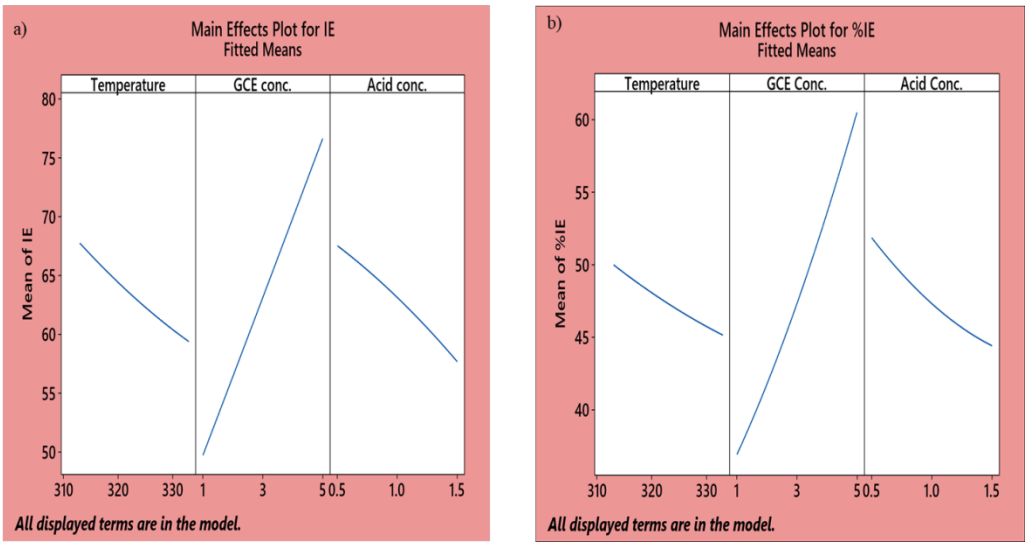

Fig. 6.18: Main effects plots for inhibition efficiency of mild steel in a) HCl b) H_2SO_4 medium

Fig. 6.19 reveals the interaction plot for inhibition efficiency in two acids which interprets any interaction between factors. If there are any crossed lines in the interaction plot, it will designate a significant interaction between the factors. Parallel or straight lines imply that there is no interaction between factors. From Fig. 6.19, it has been observed that the two-way interaction terms were inessential as there are no crossed lines in the interaction plot for inhibition efficiency in both acids. However, in HCl and H_2SO_4, parallel lines between temperature and acid concentration were not perfect, indicating some interaction. ANOVA analysis was also supplemented with these results.

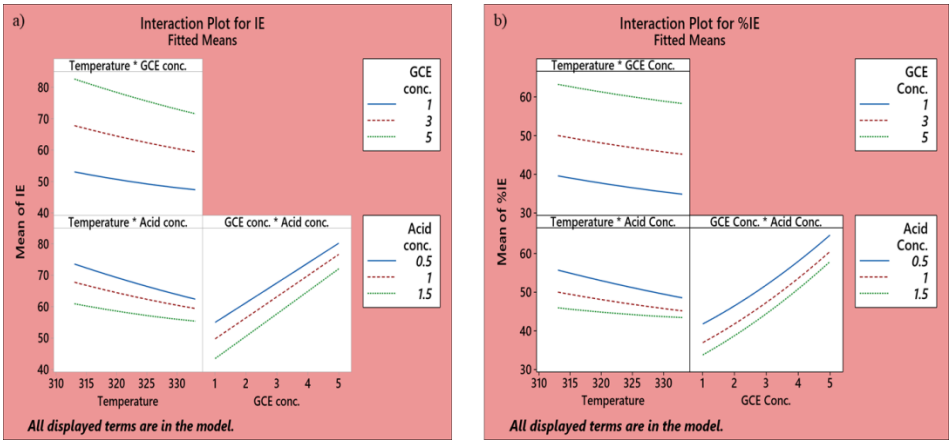

Fig. 6.19: Interaction plot for inhibition efficiency in a) HCl b) H_2SO_4 medium

Contours and 3-D surface plots delineate the inter-dependence of the tested factors on IE% and are shown in Fig. 6.20 and Fig. 6.21. It displayed that the inhibition efficiency grows tremendously when GCE concentration increases at a particular temperature. Whereas inhibition efficiency drop-down when the temperature rises. This IE%-temperature relationship can be attributed to the physical adsorption of GCE molecules on the mild steel surface. Inhibition efficiency and acid concentration are inversely proportional, indicating a higher concentration of aggressive media corrodes metal dramatically.

❖ ***Response optimization***

Quadratic equations (55) and (56) were used to optimize the independent factors such as temperature, GCE concentration and acid concentration to maximize IE. For the outstanding response, the desirability function method was adopted. Response optimization plots for IE in both media are shown in Fig. 6.22. The anticipated optimum factors observed were temperature of 313 K, GCE concentration of 5 v/v%, and acid concentration of 0.5 M and the corresponding predicted IE were 87.62% and 68.69% in HCl and H_2SO_4 solutions, respectively. Confirmation tests have been attained the perfect optimal factor settings and betterment of IE.

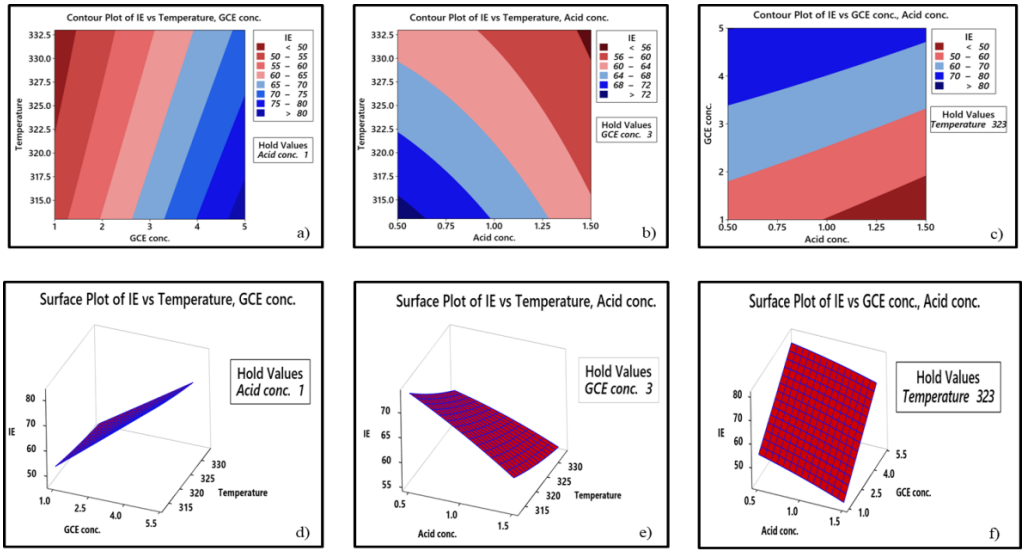

Fig. 6.20: a, b & c) Contours and d, e & f) 3-D surface plots for inhibition efficiency in HCl

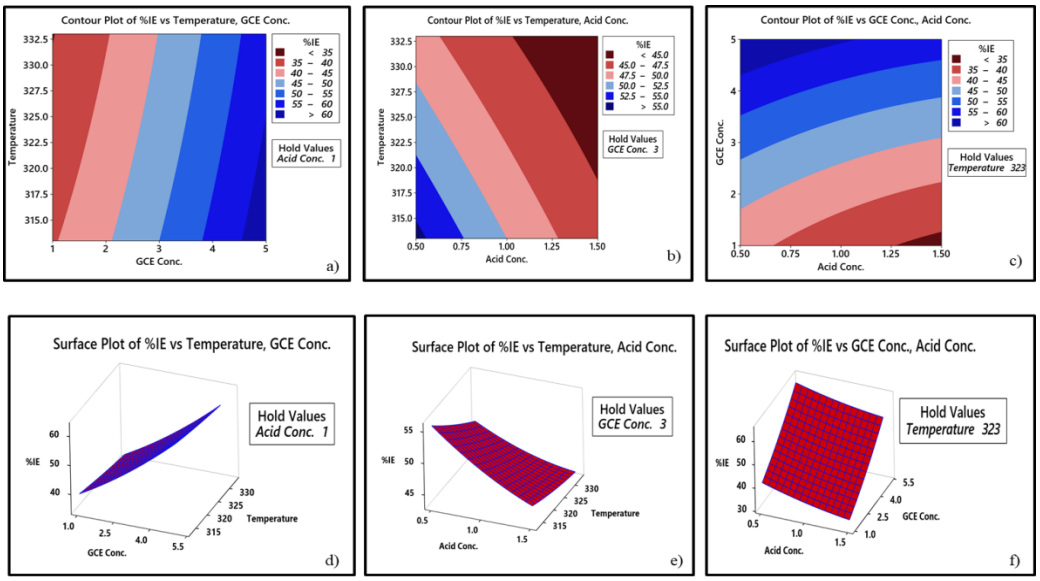

Fig. 6.21: a, b & c) Contours and d, e & f) 3-D surface plots for inhibition efficiency in H_2SO_4

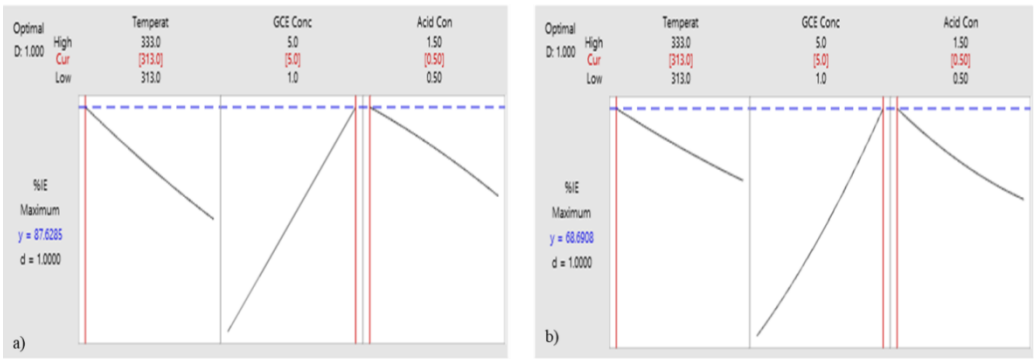

Fig. 6.22: Response optimization plot for inhibition efficiency in a) HCl b) H_2SO_4 medium

Conclusions

- *Garcinia cambogia* extract (GCE) acts as an efficient green inhibitor for corrosion of mild steel in 1 M HCl and 0.5 M H_2SO_4 medium. As the concentration of the inhibitor increases, the protecting power also increases.
- On comparing, GCE in 1 M HCl medium shows higher efficiency than 0.5 M H_2SO_4 medium. GCE exhibited 91.73% at 5 v/v% inhibition efficiency in 1 M HCL medium whereas it showed 75.53% at 5 v/v% in 0.5 M H_2SO_4 medium.
- UV-Visible spectra of extract solutions suggests the binding ability of GCE with various metals.
- Temperature and inhibition efficiency is in inverse proportional relation.
- Electrochemical impedance analysis exhibits that charge transfer resistance increases and double layer capacitance decreases according to GCE concentration.
- Potentiodynamic polarization measurements exhibit mixed type character of inhibition for GCE.
- Sharp decrease in corrosion current density pointed out that there is strong resistance in the corrosion process.
- Quantum mechanical calculations of major components - hydroxycitric acid (HCA) and hydroxycitric acid lactone (HCA lactone) present in GCE support the inhibition power of GCE.
- The adsorption studies of GCE shows that it obeys Langmuir adsorption isotherm.
- Atomic force microscopy of metal surfaces exposed in acid media with and without GCE also confirmed the protecting power of GCE.

- Statistical analysis also verified the effect of temperature and concentration of GCE and concentration of acid (both HCl and H_2SO_4) on inhibition efficiency.

CHAPTER 7

CLERODENDRUM INFORTUNATUM EXTRACT: NATURAL CORROSION INHIBITOR FOR MILD STEEL IN ACID MEDIA

The anti-corrosion properties of leaves and roots extracts of *Clerodendrum infortunatum* (CILE and CIRE) on mild steel are discussed here. The comparison of inhibition efficiency in two different acids, i.e., 1 M HCl and 0.5 M H_2SO_4, also have been studied. *Clerodendrum infortunatum* belongs to Lamiaceae family. Physicochemical, electrochemical, surface morphological and quantum mechanical studies have been employed as corrosion monitoring techniques. *Clerodendrum infortunatum* is comprised of diverse phytochemical constituents responsible for their pharmacological activities. Ethanolic extracts of CILE and CIRE contains saponins, flavonoids, steroids, tannins, and reducing sugars. Terpenoids are mainly present in the roots and negligibly present in the leaves, while alkaloids are absent in both extracts[185]. Clerodin and scutellarin are major diterpenoid and flavonoid, respectively, found in *Clerodendrum infortunatum* plants[186],[187]. Their structures are shown in Fig. 7.1. The inhibitive performance of CILE and CIRE is assessed with the concept that adsorption of its phytochemicals onto the mild steel surface made a protective barrier to the metal surface. Clerodin and scutellarin are subjected to theoretical calculations as major terpenoid and flavonoid, respectively, present in *Clerodendrum infortunatum* extracts.

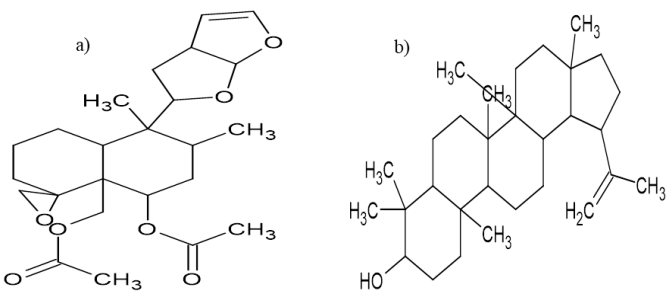

Fig. 7.1: Structure of a) clerodin b) scutellarin

Clerodendrum infortunatum

Results and discussions

Phytochemical screening of CILE and CIRE

Standard phytochemical screening tests were carried out to identify the phytochemicals in CILE and CIRE qualitatively, and the results are given in Table 7.1.

Table 7.1: Phytochemical screening of CILE and CIRE

Sl. No.	Compounds	Tests	Results of CILE	Results of CIRE
1	Alkaloids	Mayer's reagent	−−	−−
2	Steroids	Salkowaski's test	++	++
3	Phenolic compounds	Potassium ferrocyanide test	++	++
4	Flavanoids	Sodium hydroxide test	++	++
5	Saponins	Froth test	++	++
6	Tannins	Lead acetate test	++	++
7	Cardiac glycosides	Conc. sulphuric acid test	−−	−−
8	Coumarin	Alcoholic NaOH test	++	++
9	Terpenoids	Conc. sulphuric acid test	−−	++

++ (present), − − (Absent)

The phytochemical screening data were found to agree with the literature survey.

FTIR spectroscopy

Phytochemicals of plant extracts have functional groups with heteroatoms such as N, O etc., which are considered adsorption centres. It can be established by FTIR analysis of ethanolic CILE and CIRE. Fig. 7.2 a) and Fig. 7.2 b) show FTIR spectra of ethanolic CILE and CIRE, respectively. The broad absorption band at 3281 cm^{-1} for CILE and 3267 cm^{-1} for CIRE can be assigned to O–H stretching vibration. Peak corresponds to C–H stretching vibration observed at 2918 cm^{-1} for CILE and 2921 cm^{-1} for CIRE. The weak band at 2113 cm^{-1} for CILE and at 2111 cm^{-1} for CIRE may be ascribed to C-O stretching vibrations. Aliphatic and aromatic C=C stretching vibration appears at 1631 cm^{-1} for CILE and at 1603 cm^{-1} for CIRE. C-O-H in-plane bending vibrations seems at 1401 and 1413 cm^{-1} for CILE and CIRE, respectively. It may be due to the presence of phenolic acids in the extracts. The absorption bands below 1,000 cm^{-1}

can be attributed to the C–H bending vibrations. FTIR results showed that the ethanolic extracts of both CILE and CIRE consisted of functional groups like O–H, C–O, C=C, and aromatic rings, which can form an adsorption layer on the metal surface by donating pi-electrons.

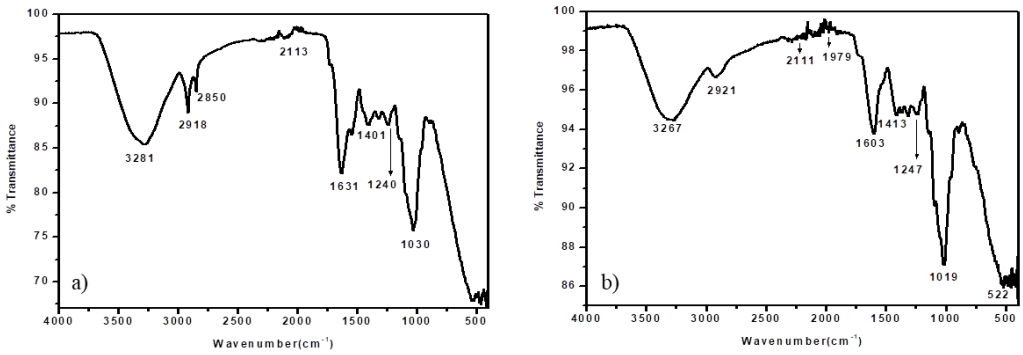

Fig. 7.2: FTIR spectra of a) CILE b) CIRE

Weight loss measurements

❖ ***Effect of concentration***

Table 7.2 represents the variation of corrosion rate (υ) and inhibition efficiency (η%) for mild steel in 1 M HCl and 0.5 M H_2SO_4 without and with CILE and CIRE at room temperatures. It has been observed from Table 7.2 that the corrosion rate of mild steel was diminished by introducing both leaves and roots extract of *Clerodendrum infortunatum* into acid media, indicating the corrosion mitigation power of the metal immersed in the presence of the extracts. Inspection of Table 7.2 also realized that inhibition efficiency is directly proportional to the concentration of extracts. The anti-corrosion performance of CILE and CIRE was ascribed to the adsorption of the phytochemical constituents of the extract at the mild steel-acid solution interface. Thus, it hindered active corrosion sites on the mild steel and decreased the rate of corrosion[188]. It was pointed out that the extract of the roots exhibits superior performance than leaves extract as a corrosion inhibitor for mild steel in both acid media. On comparing the

nature of acid media, HCl solution was more facilitated for corrosion inhibition than H_2SO_4 solution. Inhibition efficiency of 93.63% was obtained for roots and 87.56% for leaves at 303 K with 5 v/v% extract concentration in 1 M HCl. At the same time, in 0.5 M H_2SO_4, an inhibition efficiency of 65.73% was achieved for roots and 58.48% for leaves.

The variation in inhibition efficiency for roots and leaves was attributed to various phytochemicals present in CILE and CIRE. Notably, CIRE contains terpenoids, steroids, flavonoids, saponins, tannins and reducing sugars, while CILE contains all the phytochemicals in the roots except terpenoids. The presence of terpenoids in CIRE may be enhanced its anti-corrosion behaviour. The lone pair of electrons present in oxygen moieties of clerodin and scutellarin may be acted as an electron donor source.

The primary cause for the corrosion of mild steel in 1 M HCl is the adsorption of Cl^- ions onto the metal surface sites. The movement of inhibitor molecules is slower than Cl^- ions; therefore, Cl^- ions preferentially reach the metal surface. However, the inhibitor molecules can hinder Cl^- ions sterically and approach the metal surface sites[189]. The adsorption of halide ions in an inhibited solution on the metal surface is via oriented dipoles, which means cationic organic inhibitor molecules adsorb on the dipoles. So, it can be said that the rate of decrease in corrosion in the presence of both halide anions and inhibitor cations is a synergistic effect. This is why the greater inhibition efficiency of organic inhibitor molecules in HCl than H_2SO_4 medium. In the present investigation, the same is the observation, i.e., the anti-corrosion performance of CILE and CIRE were predominant in HCl solution compared to that in H_2SO_4 solution.

❖ ***Effect of temperature***

Fig. 7.3 shows the comparison of inhibition efficiency for mild steel in 1 M HCl and 0.5 M H_2SO_4 with various concentrations of CILE at different temperatures. Similar

plots for CIRE are exhibited in Fig. 7.4. It was noticed that the corrosion rate augmented with the rise in temperature with and without extracts. Inhibition efficiency was reduced with an increase in temperature in the presence of both extracts. It may be explained that the phytochemicals of both extracts were physically adsorbed on the mild steel surface.

Table 7.2: Weight loss measurements of mild steel with and without CILE and CIRE in 1 M HCl and 0.5 M H_2SO_4 at room temperature for 24 hrs

Inhibitor	Conc. (v/v %)	Corrosion rate (mm/yr)		Inhibition efficiency (η%)	
		1 M HCl	0.5 M H_2SO_4	1 M HCl	0.5 M H_2SO_4
CILE	Blank	3.95	35.57	-	-
	1	0.59	19.50	85.22	45.16
	2	0.50	17.98	87.34	49.45
	3	0.42	16.89	89.53	52.49
	4	0.30	15.55	92.48	56.28
	5	0.26	12.18	93.63	65.73
CIRE	1	1.83	20.90	53.42	41.24
	2	1.55	19.28	60.59	45.78
	3	0.88	18.21	77.58	48.79
	4	0.78	17.33	80.21	51.27
	5	0.49	14.76	87.56	58.48

Corrosion rates and inhibition efficiencies of CILE and CIRE from weight loss measurements in 1 M HCl and 0.5 M H_2SO_4 at 303, 313, 323 and 333 K are comparatively listed in Table 7.3. It has been observed from Table 7.3 that the inhibitive action of the extracts in different acid media was affected by temperature. In HCl and H_2SO_4 media, inhibition efficiency is reduced with the rise in temperature, which causes the decrease in stability of the adsorption layer[166]. This trend suggested that the phytochemicals of CILE and CIRE in HCl and H_2SO_4 media were physically adsorbed on the mild steel surface. It was also inferred from Table 7.3 that leaves and root extracts in the H_2SO_4 medium show a higher corrosion rate for mild steel at elevated temperatures. Inhibition efficiency decreased from 93.63% to 69.51% for 5 v/v% CIRE concentration, while the same concentration of CILE exhibited a sharp decrease from

87.56% to 68.23% in HCl solution when the temperature goes from 303 K to 333 K. Similarly, in the H_2SO_4 medium, corrosion inhibition capacity lowered from 65.73% to 43.67% for the highest CIRE concentration under-study, whereas, for CILE, efficacy reduced from 58.48% to 50.87% for the same concentration and temperature. An elevated temperature may be enhanced the desorption process of extracts from mild steel.

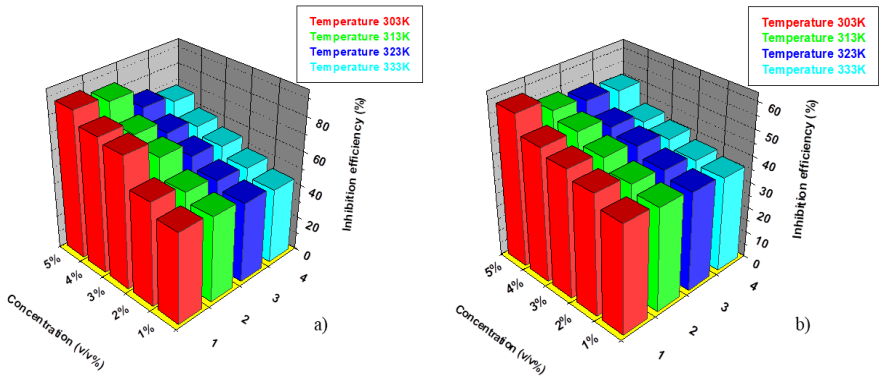

Fig. 7.3: Variation in inhibition efficiency of CILE in a) 1 M HCl b) 0.5 M H_2SO_4 at elevated temperatures

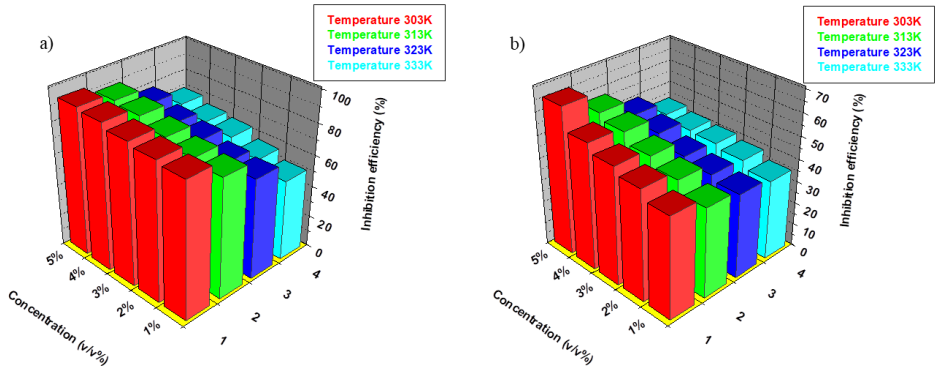

Fig. 7.4: Variation in inhibition efficiency of CIRE in a) 1 M HCl b) 0.5 M H_2SO_4 at elevated temperatures

Using the Arrhenius equation (41), the activation energy of metal corrosion was estimated. Fig. 7.5 a) and c) show the Arrhenius plots of log K vs 1/T for mild steel in 1 M HCl and 0.5 M H_2SO_4, respectively, with various CILE concentrations. Similar Arrhenius plots for CIRE are shown in Fig. 7.6 a) and Fig. 7.6 c). Thermodynamic parameters such as ΔH^* and ΔS^* values were rendered using equation (43) obtained from

transition state theory. From the slope and intercept of the plot of log K/T vs 1/T (Fig. 7.5 b) and Fig. 7.5 d)), ΔH^* and ΔS^* values for CILE inhibited metal corrosion were equated.

Table 7.3: Corrosion rate (υ) and inhibition efficiency (η%) of CIRE and CILE in 1 M HCl and 0.5 M H_2SO_4 at different temperatures for 24 hrs

Inhibitor/ Medium	Conc. (v/v%)	υ (303 K)	η% (303 K)	υ (313 K)	η% (313 K)	υ (323 K)	η% (323 K)	υ (333 K)	η% (333 K)
CILE/ 1 M HCl	Blank	3.95	-	13.11	-	22.05	-	31.77	-
	1	1.839	53.42	6.471	50.63	11.59	47.43	17.59	44.61
	2	1.556	60.59	5.822	55.59	10.63	51.77	16.01	49.60
	3	0.885	77.58	4.330	66.96	9.189	58.32	14.24	55.17
	4	0.781	80.21	3.602	72.52	7.807	64.59	12.63	60.21
	5	0.491	87.56	2.046	84.39	6.007	72.75	10.09	68.23
CILE/ 0.5 M H_2SO_4	Blank	35.57	-	58.27	-	86.25	-	106.2	-
	1	20.90	41.24	35.18	39.62	53.29	38.21	67.32	36.64
	2	19.28	45.78	33.65	42.25	51.12	40.73	65.70	38.17
	3	18.21	48.79	31.05	46.71	47.84	44.53	62.39	41.28
	4	17.33	51.27	28.56	50.98	45.82	46.87	60.23	43.31
	5	14.76	58.48	26.79	54.01	41.19	52.24	52.20	50.87
CIRE/ 1 M HCl	1	0.592	85.22	3.204	75.56	8.030	63.58	15.41	51.48
	2	0.508	87.34	2.865	78.14	7.664	65.24	13.68	56.94
	3	0.422	89.53	2.327	82.25	6.462	70.69	11.66	63.28
	4	0.306	92.48	1.672	87.24	5.849	73.47	11.01	65.32
	5	0.260	93.63	1.444	88.98	4.817	78.15	9.68	69.51
CIRE/ 0.5 M H_2SO_4	1	19.50	45.16	34.85	40.18	53.66	37.78	68.34	35.68
	2	17.98	49.45	31.78	45.46	51.63	40.13	64.66	39.14
	3	16.89	52.49	29.41	49.52	49.82	42.23	62.72	40.97
	4	15.55	56.28	26.65	54.26	45.73	46.97	61.89	41.75
	5	12.18	65.73	24.97	57.14	43.40	49.68	59.85	43.67

Similarly, ΔH^* and ΔS^* values for CIRE inhibited metal corrosion were calculated from Fig. 7.6 b) and d). Table 7.4 shows activation energy (E_a), pre-exponential factor (A), ΔH^* and ΔS^* values for mild steel corrosion with extracts of *Clerodendrum infortunatum* (CILE and CIRE) as inhibitors in acid media.

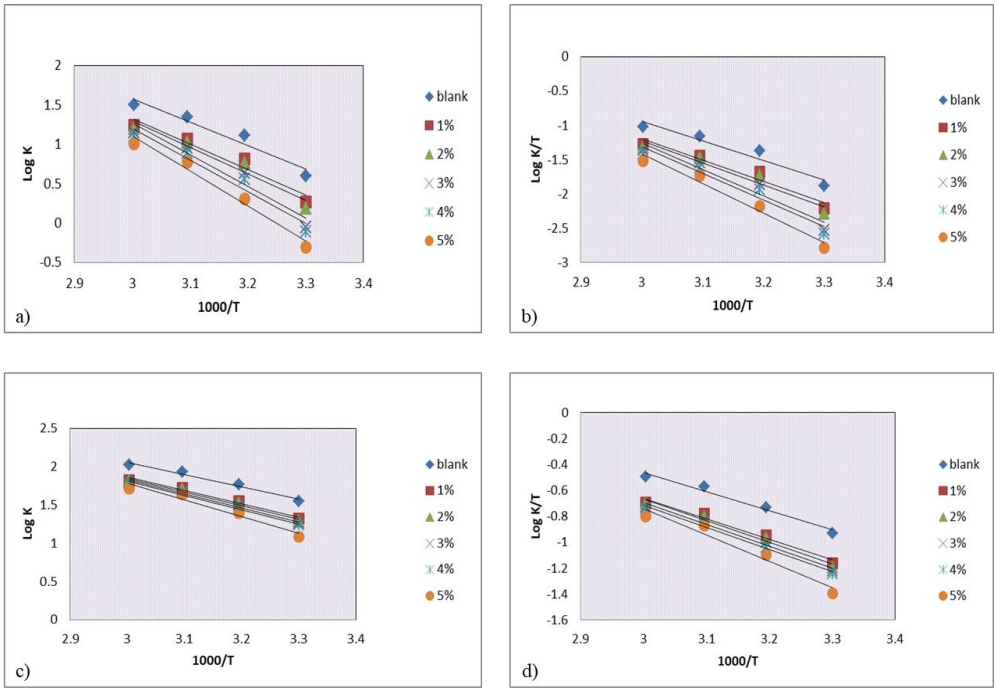

Fig. 7.5: a) Arrhenius plots b) log K/T vs 1000/T plots in 1 M HCl c) Arrhenius plots d) log K/T vs 1000/T in 0.5 M H_2SO_4 with and without CILE

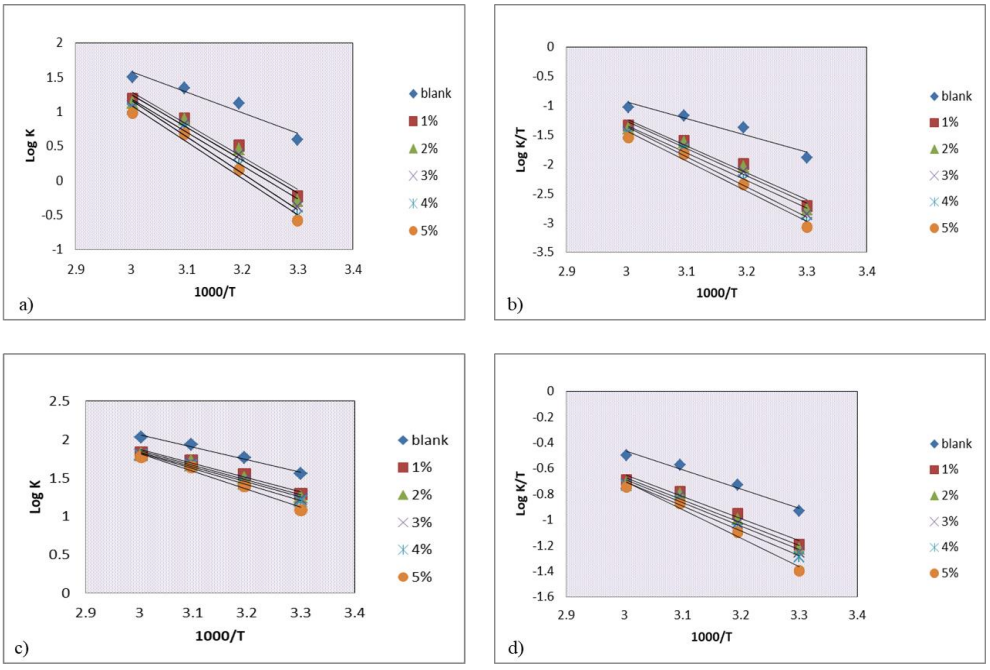

Fig. 7.6: a) Arrhenius plots b) log K/T vs 1000/T plots in 1 M HCl c) Arrhenius plots d) log K/T vs 1000/T in 0.5 M H_2SO_4 with and without CIRE

Table 7.4 revealed that the uninhibited acid media had lesser activation energy of mild steel corrosion than the inhibited acid media. The increase in E_a values with the concentration of CILE and CIRE lead to slow down the metal dissolution process. ΔH^*

and ΔS* values of the metal corrosion process were found to increase in the presence of CILE and CIRE. Positive values of the enthalpy of activation disclosed the endothermic character of metal corrosion. The observed ΔS* values for the blank experiment were negative, indicating that the rate-determining step in the metal dissolution process was an association rather than a dissociation step[190]. This association step represented a decrease in disorderliness in the formation of the activated complex from reactants. But, in the presence of CILE and CIRE as inhibitors in acids, disorderliness increased.

Adsorption isotherms

Adsorption characteristics of CILE and CIRE on mild steel surfaces were described by fitting the results obtained from weight loss measurements into various adsorption isotherm models. Langmuir adsorption isotherm was the best-fit isotherm for the adsorption of phytochemicals of both extracts by considering the tightness of the value R^2 to unity. The linear plots of Langmuir adsorption isotherm are shown in Fig. 7.7 for both extracts in 1 M HCl and 0.5 M H_2SO_4. Table 7.5 exhibits the adsorption parameters acquired from the Langmuir plots. On examining Table 7.5, it has come to the knowledge that K_{ads} value for CIRE in HCl solution was more prominent than all other inhibited solutions. This confirmed the strong adsorption of CIRE molecules onto the mild steel surface in the HCl medium[191]. The main reasons for the deviation of Langmuir isotherm slopes from unity are the interactions between adsorbed molecules on the mild steel and variations in the value of heat of adsorption.

The values of ΔG^0_{ads} are negative for both extracts. If its value is less negative than −20 kJ/mol, inhibitors adsorb physically on the metal surface but exceed −40 kJ/mol for the chemical adsorption of inhibitors. Herein, ΔG^0_{ads} values obtained for CILE and CIRE revealed mixed adsorption mode; physical and chemical adsorption in both acid media since ΔG^0_{ads} values were in between -20 kJ/mol and -40 kJ/mol.

Table 7.4: Thermodynamic parameters of mild steel corrosion with and without CILE/CIRE in 1 M HCl and 0.5 M H_2SO_4

Inhibitor/ Medium	Conc. (v/v %)	E_a (kJ mol^{-1})	A	ΔH^* (kJ mol^{-1})	ΔS^* (J $mol^{-1}K^{-1}$)
CILE/ 1 M HCl	Blank	57.24	3.58×10^{10}	54.60	-44.78
	1	62.13	1.15×10^{11}	59.49	-35.02
	2	64.16	2.22×10^{11}	61.52	-29.57
	3	76.79	1.91×10^{13}	74.15	7.84
	4	77.05	2.01×10^{13}	74.41	7.43
	5	85.53	3.25×10^{14}	82.89	31.01
CILE/ 0.5 M H_2SO_4	Blank	30.96	8.16×10^{6}	28.30	-114.51
	1	33.05	1.10×10^{7}	30.41	-112.03
	2	34.50	1.81×10^{7}	31.86	-107.88
	3	34.73	1.85×10^{7}	32.09	-107.67
	4	35.41	2.28×10^{7}	32.77	-105.97
	5	41.50	1.92×10^{8}	38.86	-88.22
CIRE/ 1 M HCl	1	90.23	2.69×10^{15}	87.59	48.60
	2	91.66	4.15×10^{15}	89.03	52.20
	3	92.62	5.00×10^{15}	89.98	53.73
	4	101.18	1.02×10^{17}	98.54	78.83
	5	101.54	1.04×10^{17}	98.90	78.99
CIRE/ 0.5 M H_2SO_4	1	35.33	2.57×10^{7}	32.69	-104.97
	2	36.45	3.66×10^{7}	33.81	-102.02
	3	37.58	5.34×10^{7}	34.94	-98.89
	4	39.40	9.91×10^{7}	36.76	-93.75
	5	44.87	7.13×10^{8}	42.23	-77.33

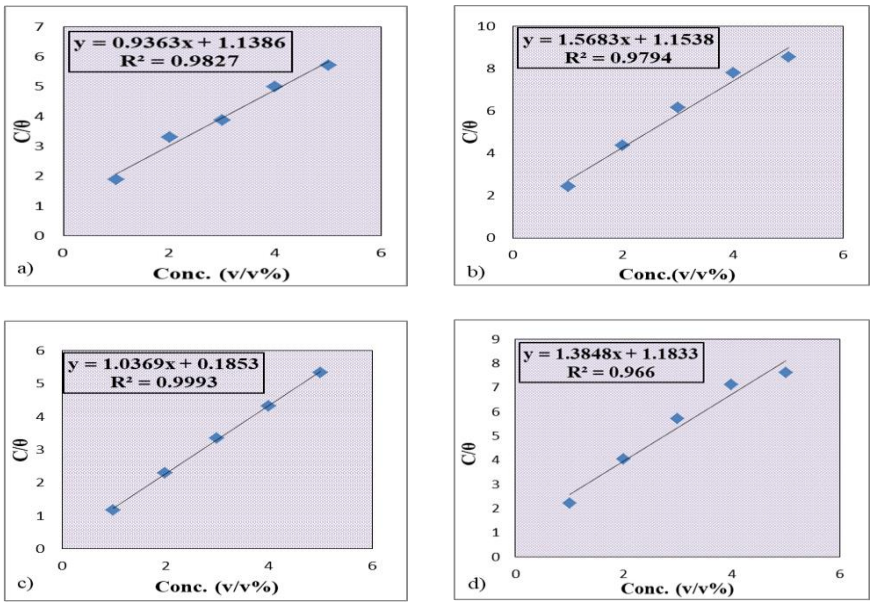

Fig. 7.7: Langmuir adsorption isotherm of CILE and CIRE on mild steel in 1 M HCl (a & c) and 0.5 M H_2SO_4 (b & d)

Table 7.5: Langmuir adsorption parameters of mild steel in 1 M HCl and 0.5 M H_2SO_4 with CILE and CIRE from weight loss measurements at room temperature

Inhibitor	Medium	ΔG^0_{ads} ($kJmol^{-1}$)	K_{ads}	R^2
CILE	1 M HCl	27.01	878.27	0.9827
	0.5 M H_2SO_4	26.97	866.70	0.9794
CIRE	1 M HCl	31.55	5396.6	0.9993
	0.5 M H_2SO_4	26.91	845.09	0.9660

Electrochemical impedance spectroscopy

Kinetics and mechanism of metal dissolution process can be interpreted using electrochemical impedance spectroscopy (EIS). Fig. 7.8 and Fig. 7.9 reveals the Nyquist and Bode plots for mild steel in 1 M HCl and 0.5 M H_2SO_4 with and without extracts of *Clerodendrum infortunatum* at room temperature. These plots have been seen with similar shapes for all concentrations, including blank, which means the mechanism of metal dissolution was almost exact for inhibited and uninhibited metal. A single capacitive loop of the impedance spectra suggested that the charge transfer reactions were predominant reactions involved in metal corrosion. The imperfect semicircular capacitive loop was observed as a consequence of the roughness and inhomogeneity on the metal surface[192].

Moreover, semicircle diameter in the presence of CILE and CIRE was more extensive than that in acid solution in the absence of extracts. On adding the concentration of extracts, the diameter of Nyquist plots magnified, reinforcing the inhibitive film. This result showed that the impedance of mild steel immersed in acid solution with CILE and CIRE increased with the concentration of extracts and caused the maintenance of excellent inhibitive power. The parameters obtained from Nyquist plots and calculated inhibition efficiencies are tabulated in Table 7.6. It has been noticed that as the concentration of CILE and CIRE increased, the double-layer capacitance (C_{dl})

lowered and charge transfer resistance (R_{ct}) enhanced. This lowering of C_{dl} values was related to imperfections on the metal surface. This relation was simulated through a constant phase element. So, capacitance can be derived using equation (51).

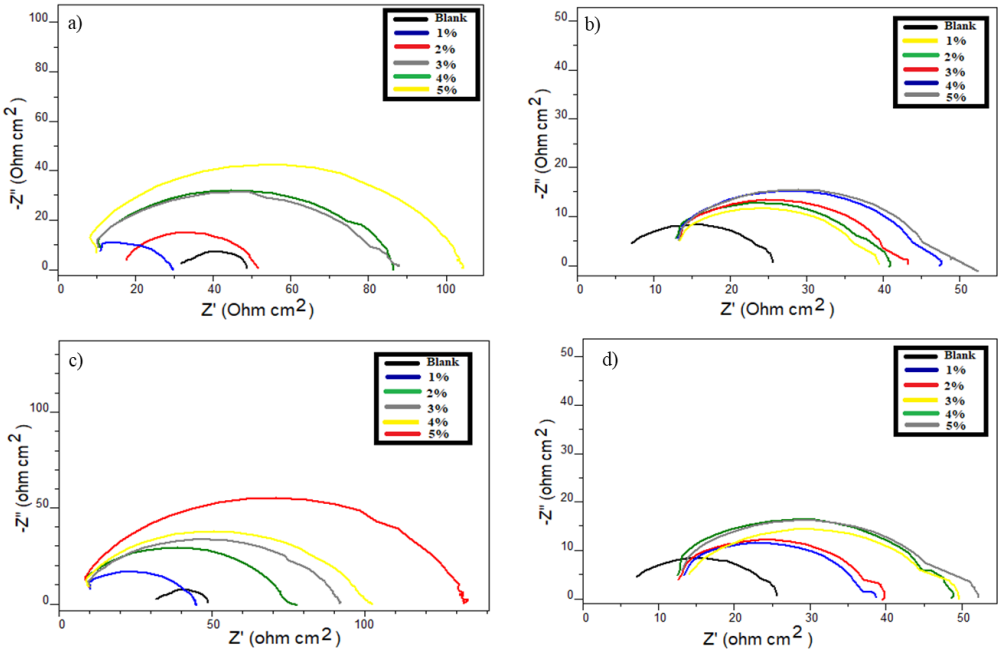

Fig. 7.8: Nyquist plots of mild steel with CILE and CIRE in 1 M HCl (a & c) and in 0.5 M H_2SO_4 (b & d)

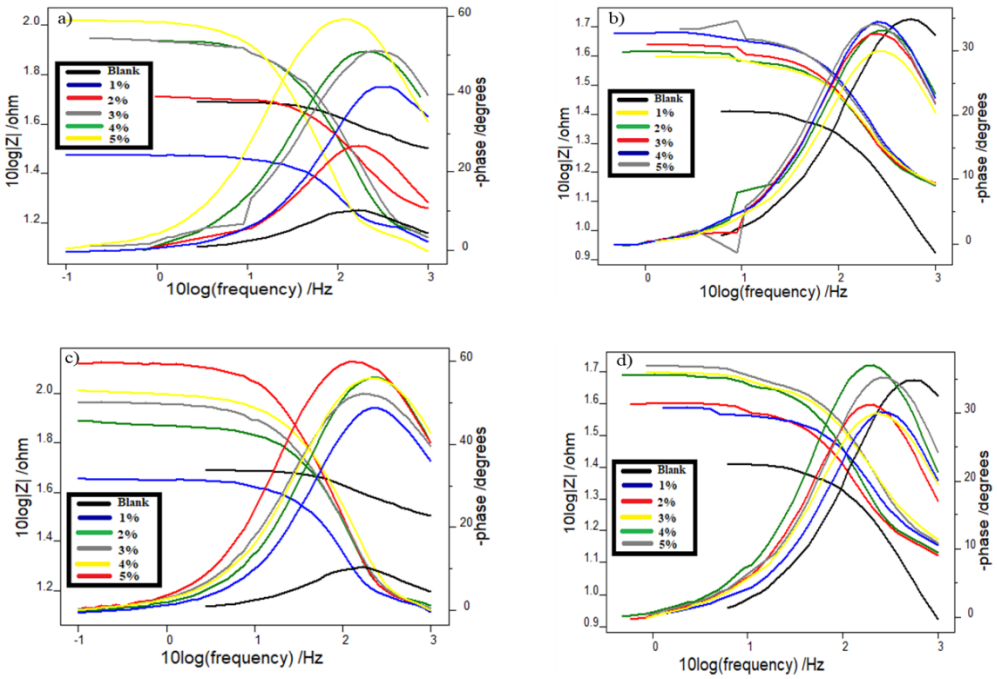

Fig. 7.9: Bode plots of mild steel with CILE and CIRE in 1 M HCl (a & c) and in 0.5 M H_2SO_4 (b & d)

A higher R_{ct} value indicates slower corroding metal. It was worth mentioning that CIRE in HCl solution possessed a higher R_{ct} value among the 4 systems of acid solutions. So, better inhibition efficiency of CIRE in 1 M HCl solution was confirmed by EIS. Bode plots demonstrated that phase angle peaks became larger and broader when the concentration of CILE and CIRE increased[193].

Electrochemical results were simulated to pure electric models by Randle's equivalent circuit (Fig. 1.8). It made possible the calculation of numerical values analogous to all the characteristics of the electrochemical system under study. Inhibition efficiencies of CILE and CIRE calculated from weight loss measurements were in exact reasonably match.

Table 7.6: Impedance parameters of mild steel in 1 M HCl and 0.5 M H_2SO_4 with and without CILE and CIRE

Inhibitor	Conc. (v/v %)	1 M HCl			0.5 M H_2SO_4		
		R_{ct} (Ωcm^2)	C_{dl} (μFcm^{-2})	η_{EIS}%	R_{ct} (Ωcm^2)	C_{dl} (μFcm^{-2})	η_{EIS}%
CILE	Blank	15.7	78.8	-	18.1	47.4	-
	1	30.8	72.8	49.02	28.9	45.2	37.37
	2	31.7	56.5	50.47	33.1	41.0	45.31
	3	70.9	54.7	77.85	33.6	40.5	46.13
	4	71.5	53.4	78.04	35.8	39.4	49.44
	5	92.4	46.2	83.01	36.3	38.8	50.13
CIRE	1	35.8	76.7	56.14	32.7	46.9	44.64
	2	64.6	60.5	75.69	34.1	45.8	46.92
	3	77.6	70.2	79.76	35.3	45.4	48.72
	4	86.8	55.9	81.91	36.5	44.6	50.14
	5	120.0	53.4	86.91	52.8	43.6	65.71

Potentiodynamic polarization studies

Tafel and linear polarization plots for mild steel in 1 M HCl and 0.5 M H_2SO_4 in the absence and presence of CILE and CIRE at room temperature are exhibited in Fig. 7.10 and Fig. 7.11. Potentiodynamic polarization parameters from both Tafel and linear polarization plots are shown in Table 7.7. Fig. 7.10 and Fig. 7.11 delineates that the shape of Tafel and linear polarization plots were the same in acid solutions with and

without extracts. However, extracts to acid solutions increased corrosion current density values (i_{corr}) and decreased corrosion rate irrespective of medium, indicating corrosion inhibition performance of extracts.

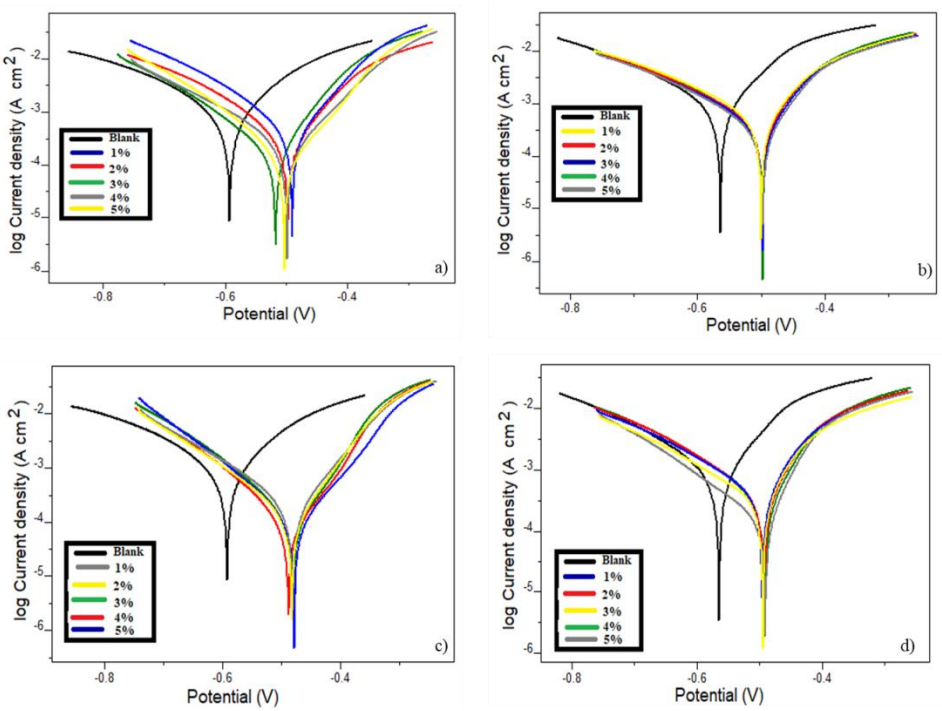

Fig. 7.10: Tafel plots of mild steel with CILE and CIRE in 1 M HCl (a & c) and in 0.5 M H_2SO_4 (b & d)

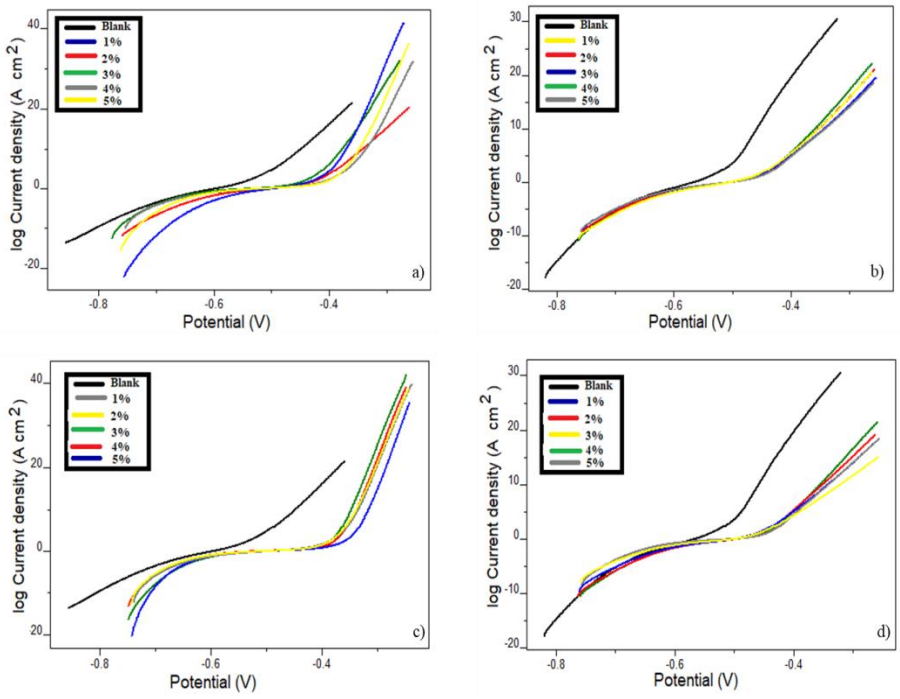

Fig. 7.11: Linear polarization plots of mild steel with CILE and CIRE in 1 M HCl (a & c) and 0.5 M H_2SO_4 (b & d)

It was inferred from Table 7.7 that the corrosion potential (E_{corr}) values of the system with CILE and CIRE shifted to noble values compared to the system without extracts. Both anodic and cathodic slopes were diverted for the sweeps at the various extract concentrations, indicating that CILE and CIRE operate as mixed-type corrosion inhibitors[194]. This result evinced that the components of both extracts in acid media get adsorbed onto both anodic and cathodic sites of the mild steel surface.

According to Tafel data, the increasing order of inhibition efficiency was $CIRE_{HCl}$> $CILE_{HCl}$>$CIRE_{H_2SO_4}$> $CILE_{H_2SO_4}$ and corresponding efficiencies were 92.57%, 87.82%, 66.09% and 51.79% respectively. Again, this result pointed up the potency of CIRE over CILE in inhibiting mild steel against acid attack and agreed with the results acquired from weight loss measurements.

Table 7.7: Potentiodynamic polarization parameters of mild steel in 1 M HCl and 0.5 M H_2SO_4 with and without CILE and CIRE

Inhibitor/ Medium	Tafel data						Polarization data	
	Conc. (v/v %)	$-E_{corr}$ (mV)	i_{corr} (μAcm^2)	b_a (mV/dec)	$-b_c$ (mV/dec)	η_{pol}%	R_p (Ω)	η_{Rp}%
CILE/ 1 M HCl	Blank	597.9	1240	166	221	-	33.14	-
	1	484.6	599.0	97	163	51.69	68.98	51.95
	2	508.9	549.0	132	171	55.72	72.36	54.20
	3	540.5	305.0	110	141	75.40	105.0	68.43
	4	489.7	255.0	96	171	78.80	139.8	76.29
	5	485.9	151.0	77	133	87.82	181.25	81.71
CILE/ 0.5 M H_2SO_4	Blank	602.2	1616	184	193	-	25.30	-
	1	540.6	987.0	188	200	38.92	42.60	40.61
	2	549.5	916.0	191	189	43.31	44.99	43.76
	3	550.8	867.0	195	191	46.34	48.09	47.39
	4	542.9	860.0	174	184	46.78	48.29	47.60
	5	548.5	779.0	185	182	51.79	51.19	50.57
CIRE/ 1 M HCl	1	476.6	220.0	86	156	82.28	109.9	81.57
	2	483.2	154.0	81	139	87.60	203.5	83.71
	3	472.7	150.0	71	129	87.92	223.2	85.15
	4	468.0	99.9	66	130	91.95	289.8	88.56
	5	460.8	92.2	71	121	92.57	211.0	89.34
CIRE/ 0.5 M H_2SO_4	1	552.4	891.0	199	187	44.96	44.96	43.72
	2	547.6	887.0	188	180	45.21	47.02	46.19
	3	543.6	805.0	174	174	50.27	47.05	46.22
	4	561.7	741.0	207	179	54.23	56.30	55.06
	5	572.2	549.0	183	145	66.09	64.11	60.53

According to polarization data, R_p values were augmented in the inhibited solution related to the uninhibited solution suggesting that CILE and CIRE protected mild steel in the acid medium. The trend of inhibition efficiency as a function of the concentration of CILE and CIRE observed for EIS and potentiodynamic polarization measurements matched linear polarization measurements.

Scanning electron microscopy

Fig. 7.12 displays SEM images of polished metal surface, mild steel surface after immersion in 1 M HCl with and without 5 v/v% CILE and CIRE for 24 hours. Fig. 7.12 a) represents SEM image of mild steel surface after polishing. Fig. 7.12 b) evident that the mild steel surface extensively corroded in HCl medium in the absence of extracts. But, in the presence of both extracts, the deterioration was diminished as disclosed in the SEM images (c) and (d), which were comparatively smooth and less damaged than the metal used in the blank experiment. It has also been noted that the mild steel surface with CIRE (d) was more smooth and undamaged than CILE (c). This observation further proved the higher inhibition power of CIRE over CILE.

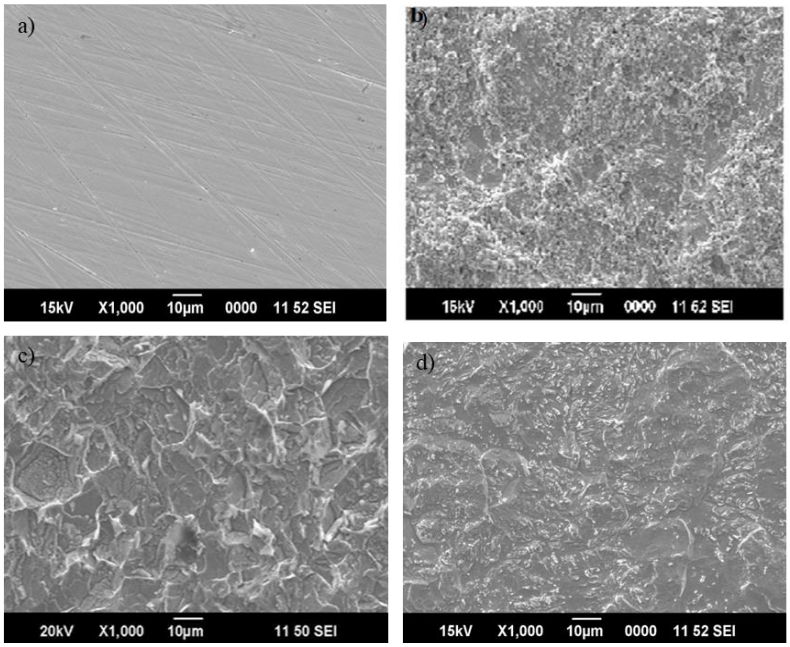

Fig. 7.12: SEM images of the surface of mild steel a) bare b) in 1 M HCl c) in 1 M HCl with CILE d) in 1 M HCl with CIRE

Quantum mechanical calculations

Spatial and electronic structures of an inhibitor have a crucial role in determining its inhibition efficiency. Quantum mechanical parameters such as energies of highest occupied molecular orbital (E_{HOMO}), lowest unoccupied molecular orbitals (E_{LUMO}), energy gap (ΔE), ionization energy (I), electron affinity (A), chemical potential (μ), electronegativity (χ), chemical hardness (η) and the number of electrons transferred (ΔN) of two significant components of *Clerodendrum infortunatum* plant extract 1) Clerodin 2) Scutellarin are given in Table 7.8. The optimized geometry, HOMO and LUMO of Clerodin and scutellarin are shown in Fig. 7.13. If the energy gap between HOMO and LUMO of an inhibitor is small, it will possess inhibition effectiveness since the ionization energy is low. Moreover, a lower ΔE value reflects the high stability of an inhibitor. Table 7.8 shows that the ΔE value of clerodin was lower than scutellarin, indicating a prominent interaction of clerodin molecules with the mild steel surface. This interaction was denoted by electron donation. Thus improved inhibition power of CIRE over CILE revealed the presence of myriads of clerodin molecules in CIRE.

According to FMO theory, E_{HOMO} values of an inhibitor determine whether it can donate its electrons to the metal surface, i.e. higher the E_{HOMO} values increase the ability to donate electrons from inhibitor to vacant metal d-orbital[53]. Or it can be said that lower the E_{LUMO} values favour the acceptance of electrons by the inhibitor molecules. From Table 7.8, it has been noted that E_{HOMO} values are as follows clerodin (-2.176 eV) > scutellarin (-3.12 eV), which recommends that the electron-donating capacity of clerodin was the highest. This was ascribed to the greater extent of adsorption of clerodin molecules over the mild steel surface.

In clerodin, the presence of oxygen moieties is relatively more than scutellarin. It may enhance the electron-donating capacity of clerodin molecules over the other.

Scutellarin has only one -OH moiety. Lower electronegativity (χ) of an inhibitor facilitates the transfer of electrons from the molecules to higher electronegativity possessed metals. During the inhibition reaction between mild steel and extract molecules, electrons move from the extract molecules with lower χ to higher χ until their chemical potentials become equal. If the value of $\Delta N < 3.6$, a molecule incline to donate electrons to the metal surface. So, the inhibition efficiency enhances with respect to electron donation of the inhibitor molecules to the metal surface. The number of electrons transferred from inhibitor molecules follows the order clerodin (1.938) > scutellarin (1.299).

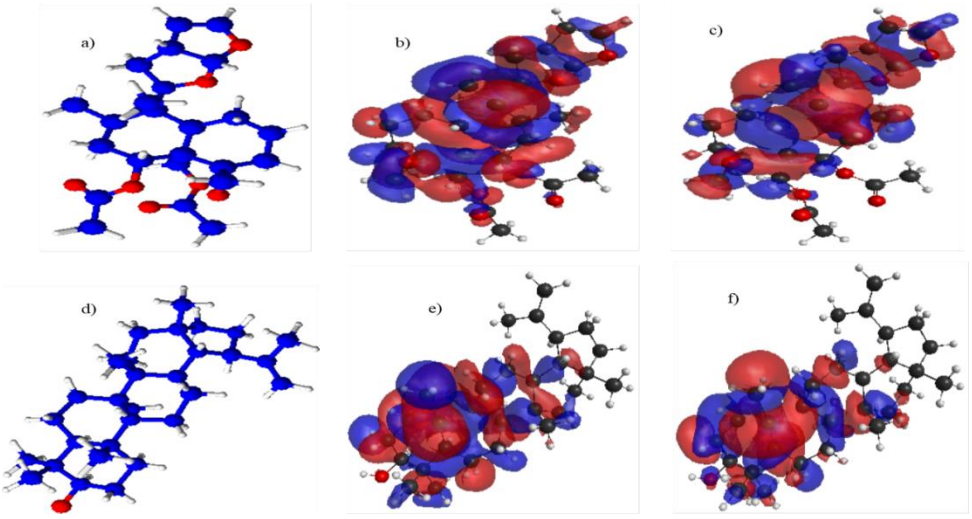

Fig. 7.13: a) Optimized geometry, b) HOMO and c) LUMO of clerodin; d) Optimized geometry, e) HOMO and f) LUMO of scutellarin

Table 7.8: Quantum mechanical parameters (in eV) of clerodin (I) and scutellarin (II)

Molecule	E_{HOMO}	E_{LUMO}	ΔE	I	A	μ	χ	η	ΔN
I	-2.176	1.177	3.35	2.17	-1.17	-0.49	0.49	1.67	1.93
II	-3.120	1.732	4.85	3.12	-1.73	-0.69	0.69	2.42	1.29

Statistical analysis

❖ ***Optimization of factors for inhibition efficiency (IE%)***

Response surface methodology (RSM) provides optimized conditions for tested parameters to acquire a good response. It was evident from weight loss measurements

that the corrosion inhibition efficiency of extracts greatly influenced its concentration and operating temperature, and CIRE showed excellent inhibition performance in 1 M HCl medium over CILE. So, corrosion inhibition efficiency of CIRE and parameters such as temperature and concentration of CIRE in 1 M HCl medium were linked through regression analysis. Two parameters used in the RSM technique are temperature in K (X_1) and concentration of CIRE in v/v% (X_2).

Central composite design (CCD) was employed to study the impact of temperature (X_1) and concentration of CIRE (X_2) on inhibition efficiency (IE%). Table 7.9 shows all the experimental runs in CCD and corresponding predicted inhibition efficiency by optimizing the two parameters.

Table 7.9: Experimental and predicted IE% from the weight loss measurements and CCD

Temp (X_1)	Conc. (X_2)	IE%		Residual
		Experimental	Predicted	
313	5	88.98	89.44	0.46753
333	1	51.48	53.37	1.89273
313	1	75.56	76.44	0.88033
333	5	69.51	70.98	1.47793
313	3	82.25	83.80	1.55793
323	5	78.15	79.18	1.03073
333	3	63.28	63.04	-0.23567
323	1	63.58	63.86	0.28953
323	3	70.69	72.38	1.69913

A full quadratic model was developed to understand the influence of inhibitor efficiency on the independent parameters in selected ranges:

$$IE = 1532 - 7.91X_1 - 13.481X_2 + 0.01037X_1^2 - 0.216X_2^2 + 0.0576X_1X_2 \quad (57)$$

Validity of this quadratic equation can be evaluated from residual plots given in Fig. 7.14. It contains four different plots. On inspection of the normal probability plot, it has been observed that this full quadratic equation for inhibition efficiency was fixed to the normal distribution. It implied that the derived model needs no response

transformation, and there were no noticeable complications with normality. Versus fits plot revealed that there was a constancy in the variance of observations for all responses. Histogram of residuals pointed out that the residuals were allocated uniformly for all frequencies. Versus order plot disclosed that points of observed runs were scattered randomly, maintaining the fixed area of residuals which substantiated the model's precision. In summary, all four plots corroborated the accuracy of the model to demonstrate the influence of parameters on the inhibition efficiency of CIRE.

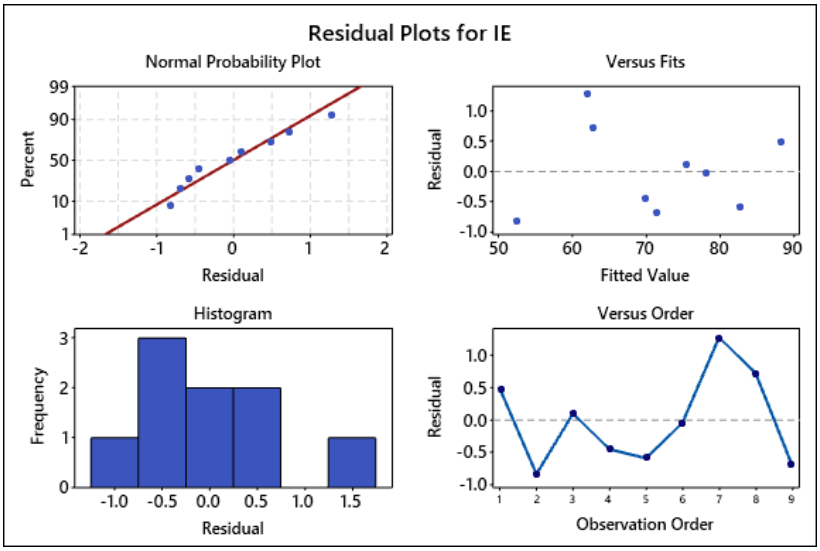

Fig. 7.14: Residual plots for inhibition efficiency

Table 7.10 describes the analysis of variance for corrosion inhibition efficiency. P-value was the superior value in Table 7.10 which establishes the significance of the variable[162]. The adopted value of α, degree of essentialness, was 0.05. On close observation to Table 7.10, it can be said that only for the linear terms the P-value was found to be less than α, which means linear terms significantly affect the response. There was little effect on IE for square and two-way interaction terms. Pareto chart (Fig. 7.15) interprets that only linear terms predominantly influenced the inhibition efficiency. Among the two linear parameters, the temperature was a more significant term than concentration. It was found that squared terms X_1^2, X_2^2 and two–way interaction term

X_1X_2 possess no considerable effect on the inhibition efficiency. Value of coefficient (R^2) obtained for the predicted model was 0.9891, which inferred the best fit quadratic model for the experimental results. Therefore, the outcomes can be easily analyzed by the model.

Table 7.10: Analysis of variance for corrosion inhibition efficiency

Source	DF	Adj SS	Adj MS	F-Value	P-Value
Model	5	1013.38	202.677	146.67	0.001
Linear	2	1004.43	502.216	363.44	0.000
Temp	1	651.46	651.458	471.45	0.000
Conc	1	352.97	352.973	255.44	0.001
Square	2	3.64	1.820	1.32	0.389
Temp *Temp	1	2.15	2.149	1.56	0.301
Conc *Conc	1	1.49	1.491	1.08	0.375
2-Way Interaction	1	5.31	5.313	3.84	0.145
Temp *Conc	1	5.31	5.313	3.84	0.145
Error	3	4.15	1.382		
Total	8	1017.53			

DF: degrees of freedom, Adj SS: adjusted sum of squares, Adj MS: adjusted mean of squares, F: Fischer's F-test value, P: probability

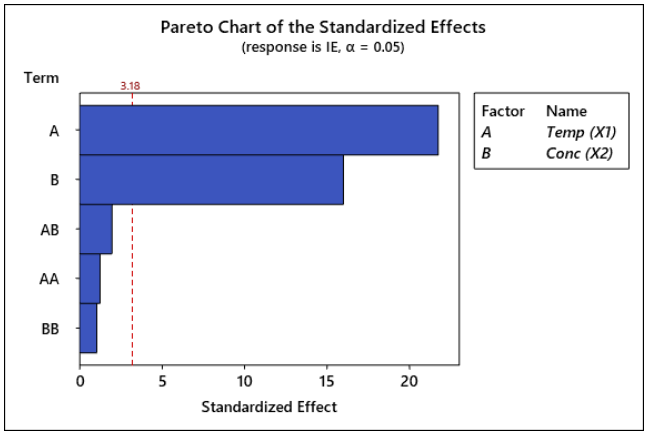

Fig. 7.15: Pareto chart of the standardized effects of mild steel

The influence of two parameters studied independently on IE% and is shown in the Main effects plots (Fig. 7.16). It was observed that temperature is inversely proportional to IE% while CIRE concentration is directly proportional to IE%. It can be inferred that CIRE molecules are adsorbed on the metal surface through physisorption mode. So, IE% decreased with higher temperatures. As the concentration of CIRE

increased, the coverage of active sites on the metal surface increased. Similar observations were found with weight loss measurements.

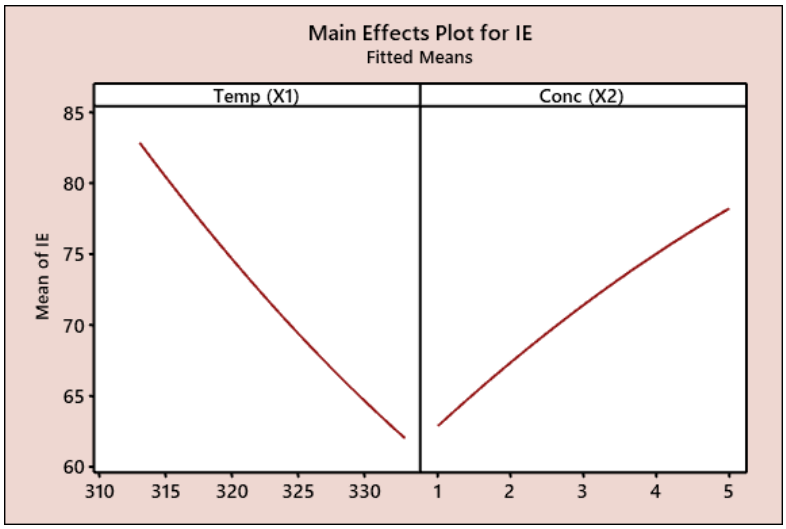

Fig. 7.16: Main effects plots for inhibition efficiency of mild steel in 1 M HCl

Interrelation of the parameters on IE% was measured using a contour and 3-D surface plot vs two independent parameters[195] in Fig. 7.17 a) and Fig. 7.17 b), respectively. It has been evident from Fig. 7.17 that the highest IE% was achieved for 5 v/v% concentration of CIRE at 313 K operating temperature. It can be said that higher temperature leads to an increase in the corrosion rate and, thus, decreased IE%.

❖ ***Response Optimization***

The CIRE concentration and temperature at which maximum IE% were acquired using the desirability function method of response optimization technique. Herein, independent parameters were optimized to maximum, and the corresponding plot is presented in Fig. 7.18. The optimum conditions of temperature and concentration were 313 K and 5 v/v %, which corresponds to 88.4931% inhibition efficiency, i.e. the best outcome for the response.

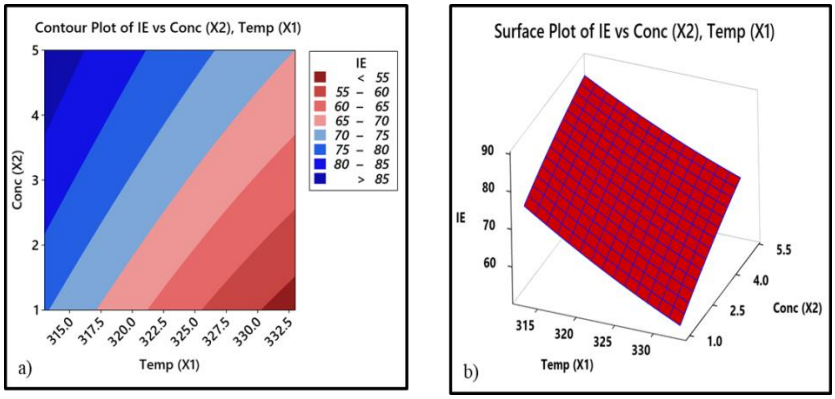

Fig. 7.17: a) Contour and b) 3-D surface plot for corrosion inhibition efficiency

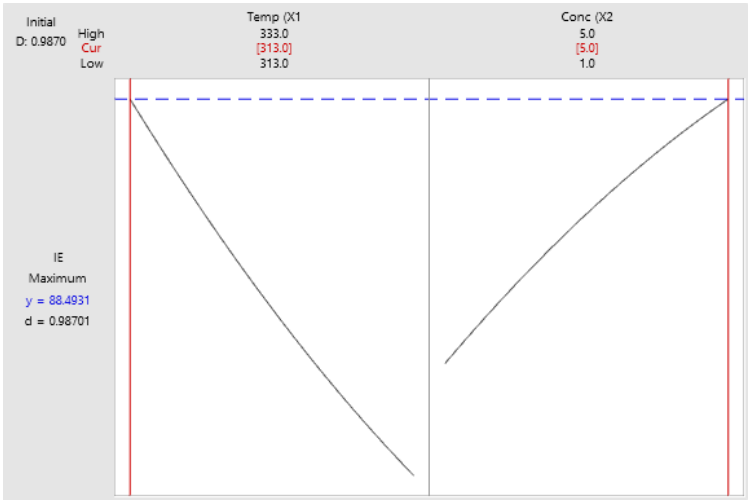

Fig. 7.18: Response optimization plot for inhibition efficiency

Conclusions

- The corrosion inhibition behaviour of *Clerodendrum infortunatum* leaf and root extracts on mild steel in 1 M HCl and 0.5 M H_2SO_4 were investigated using experimental and quantum mechanical techniques.
- Electrochemical studies disclosed that CIRE and CILE possessed fairly good inhibition efficiencies.
- The inhibition efficiencies calculated from EIS and polarization parameters were in exact agreement.
- The adsorption of CILE and CIRE on mild steel in both acid media was according to Langmuir adsorption isotherm.

- The quantum mechanical calculations for the main phytochemicals clerodin and scutellarin evidently supports the experimental results.
- The SEM images showed the protective power of the extracts on the mild steel surface.
- Predicted inhibition efficiency of CIRE at different CIRE concentrations and operating temperature in 1 M HCl evaluated by RSM was in perfect agreement with the data obtained from weight loss measurements.

CHAPTER 8

DIOSCOREA BULBIFERA EXTRACT: NATURAL CORROSION INHIBITOR FOR MILD STEEL IN ACID MEDIA

This chapter explores the potent corrosion inhibition property of green *Dioscorea bulbifera* leaf extract (DBE) on the mild steel in 1 M HCl and 0.5 M H_2SO_4 using physicochemical, electrochemical and surface morphological techniques. Even though DBE contains myriads of phytochemical constituents, three essential chemical components, bafoudiosbulbin A, diosgenin and kaempferol[196], have been subjected to quantum mechanical studies to supplement the corrosion inhibition mechanism of the leaf extract in more detail. Its structures are shown in Fig. 8.1.

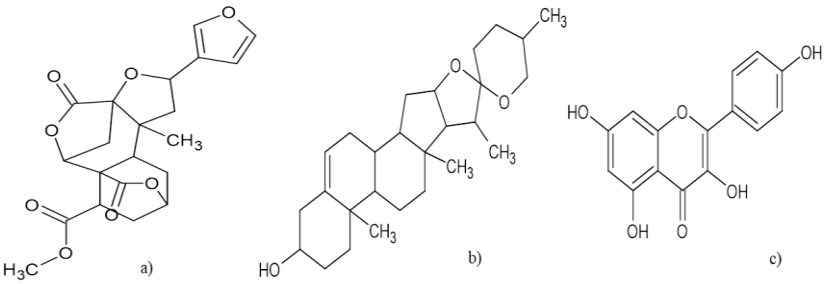

Fig. 8.1: Structures of a) bafoudiosbulbin A b) diosgenin c) kaempferol

Dioscorea bulbifera

Results and discussions

Phytochemical screening of DBE

Standard qualitative identification tests were performed to detect the phytochemicals present in DBE, and the observations are given in Table 8.1.

FTIR spectroscopy

Chemical structure and functional groups of DBE can be evaluated using FTIR spectroscopy (Fig. 8.2). An intensive and broad absorption peak at 3281 cm^{-1}, designating -OH functional groups in DBE molecules. The peak found at 2917 cm^{-1} is represented by alkyl C-H bond vibration. >C=O stretching vibration was observed at

1731 cm^{-1}. Aromatic C-C bond absorption peak was seen at 1610 cm^{-1}. Moreover, the weak peak seen at 1243 cm^{-1} corresponds to the absorption of C-O stretching vibration. In-plane bending of C-O-H was measured at 1403 cm^{-1} assigned to -COOH groups. The C-N stretching bond is seen at 1027 cm^{-1}. In short, the presence of an aromatic ring, -OH, >C=O and -COOH groups in the major chemical constituents of DBE was examined in the FTIR spectrum.

Table 8.1: Phytochemical screening of DBE

Sl. No.	Compounds	Tests	Results
1	Alkaloids	Mayer's reagent	−−
2	Steroids	Salkowaski's test	++
3	Phenolic compounds	Potassium ferrocyanide test	++
4	Flavanoids	Sodium hydroxide test	++
5	Saponins	Froth test	++
6	Tannins	Lead acetate test	−−
7	Cardiac glycosides	Conc. sulphuric acid test	++
8	Coumarin	Alcoholic NaOH test	++
9	Quinones	Conc. sulphuric acid test	++

++ (present), − − (Absent)

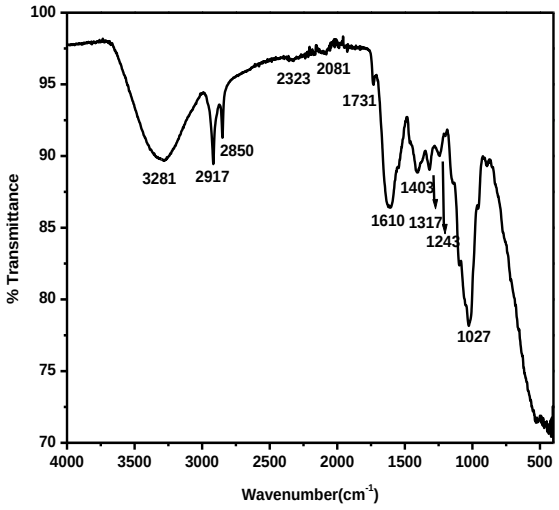

Fig. 8.2: FTIR spectrum of DBE

Weight loss measurements

Effect of concentration

According to Table 8.2, the corrosion rate (υ) of the metal treating without DBE as an inhibitor is much higher than the metals treating with DBE containing 1 M HCl and 0.5 M H_2SO_4 solutions. By increasing DBE concentration, the corrosion rate remarkably decreased. This diminution confirms the good inhibition effect of DBE. On close examination of Table 8.2, it was realized that after dissolving 5 v/v% DBE in 1 M HCl solution, the inhibition efficiency enhanced to 91.78%, whereas, in 0.5 M H_2SO_4 solution efficiency increased to 86.93%, clarifying the predominant protection power of DBE on mild steel exposed in HCl solution at room temperature[197].

Table 8.2: Weight loss measurements of mild steel with and without DBE in 1 M HCl and 0.5 M H_2SO_4 at room temperature for 24 hrs

Conc. (v/v%)	Corrosion rate (mm/yr)		Inhibition efficiency (η%)	
	1 M HCl	0.5 M H_2SO_4	1 M HCl	0.5 M H_2SO_4
Blank	3.95	35.57	-	-
1	1.16	17.69	70.52	50.26
2	0.93	16.02	76.34	54.94
3	0.72	14.03	81.53	60.55
4	0.65	12.31	83.48	65.38
5	0.32	4.648	91.78	86.93

❖ ***Effect of temperature***

Fig. 8.3 shows the comparison of inhibition efficiencies of mild steel in various concentrations of DBE in 1 M HCl and 0.5 M H_2SO_4 at different temperatures. From Fig. 8.3, it is noted that inhibition efficiency in HCl was higher than in H_2SO_4 at all temperatures under investigation. It claimed that the Cl^- ions tend to adsorb on the metal surface more quickly than SO_4^{2-} ions[64]. In HCl solution, inhibition efficiencies for all temperatures were in the range of 84-91%. The maximum inhibition efficiency was

found at 303 K for both acid media. The limited adsorbability of DBE molecules on the adsorbed SO_4^{2-} ions on the metal surface caused lower efficiency in the H_2SO_4 medium.

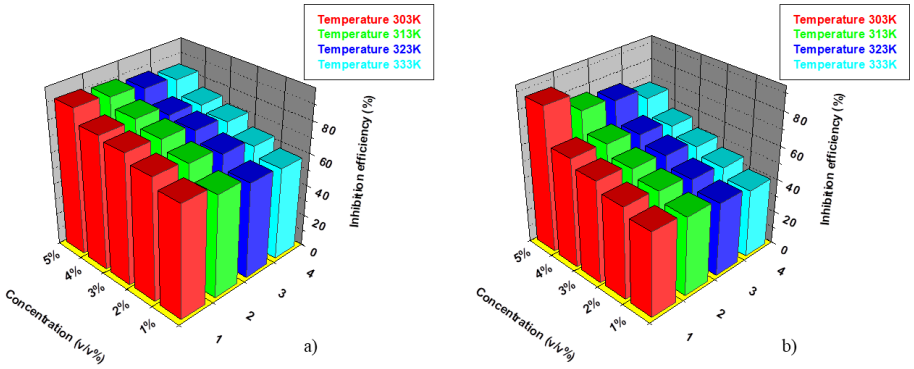

Fig. 8.3: Variation in inhibition efficiency of DBE in a) 1 M HCl b) 0.5 M H_2SO_4 at elevated temperatures

Table 8.3: Corrosion rate (υ) and inhibition efficiency (η%) of DBE in 1 M HCl and 0.5 M H_2SO_4 at different temperatures for 24 hrs

Medium	Conc. (v/v%)	υ (303 K)	η% (303 K)	υ (313 K)	η% (313 K)	υ (323 K)	η% (323 K)	υ (333 K)	η% (333 K)
1 M HCl	Blank	3.95	-	13.1	-	22.0	-	31.7	-
	1	1.16	70.5	4.66	64.3	8.79	60.1	13.2	58.3
	2	0.93	76.3	3.46	73.5	6.78	69.2	11.4	64.0
	3	0.72	81.5	2.66	79.6	5.40	75.5	8.99	71.6
	4	0.65	83.4	2.09	84.0	4.95	77.5	7.86	75.2
	5	0.32	91.7	1.32	89.8	2.90	86.8	4.99	84.2
0.5 M H_2SO_4	Blank	35.57	-	58.27	-	86.25	-	106.2	-
	1	17.69	50.26	30.73	47.25	48.15	44.17	62.65	41.04
	2	16.02	54.94	27.39	52.98	43.48	49.58	56.50	46.82
	3	14.03	60.55	24.69	57.62	38.04	55.89	51.06	51.94
	4	12.31	65.38	20.90	64.12	33.82	60.78	45.43	57.24
	5	4.648	86.93	13.86	76.21	22.56	73.84	34.60	67.43

Table 8.3 reveals that the corrosion rate significantly raised with increasing the operating temperature. This increase indicates that the mild steel dissolution rate can be signified at elevated temperatures[198]. For metals exposed to DBE containing HCl solutions, the corrosion rate lowered notably, elucidating that the DBE molecules could impressively retard the metal corrosion process.

The activation parameters can be reckoned by performing the weight loss measurements between 303 K and 333 K. The impact of temperature on mild steel corrosion in acid media with and without DBE was analyzed using Arrhenius and transition state equations (Eqs. (41) and (43)). Arrhenius and transition state plots are pictorially represented in Fig. 8.4 and Fig. 8.5 in 1 M HCl and 0.5 M H_2SO_4, respectively, and the obtained parameters are summarized in Table 8.4.

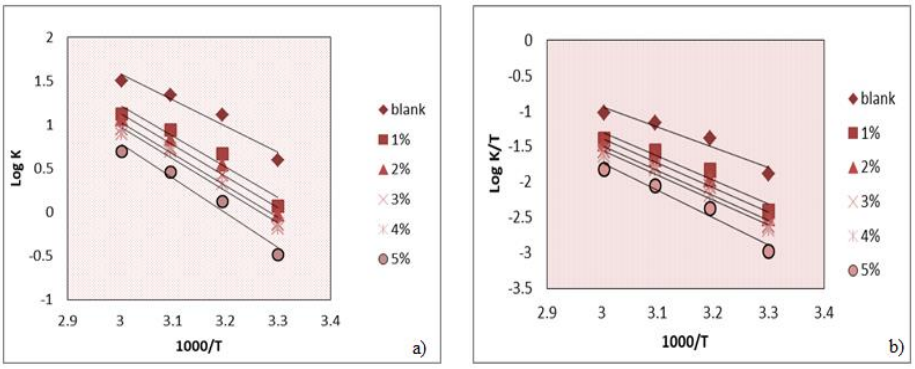

Fig. 8.4: Arrhenius plots of a) log K vs 1000/T b) log K/T vs 1000/T with and without DBE in 1 M HCl

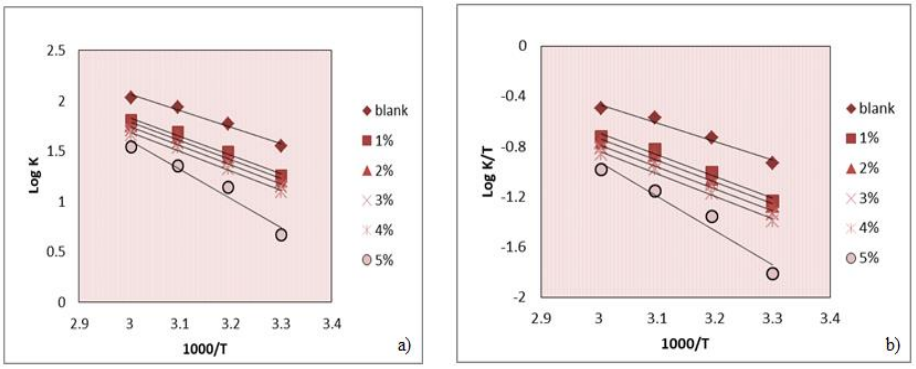

Fig. 8.5: Arrhenius plots of a) log K vs 1000/T b) log K/T vs 1000/T with and without DBE in 0.5 M H_2SO_4

On inspection of Table 8.4, it was clear that in the presence of DBE, the activation energy values shifted to higher values compared with uninhibited metal. It can be ascribed to the adsorption of DBE molecules on the mild steel surface through the physisorption mechanism. Activation parameters illustrated that the activation enthalpy (ΔH^*) and entropy (ΔS^*) values became more positive by enhancing the DBE

concentration. The positive values of ΔH* mention the endothermic process of mild steel corrosion. At the same time, ΔS* values progressed to be less negative, implies the disorderliness of DBE molecules enhancement.

Table 8.4: Thermodynamic parameters of mild steel corrosion with and without DBE in 1 M HCl and 0.5 M H_2SO_4

Medium	Conc. (v/v %)	E_a (kJ mol^{-1})	A	ΔH^* (kJ mol^{-1})	ΔS^* (J $mol^{-1}K^{-1}$)
1 M HCl	Blank	57.24	3.58×10^{10}	54.61	-44.7842
	1	66.98	5.18×10^{11}	64.34	-22.5410
	2	69.03	8.41×10^{11}	66.39	-18.5315
	3	69.51	8.95×10^{11}	66.87	-18.0203
	4	70.19	9.44×10^{11}	67.56	-17.5684
	5	75.76	4.54×10^{12}	73.12	-4.4890
0.5 M H_2SO_4	Blank	30.96	8.16×10^{6}	28.32	-114.510
	1	35.71	2.68×10^{7}	33.08	-105.524
	2	35.72	2.40×10^{7}	33.62	-104.783
	3	36.26	2.63×10^{7}	33.81	-104.628
	4	36.99	3.04×10^{7}	34.35	-103.567
	5	54.93	1.61×10^{10}	52.29	-51.378

Adsorption isotherms

Effectiveness of the adsorption of inhibitor molecules on the mild steel surface was explained by adsorption isotherm. The mechanism of inhibition by adsorption was investigated by considering various adsorption isotherms such as Langmuir, El-Awady, Frumkin, Temkin, Freundlich and Flory-Huggins isotherms. Eqs. (34)–(40) were applied for a suitable fitting. Among the isotherms, the best adsorption isotherm was Langmuir isotherm for 1 M HCl whereas, it was Frumkin isotherm for 0.5 M H_2SO_4 based on the closeness of linearity index to unity. It can be found from Fig. 8.6 a) and Fig. 8.6 b) straight line with R^2=0.9911 and R^2=0.9267 for HCl and H_2SO_4 media, respectively. Furthermore, the adsorption constant (K_{ads}) was computed. Greater the values of K_{ads} declare that the DBE molecules adsorption on the mild steel happens instinctively[82].

The observed values of ΔG_{ads}° and K_{ads} are shown in Table 8.5. The examined negative values of ΔG_{ads}° evidence that the DBE molecules effectively adsorbed on the mild steel surface. Results obtained in Table 8.5 reveals that ΔG_{ads}° value was more negative for HCl medium than H_2SO_4 medium. Current works reported that the ΔG_{ads}° values between −28 to −38 $kJ \cdot mol^{-1}$ represent the mixed type of adsorption mode by inhibitor molecules, i.e., physical and chemical adsorption. So, here DBE molecules adsorbed on the mild steel surface via physical and chemical adsorption mechanisms.

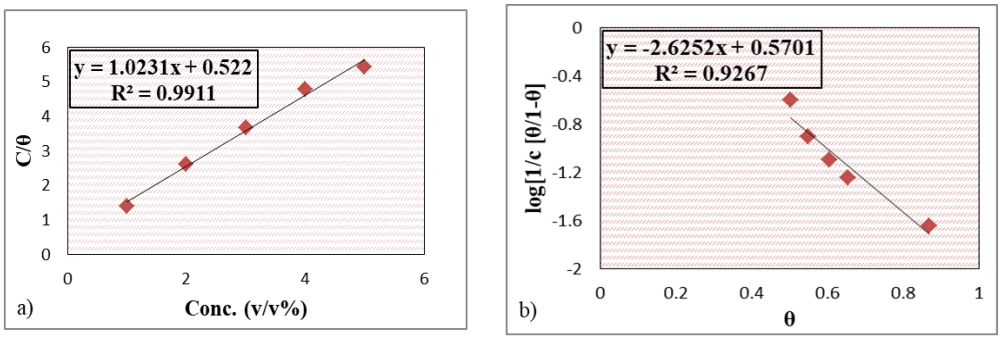

Fig. 8.6: a) Langmuir adsorption isotherm of DBE on mild steel in 1 M HCl and b) Frumkin adsorption isotherm of DBE on mild steel in 0.5 M H_2SO_4

Table 8.5: Adsorption parameters of mild steel in 1 M HCl and 0.5 M H_2SO_4 with DBE from weight loss measurements at room temperature

Medium	ΔG_{ads}^{0} ($kJmol^{-1}$)	K_{ads}	R^2
1 M HCl	28.96	1915.70	0.9911
0.5 M H_2SO_4	28.74	1754.07	0.9267

Electrochemical impedance spectroscopy

EIS illustrated the electrochemical characteristics of the mild steel exposed to 1 M HCl and 0.5 M H_2SO_4 solutions containing DBE. Fig. 8.7 and Fig. 8.8 represent Nyquist and Bode plots of metals exposed to acid solutions with and without DBE after 30 seconds of immersion. Nyquist plots displayed one capacitive semicircle, defining that the charge transfer process chiefly controls mild steel corrosion. Observing Fig. 8.7, Nyquist plots of metals dipped in acid solutions without DBE exhibited semicircles with much smaller diameters than metals subjected to acid solutions containing DBE. It has

been noticed that by enhancing the concentration of DBE, the Nyquist plot diameter becomes more extensive.

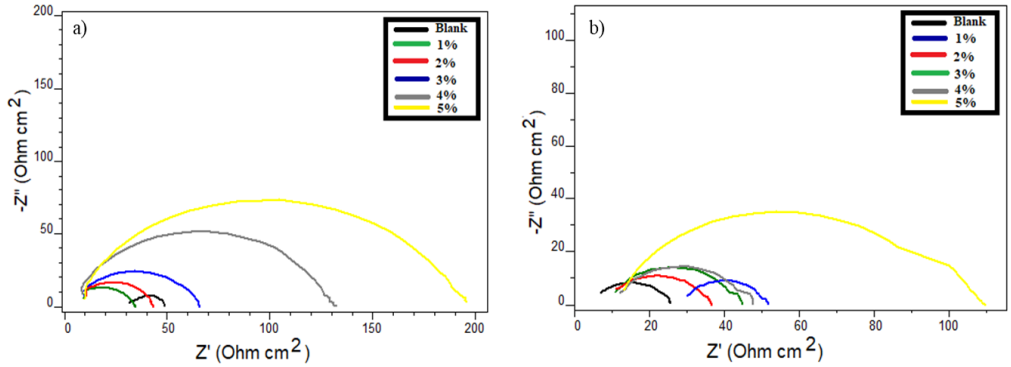

Fig. 8.7: Nyquist plots of mild steel with and without DBE in a) 1 M HCl and b) 0.5 M H_2SO_4

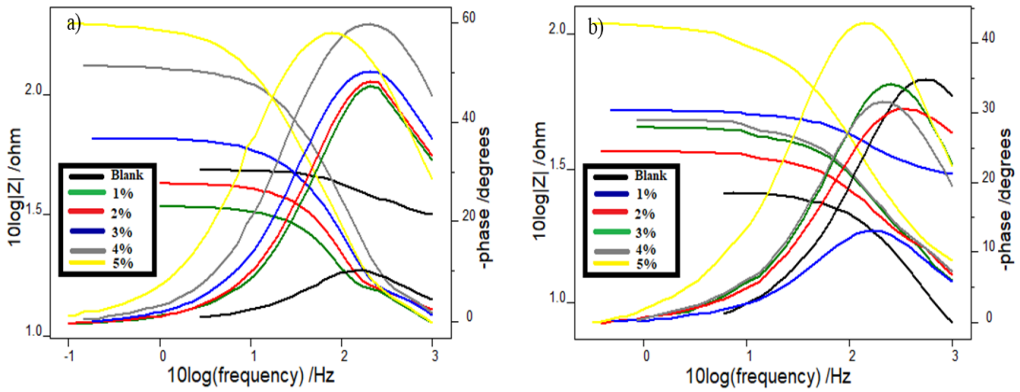

Fig. 8.8: Bode plots of mild steel with and without DBE in a) 1 M HCl and b) 0.5 M H_2SO_4

Table 8.6: Impedance parameters of mild steel in 1 M HCl and 0.5 M H_2SO_4 with and without DBE

Conc. (v/v %)	1 M HCl			0.5 M H_2SO_4		
	R_{ct} (Ωcm^2)	C_{dl} (μFcm^{-2})	η_{EIS}%	R_{ct} (Ωcm^2)	C_{dl} (μFcm^{-2})	η_{EIS}%
Blank	15.7	78.8	-	18.1	47.4	-
1	42.0	74.2	62.61	33.6	46.8	46.13
2	54.1	69.3	70.97	36.4	44.1	50.27
3	63.4	62.4	75.23	39.1	43.9	53.70
4	115	53.7	86.34	42.5	43.3	57.41
5	170	40.1	90.76	85.1	39.2	78.73

The electrochemical parameters derived from Nyquist and Bode plots fitted by suitable equivalent circuits (Randle's equivalent circuit) are tabulated in Table 8.6. On close examination of Table 8.6 revealed that by increasing DBE concentration, R_{ct} values

prominently increased, demonstrating DBE molecules adsorption on the mild steel surface. Moreover, double-layer capacitance (C_{dl}) values were estimated by maintaining a constant phase element. Table 8.6 reveals that with raising DBE concentration, C_{dl} values diminished, clarifying the local dielectric thickness depletion and the water molecules substitution with DBE molecules[199]. These observations made that DBE molecules can strongly retard the mild steel corrosion rate in 1 M HCl and 0.5 M H_2SO_4. Inhibition efficiency of DBE reached 90.76% in 1 M HCl and 78.73% in 0.5 M H_2SO_4 for the maximum DBE concentration employed in this work.

Potentiodynamic polarization studies

Fig. 8.9 and Fig. 8.10 explains Tafel and linear polarization plots of mild steel, respectively, immersed in 1 M HCl and 0.5 M H_2SO_4 solutions containing various concentrations of DBE. Electrochemical parameters obtained from Tafel plots such as corrosion current density (i_{corr}), corrosion potential (E_{corr}), Tafel slopes (b_a and b_c) and that derived from linear polarization plots such as polarization resistance (R_p) and corresponding inhibition efficiencies calculated are given in Table 8.7. Tafel plots interpret that in the presence of DBE, both the anodic and cathodic curves were repositioned in the direction of lower current densities. It caused the blocking of active sites of the mild steel surface due to the adsorption of DBE molecules.

Changes in cathodic and anodic Tafel slopes are nearly comparable when the DBE molecules added to the acid media. Values of b_c and b_a indicated that the DBE adsorption on the mild steel surface changes both the cathodic and anodic branch shapes and slopes, suggesting that the hydrogen evolution and anodic dissolution mechanism controlled by DBE adsorption[168]. In addition, the shift in E_{corr} values concerning the blank metal is less than 85 mV declares the mixed inhibition effect of DBE.

The extreme inhibition capacity on mild steel surface was found by 5% DBE concentration in HCl and H_2SO_4 media as 91.69% and 87.31%. A similar trend was observed in weight loss and EIS studies that inhibition efficiency was minor in H_2SO_4 compared to HCl medium. Linear polarization studies also have maintained this observation.

The corrosion inhibition mechanism can be explained based on the role of DBE adsorption on the mild steel surface. The chemical interaction between organic molecules of DBE and the vacant 3d orbitals of the iron surface can change the iron dissolution mechanism and inhibit mild steel corrosion. Since the DBE molecules contain various functional groups with lone pair of electrons, they can interact with the anodic sites of the metal. As discussed earlier, i_{corr} values decreased with increasing DBE concentration, associated with cathodic reaction in the solution.

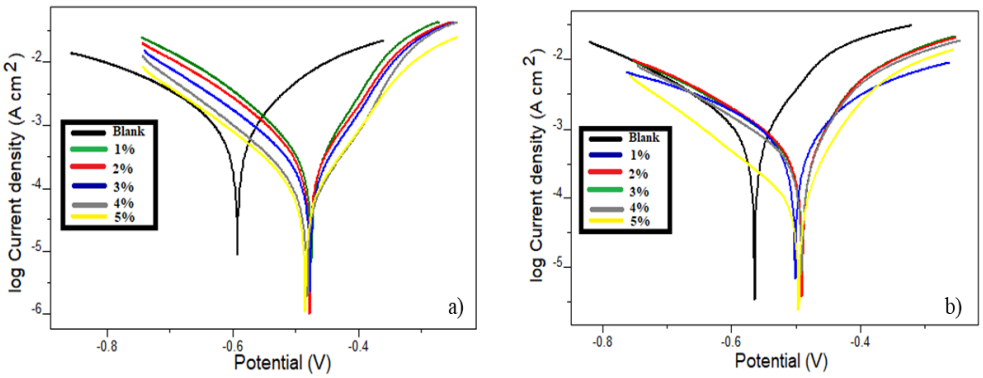

Fig. 8.9: Tafel plots of mild steel with and without DBE in a) 1 M HCl and b) 0.5 M H_2SO_4

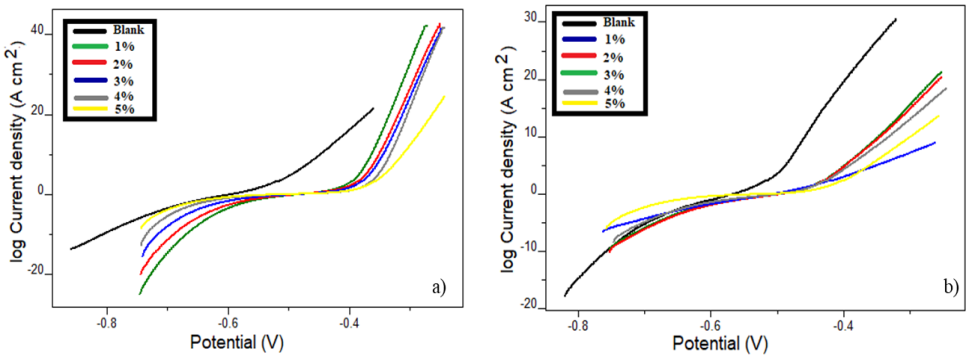

Fig. 8.10: Linear polarization plots of mild steel with and without DBE in a) 1 M HCl and b) 0.5 M H_2SO_4

Table 8.7: Potentiodynamic polarization parameters of mild steel in 1 M HCl and 0.5 M H_2SO_4 with and without DBE

Medium	Conc. (v/v %)	Tafel data				Polarization data		
		$-E_{corr}$ (mV)	i_{corr} (μAcm^2)	b_a (mV/dec)	$-b_c$ (mV/dec)	η_{pol}%	R_p (Ω)	η_{Rp}%
1 M HCl	Blank	597.9	1240	166	221	-	33.14	-
	1	529.0	430	110	146	65.32	91.15	63.64
	2	539.1	357	114	149	71.20	118.3	71.98
	3	553.6	231	98	147	81.37	129.25	74.35
	4	543.2	213	95	152	82.82	195.8	83.07
	5	546.5	103	111	159	91.69	274.0	87.90
0.5 M H_2SO_4	Blank	602.2	1616	184	193	-	25.30	-
	1	538.8	815	191	192	49.56	48.64	47.98
	2	519.5	762	227	258	52.84	51.36	50.73
	3	540.6	741	186	189	54.14	54.29	53.39
	4	551.2	685	200	184	57.61	58.51	56.75
	5	547.5	205	136	141	87.31	174.3	85.40

Electrochemical noise measurements

Shift in electrode potential is mainly used as a factor for determining pitting corrosion on mild steel. Fig. 8.11 exhibits the current noise spectra for mild steel treated with different DBE concentrations in 1 M HCl and 0.5 M H_2SO_4 solutions. It demonstrates that the current noise spectrum for metal treated without DBE was at higher amplitudes than metal dipped in DBE containing acid media reflecting adequate metal protection in the presence of DBE. PSD plots for metal fell in acid media with various DBE concentrations are portraited in Fig. 8.12. In PSD plots, when the frequency goes up, magnitudes of current noise get down. A similar observation can be seen in PSD plots as the current noise plots that the amplitudes of current for blank metal were higher than metal exposed in acid solutions with DBE. It declared metal dissolution prevention of DBE in acid media.

Pitting resistance equivalent number (PREN) is another term for the pitting index. Pitting index determines the capacity of an inhibitor to resist metal corrosion. Fig. 8.13 reveals pitting index curves for mild steel treated in acid solutions with and without DBE. Pitting index plots points out that in the presence of DBE, the pitting index value

was higher than that in the absence of DBE. Pitting index value was nobler for 5 v/v% DBE concentration in HCl medium, whereas it was lower in H_2SO_4 medium for a similar DBE concentration. Results showed that metal treated with DBE has good corrosion inhibition power in 1 M HCl and 0.5 M H_2SO_4. It also confirmed the better anti-corrosion property of DBE in 1 M HCl compared to 0.5 M H_2SO_4.

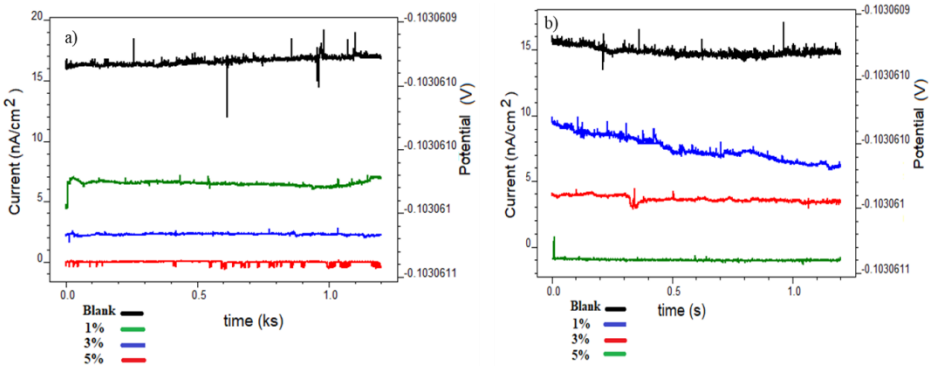

Fig. 8.11: Current noise plots of mild steel with and without DBE in a) 1 M HCl b) 0.5 M H_2SO_4

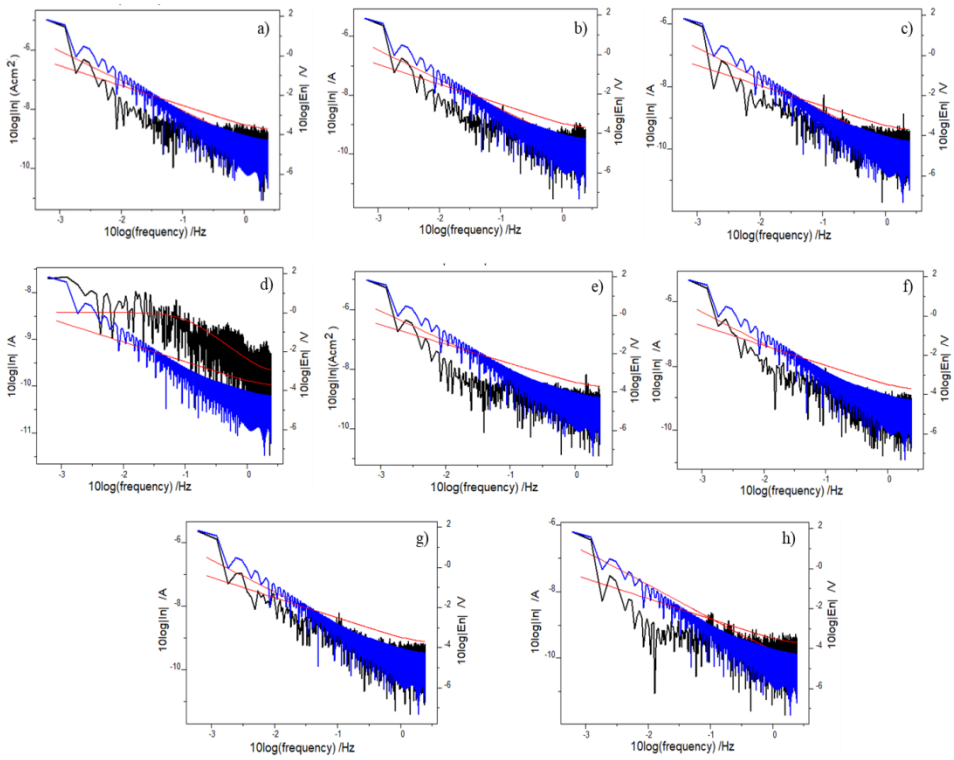

Fig. 8.12: Power spectral density plots of mild steel in 1 M HCl a) without DBE b) 1% DBE c) 3% DBE d) 5% DBE; Power spectral density plots of mild steel in 0.5 M H_2SO_4 e) without DBE f) 1% DBE g) 3% DBE h) 5% DBE

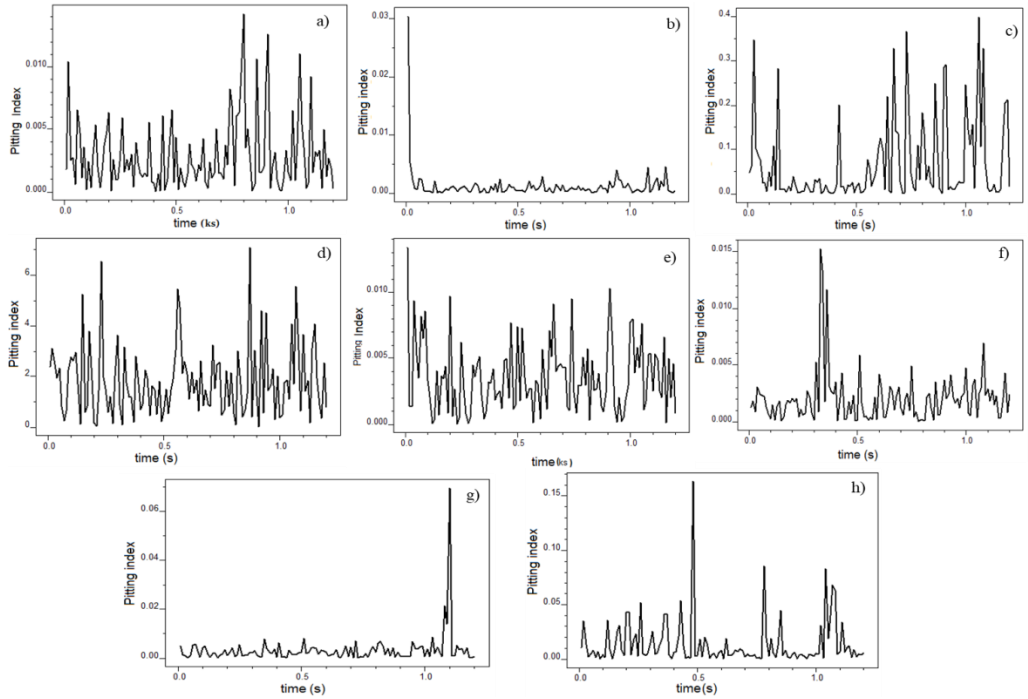

Fig. 8.13: Pitting index curves of mild steel in 1 M HCl a) without DBE b) 1% DBE c) 3% DBE d) 5% DBE; Pitting index curves of mild steel in 0.5 M H_2SO_4 e) without DBE f) 1% DBE g) 3% DBE h) 5% DBE

Scanning electron microscopy

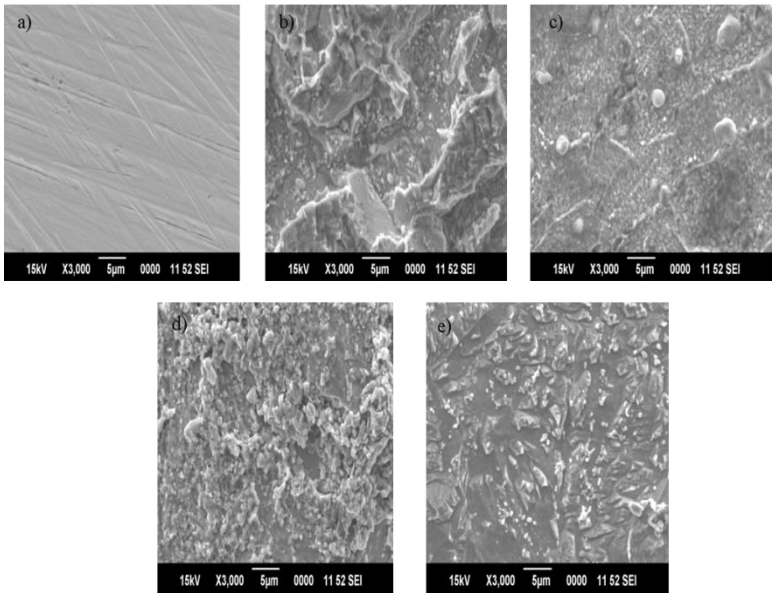

Fig. 8.14: SEM images of the surface of mild steel a) bare b) in 1 M HCl c) in 1 M HCl with DBE d) in 0.5 M H_2SO_4 e) in 0.5 M H_2SO_4 with DBE

Interaction mechanism between DBE molecules and mild steel can substantiate using SEM studies of metal coupons. Fig. 8.14 a) reveals the SEM image of the

smoothened surface of mild steel. SEM images of the surface of mild steel in 1 M HCl (Fig. 8.14 b & c) and 0.5 M H_2SO_4 (Fig. 8.14 d & e) were presented in the absence and presence of DBE, respectively. It showed that the lack of DBE severely damaged the surface of the mild steel. Also noticed that the metal destruction is predominant in the 0.5 M H_2SO_4 solution than in 1 M HCl solution. The metal surface became more refined and smooth in the presence of DBE molecules[188]. Therefore, it can be established that DBE behaves as an efficient corrosion inhibitor in acidic media.

Quantum mechanical calculations

According to the electronic perspective, donor-acceptor interactions cause the adsorption of inhibitors on the metal. Three important chemical constituents in the leaves of *Dioscorea bulbifera* are Bafoudiosbulbin A, Diosgenin and Kaempferol, which were subjected to quantum mechanical studies. From HOMO/LUMO plots and quantum mechanical parameters (Fig. 8.15 & Table 8.8), it is noted that the electron-rich centres of DBE molecules such as aromatic rings, double bonds and O heteroatoms could donate their electrons to proper nucleophiles or vacant orbitals of Fe atoms on mild steel. This electron donation of DBE molecules ensures their chemisorption.

Results showed that the ΔE value of the kaempferol was relatively lower than bafoudiosbulbin A and diosgenin, indicating a significant interaction of kaempferol molecules with the mild steel surface. Thus better electron donation of kaempferol results in improved inhibition capacity of DBE molecules. The presence of hydroxyl groups in aromatic rings enhances the electron-donating ability of kaempferol. The order of ΔE values of the components was kaempferol (4.155 eV) < bafoudiosbulbin A (5.171 eV) < diosgenin (5.249 eV).

Lower electronegativity (χ) of kaempferol (1.0245) supports the transfer of electrons to metals which having higher electronegativity. The number of electrons

transferred (ΔN) also determine the electron donation power of inhibitor molecules[53]. ΔN values of molecules in the order of kaempferol (1.43) > bafoudiosbulbin A (1.057) >diosgenin (1.05). All the values are less than 3.6, which leads to efficient metal corrosion inhibition.

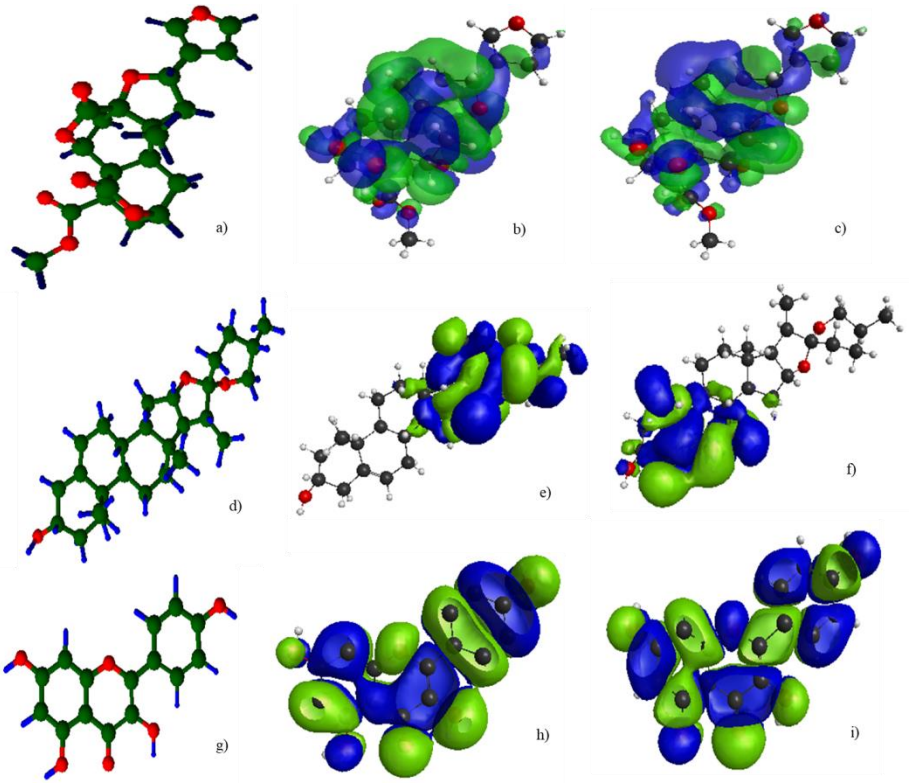

Fig. 8.15: a) Optimized geometry, b) HOMO and c) LUMO of bafoudiosbulbin A; d) Optimized geometry, e) HOMO and f) LUMO of diosgenin; g) Optimized geometry, h) HOMO and i) LUMO of kaempferol

Table 8.8: Quantum mechanical parameters (in eV) of bafoudiosbulbin A (I), diosgenin (II) and kaempferol (III)

Molecule	E_{HOMO}	E_{LUMO}	ΔE	I	A	μ	χ	η	ΔN
I	-4.118	1.053	5.171	4.118	-1.053	-1.53	1.53	2.58	1.057
II	-4.112	1.137	5.249	4.112	-1.137	-1.48	1.48	2.62	1.050
III	-3.102	1.053	4.155	3.102	-1.053	-1.02	1.02	2.07	1.438

Statistical analysis

❖ ***Optimization of factors for inhibition efficiency (IE%)***

Experimental results disclosed three predominant factors, i.e., temperature, DBE concentration, and acid concentration which affected the corrosion inhibition efficiency.

So they opted as independent factors for statistical analysis. Weight loss studies revealed that the corrosion rate was improved in H_2SO_4 than in HCl medium. So, HCl concentration was selected as an acid concentration. The structure of the design and the three levels of BBD are shown in Table 8.9, including experimental results and predicted response. A total of 15 experimental runs were performed in it. To identify the proper combination of the three factors used in this analysis for obtaining the highest efficiency, RSM was employed as an optimization technique. The regression model satisfying the test factors and the inhibition efficiency is given in equation (58).

$$IE = 379 - 1.36\ X_1 + 7.3\ X_2 - 52.0\ X_3 + 0.0011\ X_1^2 - 0.350\ X_2^2 - 14.35\ X_3^2 + 0.0060\ X_1X_2 + 0.217\ X_1X_3 - 0.83\ X_2X_3 \quad (58)$$

This full quadratic model was used to perform analysis of variance (ANOVA)[200]. ANOVA results with a significance level of 95% are demonstrated in Table 8.10. P-value is the most remarkable parameter in this Table. P-value predicts whether the impact of a factor on response significant or not. The degree of essentialness (α) was chosen to be 0.05. Results showed that P-value was lower than 0.05 for all the linear and one of the square terms. It explained that temperature, DBE concentration, HCl concentration and square term of HCl concentration were significant factors. The same results were obtained in Pareto chart (Fig. 8.16). It illustrates that DBE concentration has the most appreciable impact on the inhibition efficiency. Squared terms of temperature and DBE concentration were observed to influence the inhibition efficiency (IE%) negatively. Similarly, the interaction terms X_1X_3, X_1X_2 and X_2X_3 did not impact inhibition efficiency.

The suitable fit model for experimental results verified by the closeness of R^2 and R^2(adj) value to unity. Here, the R^2 and R^2(adj) values were 0.9888 and 0.9686,

respectively, suggesting the best-fit regression model for experimental values. Therefore, the results can be evaluated by this full quadratic model.

Table 8.9: Experimental and predicted IE% from weight loss measurements and BBD

Run order	Actual level of factors			IE%		Residual
	X_1	X_2	X_3	Experimental	Predicted	
1	323	3	1	75.51	80.29	4.7869
2	323	1	1.5	53.06	56.97	3.9139
3	313	5	1	89.87	95.64	5.7769
4	333	3	1.5	60.17	67.21	7.0409
5	323	1	0.5	63.48	68.41	4.9329
6	323	3	1	75.51	80.29	4.7869
7	333	5	1	84.28	87.59	3.3189
8	333	3	0.5	72.08	78.13	6.0599
9	323	3	1	75.51	80.29	4.7869
10	313	3	0.5	86.06	88.59	2.5379
11	323	5	0.5	89.65	95.30	5.6549
12	313	1	1	64.39	70.65	6.2649
13	313	3	1.5	69.81	73.32	3.5189
14	333	1	1	58.32	62.12	3.8069
15	323	5	1.5	75.9	80.54	4.6459

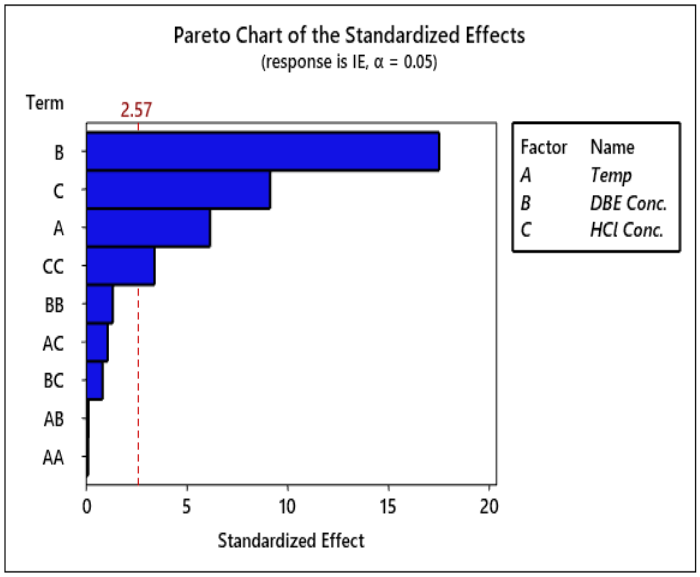

Fig. 8.16: Pareto chart of the standardized effects of mild steel

Main effects plots indicate the influence of tested factors on the response. Fig. 8.17 elucidates the main effects plots for the fitted means of inhibition efficiency. It revealed that the highest inhibition efficiency was found for 5 v/v% concentration of

DBE at a working temperature of 313 K at 0.5 M concentration of HCl. Kinetic energy of DBE molecules and the speed of bombardment between the molecules increases at higher temperatures. This trend prevents and destroys the formation of adsorbed film by inhibitors on the metal surface. So, at elevated temperatures, inhibition efficiency decreases.

Table 8.10: Analysis of variance for corrosion inhibition efficiency

Source	DF	Adj SS	Adj MS	F-Value	P-Value
Model	9	1819.69	202.19	49.05	0.000
Linear	3	1759.16	586.39	142.27	0.000
Temp	1	155.58	155.58	37.75	0.002
DBE Conc.	1	1261.28	1261.28	306.01	0.000
HCl Conc.	1	342.30	342.30	83.05	0.000
Square	3	52.99	17.66	4.29	0.076
Temp*Temp	1	0.04	0.04	0.01	0.924
DBE Conc.*DBE Conc.	1	7.25	7.25	1.76	0.242
HCl Conc.*HCl Conc.	1	47.49	47.49	11.52	0.019
2-Way Interaction	3	7.54	2.51	0.61	0.637
Temp*DBE Conc.	1	0.06	0.06	0.01	0.910
Temp*HCl Conc.	1	4.71	4.71	1.14	0.334
DBE Conc.*HCl Conc.	1	2.77	2.77	0.67	0.449
Error	5	20.61	4.12		
Lack-of-Fit	3	20.61	6.87	*	*
Pure Error	2	0.00	0.00		
Total	14	1840.30			

DF: degrees of freedom, Adj SS: adjusted sum of squares, Adj MS: adjusted mean of squares, F: Fischer's F-test value, P: probability

Similarly, when HCl concentration raised from 0.5 M to 1.5 M, inhibition efficiency decreased. In contrast, inhibition power was directly proportional to DBE concentration. The corrosion rate was tremendously boosted in the absence of an inhibitor and dropped when the inhibitor was present. Thus, the adsorption of inhibitor molecules enhances, and efficiency also increases.

Accuracy of this full quadratic equation (58) can be interpreted from residual plots given in Fig. 8.18. It consists of four different plots. Normal probability plot observed that this full quadratic equation for inhibition efficiency was fixed to the normal distribution. It indicated that the obtained model required no response transformation.

Versus fits plot revealed that the range of variance of observations was constant for all responses. Histogram of residuals pointed out that the residuals were allocated symmetrically for all frequencies. The fine uniform shape of this histogram validates the accuracy of the regression model. Versus order plot exhibited that points of observed runs were scattered randomly, keeping the fixed area of residuals which substantiated the model's precision. In conclusion, all four plots confirmed the accuracy of the model to demonstrate the influence of factors on the inhibition efficiency.

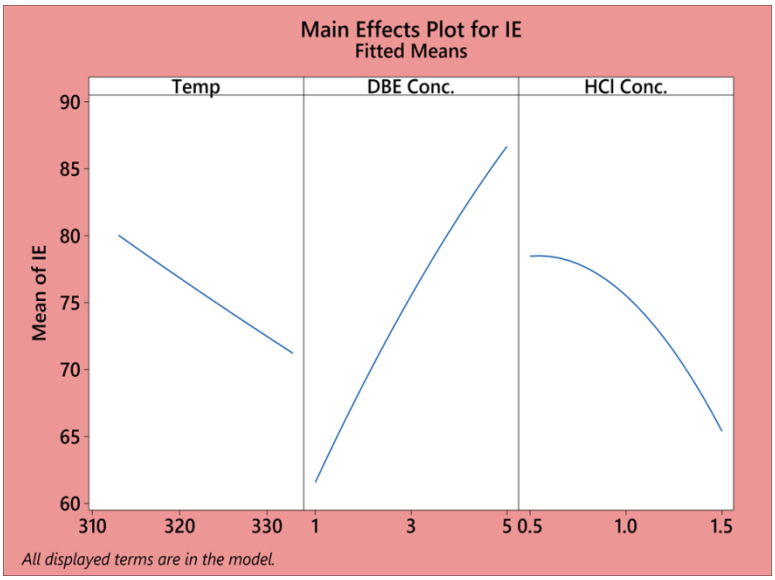

Fig. 8.17: Main effects plots for inhibition efficiency of mild steel in HCl medium

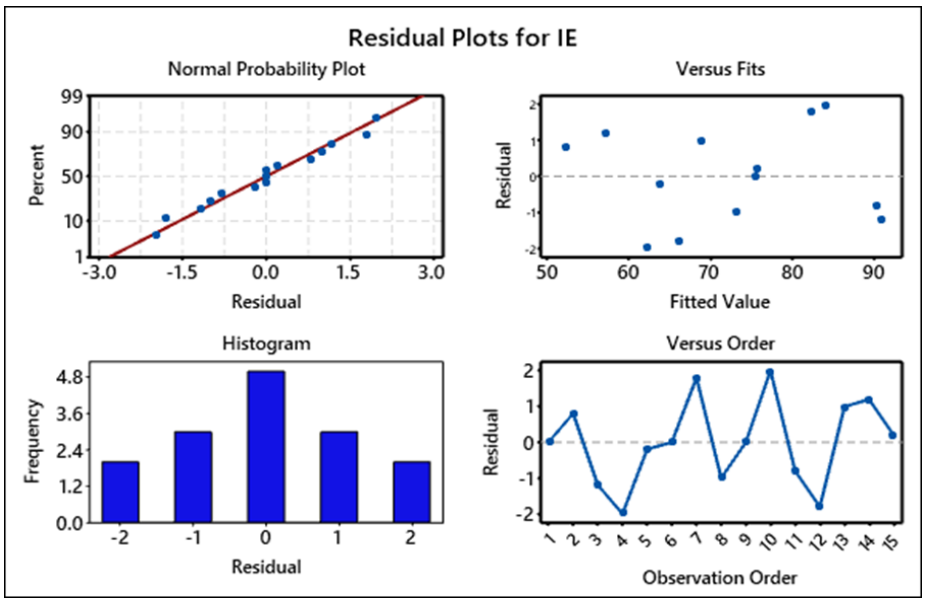

Fig. 8.18: Residual plots for inhibition efficiency

Contours and 3-D surface plots describe the inter-dependence of the tested factors on IE% and are shown in Fig. 8.19. It was realized that IE% goes up when DBE concentration rises for a given temperature. But, inhibition efficiency and temperature have an inverse relationship. This inclination can be attributed to the physical adsorption of DBE molecules on the mild steel surface. Because, as temperature rises, the rate of desorption increases. Similarly, inhibition efficiency and HCl concentration are inversely proportional.

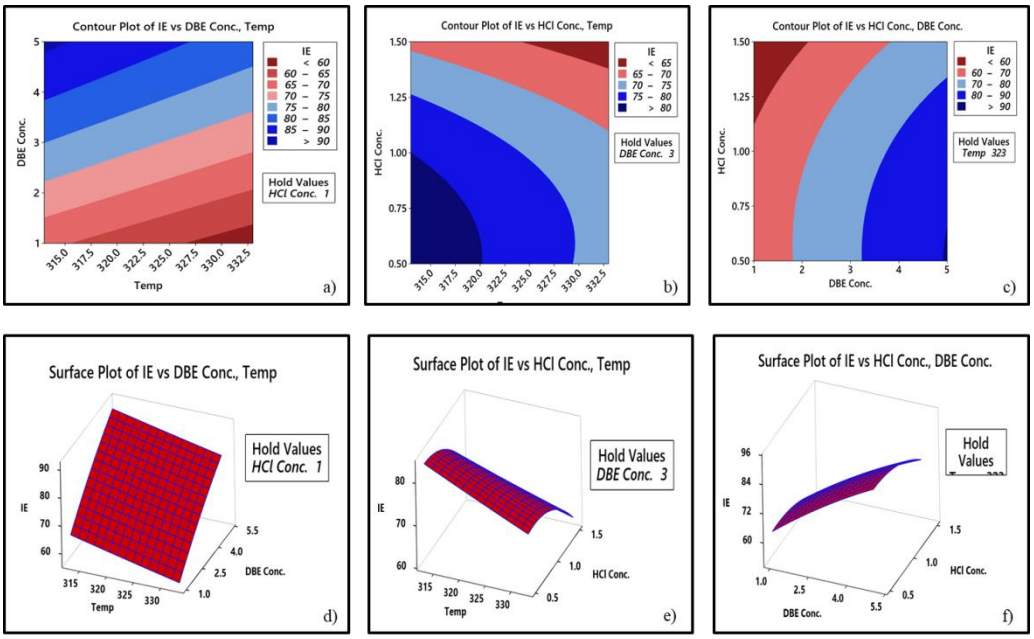

Fig. 8.19: a, b & c) Contours and d, e & f) 3-D surface plots for inhibition efficiency

❖ ***Response optimization***

A well-organized numerical model in quadratic equation (58) was applied to optimize the independent factors such as temperature, DBE concentration, and HCl concentration to achieve the maximum IE%. Desirability function method was employed for optimization. Response optimization plot for IE% is exhibited in Fig. 8.20. The optimum conditions for best IE% were temperature (313 K), DBE concentration (5 v/v %), and HCl concentration (0.5 M) and the corresponding predicted IE% was

95.9337%, as shown in Fig. 8.20. This optimization technique helped to verify the recurrence of the experimental outcomes and approve the validity of the model.

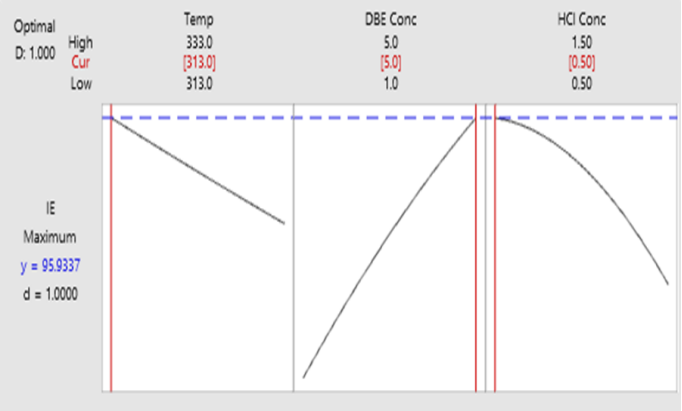

Fig. 8.20: Response optimization plot for inhibition efficiency

Conclusions

- DBE was found to be an efficient corrosion inhibitor for mild steel corrosion exposed in 1 M HCl and 0.5 M H_2SO_4.
- Weight loss studies exhibited that increasing the DBE concentration leads to an increase in inhibition efficiency. It is due to the adsorption of DBE molecules on the metal surface. In comparison, at higher temperatures, inhibition potential reduces due to the desorption of the adsorbed layer.
- Maximum inhibition capacity of DBE in 1 M HCl and 0.5 M H_2SO_4 was estimated as 91.78% and 86.93%, respectively.
- Langmuir adsorption isotherm was identified as good adsorption of DBE molecules on mild steel surface in HCl medium, while Frumkin was the best isotherm in the H_2SO_4 medium.
- Surface morphology of mild steel was studied by SEM, which supplemented strong evidence for forming a protective film on mild steel with DBE in acidic environments.

- Quantum mechanical calculations of three important phytochemicals were also supported the good inhibition efficiency of DBE.
- Response surface methodology was applied to validate the interdependence between DBE concentration, HCl concentration, and temperature on the inhibition efficiency by designing BBD. Regression equation could describe the results obtained from experiments in good agreement.

CHAPTER 9

SCHIFF BASES DERIVED FROM PYRIDINE CARBONYL COMPOUNDS: SYNTHETIC MICROBIAL INDUCED CORROSION INHIBITOR FOR MILD STEEL IN MARINE ENVIRONMENT

This chapter deals with microbial induced corrosion (MIC) behaviour of four synthetic inhibitors derived from pyridine carbaldehyde and acetyl pyridine on mild steel in the artificial seawater medium, 1) *N*-hydroxy-1-(pyridin-2-yl)methanimine, NHP2M 2) *N*-hydroxy-1-(pyridin-3-yl)methanimine, NHP3M 3) (E)-2-(1-(2-phenylhydrazono) ethyl)pyridine, 2PHEP and 4) (E)-2-(1-triazylidineethyl)pyridine, 2TAEP. It includes physicochemical and electrochemical techniques of these Schiff bases to monitor MIC.

Results and discussions

Identification of corrosion causing bacterium

Microorganisms inducing corrosion were selectively enriched by repeated subculturing in artificial seawater media. Streak plating techniques is used to obtain pure cultures of bacterial[101]. Individual isolates were re-tested to confirm the corrosion-inducing property of the strain. The cultures retaining the corrosion-inducing properties were systematically named and stored for further studies. The isolate labelled MICBT7 has shown significant metal deterioration activity on liquid media and agar medium. So, the strain MICBT7 was chosen as the active colony for corrosion enhancement in the present study. Table 9.1 gives the morphological characteristics of the selected bacterial isolate MICBT7.

❖ ***Polymerase Chain Reaction (PCR)***

PCR-based rDNA amplification and sequencing[201] were used for the identification of bacterial isolate MICBT7. The whole genomic DNA of the isolated colony was isolated using the phenol-chloroform method. Quantity and purity of DNA isolate was accessed by 260/280 spectrophotometric analysis. Resulting DNA was

amplified using a pair of universal primers for rDNA in a PCR reaction. DNA amplification was confirmed by agarose gel electrophoresis and visualization in a UV transilluminator[202]. Sequencing of the resulting culture showed the possibility of mixed culture of related bacteria in the isolate. Further steps are needed to separate and obtain pure cultures of the mixed isolate.

Table 9.1: Morphological characteristics of bacterial isolate MICBT7

Variable	Characteristics
Colony shape	Round
Colony size	Small
Edge	Entire
Surface	Smooth
Opacity	Opaque
Elevation	Raised
Colour	Light brown
Motility	Nonmotile
Cell shape	Rod
Cell size	Small

Weight loss measurements

Corrosion rate (υ) and inhibition efficiency (η%) of mild steel in control, biotic and inhibitor (100 ppm) systems for 21 days are summarized in Table 9.2. It was noted that the corrosion rate of 2.3620 mm/yr in the control system after 21 days, whereas, in the biotic system, it was 2.8207 mm/yr. The increase in corrosion rate for the latter may be due to forming a thick layer of biofilm on the metal surface[203]. It increased microbial induced corrosion rates of mild steel and changed cathodic or anodic reactions by creating an electrolytic environment. It has come to the knowledge that in the presence of Schiff base inhibitors, lower corrosion rates were identified, and a significant decrease in corrosion rate was noted with NHP3M compared to all other Schiff base inhibitors. On comparing the corrosion rate of the mild steel immersed in the control and biotic systems, all the four Schiff bases retarded the MIC rate of mild steel considerably. The decreasing order of inhibition efficiency of Schiff bases was NHP3M > 2PHEP >

NHP2M > 2TAEP. NHP3M attained a maximum inhibition efficiency of 60.3% at 100 ppm concentration. NHP3M and 2PHEP showed inhibition efficiency above 50%, while NHP2M and 2TAEP were achieved about 30% inhibition efficiency.

Appreciable efficiency of these Schiff bases may be ascribed to their molecular structure[204]. Presence of heteroatoms, aromatic ring systems, the possibility of forming intermolecular hydrogen bonding and intramolecular hydrogen bonding leads to effective binding of inhibitor molecules on the mild steel surface. Such a binding interaction may disturb the development of microbial growth. This hindrance to biofilm formation by adsorbing on the metal surface makes Schiff bases potent corrosion inhibitors. Inhibition efficiency of NHP2M and NHP3M can be attributed to hydrogen bonding[92]. As NHP3M molecules prefer intermolecular hydrogen bonding, the molecular assembly can sufficiently adsorb the mild steel surface. It may cause a noticeable decrease in the exposed surface area of the metal on which microorganisms can attack to form biofilm. NHP2M molecules interact with intramolecular hydrogen bonding. So NHP2M molecules can bind the metal surface separately, which means no interaction between the adsorbed molecules. It may cause the attack of microorganisms on the active sites of the metal surface, which are not blocking with inhibitors. So, the former reduces the MIC rate significantly than the latter.

It was reported that 2PHEP possessed a perfect planar geometry[129]. The high inhibition efficiency of 2PHEP over 2TAEP can be ascribed to the presence of two aromatic rings in the former. It enhances pi-electron cloud and facilitates a strong adhesion to the metallic surface, which blocks active sites on the mild steel surface from the biofilm formation by microbes. Due to the absence of electron-rich centres other than azomethine linkage on 2TAEP behaved as a weak corrosion inhibitor.

From Table 9.2, it was apparent that all the four Schiff bases acted as inhibitors preventing biofilm formation and successfully reducing MIC rate. The corrosion rate of Schiff bases was increased to the maximum of about 1.6393 mm/year, which was lower than control (2.3620 mm/year) and biotic system (2.8207 mm/year). So, Schiff bases inhibited bacterial growth on the mild steel surface by adsorbing on the metal surface. It was proved that these Schiff bases could form a protective layer on the metal surface by the phenomenon of adsorption.

Table 9.2: Weight loss measurements of mild steel in control, biotic and Schiff base inhibitor systems

System	Corrosion rate (υ) (mm/yr)	Inhibition efficiency (η%)
Control	2.3620	-
Biotic	2.8207	-
NHP2M	1.6306	30.9%
NHP3M	0.9385	60.3%
2PHEP	1.1163	52.7%
2TAEP	1.6393	30.5%

Electrochemical impedance spectroscopy

Nyquist plots for the mild steel containing six biocorrosion systems for 21 days of incubation are exhibited in Fig. 9.1a). The corresponding impedance parameters such as charge transfer resistance (R_{ct}) and double-layer capacitance (C_{dl}) are shown in Table 9.3. Nyquist plot was seen in a semicircular shape for Schiff base inhibitor systems whereas, in the biotic systems, its curve was weakened at high-frequency values. This depression in the curve may occur due to the formation of a biofilm on the mild steel surface[205]. Similarly, Nyquist plot for the control system also showed depressed semicircle and lower R_{ct} (40.79 Ω cm^2) values than Schiff base inhibitor systems (Table 9.3), which recommends the localized corrosion on a metal surface. It has been realized that R_{ct} value was lower (29.18 Ω cm^2) for the biotic system than the control system, suggesting that microorganisms can form thick film on the mild steel surface and

enhance the corrosion process[206]. The higher R_{ct} values of the Schiff base inhibitor system were ascribed to the adsorption of inhibitor molecules and thus restriction of cathodic/anodic reaction on the mild steel surface.

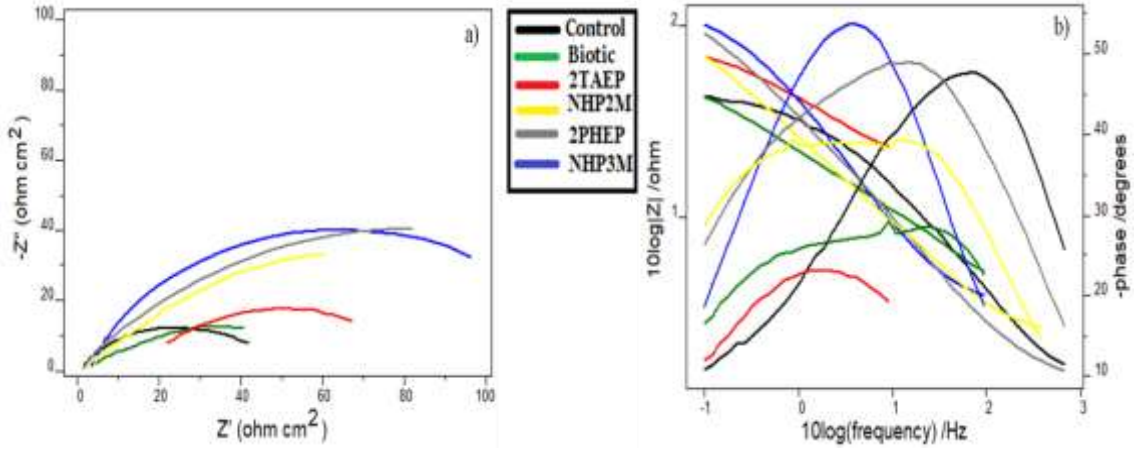

Fig. 9.1: a) Nyquist plots b) Bode plots of mild steel in control, biotic and Schiff base inhibitor systems

Table 9.3: Impedance parameters for mild steel in control, biotic and Schiff base inhibitor systems

System	C_{dl} (μFcm^{-2})	R_{ct} (Ω	η_{EIS}%
Control	0.006991	40.79	-
Biotic	0.009811	29.18	-
NHP2M	0.006447	62.25	34.47
NHP3M	0.004483	89.68	54.52
2PHEP	0.006021	80.82	49.52
2TAEP	0.006344	61.42	33.58

The lower C_{dl} values obtained for Schiff base inhibitor systems can be attributed to reducing local dielectric constant or increment in the electrical double layer thickness. This action may be due to the adsorption of these compounds at the metal–solution interface.

The Schiff base inhibitor systems NHP3M exhibited the highest corrosion inhibition efficiency, i.e. 54.52% at 100 ppm concentration. The decreasing order of inhibition efficiency of Schiff base inhibitor systems as follows: NHP3M > 2PHEP >

NHP2M > 2TAEP. This result was going along with data obtained in weight loss measurements.

Fig. 9.1 b) shows a Bode plot for the control, biotic and Schiff base inhibitor systems. It was observed that a sharp drop in |Z| values at the low-frequency region for biotic and control systems, implying the accumulation of microorganisms and development of a biofilm on the mild steel surface[207]. In contrast, Bode plots for Schiff base inhibitor systems |Z| values were tremendously higher at the low-frequency region even though there was no difference in the shapes of the Bode plots, inferring MIC inhibition capacity. The impedance spectra for all the systems were fitted with an equivalent circuit consisting of a solution resistance (R_s) in series with a parallel combination of charge transfer resistance (R_p) and double-layer capacitance (C_{dl}) as represented in Fig.1.7. The double-layer capacitance was replaced by a constant phase element because the roughness of a surface or biofilm deformity on the metal surface caused the dispersion effects. To summarize, electrochemical studies suggest the inhibition effect of the Schiff base inhibitors for the microorganism caused MIC of mild steel.

MIC inhibition of these Schiff base inhibitors can be explained as they appreciably reduced the contribution of microorganisms in the corrosion process. The studied Schiff base inhibitors minimized the growth of microorganisms and biofilm development by forming an adsorption layer that prevents the colonization of microbes on the metal surface. The protective shielding offered by Schiff bases may be attributed to adsorbed intermediates formed on the mild steel surface. Sini C V et al. investigated the inhibition efficiency of *N*-hydroxy-1-(pyridin-2-yl)methanimine and *N*-hydroxy-1-(pyridin-3-yl)methanimine on carbon steel corrosion in 1 M HCl and 0.5 M H_2SO_4 media[92]. Bincy M Paulson et al. studied the corrosion inhibition behaviour of (E)-2-(1-

(2-phenylhydrazono)ethyl)pyridine and (E)-2-(1-triazylidineethyl)pyridine on mild steel in acidic environments[129]. Their findings recommended that these compounds acted as suitable metal corrosion inhibitors in acid solutions due to the chemical and physical adsorption of the compounds on the metal surface.

Potentiodynamic polarization studies

Fig. 9.2 reveals linear polarization and Tafel plots, and Table 9.4 presents corresponding potentiodynamic polarization parameters of mild steel in control, biotic and Schiff base inhibitor systems after 21 days of incubation. Fig. 9.2 b) displayed that the cathodic peak was changed to lower potential, and cathodic current density was increased (260 µA/cm^2) in the biotic system, suggesting the biofilm formation on the metal surface by microorganism.

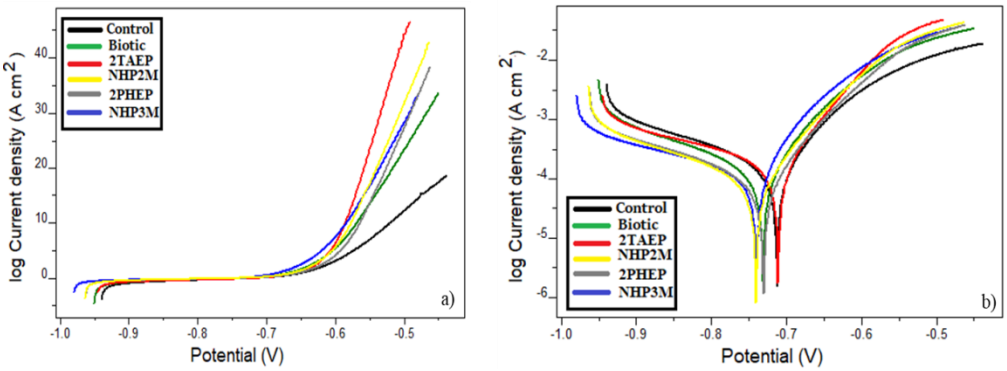

Fig. 9.2: a) Linear polarization and b) Tafel plots in control, biotic and Schiff base inhibitor systems

It has been observed that the corrosion current density for the control system (208 µA/cm^2) was lower when compared to the biotic system. Accumulation of microbes leads to high oxygen diffusion, which facilitates high i_{corr} in the biotic system[208]. At the same time, in the presence of Schiff base inhibitors, i_{corr} values were significantly smaller than control and biotic systems, which can be ascribed to absorption of these compounds on the metal surface.

Table 9.4: Potentiodynamic polarization parameters for control, biotic and Schiff base inhibitor systems

System	Tafel data					Polarization data	
	$-E_{corr}$ (mV)	i_{corr} ($\mu A/cm^2$)	b_a (mV/dec)	$-b_c$ (mV/dec)	η_{pol}%	R_p (Ω)	η_{Rp}%
Control	773.0	208	124	235	-	169.6	-
Biotic	761.8	260	150	256	-	158.2	-
NHP2M	736.3	121	77	224	41.82	295.4	42.58
NHP3M	714.6	100	121	244	51.92	374.2	54.67
2PHEP	746.3	115	95	217	44.71	310.0	45.29
2TAEP	759.7	125	96	234	39.90	281.2	39.68

It has been noted that the corrosion potential (E_{corr}) for the Schiff base inhibitor system was shifted to a positive potential indicating less susception. This tendency revealed a better corrosion resistance on the metal surface. Herein, the change in corrosion potential was within 85 mV from the control system. So, these compounds were acted as a mixed-type inhibitor. Anodic and cathodic slope (b_a and b_c) values implied that Schiff base inhibitors affected cathodic and anodic branches of the Tafel plot and acted as a mixed type inhibitor. Previous studies reported that inhibition behaviour of these Schiff bases was mixed-type in acidic environments. From Table 9.4, it has been summarized that the polarization resistance (R_p) for the biotic system was dramatically lowered (158.2 Ω cm^2). In contrast, it was very much higher for Schiff bases and reached 374.2 Ω cm^2 for NHP3M. The order of R_p values for Schiff bases was NHP3M > 2PHEP > NHP2M > 2TAEP. Hence, it was evident that NHP3M functioned as the best MIC inhibitor in the saline medium. Inhibition efficiency obtained from Tafel and linear polarization data was found to be in good agreement.

In vitro antibacterial effects of inhibitors

In *vitro* antibacterial effects of the Schiff base inhibitors NHP2M, NHP3M, 2PHEP and 2TAEP against *Escherichia coli* were performed at 500 $\mu g disc^{-1}$ in DMSO. Tetracycline was used as a standard antibiotic to verify the activity of Schiff base inhibitors. Table 9.5 and Fig. 9.3 exhibits the antibacterial effects of the Schiff base

inhibitors. Diameter of the zone of inhibition shown by tetracycline in *E. coli* is 20 mm. All the Schiff base inhibitors exhibited a zone of inhibition except NHP3M. 2TAEP showed a maximum zone of inhibition of about 19 mm. The order of antibacterial effect was NHP3M < NHP2M < 2PHEP < 2TAEP.

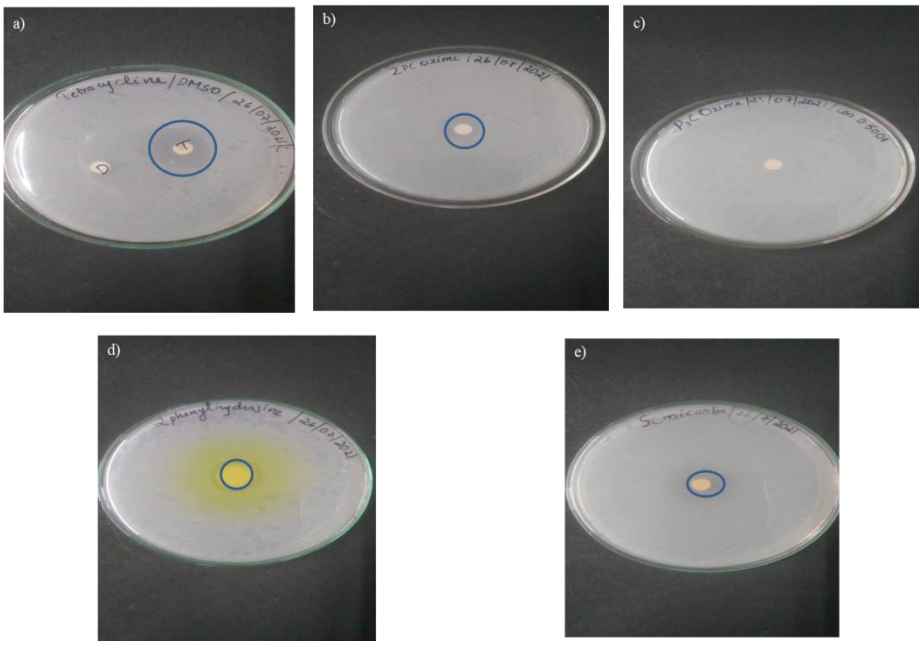

Fig. 9.3: Antibacterial effects of a) Tetracycline b) NHP2M c) NHP3M d) 2PHEP e) 2TAEP against *E. coli* at 500 µgdisc^{-1} in DMSO

Table 9.5: Antibacterial effects of the Schiff base inhibitors at 500 µgdisc^{-1} in DMSO against *Escherichia coli*

Inhibitor	Zone of inhibition (mm)
NHP2M	15
NHP3M	No zone of inhibition
2PHEP	18
2TAEP	19
Tetracycline	20

It has been noted that NHP3M was the inhibitor with the highest MIC inhibition efficiency. But it is not an antibacterial agent. So, the proposed mechanism of inhibition is that Schiff base molecules destabilize biofilm formation by adsorption of Schiff base molecules on the mild steel surface, not by killing the microorganism. 2TAEP was found to be the inhibitor with the comparatively highest antibacterial activity. But, it was not a suitable MIC inhibitor. In this case, the binding interaction of 2TAEP with the

metal surface was not sufficient to disturb the biofilm growth formed on the metal surface. This result revealed the relevance of these Schiff base inhibitors in inhibiting MIC rather than toxic and harmful antibacterial agents. So, the selected Schiff base inhibitors can be applied as MIC inhibitors for mild steel in the marine environment.

Mechanism of MIC inhibition

Mechanism of MIC inhibition by Schiff base inhibitors can be established by surface analysis, microscopic surface analysis and UV-Visible spectroscopy.

❖ ***Surface analysis***

FTIR spectroscopy

FTIR spectroscopy of the corrosion products furnishes an idea about the interaction of Schiff base inhibitors on the mild steel exposed in the biotic medium. Fig. 9.4 gives the FTIR spectra of corrosion products obtained from the mild steel surface exposed to control, biotic and Schiff base inhibitor systems at the end of 21 days of the incubation period. The broad peak was observed at 3200–3400 cm^{-1} for NHP3M and 2PHEP systems due to -OH and -NH stretching vibrations of hydroxyl groups and aromatic amines deposited on the mild steel surface, respectively. The distinguishing peak observed for Schiff base inhibitor systems was at 1347 cm^{-1}, attributed to C-N stretching vibration. This stretching frequency confirmed the adsorption of the imine group on the mild steel surface. These intense peaks were absent in the spectrum of control and biotic systems.

These noticeable changes in the IR spectra give the mechanism of MIC inhibition by Schiff base molecules. The presence of Schiff base inhibitors as corrosion products on the mild steel surface may cause interaction of Schiff base molecules with the biofilm formed on the metal surface. Schiff base molecules may be locked on the biofilm and cause destabilization of biofilm. Schiff base inhibitors may act as destabilizing agents for

biofilm growth by adsorbing on the metal surface. FTIR revealed the role of Schiff base molecules in inhibiting microbially influenced corrosion.

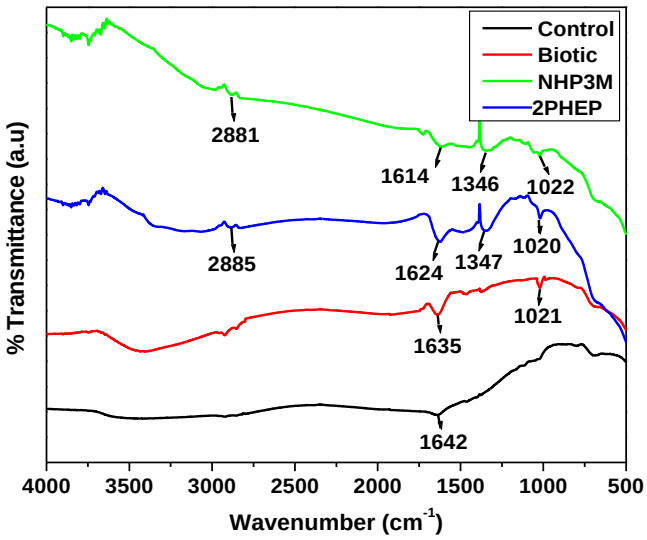

Fig. 9.4: FTIR spectra of corrosion products formed on mild steel surfaces of control, biotic and inhibitor systems

X-ray diffraction spectroscopy (XRD)

Fig. 9.5 shows the XRD spectra of the mild steel surface immersed in control, biotic and inhibitor systems after 21 days of incubation. High-intensity peaks observed in all systems at 44.7º, 65.1º and 82.3º indicated Fe (0) metal[209]. Peak at 35.1º in the control and biotic systems represented Fe_2O_3 formed as corrosion products[210]. In the presence of Schiff base inhibitors, the intensity of peak at 35.1º was decreased due to the prevention of the bacterial biofilm formation on the mild steel surface. In the biotic system, another corrosion product FeO was detected at 42.7º with low intensity. Similarly, in the 2TAEP system, significantly lower intensity of iron oxide peak was observed, which indicated relatively lower inhibition efficiency of 2TAEP than all other inhibitor systems.

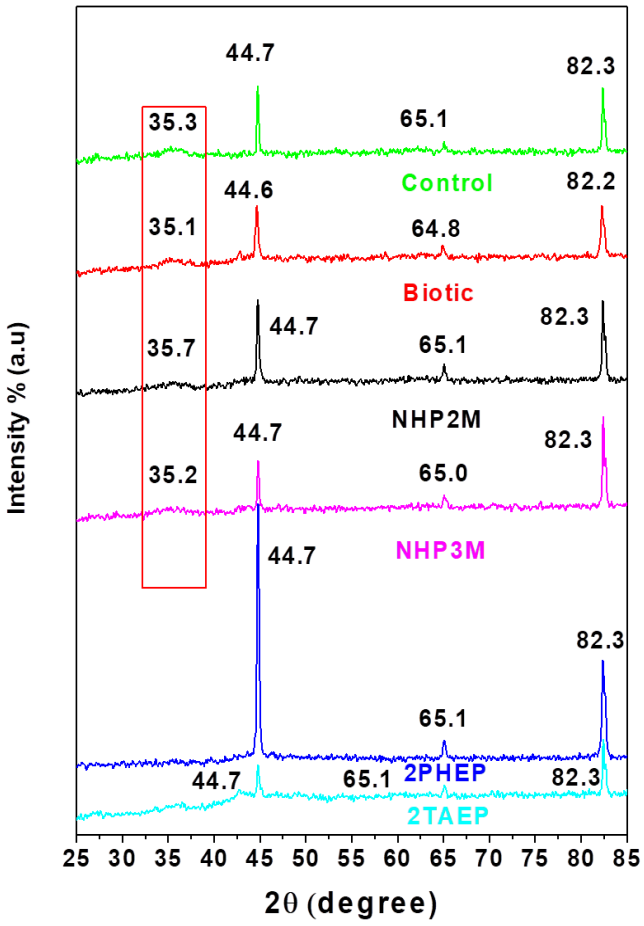

Fig. 9.5: XRD spectra of mild steel surface immersed in control, biotic and inhibitor systems

❖ ***Microscopic surface analysis***

Optical microscopic images[211] of the mild steel coupons exposed in control, biotic and inhibitor systems after 21 days are exhibited in Fig. 9.6. The more hydrated ferric oxide was present on the mild steel coupon exposed in the biotic medium than other metal coupons. It is established that the mild steel coupon exposed in the biotic medium has enhanced corrosion due to the stable and quick biofilm formation on the metal surface. Biofilm causes metal destruction gradually. In comparison, the mild steel coupon exposed in inhibitor systems like NHP3M has only little oxide content. Mild steel exposed in 2TAEP were found to be more corrosive compared to all other inhibitors. Mild steel coupons exposed in 2PHEP and NHP2M

were observed as a better MIC inhibitor than 2TAEP. Thus the capacity of inhibitor systems to prevent the MIC in the artificial sea water medium was again verified and successfully analyzed by this method.

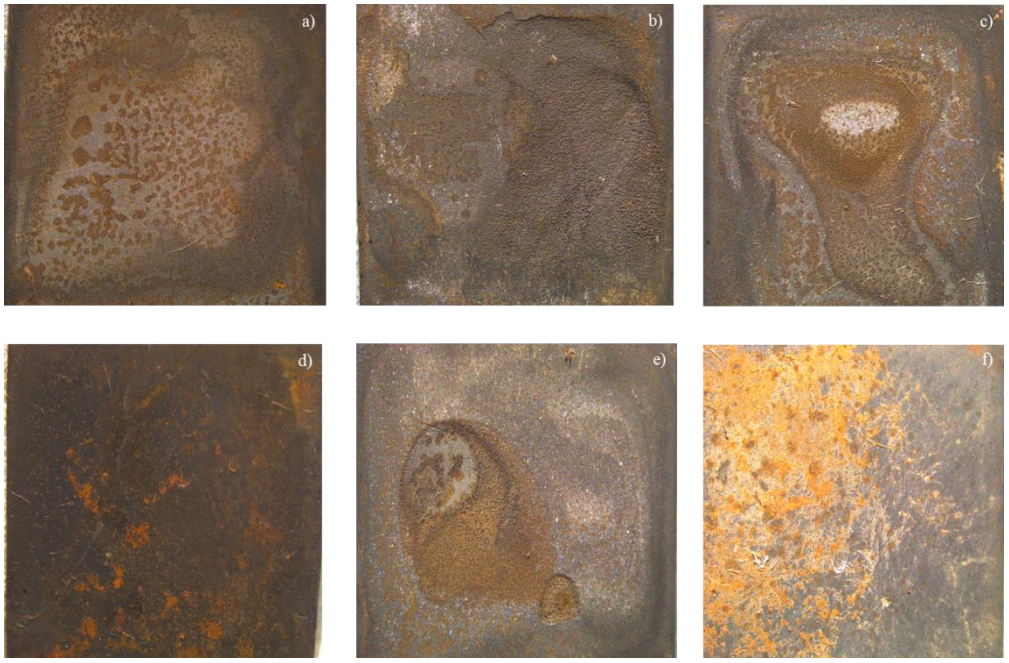

Fig. 9.6: Optical micrographs of mild steel coupons exposed in a) control b) biotic c) NHP2M d) NHP3M e) 2PHEP f) 2TAEP

❖ ***UV-Visible spectroscopy***

The mechanism of MIC inhibition can be further interpreted by UV-Visible spectroscopy. The affinity of Schiff base inhibitor towards metal surface can be confirmed by taking UV-Visible spectra of inhibitor and ferric salt solutions individually and combined. Almost all ferrous ions will convert into ferric ions in the artificial sea water medium (pH=7.5 ± 0.5). So the interaction between Schiff base inhibitor and mild steel metal can be studied by employing the ferric salt solution and inhibitor.

Fig. 9.7 shows UV-Visible spectra of 2PHEP, $FeCl_3$ and an equal mixture of 2PHEP and $FeCl_3$. 2PHEP shows 3 distinct peaks at 407 nm, 316.5 nm and 265.5 nm, which can be attributed to $n \rightarrow \pi^*$ (R-band), $\pi \rightarrow \pi^*$(benzenoid band) and $\pi \rightarrow \pi^*$(K band) transitions respectively. After mixing 2PHEP with ferric salt solution, there is a notable difference in absorbance values for the $FeCl_3$-2PHEP spectrum from the individual

spectra. The peak at 407 nm due to 2PHEP is shifted to 402.5 nm. The value of absorbance for the $FeCl_3$-2PHEP mixture was found to be decreased. This blue shift can be ascribed to the transfer/adsorption of 2PHEP molecules from the medium to the mild steel surface. A significant decrease in intensity observed at 402.5 nm for $FeCl_3$-2PHEP mixture clearly show strong binding interaction between 2PHEP molecules and $FeCl_3$ due to quenching. The substantial changes in the characteristics of the UV-Visible spectra pointed out the possible complexation between Schiff base inhibitor and metal.

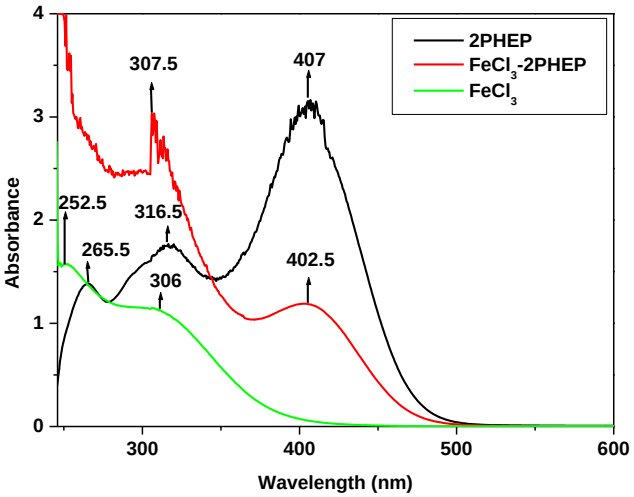

Fig. 9.7: UV-Visible spectra of 2PHEP, $FeCl_3$ and 1:1 mixture of 2PHEP and $FeCl_3$

Conclusions

- Schiff base inhibitors derived from pyridine carbaldehyde and acetyl pyridine 1) *N*-hydroxy-1-(pyridin-2-yl)methanimine, NHP2M 2) *N*-hydroxy-1-(pyridin-3-yl)methanimine, NHP3M 3) (E)-2-(1-(2-phenylhydrazono)ethyl)pyridine, 2PHEP and 4) (E)-2-(1-triazylidineethyl)pyridine, 2TAEP were applied as MIC inhibitor on mild steel in the artificial seawater medium.

- All the Schiff base inhibitors showed appreciable inhibition efficiency. The decreasing order of inhibition efficiency of Schiff base inhibitor systems as follows: NHP3M > 2PHEP > NHP2M > 2TAEP.
- Isolation and identification of the resulting culture showed the possibility of mixed culture of related bacteria in the isolate from original seawater.
- Impedance parameters were going along with data obtained in weight loss measurements.
- Shifting of corrosion potential (E_{corr}) for the Schiff base inhibitor system to a positive potential revealed a better corrosion resistance on the metal surface.
- Potentiodynamic polarization studies revealed that Schiff base inhibitors were acted as a mixed-type inhibitor.
- In vitro antibactereial effects of inhibitors showed that the order of antibacterial effect was NHP3M < NHP2M < 2PHEP < 2TAEP. So, the mechanism of inhibition was proposed that Schiff base molecules destabilize biofilm formation by adsorption of Schiff base molecules on the mild steel surface, not by killing the microorganism.
- Proposed mechanism was established by surface analysis like XRD and FTIR of corrosion products. XRD spectrum of metal dipped in the biotic system showed an intense peak of Fe_2O_3, which represents increased corrosion by the influence of microorganisms. FTIR spectra of corrosion products of inhibitor systems revealed that Schiff bases could act as destabilizing agents for biofilm formation.
- Microscopic surface analysis of metal surfaces exposed in Schiff base inhibitor systems showed the protective nature of inhibitors.

- The affinity of Schiff base inhibitor towards metal surface proved by UV-Visible spectra. Decrease in intensity for $FeCl_3$-2PHEP mixture showed strong binding interaction between 2PHEP molecules and $FeCl_3$.

SUMMARY

This thesis incorporated the preparation, phytochemical screening, and FTIR spectroscopy of seven natural plant extracts as corrosion inhibitors for mild steel in acid media. *Ixora coccinea* extract (ICE), *Croton persimilis* extract (CPE), *Tinospora cordifolia* extract (TCE), *Garcinia cambogia* extract (GCE), *Clerodendrum infortunatum* extract (CILE and CIRE) and *Dioscorea bulbifera* extract (DBE) were the plant extracts applied as green corrosion inhibitors. Phytochemical screening of all the extracts showed the same results as in the literature review. Characterization of the extracts was carried out using FTIR spectroscopy.

Corrosion inhibition efficiency of these seven extracts was screened on mild steel in 1.0 M HCl and 0.5 M H_2SO_4 using weight loss measurements and electrochemical studies such as electrochemical impedance spectroscopy, potentiodynamic polarization and electrochemical noise measurements. Evaluation of the adsorption phenomenon of the extracts on mild steel surface was carried out using various adsorption isotherms to derive the inhibition mechanism. All the inhibitors showed both physisorption and chemisorption during the adsorption process. The metal binding ability of these extracts was proved by UV-Visible spectroscopy. Surface morphological studies like SEM and AFM were performed to confirm the adsorption behaviour of extracts. Temperature studies revealed that inhibition potential reduces at higher temperatures due to the desorption of the adsorbed layer for all the extracts. Potentiodynamic polarization studies showed that all the inhibitors are mixed-type inhibitors. It has been found that, generally, inhibition efficiency in the HCl medium was more predominant than H_2SO_4 medium, except in the case of CPE.

Scanning electron microscopy and atomic force microscopy were recorded to establish the protective nature of plant extracts on the mild steel surface. All the metal

surfaces exposed in the inhibitor solution were found to be more fine and smooth than in blank solution. Quantum mechanical calculations of major components of all the extracts were also done to predict theoretical corrosion inhibition efficiency. Statistical analysis was performed to optimize factors like temperature, inhibitor concentration and acid concentration on inhibition efficiency using Response surface methodology and BBD/CCD design. Regression model could describe the interdependence between factors on the inhibition efficiency and the results obtained from experiments in good agreement.

Four synthetic Schiff base inhibitors derived from pyridine carbonyl compounds such as N-hydroxy-1-(pyridin-2-yl) methanimine (NHP2M), N-hydroxy-1-(pyridin-3-yl) methanimine (NHP3M), (E)-2-(1-(2-phenylhydrazono) ethyl)pyridine (2PHEP) and (E)-2-(1-triazylidineethyl) pyridine (2TAEP) were applied as microbial induced corrosion (MIC) inhibitors for mild steel in marine environment. Isolation and identification of the resulting culture showed the possibility of mixed culture of related bacteria in the isolate from original seawater. MIC inhibition studies such as weight loss measurements and electrochemical studies such as electrochemical impedance spectroscopy and potentiodynamic polarization studies were performed. NHP3M was found to be more efficient than all other inhibitors. The decreasing order of inhibition efficiency of Schiff base inhibitor systems is as follows: NHP3M > 2PHEP > NHP2M > 2TAEP. Potentiodynamic polarization studies revealed that Schiff base inhibitors were acted as mixed-type inhibitors. Mechanism of MIC inhibition was established using surface analysis like XRD, FTIR spectroscopy and microscopic surface analysis, *in vitro* antibacterial effects of inhibitors and UV-Visible spectroscopy. The proposed mechanism of inhibition was described as Schiff base inhibitors disturbing biofilm formation by adsorbing on the metal surface, not by killing microorganisms.

REFERENCES

1. Shreir, L. L., Burstein, G. T. & Jarman, R. A. *Corrosion Control*, Third Edition, Butterworth-Heinemann (1994).

2. Cicek, V. & Bayan, A. *Corrosion Chemistry*, First Edition, Scrivener publishing (2011).

3. Bradford, S. A. *Corrosion Contr*ol, Second Edition , CASTI Publishing Inc. (2001).

4. Peter, M. & Peter, P. *Handbook of Hot-dip Galvanization*, First Edition, Wiley-VCH verlag GmbH & Co. (2011) .

5. Bockris, John, O.M., Khan. & Shahad, U. M. *Surface Electrochemistry: A Molecular Level Approach*, Springer US (1993).

6. Wagner, C. & Traud, W. On the interpretation of corrosion processes through the superposition of electrochemical partial processes and on the potential of mixed electrodes. *Corrosion* **62**, 844–855 (2006).

7. Landrum, R. J. *Fundamentals of Designing for Corrosion Control : A Corrosion Aid for the Designer*, Second Edition, NACE (1992).

8. Prion, D. L. *The Electrochemistry of Corrosion*, First Edition, NACE (1991).

9. Walsh, F. C.& Plectcher, D. *Industrial Electrochemistry*, Second Edition, Springer Netherlands (1990).

10. Hoar, T. P. *Report of the Committee on Corrosion and Protection : A Survey of Corrosion and Protection in the United Kingdom*, First Edition, H.M.S.O London (1971).

11. Bennett, L. H. *Economic Effects of Metallic Corrosion in the United States: A Report to the Congress by the National Bureau of Standards, NBS Special Publication*, U S Govt. Printing Office, Washington (1978).

12. Strehblow, H. H. & Marcus, P. *Corrosion Mechanisms in Theory and Practice*, Third Edition, CRC Press (2011).

13. Gellings, P. J. *Introduction to corrosion prevention and control*, First Edition, Delft University Press (1984).

14. Pierre, R. R. *Handbook of corrosion engineering*, Second Edition, Mc Graw Hill, New York (2012).

15. Ghali, E., Sastri, V. S. & Elboujdaini, M. *Corrosion prevention and protection: practical solutions*, First Edition, John Wiley & Sons, Ltd. (2007).

16. Kuruvilla, M. *Amino acid based green inhibitors for the corrosion of mild steel and copper in different media*, Ph.D Thesis, University of Calicut (2016).

17. Cramer, S. D. & Covino, B. S. Corrosion : *Fundementals, Testing, and Protection,*

First Edition, Vol. 13A, ASM International (2003).

18. Azim, S., Muralidharan, S., Iyer, S., Muralidharan, B. & Vasudevan, T. Synergistic influence of iodide ions on inhibition of corrosion of mild steel in H_2SO_4 by N-phenyl thiourea. *Br. Corros. J.* **33**, 297–301 (1998).

19. Subramanian, A., Natesan, M., Muralidharan, V. S., Balakrishnan, K. & Vasudevan, T. An overview: Vapor phase corrosion inhibitors. *Corrosion* **56**, 144–155 (2000).

20. Cramer, S. D. & Covino, B. S. *Corrosion : Fundamentals, Testing, and Protection*, First Edition, Vol. 13A, ASM International (2003).

21. Musa, A. Y., Jalgham Ramzi, T. T. & Mohamad, A. B. Molecular dynamic and quantum chemical calculations for phthalazine derivatives as corrosion inhibitors of mild steel in 1M HCl. *Corros. Sci.* **56**, 176–183 (2012).

22. Nataraja, S. E., Venkatesha, T. V. & Tandon, H. C. Computational and experimental evaluation of the acid corrosion inhibition of steel by tacrine. *Corros. Sci.* **60**, 214–223 (2012).

23. Cottis, R. A. & Shreir, L. L. *Shreir's Corrosion*, Fourth Edition, Elsevier, London, 2857-2889 (2010).

24. Cottis, R. A. & Shreir, L. L. *Shreir's Corrosion*, Fourt Edition, Elsevier, London, 3207-3229 (2010).

25. Bahadori, A. *Cathodic Corrosion Protection Systems A Guide for Oil and Gas Industries*, First Edition, Gulf Professional Publishing, Elsevier (2014).

26. Bard, A. J. & Faulkner, L. R. *Electrochemical Methods: Fundamentals and Applications*, Second Edition, Wiley (2004).

27. Xiao-ZiRiny, Y., Chaojie, S., & Haijiang, W. *Electrochemical Impedance Spectroscopy in PEM Fuel Cells*, First Edition, Springer-Verlag London (2010).

28. Hamdy Makhlouf, A. S., El-Shenawy, E. & El-Bitar, T. Electrochemical impedance spectroscopy study of the corrosion behavior of some niobium bearing stainless steels in 3.5% NaCl. *Int. J. Electrochem. Sci.* **1**, 171–180 (2006).

29. Haynes, G. S. *Laboratory Corrosion Tests and Standards*, First Edition, ASTM International (1985).

30. Rammelt, U. & Reinhard, G. Application of electrochemical impedance spectroscopy (EIS) for characterizing the corrosion-protective performance of organic coatings on metals. *Prog. Org. Coatings* **21**, 205–226 (1992).

31. Fontana, M. G. *Corrosion Engineering*, Third Edition, McGraw-Hill (1986).

32. Wagner, C., Traud, W. 'On the interpretation of corrosion processes through the superposition of electrochemical partial processes and on the potential of mixed electrodes,' with a perspective by F. Mansfeld. *Corrosion* **62**, 843–855 (2006).

33. Wandelt, K. *Encyclopedia of Interfacial Chemistry*, First Edition, Elsevier (2018).

34. Popov, B. N. *Corrosion Engineering Principles and Solved Problems*, First Edition, Elsevier (2015).

35. Kolotyrkin, Y. M. Electrochemical aspects of the corrosion of metals. *Prot. Met.* **11**, 635–644 (1975).

36. Babu, S. *Advances in Chemical Mechanical Planarization (CMP)*, First Edition, Woodhead Publishing (2016).

37. Lee, Y., Pan, J., Hathaway, R. B., & Barkey, M. E. *Fatigue Testing and Analysis: Theory and Practice*, First Edition, Butterworth-Heinemann, Elsevier (2005).

38. Loto, C. A. Electrochemical noise evaluation and data statistical analysis of stressed aluminium alloy in NaCl solution. *Alexandria Eng. J.* **57**, 1313–1321 (2018).

39. Rulph, C. & Donald, R. *Digital Signal Processing and Applications with the TMS320C6713 and TMS320C6416 DSK*, Second Edition, Wiley-IEEE Press, (2003).

40. Thomson, R. E. & Emery, W. J. *Data Analysis Methods in Physical Oceanography*, Third Edition, Elsevier Science (2014).

41. Begum, A. S., Mallika, J. & Gayathri, P. Corrosion inhibition property of some 1, 3, 4- Thiadiazolines on mild steel in acidic medium. *E-Journal Chem.* **7**, 185–197 (2010).

42. Elayyachy, M., El Idrissi, A. & Hammouti, B. New thio-compounds as corrosion inhibitor for steel in 1M HCl. *Corros. Sci.* **48**, 2470–2479 (2006).

43. Loto, R. T., Loto, C. A. & Popoola, A. P. I. Corrosion inhibition of thiourea and thiadiazole derivatives: A review. *J. Mater. Environ. Sci.* **3**, 885–894 (2012).

44. Kooliyat, R., Kakkassery, J. T., Raphael, V. P., Cheruvathur, S. V. & Paulson, B. M. Synthesis, cyclic voltammetric, electrochemical, and gravimetric corrosion inhibition investigations of Schiff base derived from 5,5-Dimethyl-1,3-cyclohexanedione and 2-Aminophenol on mild steel in 1 M HCl and 0.5 M H_2SO_4. *Int. J. Electrochem.* **2019,** 1094148 (2019).

45. Cang, H., Fei, Z., Shao, J., Shi, W. & Xu, Q. Corrosion inhibition of mild steel by Aloes extract in HCl solution medium. *Int. J. Electrochem. Sci.* **8**, 720–734 (2013).

46. Ayawei, N., Ebelegi, A. N. & Wankasi, D. Modelling and interpretation of adsorption isotherms. *J. Chem.* **2017** 3039817 (2017).

47. Chen, Q., Tian, Y. & Li, P. Study on shale adsorption equation based on monolayer adsorption, multilayer adsorption and capillary condensation. *J. Chem.* **2017** 1496463 (2017).

48. Shainy, K., Anupama, K. & Joseph, A. Excellent anticorrosion behavior of *Ruta graveolens* extract (RGE) for mild steel in hydrochloric acid : electro analytical studies on the effect of time, temperature and inhibitor concentration. *J. Bio-Tribo-Corrosion* **2**, 1–10 (2016).

49. Bidi, M. A., Azadi, M. & Rassouli, M. A new green inhibitor for lowering the corrosion rate of carbon steel in 1 M HCl solution: Hyalomma tick extract. *Mater. Today Commun.* **24**, 100996 (2020).

50. Umoren, S. A., Solomon, M. M., Obot, I. B. & Suleiman, R. K. Comparative studies on the corrosion inhibition efficacy of ethanolic extracts of date palm leaves and seeds on carbon steel corrosion in 15% HCl solution. *J. Adhes. Sci. Technol.* **32**, 1934–1951 (2018).

51. Dehghani, A., Bahlakeh, G., Ramezanzadeh, B. & Ramezanzadeh, M. Experimental complemented with microscopic (electronic/atomic)-level modeling explorations of *Laurus nobilis* extract as green inhibitor for carbon steel in acidic solution. *J. Ind. Eng. Chem.* **84**, 52–71 (2020).

52. Leite, F. L., Bueno, C. C., Da Róz, A. L., Ziemath, E. C. & Oliveira, O. N. Theoretical models for surface forces and adhesion and their measurement using atomic force microscopy. *Int. J. Mol. Sci.* **13**, 12773–12856 (2012).

53. Asadi, N., Ramezanzadeh, M., Bahlakeh, G. & Ramezanzadeh, B. Utilizing Lemon Balm extract as an effective green corrosion inhibitor for mild steel in 1M HCl solution: A detailed experimental, molecular dynamics, Monte Carlo and quantum mechanics study. *J. Taiwan Inst. Chem. Eng.* **95**, 252–272 (2019).

54. Raphael, V. P., Kakkassery, J. T., Shanmughan, S. K. & Varghese, S. Interaction of two water soluble heterocyclic hydrazones on copper in nitric acid: electrochemical, surface morphological, and quantum chemical investigations. *Int. J. Met.* **2016**, 1–8 (2016).

55. Singh, A., Ansari, K. R., Chauhan, D. S., Quraishi, M. A., Lgaz, H. & Ill-Min, C. Comprehensive investigation of steel corrosion inhibition at macro/micro level by ecofriendly green corrosion inhibitor in 15% HCl medium. *J. Colloid Interface Sci.* **560**, 225–236 (2020).

56. Vidhya, T. K., Joby, T. K., Raphael, V. P., Ragi, K. & Reeja, J. *Ixora coccinea* extract as an efficient eco-friendly corrosion inhibitor in acidic media: Experimental and theoretical approach. *Curr. Chem. Lett.* **10**, 139–150 (2021).

57. Salmerón-Manzano, E., Garrido-Cardenas, J. A. & Manzano-Agugliaro, F. Worldwide research trends on medicinal plants. *Int. J. Environ. Res. Public Health* **17**, 3376 (2020).

58. Saxena, A., Prasad, D., Thakur, K. K. & Kaur, J. PDP, EIS, and surface studies of the low-carbon steel by the extract of *Tinospora cordifolia*: A green approach to the corrosion inhibition. *Arab. J. Sci. Eng.* **46**, 425–436 (2020) doi:10.1007/s13369-020-04894-9.

59. Saxena, A., Thakur, K. K., Saxena, K. K., Chambyal, S. & Sharma, A. Electrochemical studies and surface examination of low carbon steel by applying the extract of *Terminalia chebula*. *Mater. Today Proc.* **26**, 1360–1367 (2019).

60. Haldhar, R., Prasad, D., Saxena, A. & Kumar, R. Experimental and theoretical studies of *Ficus religiosa* as green corrosion inhibitor for mild steel in 0.5 M H_2SO_4 solution. *Sustain. Chem. Pharm.* **9**, 95–105 (2018).

61. Saxena, A., Prasad, D. & Haldhar, R. Investigation of corroscon inhibition effect and adsorption activities of *Achyranthes aspera* extract for mild steel in 0.5 M H_2SO_4. *J. Fail. Anal. Prev.* **18**, 957–968 (2018).

62. Ayoola, A., Ojo Sunday, I. F., Godwin, A., Ayeni, A. O., Oluranti, A., Oyinola, O., Olubunmi, A., Chiderah, C. Inhibitive corrosion performance of the eco-friendly Aloe vera in acidic media of mild and stainless steels. *J. Bio- Tribo-Corrosion* **6**, 1–13 (2020).

63. Anupama, K. K. & Joseph, A. Experimental and theortical studies on *Cinnamomum verum* leaf extract and one of its major components, eugenol as environmentally benign corrosion inhibitors for mild steel in acid media. *J. Bio-Tribo-Corrosion* **4**, 30 (2018).

64. Ji, G., Dwivedi, P., Sundaram, S. & Prakash, R. Inhibitive effect of *Chlorophytum borivilianum* root extract on mild steel corrosion in HCl and H_2SO_4 solutions. *Ind. Eng. Chem. Res.* **52**, 10673–10681 (2013).

65. Chidiebere, M. A., Ogukwe, C. E., Oguzie, K. L., Eneh, C. N. & Oguzie, E. E. Corrosion inhibition and adsorption behavior of *Punica granatum* extract on mild steel in acidic environments: experimental and theoretical studies. *Ind. Eng. Chem. Res.* **51**, 668–677 (2012).

66. Karthiga, N. K., Rajendran, S., Prabhakar, P., Al-Hashem, A. & Shanmugapriya, S. Corrosion inhibition of mild steel by an aqueous extract of *Allium sativum*. *Eur. J. Biomed. Pharm. Sci.* **5**, 838–843 (2018).

67. Faustin, M., Maciuk, A., Salvin, P., Roos, C. & Lebrini, M. Corrosion inhibition of C38 steel by alkaloids extract of *Geissospermum laeve* in 1M hydrochloric acid: electrochemical and phytochemical studies. *Corros. Sci.* **92**, 287–300 (2015).

68. Deyab, M. A., Osman, M. M., Elkholy, A. E. & El-Taib Heakal, F. Green approach towards corrosion inhibition of carbon steel in produced oilfield water using lemongrass extract. *RSC Adv.* **7**, 45241–45251 (2017).

69. Savita, Mourya, P., Namrata, C., Surendra, K., Singh, V. K. & Singh, M. M. *Strychnos nuxvomica*, *Piper longum* and *Mucuna pruriens* seed extracts as eco-friendly corrosion inhibitors for copper in nitric acid. *RSC Adv.* **6**, 95644–95655 (2016).

70. El-Etre, A. Y. Inhibition of acid corrosion of carbon steel using aqueous extract of olive leaves. *J. Colloid Interface Sci.* **314**, 578–583 (2007).

71. Mayakrishnan, P., Seung Hyun, K., Asokan, S., Hemapriya, V. & Chung, I. M. β-Sitosterol isolated from rice hulls as an efficient corrosion inhibitor for mild steel in acidic environments. *New J. Chem.* **41**, 3900–3907 (2017).

72. Saxena, A., Prasad, D., Haldhar, R., Singh, G. & Kumar, A. Use of *Saraca ashoka* extract as green corrosion inhibitor for mild steel in 0.5 M H_2SO_4. *J. Mol. Liq.* **258**, 89-97 (2018).

73. Ji, G., Anjum, S., Sundaram, S. & Prakash, R. *Musa paradisica* peel extract as green corrosion inhibitor for mild steel in HCl solution. *Corros. Sci.* **90**, 107-117

(2014).

74. Lahhit, N. N., Bouyanzer, A., Desjobert, J. M., Hammouti, B., Salghi, R., Costa, J., Jama, C., Bentiss, F. & Majidi, L. Fennel (*Foeniculum Vulgare*) essential oil as green corrosion inhibitor of carbon steel in hydrochloric acid solution. *Port. Electrochim. Acta* **29**, 127–138 (2011).

75. Dahmani, K., Galai, M., Cherkaoui, M., El hasnaoui, A. & El Hessni, A. Cinnamon essential oil as a novel eco-friendly corrosion inhibitor of copper in 0.5 M sulfuric acid medium. *J. Mater. Environ. Sci.* **8**, 1676–1689 (2017).

76. Fekry, A. M. & Ameer, M. A. Corrosion inhibition of mild steel in acidic media using newly synthesized heterocyclic organic molecules. *Int. J. Hydrogen Energy* **35**, 7641–7651 (2010).

77. Sutter, E. M. M., Ammeloot, F., Pouet, M. J., Fiaud, C. & Couffignal, R. Heterocyclic compounds used as corrosion inhibitors: correlation between ^{13}C and ^{1}H NMR spectroscopy and inhibition efficiency. *Corros. Sci.* **41**, 105–115 (1999).

78. Rohira, B. & Singh, G. Adsorption kinetics of dihydroxypyrimidine on mild steel in 1 N phosphoric acid. *Indian J. Chem. Technol.* **3**, 263–268 (1996).

79. Ezhilarasi, M. R., Prabha, B. & Santhi, T. Novel pyrazole based ionic liquid as a corrosion inhibitor for mild steel in acidic media. *Chem. Sci. Trans.* **4**, 758–767 (2015).

80. Mushtaq, J. & Meften, M. Synthesis, characterization and study of a new heterocyclic compound as corrosion inhibitor in 15% HCl solution. *Int. J. Innov. Res. Sci. Eng. Technol.* **5**, 13685-13696 (2007).

81. Fouda, A., El-Aziz, S., Abd el-Maksoud, S. A., El-Sayed, E. H., Elbaz, H. A. & Abousalem, A. S. Effectiveness of some novel heterocyclic compounds as corrosion inhibitors for carbon steel in 1 M HCl using practical and theoretical methods. *RSC Adv.* **11**, 19294–19309 (2021).

82. Aljourani, J., Golozar, M. A. & Raeissi, K. The inhibition of carbon steel corrosion in hydrochloric and sulfuric acid media using some benzimidazole derivatives. *Mater. Chem. Phys.* **121**, 320–325 (2010).

83. Shanmughan, S. K., Kakkassery, J. T., Raphael, V. P. & Paul, A. Electrochemical and surface morphological studies of carbon steel corrosion by a novel polynuclear Schiff base in HCl solution. *ISRN Electrochem.* **2013**, 820548 (2013).

84. Kuriakose, N., Kakkassery, J. T., Raphael, V. P. & Shanmughan, S. K. Electrochemical impedance spectroscopy and potentiodynamic polarization analysis on anticorrosive activity of Thiophene-2-Carbaldehyde derivative in acid medium. *Indian J. Mater. Sci.* **2014**, 124065 (2014).

85. Abd El-Lateef, H. M. Experimental and computational investigation on the corrosion inhibition characteristics of mild steel by some novel synthesized imines in hydrochloric acid solutions. *Corros. Sci.* **92**, 104–117 (2015).

86. Paul, A., Thomas, K. J., Raphael, V. P. & Shaju, K. S. 3-Formylindole-4-aminobenzoic acid: A potential corrosion inhibitor for mild steel and copper in

hydrochloric acid media. *ISRN Corros.* **2012**, 1–9 (2012).

87. Meng, Y., Wenbo, N., Xu, B., Yang, W., Zhang, K., Chen, Y., Li, L., Liu, X., Zheng, J. & Zhang, Y. Inhibition of mild steel corrosion in hydrochloric acid using two novel pyridine Schiff base derivatives: A comparative study of experimental and theoretical results. *RSC Adv.* **7**, 43014–43029 (2017).

88. Dohare, P., Quraishi, M. A. & Obot, I. B. A combined electrochemical and theoretical study of pyridine-based Schiff bases as novel corrosion inhibitors for mild steel in hydrochloric acid medium. *J. Chem. Sci.* **130**, 1–19 (2018).

89. John, S., Jeevana, R., Aravindakshan, K. K. & Joseph, A. Corrosion inhibition of mild steel by N(4)-substituted thiosemicarbazone in hydrochloric acid media. *Egypt. J. Pet.* **26**, 405–412 (2017).

90. Yurt, A., Balaban, A., Kandemir, S. U., Bereket, G. & Erk, B. Investigation on some Schiff bases as HCl corrosion inhibitors for carbon steel. *Mater. Chem. Phys.* **85**, 420–426 (2004).

91. Hosseini, M. G., Ehteshamzadeh, M. & Shahrabi, T. Protection of mild steel corrosion with Schiff bases in 0.5 M H_2SO_4 solution. *Electrochim. Acta* **52**, 3680–3685 (2007).

92. Sini, V., Joby, T., Vinod, R. & Shaju, K. S. Corrosion inhibition capacity of two heterocyclic oximes on copper in nitric acid: electrochemical, quantum chemical and surface morphological investigations. *Curr. Chem. Lett.* **8**, 1–12 (2019).

93. Mansouri, H. & Alavi, S. A study of microbial influenced corrosion in oil and gas industry. *First International Conference of Oil, Gas, Petrochemical and Power Plant*, Tehran, Iran (2012). doi:10.13140/RG.2.1.3117.8089.

94. Costerton, J. W., Geesey, G. G. & Cheng, K.-J. How bacteria stick. Sci. Am. 238, 86–95, This week's Citation classic CC/Number 48 (1978).

95. Trevors, J., & Gurtler, V. *Microbiology of Atypical Environments*, First Edition, Academic Press, Vol. 45, 123–144 (2018).

96. Mara, D. & Horan, N. *Handbook of Water and Wastewater Microbiology*, First Edition, Academic Press (2003).

97. Huber, B., Herzog, B., Drewes, J. E., Koch, K. & Müller, E. Characterization of sulfur oxidizing bacteria related to biogenic sulfuric acid corrosion in sludge digesters. *BMC Microbiol.* **16**, 153 (2016).

98. Glasauer, S. M., Beveridge, T. J., Burford, E. P., Harper, F. A. & Gadd, G. M. Metals and metalloids, transformation by microorganisms. *Sci. Prog.* **86**, 179–202 (2013).

99. Gu, T. Theoretical modeling of the possibility of acid producing bacteria causing fast pitting biocorrosion. *J. Microb. Biochem. Technol.* **06**, 68-74 (2014).

100. Enning, D. & Garrelfs, J. Corrosion of iron by sulfate-reducing bacteria: new views of an old problem. *Appl. Environ. Microbiol.* **80**, 1226–1236 (2014).

101. Kielemoes, J., Bultinck, I., Storms, H., Boon, N. & Verstraete, W. Occurrence of manganese-oxidizing microorganisms and manganese deposition during biofilm formation on stainless steel in a brackish surface water. *FEMS Microbiol. Ecol.* **39**, 41–55 (2002).

102. Kermani, B. & Harrop, D. *Corrosion and Materials in Hydrocarbon Production: A Compendium of Operational and Engineering Aspects*, First Edition, Wiley-ASME Press Series (2019).

103. Javaherdashti, R. *Microbiologically Influenced Corrosion, An Engineering Insight*, First Edition, Springer-Verlag London (2008).

104. Skovhus T L, Enning D & Lee J S. *Microbiologically Influenced Corrosion in the Upstream Oil and Gas Industry*, CRC Press (2017).

105. STG 31- Oil and Gas Production. *Selection, application, and evaluation of biocides in the oil and gas industry*, NACE 31205-2006-SG (2006).

106. Javaherdashti, R., & Akvan, F. *Hydrostatic Testing, Corrosion, and Microbiologically Influenced Corrosion: A Field Manual for Control and Prevention*, First Edition, CRC Press (2017).

107. Flynn, D. J. & Nalco Company. *The Nalco water handbook*, Third Edition, McGraw-Hill (2009).

108. Heidersbach, R. *Metallurgy and Corrosion Control in Oil and Gas Production*, Second Edition, Wiley (2018).

109. Hsu, C. W., Chen, T. E., Lo, K. Y. & Lee, Y. L. Inhibitive properties of Benzyldimethyldodecylammonium chloride on microbial corrosion of 304 stainless steel in a Desulfovibrio desulfuricans-inoculated medium. *Materials.* **12**, 307 (2019).

110. Wang, J., Hou, B., Xiang, J., Chen, X., Gu, T. & Liu, H. The performance and mechanism of bifunctional biocide sodium pyrithione against sulfate reducing bacteria in X80 carbon steel corrosion. *Corros. Sci.* **150**, 296–308 (2019).

111. Shaban, S. M., Aiad, I., Moustafa, A. H. & Aljoboury, O. H. Some alginates polymeric cationic surfactants; surface study and their evaluation as biocide and corrosion inhibitors. *J. Mol. Liq.* **273**, 164–176 (2019).

112. Vaithiyanathan, S., Chandrasekaran, K. & Barik, R. C. Green biocide for mitigating sulfate-reducing bacteria influenced microbial corrosion. *3 Biotech* **8**, 495 (2018).

113. Rasool, K., Gheyath, K. N., Nadin, Y., Ravi, P. P., Abdul Rasheed, P. & Mahmoud, K. A. "Green" ZnO-interlinked chitosan nanoparticles for the efficient inhibition of sulfate-reducing bacteria in inject seawater. *ACS Sustain. Chem. Eng.* **6**, 3896–3906 (2018).

114. Carlson, H. K., Mullan, M. R., Mosqueda, L. A., Chen, S., Arkin, M. R. & John, D. C. High-throughput screening to identify potent and specific inhibitors of microbial sulfate reduction. *Environ. Sci. Technol.* **51**, 7278–7285 (2017).

115. Narenkumar, J., Parthipan, P., Usha Raja, N. A., Benelli, G., Murugan, K. & Rajasekar, A. Ginger extract as green biocide to control microbial corrosion of mild steel. *Biotech* **7**, 1–11 (2017).

116. Labena, A., Hegazy, M. A., Horn, H. & Müller, E. The biocidal effect of a novel synthesized gemini surfactant on environmental sulfidogenic bacteria: planktonic cells and biofilms. *Mater. Sci. Eng. C. Mater. Biol. Appl.* **47**, 367–375 (2015).

117. Labena, A., Hegazy, M. A., Horn, H. & Müller, E. Cationic gemini surfactant as a corrosion inhibitor and a biocide for high salinity Sulfidogenic bacteria originating from an oil-field water tank. *J. Surfactants Deterg.* **17**, 419–431 (2014).

118. Shaban, S., Aiad, I., Tawfik, S., Abd-Elaal, A. A. & El-Shafie, M. Enhancing of corrosion inhibition and the biocidal effect of phosphonium surfactant compounds for oil field equipment. *J. Surfactants Deterg.* **17**, 391–401 (2013).

119. Bhola, S. M., Faisa,l M. A., Bhola, R., Spear, J. R., Mishra, B., Olson, D. L. & Anthony, E. K. Neem extract as an inhibitor for biocorrosion influenced by sulfate reducing bacteria: A preliminary investigation. *Eng. Fail. Anal.* **36**, 92–103 (2014).

120. Parthipan, P., Elumalai, P., Narenkumar, J., Machuca, L. L., Murugan, K., Obuli, P. K. & Aruliah, R. *Allium sativum* (garlic extract) as a green corrosion inhibitor with biocidal properties for the control of MIC in carbon steel and stainless steel in oilfield environments. *Int. Biodeterior. Biodegrad.* **132**, 66–73 (2018).

121. Negm, N. A., El Farargy, A. F., Al Sabagh, A. M. & Abdelrahman, N. R. New Schiff base cationic surfactants: surface and thermodynamic properties and applicability in bacterial growth and metal corrosion prevention. *J. Surfactants Deterg.* **14**, 505–514 (2011).

122. Kobisy, A. S., Nassar, H. N., Tawfik, S. M., Elshatoury, E. H. & Aiad, I. Mitigation of eco-unfriendly and costly microbial induced corrosion using novel synthesized Schiff base cationic surfactants. *J. Chem. Technol. Biotechnol.* **96**, 941–952 (2021).

123. Shaban, S. M., Saied, A., Tawfik, S. M., Abd-Elaal, A. & Aiad, I. Corrosion inhibition and biocidal effect of some cationic surfactants based on Schiff base. *J. Ind. Eng. Chem.* **19**, 2004–2009 (2013).

124. Negm, N. A., Zaki, M. F. & Salem, M. A. I. Cationic Schiff base amphiphiles and their metal complexes: surface and biocidal activities against bacteria and fungi. *Colloids Surf. B.* **77**, 96–103 (2010).

125. Chhabra, S. C., Uiso, F. C. & Mshiu, E. N. Phytochemical screening of tazanian medical plants. *I. J. etnopharmacology* **11**, 157–179 (1984).

126. Roopashree, T. S., Dang, R., Rani, S. R. H. & Narendra, C. Antibacterial activity of antipsoriatic herbs: *Cassia tora*, *Momordica charantia* and *Calendula officinalis*. *Int. J. Appl. Res. Nat. Prod.* **1**, 20–28 (2008).

127. Sofowora, A. Recent trends in research into African medicinal plants. *J. Ethnopharmacol.* **38**, 197–208 (1993).

128. Rami, E., Sipai, S. & Patel, I. Studies on qualitative and quantitative phytochemical analysis of *Piper longum* linn. *Int. J. Pharma Bio Sci.* **4**, 11–17 (2013).

129. Binsi, M. P., Joby, T. K., Ragi, K., Sini, V. C. & Reeja, J. Interaction of two heterocyclic schiff bases derived from 2-acetyl pyridine on mild steel in hydrochloric acid: physicochemical and corrosion inhibition investigations. *Curr. Chem. Lett.* **9**, 19–30 (2020).

130. Sanni, O. & Popoola, A. P. I. Assessment of concentration, temperature and exposure time effect on waste product as a sustainable inhibitor for stainless steel corrosion: optimization using response surface method. *J. Bio- Tribo-Corrosion* **5**, 1–14 (2019).

131. Bhattacharya, S. *Central Composite Design for response surface methodology and its application in pharmacy in Response Surface Methodology in Engineering Science 1–19*, IntechOpen Book series (2021).

132. Prabhu, D., Prabhu, P. R. & Rao, P. Thermodynamics, adsorption, and response surface methodology investigation of the corrosion inhibition of aluminum by *Terminalia chebula* Ritz. extract in H_3PO_4. *Chem. Pap.* **75**, 653–667 (2020) doi:10.1007/s11696-020-01318-8.

133. El-Shamy, A. M., El-Hadek, M. A., Nassef, A. E. & El-Bindary, R. A. Optimization of the influencing variables on the corrosion property of steel alloy 4130 in 3.5 wt.% NaCl solution. *J. Chem.* **2020**, 9212491 (2020).

134. Ajeigbe, S. O., Basar, N., Hassan, M. A. & Aziz, M. Optimization of corrosion inhibition of essential oils of *Alpinia galanga* on mild steel using response surface methodology. *ARPN J. Eng. Appl. Sci.* **12**, 2763–2771 (2017).

135. Okewale, A. O. & Adebayo, T. Investigation of pumpkin pod extract as corrosion inhibitor for carbon steel in HCl solution. *Niger. J. Technol.* **39**, 173–181 (2020).

136. Ferreira, S. L. C., Bruns, R. E., Ferreira, H. S., Matos, G. D., David, J. M., Brandao, G. C., Da Silva, E. G. P., Portugal, L. A., Dos Reis, P. S., Souza, A. S. & Dos Santos, W. N. L. Box-Behnken design: An alternative for the optimization of analytical methods. *Anal. Chim. Acta* **597**, 179–186 (2007).

137. Krishna, J. G. *Pigment production by marine Serratia sp. BTW J8*. Ph. D Thesis, CUSAT, Cochin (2008).

138. Stolp, H., Starr, M. P., Truper, H. G., Balows, A. & Schlegel, H. G. *The Prokaryotes: A Handbook on Habitats, Isolation, and Identification of Bacteria*, Springer-Verlag Berlin Heidelberg (1981).

139. Norman, D. L. *Bergey's Manual of Determinative Bacteriology*, Eightth Edition, Williams & Wilkins Co., vol. 22 (1975).

140. Green, M. R. & Sambrook, J. Molecular Cloning: A Laboratory Manual, Fourth Edition, Cold Spring Harbor Laboratory Press Bookstore, vol. 1 (2014).

141. Reddy, G. S., Aggarwal, R. K., Matsumoto, G. I. & Shivaji, S. Arthrobacter flavus sp. nov., a psychrophilic bacterium isolated from a pond in McMurdo Dry Valley,

Antarctica. *Int. J. Syst. Evol. Microbiol.* **50**, 1553–1561 (2000).

142. Bauer, A. W., Kirby, W. M. M., Sherris, J. C. & Turck, M. Antibiotic susceptibility testing by a standardized single disk method. *Am. J. Clin. Pathol.* **45**, 493–496 (1966).

143. Mueller, J. H. & Hinton, J. A protein-free medium for primary isolation of the Gonococcus and Meningococcus. *Proc. Soc. Exp. Biol. Med.* **48**, 330–333 (1941).

144. Ikram, A., Muhammad Ali, V., Shumaila, S., Salman Khalid, A., Syed Tahir, A. & Shaheen, F. Ixorene, a new dammarane triterpene from the leaves of *Ixora coccinea* linn. *Rec. Nat. Prod.* **7**, 302–306 (2013).

145. Hamdy, A. & El-Gendy, N. S. Thermodynamic, adsorption and electrochemical studies for corrosion inhibition of carbon steel by henna extract in acid medium. *Egypt. J. Pet.* **22**, 17–25 (2013).

146. Saxena, A. & Kumar, J. Phytochemical screening, metal-binding studies and applications of floral extract of *Sonchus oleraceus* as a corrosion inhibitor. *J. Bio-Tribo-Corrosion* **6**, 1–10 (2020).

147. Zheng, X. Corrosion inhibition of mild steel in sulfuric acid solution by *Houttuynia cordata* extract. *Int. J. Electrochem. Sci.* **12**, 6232–6244 (2017).

148. Kurniawan, F. & Madurani, K. Electrochemical and optical microscopy study of red pepper seed oil corrosion inhibition by self-assembled monolayers (SAM) on 304 SS. *Prog. Org. Coatings* **88**, 256–262 (2015).

149. Idris, M. N., Daud, A. R. & Othman, N. K. Electrochemical impedance spectroscopy study on corrosion inhibition of benzyltriethylammonium chloride. *AIP Conf. Proc.* **1571**, 23–28 (2013).

150. El-Lateef, H. M. A., El-Sayed, A. R., Mohran, H. S. & Shilkamy, H. A. S. Corrosion inhibition and adsorption behavior of phytic acid on Pb and Pb–In alloy surfaces in acidic chloride solution. *Int. J. Ind. Chem.* **10**, 31–47 (2019).

151. Oonincx, P. J., Homborg, A. M., Van Westing, E. P. M., Tinga, T., Zhang, X., Ferrari, G. M., Dewit, J. H. W. & Mol, J. M. C. Novel time–frequency characterization of electrochemical noise data in corrosion studies using Hilbert spectra. *Corros. Sci.* **66**, 97–110 (2013).

152. Ragi, K., Kakkassery, J. T., Raphael, V. P., Paulson, B. M. & Johnson, R. Corrosion inhibition of mild steel by N, N'-(5,5- dimethylcyclohexane-1,3-diylidene) dianiline in acid media: gravimetric and electrochemical evaluations. *Curr. Chem. Lett.* **10**, 67–80 (2021).

153. Singh, A., Ansari, K. R., Chauhan, D. S., Quraishi, M. A., Lgaz, H. & Ill-Min, C. Comprehensive investigation of steel corrosion inhibition at macro/micro level by ecofriendly green corrosion inhibitor in 15% HCl medium. *J. Colloid Interface Sci.* **560**, 225–236 (2020).

154. Raphael, V. P., Shanmughan, S. K. & Kakkassery, J. T. Monitoring the interaction of two heterocyclic compounds on carbon steel by electrochemical polarization, noise, and quantum chemical studies. *Int. J. Corros.* **2016**, 4204532 (2016).

155. Abbas, D., Resan, K. & Takhakh, A. Optimization of Ni-Ti-Cu shape memory effect using minitab program. *Int. J. Energy Environ. Spec. Issue Appl. Mech. Res.* **7**, 263–268 (2016).

156. Manescu, R., Nedelcu, A. & Adela-Eliza, D. Improvement the quality of industrial products by applying the pareto chart. *Rev. Air Force Acad.* **13**, 169–172 (2015).

157. Mathew, A., Areekara, S. & Sabu, A. S. Sensitivity analysis on radiative heat transfer of hydromagnetic Carreau nanoliquid flow over an elongating cylinder using Bulirsch-Stoer algorithm. *Therm. Sci. Eng. Prog.* **25**, 101038 (2021).

158. Achayindee, S. Roengsumran, S. & Mahatumaratana, C. Chemical constituents of the leaf of *Croton oblongifolius* Roxb., Chulalongkorn University (1996) http://cuir.car.chula.ac.th/handle/123456789/42340.

159. Saxena, A., Kishor, K. & Bhardwaj, N. Electrochemical studies and surface examination of low carbon steel by applying the extract of *Musa acuminata*. *Surf. Interfaces.* **18,** 100436 (2020).

160. Farhadian, A., Rahimi, A., Nehzat, S., Shaabani, A., Majid, A. & Alavi, A. A theoretical and experimental study of castor oil-based inhibitor for corrosion inhibition of mild steel in acidic medium at elevated temperatures. *Corros. Sci.* **175**, 108871 (2020).

161. Mathew, A., Neethu, T. S. & Areekara, S. Three-dimensional hydromagnetic hybrid nanoliquid flow and heat transfer between two vertical porous plates moving in opposite directions: Sensitivity analysis. *Heat Transf.* **50**, 1–24 (2021) doi:10.1002/htj.22192.

162. Luo, X., Bai, R., Zhen, D., Yang, Z., Huang, D., Mao, H., Li, X., Zou, H., Xiang, Y., Liu, K., Wen, Z. & Fu, C. Response surface optimization of the enzyme-based ultrasound-assisted extraction of acorn tannins and their corrosion inhibition properties. *Ind. Crops Prod.* **129**, 405–413 (2019).

163. Reddi, K. K. & Tetali, S. D. Dry leaf extracts of *Tinospora cordifolia* (Willd.) Miers attenuate oxidative stress and inflammatory condition in human monocytic (THP-1) cells. *Phytomedicine* **61**, 152831 (2019).

164. Erna, M., Herdini, H. & Futra, D. Corrosion inhibition mechanism of mild steel by amylose-acetate/carboxymethyl chitosan composites in acidic media. *Int. J. Chem. Eng.* **2019**, 8514132 (2019).

165. Dagdag, O., Zaki, S., Erramli, H., Nuha, W., Lei, G., Verma, C., Ebenso, E. E., Kaya, S. & El Harfi, A. Epoxy prepolymer as a novel anti-corrosive material for carbon steel in acidic solution: electrochemical, surface and computational studies. *Mater. Today Commun.* **22**, 100800 (2020).

166. Muthamma, K., Kumari, P., Lavanya, M. & Rao, S. A. Corrosion inhibition of mild steel in acidic media by N-[(3,4-dimethoxyphenyl)methyleneamino]-4-hydroxy-benzamide. *J. Bio- Tribo-Corrosion* **7**, 1–19 (2021).

167. Anupama, K. K., Ramya, K. & Joseph, A. Electrochemical measurements and theoretical calculations on the inhibitive interaction of *Plectranthus amboinicus*

leaf extract with mild steel in hydrochloric acid. *Meas. J. Int. Meas. Confed.* **95**, 297–305 (2017).

168. Preethi Kumari, P., Shetty, P. & Rao, S. A. Electrochemical measurements for the corrosion inhibition of mild steel in 1 M hydrochloric acid by using an aromatic hydrazide derivative. *Arab. J. Chem.* **10**, 653–663 (2017).

169. Chira, A., Bucur, B. & Radu, G. L. Electrodeposited organic layers formed from aryl diazonium salts for inhibition of copper corrosion. *Materials.* **10**, 235 (2017).

170. Anadebe, V. C., Onukwuli, O. D., Omotioma, M. & Okafor, N. A. Optimization and electrochemical study on the control of mild steel corrosion in hydrochloric acid solution with bitter kola leaf extract as inhibitor. *South African J. Chem.* **71**, 51–61 (2018).

171. Prabhu, P. R., Prabhu, D. & Rao, P. Analysis of *Garcinia indica* Choisy extract as eco-friendly corrosion inhibitor for aluminum in phosphoric acid using the design of experiment. *J. Mater. Res. Technol.* **9**, 3622–3631 (2020).

172. Prabhu, P. R., Prabhu, D., Sharma, S. & Kulkarni, S. M. Surface properties and corrosion behavior of turn-assisted deep-cold-rolled AISI 4140 steel. *J. Mater. Eng. Perform.* **29**, 5871–5885 (2020).

173. Rameshkumar K B. Diversity of Garcinia species in the western ghats: phytochemical perspective. Jawaharlal Nehru Tropical Botanic Garden and Research Institute, Thiruvananthapuram (2016).

174. Priya, S. V.Corrosion inhibition of mild steel in 1 M HCl and 0.5 M H_2SO_4 by natural product extract - A comparative analysis by electrochemical studies. *Int. J. Adv. Res. Chem. Chem. Eng.* **1**, 0–7 (2019).

175. Tsoeunyane, M. G., Makhatha, M. E. & Arotiba, O. A. Corrosion inhibition of mild steel by Poly(butylene succinate)-L-histidine extended with 1,6-diisocynatohexane polymer composite in 1 M HCl. *Int. J. Corros.* **2019**, 7406409 (2019).

176. Lima, K. C. D. S. De., Paiva, V. M., Perrone, D., Ripper, B., Grazieli, S., Maria, L. M. R., Amanda, G. da V. & Eliane, D. Glycine max meal extracts as corrosion inhibitor for mild steel in sulphuric acid solution. *J. Mater. Res. Technol.* **9**, 12756–12772 (2020).

177. Kumar, J., Kaur, A. & Narang, P. Phytochemical screening and metal binding studies on floral extract of *Solanum nigrum*. *Mater. Today Proc.* **26**, 3332–3336 (2019).

178. Mei, B.-A., Munteshari, O., Lau, J., Dunn, B. & Pilon, L. Physical interpretations of Nyquist plots for EDLC electrodes and devices. *J. Phys. Chem. C.* **122**, 194–206 (2017).

179. Loto, R. T., Loto, C. A. & Fedotova, T. Electrochemical studies of mild steel corrosion inhibition in sulfuric acid chloride by aniline. *Res. Chem. Intermed.* **40**, 1501–1516 (2014).

180. Ameer, M. & Fekry, A. Corrosion inhibition of mild steel by natural product

compound. *Prog. Org. Coatings* **71**, 343–349 (2011).

181. Mehdipour, M., Ramezanzadeh, B. & Arman, S. Y. Electrochemical noise investigation of Aloe plant extract as green inhibitor on the corrosion of stainless steel in 1M H_2SO_4. *J. Ind. Eng. Chem.* **21**, 318–327 (2015).

182. Makhlouf A S H & Aliofkhazraei M. Handbook of Materials Failure Analysis With Case Studies from the Aerospace and Automotive Industries, Butterworth Heinemann, Elsevier (2016).

183. Allal, H., Belhocine, Y. & Emna, Z. Computational study of some thiophene derivatives as aluminium corrosion inhibitors. *J. Mol. Liq.* **265**, 668-678 (2018).

184. Olawale, O., Bello, O. J., Ogunsemi, B. T., Uchella, U. C., Oluyori, A. P. & Oladejo, N. K. Optimization of chicken nail extracts as corrosion inhibitor on mild steel in 2M H_2SO_4. *Heliyon* **5**, e02821 (2019).

185. Haris, M., Mahmood, R., Rahman, H. & Rahman, N. *In vitro* cytotoxic activity of clerodendrum infortunatum L. against T47D, PC-3, A549 and HCT-116 human cancer cell lines and its phytochemical screening. *Int. J. Pharm. Pharm. Sci.* **8**, 439–444 (2016).

186. Subramanian, S., Nair, A. Scutellarin and hispidulin-7-0-glucuronide from the leaves of *Clerodendrum indicum* and *Clerodendrum infortunatum*. *Phytochemistry* **12**, 1195 (1973).

187. Das, B., Pal, D. & Haldar, A. A review on biological activities and medicinal properties of *Clerodendrum infortunatum* linn. *Int. J. Pharm. Pharm. Sci.* **6**, 41–43 (2014).

188. Akens, H. A., Nkem, B. I. Corrosion inhibition of API 5L X80 pipeline steel in acidic environment using aqueous extract of *Thevetia peruviana*. *Chem. Int.* **6**, 117–128 (2020).

189. Zhang, W., Hui-Jing, L., Meirong, W., Li-Juan, W., Ai-Han, Z. & Yan-Chao, W. Highly effective inhibition of mild steel corrosion in HCl solution by using pyrido[1,2-a]benzimidazoles. *New J. Chem.* **43**, 413–426 (2019).

190. Shivakumar, S. S. & Mohana, K. N. Corrosion behavior and adsorption thermodynamics of some Schiff bases on mild steel corrosion in industrial water medium. *Int. J. Corros.* **2013**, 543204 (2013).

191. Manimegalai, S. & Manjula, P. Thermodynamic and adsorption studies for corrosion inhibition of mild steel in aqueous media by *Sargasam swartzii* (Brown algae). *J. Mater. Environ. Sci.* **6**, 1629–1637 (2015).

192. Praveen, B. M., Alhadhrami, A., Prasanna, B. M., Hebbar, N. & Prabhu, R. Anti-corrosion behavior of olmesartan for soft-cast steel in 1 mol dm^{-3} HCl. *Coatings* **11**, 965 (2021).

193. Akinbulumo, O. A., Odejobi, O. J. & Odekanle, E. L. Thermodynamics and adsorption study of the corrosion inhibition of mild steel by *Euphorbia heterophylla* L. extract in 1.5 M HCl. *Results Mater.* **5**, 100074 (2020).

194. Tan, B., Bin, X., Shengtao, Z., Yujie, Q., Lihui, X., Shijin, C. & Jiahong, H. Papaya leaves extract as a novel eco-friendly corrosion inhibitor for Cu in H_2SO_4 medium. *J. Colloid Interface Sci.* **582**, 918–931 (2021).

195. Akinbulumo, O. A. & Odejobi, O. J. Modeling and optimization of the inhibition efficiency of *Euphorbia heterophylla* extracts based corrosion inhibitor of mild steel corrosion in HCl media using a response surface methodology. *J. Chem. Technol. Metall.* **54**, 217–232 (2018).

196. Kundu, B. B., Karan, V., Ayesha, F., Priyanka, J., Devendra, K. P. & Vijay, K. *Dioscorea bulbifera* L. (Dioscoreaceae): A review of its ethnobotany, pharmacology and conservation needs. *South African J. Bot.* **140**, 365-374 (2020) doi:10.1016/j.sajb.2020.07.028.

197. Chen, S., Zhu, B. & Liang, X. Corrosion inhibition performance of coconut leaf extract as a green corrosion inhibitor for X65 steel in hydrochloric acid solution. *Int. J. Electrochem. Sci.* **15**, 1–15 (2020).

198. Umoren, S. A., Eduok, U. M., Solomon, M. M. & Udoh, A. P. Corrosion inhibition by leaves and stem extracts of *Sida acuta* for mild steel in 1 M H_2SO_4 solutions investigated by chemical and spectroscopic techniques. *Arab. J. Chem.* **9**, S209–S224 (2016).

199. Oguzie, E. E. Kanayo, L. O., Chris, O. A., Irene, O. U., Jude, N. O. & Victor, O. N. Natural products for materials protection: corrosion and microbial growth inhibition using *Capsicum frutescens* biomass extracts. *ACS Sustain. Chem. Eng.* **1**, 214–225 (2013).

200. Ali, A., Falih, S., Yousif, N., Rezgar, R. & Kamal, I. Modeling and optimization of structural steel corrosion inhibition using barely grass extract as green inhibitor. *Am. J. Environ. Eng.* **7**, 73–81 (2017).

201. Schuurman, T., De Boer, R. F., Kooistra-Smid, A. M. D. & Van Zwet, A. A. Prospective study of use of PCR amplification and sequencing of 16S ribosomal DNA from cerebrospinal fluid for diagnosis of bacterial meningitis in a clinical setting. *J. Clin. Microbiol.* **42**, 734–740 (2004).

202. Chaijarasphong, T., Thammachai, T., Itsathitphaisarn, O., Sritunyalucksana, K. & Suebsing, R. Potential application of CRISPR-Cas12a fluorescence assay coupled with rapid nucleic acid amplification for detection of white spot syndrome virus in shrimp. *Aquaculture* **512**, 734340 (2019).

203. AlAbbas, F. M., Charles, W., Shaily, M. B., John, R. S., David, L. O., Brajendra, M. & Anthony E. K. Influence of sulfate reducing bacterial biofilm on corrosion behavior of low-alloy, high-strength steel (API-5L X80). *Int. Biodeterior. Biodegradation* **78**, 34–42 (2013).

204. Behpour, M., Ghoreishi, S. M., Soltani, N. & Salavati-Niasari, M. The inhibitive effect of some bis-N,S-bidentate Schiff bases on corrosion behaviour of 304 stainless steel in hydrochloric acid solution. *Corros. Sci.* **51**, 1073–1082 (2009).

205. Delaunois, F., Tosar, F. & Vitry, V. Corrosion behaviour and biocorrosion of galvanized steel water distribution systems. *Bioelectrochemistry* **97**, 110–119

(2014).

206. Al Abbas, F. M., Bhola, R., Spear, J. R., Olson, D. L. & Mishra, B. Electrochemical characterization of microbiologically influenced corrosion on linepipe steel exposed to facultative anaerobic Desulfovibrio sp. *Int. J. Electrochem. Sci.* **8**, 859–871 (2013).

207. Li, X., Chen, H., Chen, P., Qing, C. & Li, H. Microbial activities' influence on three kinds of metal material corrosion behaviors. *J. Mater. Eng. Perform.* **26**, 2102–2109 (2017).

208. Chandrasatheesh, C. & Jayapriya, J. *Bioelectrochemical Interface Engineering*, John Wiley & Sons, Inc., First Edition, 77–90 (2019) doi:https://doi.org/10.1002/9781119611103.ch5.

209. Xi, Y., Mallavarapu, M. & Naidu, R. Reduction and adsorption of Pb^{2+} in aqueous solution by nano-zero-valent iron — A SEM , TEM and XPS study. *Mater. Res. Bull.* **45**, 1361–1367 (2010).

210. Jorgensen, J.-E., Mosegaard, L., Thomsen, L. E., Jensen, T. R. & Hanson, J. C. Formation of γ-Fe_2O_3 nanoparticles and vacancy ordering: An in situ X-ray powder diffraction study. *J. Solid State Chem.* **180**, 180–185 (2007).

211. Paulson, B., Kakkassery, J., Raphael, V. & Shanmughan, S. Prevention of reinforcement corrosion in concrete by sodium lauryl sulphate: electrochemical and gravimetric investigations. *Int. J. Corros.* **2018**, 1–10 (2018).

LIST OF PUBLICATIONS

- **Vidhya Thomas K**, Joby Thomas K, Vinod Rapheal P, A.S. Sabu, K. Ragi, Reeja Johnson. "*Tinospora cordifolia* extract as an environmentally benign green corrosion inhibitor in acid media: electrochemical, surface morphological, quantum chemical, and statistical investigations", *Materials Today Sustainability*, vol.13, 100076 (2021) https://doi.org/10.1016/j.mtsust.2021.100076

- **Vidhya K Thomas,** Joby K Thomas, Vinod P Raphael, K Ragi, Reeja Johnson, Ramesh Babu."Green corrosion inhibition properties of *Croton persimilis* extract on mild steel in acid media", *Journal of Bio and Tribo Corrosion*, vol.7, 121 (2021) https://doi.org/10.1007/s40735-021-00554-z

- **Vidhya Thomas K**, Joby Thomas Kakkassery, Vinod P Raphael, K Ragi, Reeja Johnson. "*Ixora coccinea* extract as an efficient eco-friendly corrosion inhibitor in acidic media: experimental and theoretical approach", *Current Chemistry Letters*, vol.10, 139-150(2021) http://dx.doi.org/10.5267/j.ccl.2020.12.001

- Ragi. K, Joby Thomas Kakkassery, Vinod P. Raphael, Reeja Johnson, **Vidhya Thomas K**. "*In vitro* antibacterial and *in silico* docking studies of two Schiff bases on *Staphylococcus aureus* and its protein targets" , *Future Journal of Pharmaceutical Sciences*, vol.7, 1-9(2021) https://doi.org/10.1186/s43094-021-00225-3

- Reeja Johnson, Joby Thomas Kakkassery, Vinod Raphael Palayoor, Ragi Kooliyat and **Vidhya Thomas Kannanaikkal**. "Experimental and theoretical investigations on the corrosion inhibition action of Thiadiazole derivatives on carbon steel in 1M HCl medium", *Oriental Journal of Chemistry*, vol.36(6), 1179-1188(2020) http://dx.doi.org/10.13005/ojc/360624

LIST OF CONFERENCE PAPERS

- **Vidhya Thomas K**, Joby Thomas K, Ragi K, Reeja Johnson."Excellent eco-friendly corrosion inhibition behaviour of *Croton persimilis* extract (CPE) for mild steel in acidic media: physicochemical, electrochemical and surface morphological studies", *National seminar on Current Trends in Chemistry (CTriC 2020),* CUSAT, February 2020

- Aby Paul, Joby Thomas K, **Vidhya Thomas K**, Vinod P Rapheal."Synthesis, characterisation and antimicrobial studies of transition metal complexes of Schiff base ligand", *KSCSTE Sponsored National Seminar on Recent Trends in Computational Chemistry and Drug Design*,St. Joseph's College(autonomous), Irinjalakuda, January 2019

- Nimmy Kuriakose, Joby Thomas K, **Vidhya Thomas K**,Vinod P Rapheal. "Synthesis, characterization and antitumor studies of Cu(II) complexes of heterocyclic Schiff base ligands", *International Conference on Chemistry and Physics of Materials*, St.Thomas' College(autonomous), Thrissur, January 2019

- Shaju K S, Joby Thomas K, **Vidhya Thomas K**, Vinod P Rapheal."Synthesis, characterization and redox properties of Schiff base derived from 3-mercapto propanoic acid and its Cu(II) complex", *KSCSTE Sponsored National Seminar on Interdisciplinary Chemical Research*, St Joseph's College(autonomous), Irinjalakuda, February 2018.

- Shaju K S, Joby Thomas K, **Vidhya Thomas K**,Vinod P Rapheal. "Cyclic voltammetric studies of Schiff base derived from 3-Phenylpropanoic acid and its Cu(II) complex in DMSO at the surface of glassy carbon", *UGC sponsored National seminar on Recent Advances in Chemistry*, Vimala College,Thrissur,January2017

PAPERS TO BE COMMUNICATED

- Schiff bases derived from pyridine carbonyl compounds as synthetic microbial induced corrosion inhibitor for mild steel in marine environment.

- Influence of leaves and roots extracts of *Clerodendrum infortunatum* as eco-friendly corrosion inhibitor on mild steel in acid media: Experimental and theoretical approach

Format for plagiarism check certificate

UNIVERSITY OF CALICUT
CERTIFICATE ON PLAGIARISM CHECK

1.	Name of the research scholar	Vidhya Thomas K		
2.	Title of thesis/dissertation	Synthetic and natural organic inhibitors for meta corrosion: physicochemical, electrochemical, morphological and quantum mechanical investigation		
3.	Name of the supervisor	Dr. Joby Thomas K		
4.	Department/Institution	Dept. of Chemistry St. Thomas' College (Autonomous) Thrissu		
5.		**Introduction/ Review of literature**	**Materials and Methods**	**Result/ Discussion/Summary/ Conclusion**
	Similar content (%) identified	2%	2%	4%
	Acceptable maximum limit (%)	25 /35	25	10
6.	Software used	Urkund		
7.	Date of verification	9/9/2021		

**Report on plagiarism check, specifying included/excluded items with % of similarity to be attached.*

Checked by (with name, designation & signature) Dr. VINOD. V. M
Assistant Librarian(Sr.Scale)
University of Calicut

Name & Signature of the Researcher Vidhya Thomas K

Name & Signature of the Supervisor

The Doctoral Committee* has verified the report on plagiarism check with the contents of the thesis, as summarized above and appropriate measures have been taken to ensure originality of the Research accomplished herein.

Name & Signature of the HoD/HoI (Chairperson of the Doctoral Committee)

Dr. Martin K. A.
Assistant Professor
In charge of Principal
St. Thomas College (Autonomous)
Thrissur - 680 001

** In case of languages like Malayalam, Tamil, etc. on which no software is available for plagiarism check, a manual check shall be made by the Doctoral Committee, for which an additional certificate has to be attached*